EFFECT OF PRIOR EXPOSURE AT ELEVATED TEMPERATURES ON TENSILE PROPERTIES AND STRESS-STRAIN BEHAVIOR OF FOUR NON-OXIDE CERAMIC MATRIX COMPOSITES

THESIS
JUNE 2015

Sarah M. Wallentine, Captain, USAF

AFIT-ENY-MS-15-J-048

DEPARTMENT OF THE AIR FORCE
AIR UNIVERSITY
AIR FORCE INSTITUTE OF TECHNOLOGY

Wright-Patterson Air Force Base, Ohio

AFIT-ENY-MS-15-J-048

EFFECT OF PRIOR EXPOSURE AT ELEVATED TEMPERATURES ON TENSILE PROPERTIES AND STRESS-STRAIN BEHAVIOR OF FOUR NON-OXIDE CERAMIC MATRIX COMPOSITES

THESIS

Presented to the Faculty

Department of Aeronautics and Astronautics

Graduate School of Engineering and Management

Air Force Institute of Technology

Air University

Air Education and Training Command

In Partial Fulfillment of the Requirements for the

Degree of Master of Science in Aeronautical Engineering

Sarah M. Wallentine, BS

Captain, USAF

June 2015

AFIT-ENY-15-J-048

EFFECT OF PRIOR EXPOSURE AT ELEVATED TEMPERATURES ON TENSILE PROPERTIES AND STRESS-STRAIN BEHAVIOR OF FOUR NON-OXIDE CERAMIC MATRIX COMPOSITES

Sarah M. Wallentine, BS
Captain, USAF

Committee Membership:

Dr. Marina B. Ruggles-Wrenn, PhD
Chair

Dr. Thomas G. Eason III
Member

Dr. Richard B. Hall
Member

Abstract

Thermal stability of four non-oxide ceramic matrix composites was studied. The materials studied were: SiC/SiNC; C/SiC; C/SiC-B_4C (C/HYPR-SiC™); and SiC/SiC-B_4C (SiC/HYPR-SiC™). All are commercially available composites. COI Ceramics, San Diego, CA, manufactured the SiC/SiNC and C/SiC composites using polymer infiltration and pyrolysis (PIP). The C/HYPR-SiC™ and SiC/HYPR-SiC™ CMCs were manufactured by Hyper-Therm High-Temperature Composites (Hyper-Therm HTC), Inc., Huntington Beach, CA using chemical vapor infiltration (CVI). The SiC/SiNC composite consists of an amorphous silicon nitrocarbide matrix reinforced by woven laminates of Hi-Nicalon™ silicon carbide fibers. The C/SiC composite consists of a crystalline silicon carbide matrix reinforced by woven laminates of HexTow® IM7 PAN-based carbon fibers. The C/HYPR-SiC™ and SiC/HYPR-SiC™ composites consist of a layered silicon carbide and boron carbide matrix reinforced by woven laminates of T300-1K carbon fibers and Hi-Nicalon™ silicon carbide fibers, respectively. All four composites rely on a dense matrix for strength, stiffness, and oxidation protection. Fiber coating provides a fiber-matrix interface that allows fiber-matrix debonding and fiber pullout to occur, imparting fracture toughness to the CMC. The SiC/SiNC, C/SiC, and C/HYPR-SiC™ composites were heat treated in laboratory air for 10 h, 20 h, 40 h, and 100 h at over-temp (1300°C) and for 100 h at operating temperature (1200°C). The SiC/HYPR-SiC™ composite was heat treated in laboratory air for 10 h, 20 h, 40 h, and 100 h at over-temp (1400°C) and for 100 h at operating temperature

(1300°C). Room-temperature tensile properties of heat treated and virgin material were measured, and effect of prior heat treatment on tensile properties was evaluated.

Prior heat treatment caused a reduction of tensile strength of at least 10% for all materials. The C/HYPR-SiC™ CMC exhibited the best thermal stability, retaining 89% of its tensile strength after 100 h duration exposure at over-temp. The SiC/SiNC composite exhibited 80%, and the C/SiC composite exhibited 73% strength retention after heat treatment for 100 h at over-temp. Heat treatment at operating temperature had little effect on tensile strength relative to heat treatment at over-temp. Tensile strength of the SiC/HYPR-SiC™ composite exhibited a drastic 32% decrease following heat treatment for 10 h at over-temp. 20 h, 40 h, and 100 h heat treatments at over-temp and 100 h at operating temperature had little additional effect on tensile strength of the composite compared to the 10 h exposure time. Both PIP-produced CMCs exhibited increased fiber-matrix bonding due to high temperature exposures, contributing to brittle fracture of clumped fiber bundles and thus reduced tensile strength. Both CVI-produced CMCs exhibited considerable matrix voids due to poor infiltration during fabrication. Void prevalence and the associated stress concentrations contributed to premature matrix cracking and composite failure. The CVI CMCs were susceptible to degraded tensile properties and brittle composite fracture due to strengthened fiber-matrix interfaces and fiber degradation caused by prior heat treatment.

Acknowledgements

First and foremost, I would like to express my sincere gratitude to my research and thesis advisor, Dr. Marina B. Ruggles-Wrenn. It is her passion for and dedication to research and education that has enabled this research effort. Her expertise and tireless guidance and support are what made the successful completion of my research and thesis a reality. In the words made famous by Sir Isaac Newton, “If I have seen further, it is by standing on the shoulders of giants.”

Thank you to Dr. Larry Zawada and AFRL/RXCC for sponsorship of my research. Thank you to Dr. Kristin Keller (AFRL/RXCCM), Ms. Jennifer Pierce (AFRL/RXCM), Mr. Randall Corns (AFRL/RXCCM), and Dr. Kathleen Shugart (AFRL/RXCC) for their support through resources and training necessitated by my research. Thank you to Dr. Thomas Eason (AFRL/RQHF) and Dr. Richard Hall (AFRL/RXCCP) for their membership and support on my thesis committee.

I would also like to thank the AFIT/ENY laboratory technicians Mr. Barry Page, Mr. Wilber Lacy, and Mr. John Hixenbaugh for their persistent support with lab equipment – from training to maintaining. AFIT Model Fabrication Shop staff Mr. Jan LeValley, Mr. Brian Crabtree, and Mr. Daniel Ryan provided invaluable support and machining expertise that was critical to the completion of my research.

A special thanks to my family and friends for the personal and moral support throughout my graduate education experience. Especially to my parents, for their enduring love and their endless support for all that I do. Without them I would not be here today.

Sarah M. Wallentine

Table of Contents

List of Figures

Page

List of Tables

Page

EFFECT OF PRIOR EXPOSURE AT ELEVATED TEMPERATURES ON TENSILE PROPERTIES AND STRESS-STRAIN BEHAVIOR OF FOUR NON-OXIDE CERAMIC MATRIX COMPOSITES

I. Introduction

> "The best and safest method of philosophizing seems to be, first to enquire diligently into the properties of things, and to establish these properties by experiment, and then to proceed more slowly to hypotheses for the explanation of them. For hypotheses should be employed only in explaining the properties of things, but not assumed in determining them, unless so far as they may furnish experiments." [1]

1.1 Motivation

Demand for increasing capability, performance, and efficiency of air and space vehicles has persisted since their inception. Key factors in addressing these demands include: weight savings; increased engine burning temperatures; and structural components that can handle higher temperatures. There thus exists a requirement to integrate or replace historically employed materials with new materials that have comparable or better structural and mechanical characteristics, as well as improved thermal properties. Development and application of advanced materials is critical in enabling the technology maturation required to remain on the cutting edge of air and space vehicle advancement.

As mentioned above, advancements in aerospace and air vehicle technology rely heavily on the development of structural materials that maintain mechanical performance at elevated temperatures. Figure 1 illustrates this relationship of air and space vehicle development to increased operating temperatures. Examples of components that are exposed to extreme temperature environments include engine-related components (engine ducts, engine vanes, exhaust flaps),

structural components of hypersonic air vehicles, and thermal protection systems (TPSs). Metals and metallic super-alloys have been developed to increased temperature capability, but their melting temperatures are being met and exceeded by current and future operating conditions [2]. The temperature limitation imparted by metals and metallic alloys is cause for further material development on other fronts.

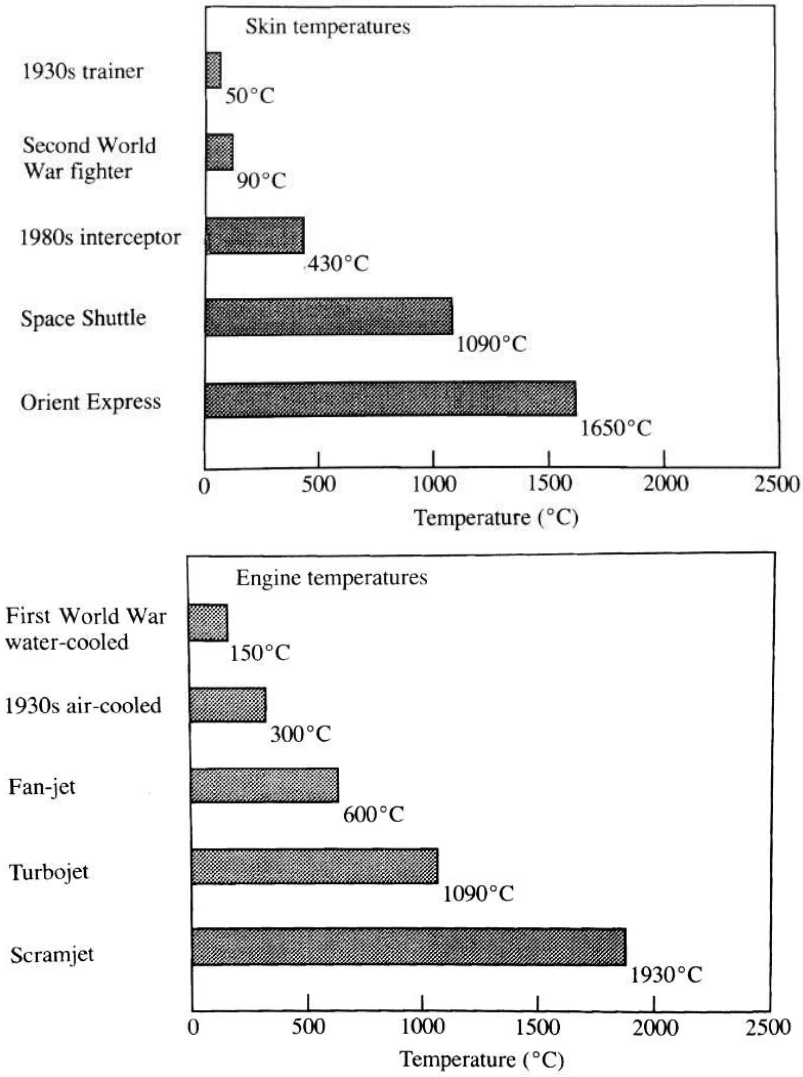

Figure 1: Air and space vehicle development related to increase in operating temperatures [3]

As seen in Figure 2, the temperature capability of high performance monolithic ceramic materials far exceeds that of polymers and metals. This makes ceramics an obvious candidate for high temperature applications.

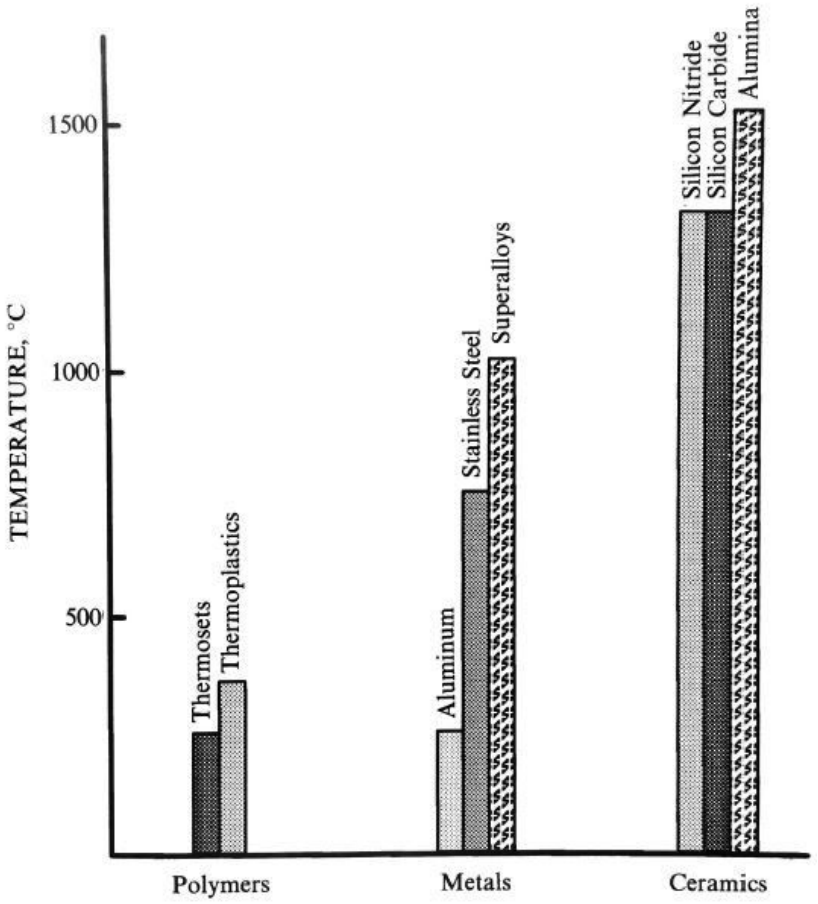

Figure 2: Service temperature limits of polymers, metals, and ceramics [4]

However, high temperature performance is not the only consideration. Mechanical performance of any material that is candidate for structural application must also be considered. In addition to excellent high-temperature characteristics, high performance monolithic ceramics are characterized by high strength and hardness, chemical inertness, wear resistance, and low density. On

the other hand, even these high performance monolithic ceramics do not perform well under impact loading and are prone to catastrophic failure under mechanical or thermal loading. It is the absence of energy-dissipating mechanisms in these monolithic ceramics that causes such catastrophic failure [4]. In other words, once a monolithic ceramic begins to develop a crack either during loading or from a manufacturing defect, the material provides no mechanism to impede or prevent crack propagation. An unobstructed propagating crack easily grows to a critical size, leading to fracture and catastrophic failure. The measure of tolerance to crack-like defects of a material is a property known as fracture toughness. It is the extremely low fracture toughness of monolithic ceramics that precludes their use as structural components.

Altering high performance monolithic ceramics to include more energy-absorbing mechanisms, thus increasing fracture toughness, will manage the concern of catastrophic failure. The incorporation of reinforcements in a ceramic matrix, forming a ceramic matrix composite (CMC), has been found to drastically improve the fracture toughness over that of monolithic ceramics. CMCs provide a combination of the outstanding thermal and mechanical properties of ceramics with an increased fracture toughness afforded by the reinforcement phase. The resulting material has a vastly improved damage tolerance and is ideal for use as a structural or other component in high-temperature applications.

CMCs have thus been identified as leading high-performance material systems for use in air and space vehicle structures and components, to include TPSs. However, because development of CMCs is in the relatively early stages,

there exists much work to be done in the identification, testing, and characterization of different CMC systems under a variety of conditions. The emphasis of the current research is on characterization through experimental investigation of four different CMC material systems that are being considered for use as thermal protection systems.

1.2 Problem Statement

When structural components of air and space vehicles are subjected to extremely high temperatures, the structural integrity of the vehicle is put at increased risk. It is of utmost importance that structural components of these vehicles consist of materials that can withstand such operating environments while maintaining a high level of performance. One promising solution is the utilization of CMCs as thermal protection systems for the components in question.

Prior to employment, thermal and mechanical properties of CMCs must be extensively characterized and understood. This includes establishing a baseline of the given CMC properties at room-temperature, prior to any environmental exposure, as well as investigation of CMC behavior after exposure to simulated operating conditions. Material properties are largely determined through macroscopic testing. Prior to advancing to more complex loading and material behavior, fundamental material properties must be established. This is best accomplished with the tensile test – the most basic mechanical test [5, 6]. Thus, tensile testing was employed in this research to establish the fundamental

mechanical properties of four CMC systems that are being considered for use as TPSs. Virgin material and material exposed to various time-temperature histories were experimentally investigated.

1.3 Research Objective

The objective of this research is to characterize the room-temperature tensile properties of four different CMC systems following heat treatments that simulate large acreage TPS panel service conditions. Tensile properties were established experimentally by performing uniaxial monotonic tensile tests on both virgin specimens and specimens exposed to various time-temperature histories. The four material systems (indicated by MS1, MS2, MS3, and MS4) evaluated were:

MS1: SiC/SiNC – CMC reinforced with Hi-Nicalon™ SiC fibers in a SiNC matrix derived by polymer infiltration and pyrolysis (PIP) (manufactured by COI Ceramics, San Diego, CA)

MS2: C/SiC – CMC reinforced with HexTow® IM7 PAN-based carbon fibers in a PIP-derived SiC matrix with oxidation inhibitors, and seal-coated with PIP-derived SiC (manufactured by COI Ceramics, San Diego, CA)

MS3: C/SiC-B_4C – CMC reinforced with T300-1K carbon fibers, consisting of alternating layers of SiC and B_4C matrices, processed by chemical vapor infiltration (CVI), and coated with a SiC-based glaze (manufactured by Hyper-Therm High-Temperature Composites, Inc., Huntington Beach, CA)

MS4: SiC/SiC-B_4C – CMC reinforced with Hi-Nicalon™ SiC fibers, consisting of alternating layers of SiC and B_4C matrices, processed by CVI (manufactured by Hyper-Therm High-Temperature Composites, Inc., Huntington Beach, CA)

Uniaxial monotonic tensile tests to failure were conducted on each material system following subjection to various prescribed time-temperature histories.

Each CMC was exposed to two temperatures: manufacturer recommended operating temperature and 100°C over-temperature. MS1, MS2, and MS3 were subjected to 1300°C for 10, 20, 40, and 100 hours, and to 1200°C for 100 hours. MS4 was subjected to 1400°C for 10, 20, 40, and 100 hours, and to 1300°C for 100 hours.

1.4 Methodology

The research objective outlined above was accomplished using the following methodology:

1. Perform monotonic tension to failure tests on virgin specimens of all material systems
2. Perform monotonic tension to failure tests on pre-heat treated specimens
3. Evaluate change in tensile properties and stress-strain behavior due to heat treatment
4. Examine all tested specimens using an optical and a scanning electron microscope (SEM) to assess failure mechanisms of the composites and microstructural changes caused by heat treatment

II. Background

2.1 Ceramics

Ceramics refers to a wide variety of inorganic, generally non-metallic materials that are typically processed at high temperatures. Over time, ceramics have been further categorized into two classes: traditional/conventional ceramics and advanced/high-performance ceramics [4]. The two classes of ceramics are distinguished in most part by: level of sophistication in processing methods; material properties; and the typical applications for their use. Traditional or conventional ceramics are most often monolithic in form and include various clay, cement, and silicate glass products. Some common examples are pottery, porcelain, bricks, tiles, cements and glasses [4, 7]. Advanced or high-performance ceramics most often involve very sophisticated processing techniques and have superior material properties, which are a function of the quality and purity of raw materials that comprise them. Some examples include structural, electrical, and chemical processing products, among others [4, 7, 8].

Due to their superior material properties, high-performance ceramics have become commonplace in various engineering applications. Some outstanding material characteristics of these high-performance ceramics include their extremely high resistance to heat, chemicals, abrasion, and wear. They are also typified by chemical inertness, low density, and high strength and hardness [4]. However, in a monolithic form, even these advanced ceramics have their limitations.

The benefit of the very high strength and hardness of ceramics is accompanied by the drawback of extremely low damage tolerance (i.e. low fracture toughness), causing them to be highly vulnerable to catastrophic failure. As discussed before, this low fracture toughness of monolithic ceramics is an effect of their lack of energy dissipating mechanisms [4]. In other words, once a crack begins to develop (either during loading or from a manufacturing defect), there are no mechanisms to impede or prevent the crack from easily growing to a critical size, causing the structure to catastrophically fail in fracture.

In order for these high-performance ceramics to also become advantageous in structural applications, the issue of low fracture toughness must be resolved. It is with this in mind that research and development of high-performance ceramics has evolved into that of ceramic composites. The incorporation of reinforcements in a ceramic matrix, forming a ceramic matrix composite (CMC), has been found to drastically improve the fracture toughness over that of monolithic ceramics. As mentioned before, the combination of outstanding thermal and mechanical properties of ceramics, with increased fracture toughness and damage tolerance afforded by reinforcements, makes CMCs ideal candidates for use as structural or other components in high-temperature applications.

2.2 Ceramic Matrix Composites

A composite is a material system consisting of two or more phases (matrix and reinforcement) whose mechanical performance and properties are designed to be superior to those of the constituent phases acting independently [9]. As

illustrated by Figure 3, the matrix is a continuous phase in which the reinforcement phase is distributed.

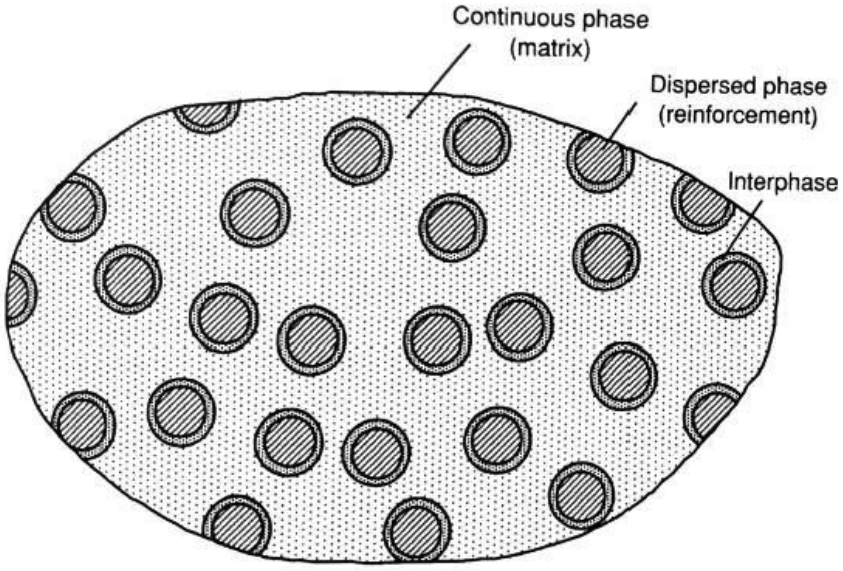

Figure 3: Schematic of composite phases [9]

The choice of material for the matrix and reinforcement phases, as well as the type of reinforcement used can vary from case-to-case, and is dependent upon the desired ultimate performance of the composite. For example, the matrix can be composed of polymer, metal, or ceramic material, and the reinforcement phase can be in the form of particles, whiskers, short fibers, or continuous fibers. The choice of material for each phase, as well as the nature of interaction between the phases (i.e. the interface) plays a critical role in overall composite performance.

In the case of polymer matrix composites (PMCs) and metal matrix composites (MMCs), the design objective is typically to achieve a relatively high modulus ratio of reinforcement to matrix, usually in the range of 10 – 100:1.

Reinforcement in a PMC provides the majority of strength and stiffness to the composite, and load transfer from matrix to reinforcement is achieved efficiently through a strong matrix-reinforcement interface [4, 3]. On the other hand, the reinforcement to matrix modulus ratio of CMCs is relatively low, often 1:1 or less [4]. CMC design does not emphasize utilization of a strong matrix-reinforcement interface to improve strength or stiffness properties of the composite. A ceramic matrix already provides the desired high strength and stiffness. So, the primary purpose of reinforcements in CMCs is to increase fracture toughness of the otherwise brittle ceramic matrix. This is accomplished by adding reinforcements, introducing to the matrix a great energy-dissipating mechanism that it intrinsically lacks. The nature of the matrix-reinforcement interface in PMCs, MMCs, and CMCs is what enables the desired effects of creating a composite material.

In order for the reinforcements of a CMC to contribute the desired energy-dissipating and fracture toughness functions, the matrix-reinforcement interface must be weak in nature. In other words, the mechanical and/or chemical bond between the two phases must not be strong. In CMCs, the method of coating the reinforcement material is often resorted to in order to reduce or avoid chemical interaction in the interface, thus minimizing the issue of chemical bonding and leaving only mechanical bonding to be greatly concerned with [4]. As depicted in Figure 4, a strong interfacial bond will cause the CMC to behave in a brittle manner, not unlike monolithic ceramics, therefore subjecting the CMC to planar fracture and catastrophic failure. On the other hand, as shown on the right in Figure 4, a weak interfacial bond will allow for crack deflection by the

reinforcement phase (typically a ceramic fiber in a CMC), which increases fracture toughness and resistance to catastrophic fracture of the CMC [4]. Consider a continuous fiber-reinforced CMC. The strong interfacial bond in the first case allows a crack propagating through the matrix to easily continue through the fiber reinforcement without obstruction, eventually making its way through the entire structure, resulting in catastrophic fracture and an often planar and smooth fracture surface. In the case of a weak interfacial bond, once the propagating crack meets the fiber, it can no longer easily transition from the matrix and through or across the fiber, but is instead arrested at the interface and is deflected from the original path to one along the direction of the fiber. This process dissipates the energy stored in the crack, reducing its ability to catastrophically damage the CMC, and thus increases the fracture toughness of the CMC.

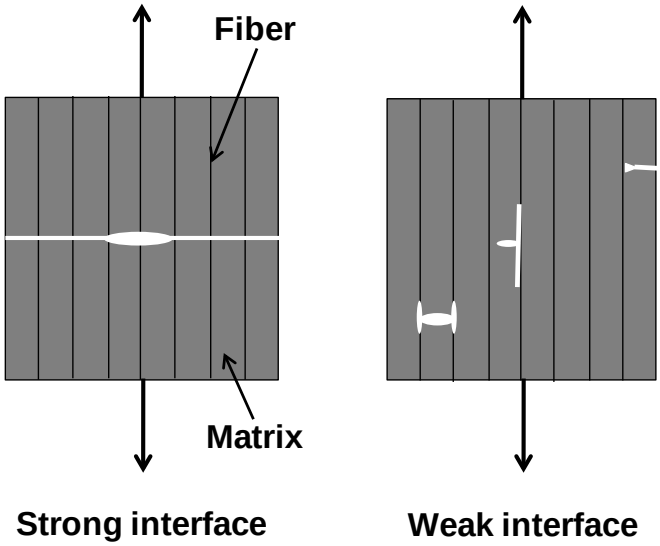

Figure 4: Failure schematic of CMCs containing strong and weak fiber-matrix interface [4]

2.3 Mechanical behavior of CMCs under monotonic tensile loading

The monotonic tensile test is commonly used to establish mechanical characteristics of CMCs [5]. It should be mentioned that flexure testing is also used in practice. Although less complicated to perform than a tensile test, the interpretation of flexure test data is much less straightforward, often leaving the tensile test as the most desirable option [4].

Having two constituents, often with different mechanical properties, the mechanical behavior of a CMC under tensile loading will be dominated by either one of the constituents. Considering a continuous fiber-reinforced CMC, either the failure strain of the fiber or matrix will dominate, determined by which is lesser in value. If the failure strain of the fiber dominates (i.e. is less than that of the matrix), single-fracture failure is likely to occur [4]. This scenario is depicted in Figure 5(a). Shown are the stress-strain curve (left) and variation of composite strength as a function of fiber volume fraction (right). However, the case of fiber failure strain being less than that of the matrix is uninteresting and uncommon in the case of CMCs.

In the other case, which is most common and of great interest in CMCs, the failure strain of the fiber is greater than that of the matrix, causing the matrix to fail first and the load to be transferred to the fibers [4]. Depending on the volume ratio of fibers to matrix, the fibers will either be able to sustain the load transfer or will not. This scenario is depicted in Figure 5(b).

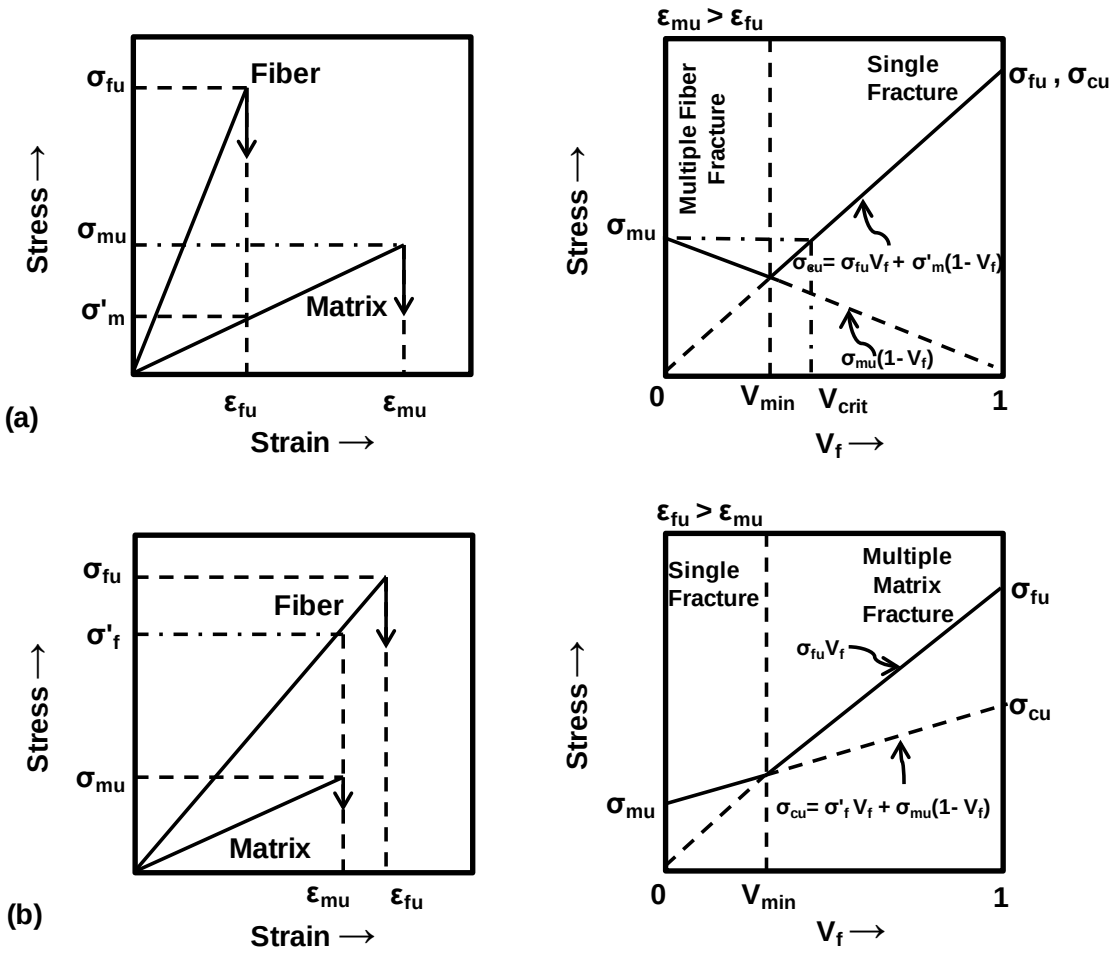

Figure 5: Unidirectional fiber reinforced composite stress-strain curves (left) and composite strength vs. fiber volume fraction (right); (a) matrix failure strain greater than that of the fiber; (b) matrix failure strain less than that of the fiber [4]

If the volume ratio is at or below the critical value, the fibers will be unable to carry the extra load and will fail. If the volume ratio is above the critical value, the fibers will carry the extra load, transferring some load back to the matrix (assuming the interface remains intact), which causes additional cracking in the matrix. Once the composite ultimate failure is reached (again, dominated by fiber failure stress), the fibers fracture and begin to pull out of the matrix (referred to as

fiber pullout) [4]. Figure 6 illustrates the stress-strain behavior of a continuous fiber-reinforced CMC with fiber-matrix volume ratio greater than the critical value.

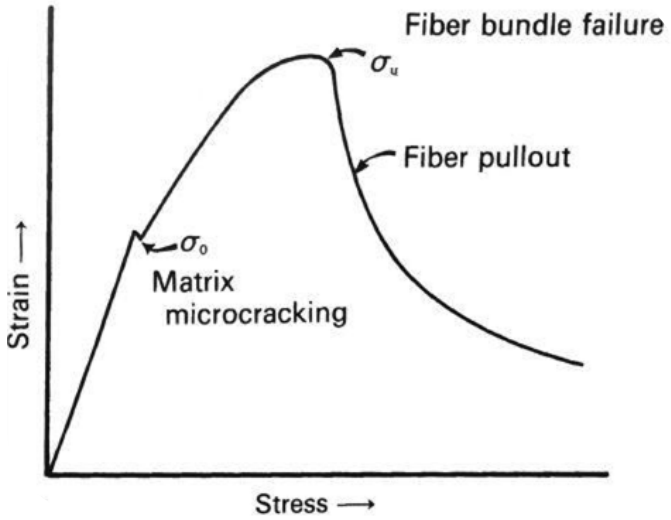

Figure 6: Representative stress-strain curve of continuous fiber-reinforced CMC with fiber-dominated failure [4]

2.4 Oxide and Non-oxide CMCs

The constituents of a CMC are typically composed of either oxide or non-oxide compounds. CMC matrix materials can be composed of either oxide or non-oxide compounds. Reinforcements can also be composed of either oxide or non-oxide compounds, including carbon. Considering CMCs for structural and very high temperature applications, there are benefits and drawbacks with each the oxide and the non-oxide family of constituents.

Oxide materials are characterized by high tensile strength and modulus and are highly resistant to oxidation at very high temperatures. However, oxides are typically fine-grained material, causing them to be prone to grain-boundary sliding and creep at temperatures at or above 1100°C [4, 10]. Therefore,

oxide/oxide CMCs are limited in their application to operating environments involving long-term exposure at very high temperatures. None of the material systems in this research are composed of oxide constituents.

Non-oxide materials also possess high tensile strength and modulus, but unlike oxides, they are rather susceptible to oxidation and thus degradation at very high temperatures. An advantage of non-oxides is that creep rates are low at very high temperatures [10]. All material systems in this research are composed of non-oxide matrix materials: SiNC (MS1); SiC (MS2); and alternating layers of SiC and B_4C (MS3 and MS4). MS1 and MS4 contain continuous non-oxide fiber reinforcements (Hi-Nicalon™ SiC), while MS2 and MS3 are comprised of continuous carbon fiber reinforcements.

The strength and modulus properties of carbon fibers are highly dependent on the fiber fabrication process and can vary in value from relatively low to very high. Further, carbon fibers will oxidize and deteriorate rather quickly at high temperatures, but can be protected by either the surrounding matrix or a protective fiber coating [10]. Thus, the range of suitable applications for carbon fiber reinforcements is broad and in most part the fabrication process can be coordinated to suit the desired application. MS2 is a non-oxide matrix CMC reinforced with IM7 PAN-based carbon fibers, which are derived from polyacrylonitrile (PAN) fibers and are of intermediate modulus (275-350 GPa). MS3 is a non-oxide matrix CMC reinforced with T300-1K carbon fibers, which are considered high tensile (HT) fibers [10].

2.5 Previous Research

The present research involves some specific material systems that have been previously studied as well as some that are new and have not yet been fully characterized. In the case of the CMCs that have not yet been fully characterized, some previous studies have been performed on similar material systems and similar constituent materials. It is important to examine the past research involving these materials and material systems in order to better understand the behavior exhibited by the material systems of the current study.

Ruggles-Wrenn et al [11, 12, 13] have performed multiple studies on Hi-Nicalon™/SiC-B_4C CMCs, which are that of MS4 in the present study. The majority of these efforts were focused towards characterizing the fatigue and creep behavior of the CMC at 1200°C in air and in steam. However, in one study the mechanical behavior of the CMC in monotonic tension in air at 1200°C was also characterized and compared to that of a Hi-Nicalon™/SiC CMC [11]. It was found that both CMCs exhibit a nearly bilinear stress-strain behavior. The stress-strain curves are linear up to the proportional limit, where nonlinear behavior occurs due to matrix cracking. The stress-strain curves then continue with a decreased slope. The ultimate tensile strength (UTS) and failure strain of the Hi-Nicalon™/SiC-B_4C were both considerably higher than that of the Hi-Nicalon™/SiC composite. However, the elastic modulus and average proportional limit of the Hi-Nicalon™/SiC composite was higher than that of the Hi-Nicalon™/SiC-B_4C (240 GPa and ~51% UTS versus 208 GPa and ~38% UTS, respectively). Additionally, the effect of prior tension-tension fatigue on the

tensile strength of the Hi-Nicalon™/SiC-B_4C composite was assessed. It was determined that prior fatigue at 1200°C in air and in steam causes a significant reduction in tensile strength. The degradation was attributed to an intrinsic creep-controlled flaw growth mechanism, and it was concluded that the multilayered matrix limited oxidation embrittlement of the fibers [11].

Ma, et al, and Mei, et al, [14, 15, 16] investigated the tensile behavior and thermal effects, respectively, on C/SiC composites. Ma, et al, determined the tensile behavior of a 2.5D woven method T300 carbon fiber reinforced C/SiC CMC processed by chemical vapor infiltration (CVI) [14]. Tensile stress-strain curves in both weft and warp direction showed mostly nonlinear material behavior, though the tensile properties of the two directions were significantly different. The difference in tensile properties between directions was attributed to weave architecture. Further, scanning electron microscope (SEM) imaging of the fracture surfaces indicated multi-step fiber fracture and extensive fiber pullout [14].

Mei, et al, investigated effects of high-temperature thermal cycling under constant load in a wet oxygen atmosphere on T300-1K carbon fiber reinforced C/SiC composites processed by isothermal CVI [15, 16]. In Reference 14, a series of three sets of thermal cyclic loading at constant tensile stress levels were performed. The maximum temperature reached for all cycles was 1200°C, and the series of cycles were as follows: 25 cycles for ΔT_1 of 500°C at 50 MPa; 35 cycles for ΔT_2 of 400°C at 100 MPa; 44 cycles for ΔT_3 of 300°C at 150 MPa. After the 144 cycles were complete, the residual material properties were

measured and compared to that of the virgin specimen. The strength, modulus, and failure strain retained 60.29%, 84.2%, and 59% of initial properties, respectively. Additionally, it was shown that thermo-elastic strain range is dependent on the temperature gradient magnitude but independent of applied stress level. SEM micrographs of the fracture surfaces showed that the composites exhibited a brittle and catastrophic damage characteristic, which was attributed to extensive matrix cracking, fiber debonding and breaking, as well as the oxidation of carbon fibers along the open and propagating cracks [15].

In Reference 15, thermal cycling from 900°C to 1200°C (ΔT of 300°C) was carried out over a total of 120 seconds. Under a constant tensile load of 60 MPa, temperature was held at 900°C for 30 s, heated to 1200°C in 60 s, held for 30 s, then cooled immediately down to 900°C. This cycle was repeated 50 times, and the monotonic tensile behavior was subsequently determined. The elastic modulus was reduced by 50%, UTS retained 82% of initial strength, and the failure strain decreased by approximately 50%. Additionally, it was deduced that thermal cycling causes nonreversible damage in the composite, resulting in an increase of the strain rate. Inspection of SEM micrographs showed matrix and coating cracks as well as oxidation along the opening cracks and beneath the coating. The cracking and oxidation were ascribed to the thermal and tensile loading as well as the wet oxygen atmosphere and particular structure of the investigated composites [16].

In attempting to identify additional mechanisms to improve damage tolerance of CMCs, References 16 and 17 examined the effects of a multilayered matrix on

the performance of carbon fiber reinforced CMCs. Multilayered CMCs are commonly identified in shorthand by MCMCs, and MS3 and MS4 in the current study are both MCMCs. Lamouroux, et al, conducted tensile and four-point bending tests of unidirectional and 2.5D woven configuration C/Si-B-C MCMC, a multilayer Si-B-C matrix composite reinforced with carbon fibers, and C/SiC CMC at ambient- and high-temperature in order to compare the lifetime of the multi- versus mono-layered matrix CMCs. Upon examination of test data as well as SEM micrographs for all tests, the authors concluded that a C/Si-B-C MCMC is more efficient in terms of providing oxidation resistance to the carbon fibers, and thus has a longer lifetime compared to that of the classical anti-oxidation systems based on coating carbon fibers to reduce oxygen permeation. This highly efficient oxidation resistant behavior of the multilayer matrix was accredited to a better control of crack propagation through the matrix, better damage configuration, and ability to select matrix layer materials based on the nature of a given aggressive environment. It was further asserted that the study proves carbon fibers can be used in an oxidizing environment, when used in reinforcing a multilayer ceramic matrix, even if the matrix is damaged [17].

Zhang, et al, examined the mechanical properties of a 2D weave T-300 carbon fiber reinforced C/Si-B-C MCMC prepared through low-pressure CVI. Monotonic tensile, interlaminar and in-plane shear tests were conducted from room temperature to 1200°C. Tests at room temperature were conducted in air while those at elevated temperatures were conducted in vacuum. It was experimentally determined that tensile, interlaminar shear and in-plane shear

strengths are highly dependent on temperature, with a continuous increase in the properties until a threshold of 1000°C is reached, after which point the properties exhibit a degradation. Further, it was observed that above this temperature threshold the composite exhibited an almost brittle fracture under tension, which was attributed to an increase in strength of the interfacial bond between fibers and matrix. In interlaminar shear, a stepwise matrix fracturing was observed, and in in-plane shear, all 90° fibers on the fracture plane failed with high crack density and short pullout length while all 0° fibers were intact. The stepwise matrix fracturing in interlaminar shear was attributed to crack deflection and debonding of the interface between matrix layers. The high crack density and short pullout length of the 90° fibers in in-plane shear failure was attributed to a strong fiber-matrix interface. Overall, it was concluded that strength of the MCMC was greatly dependent on temperature, with a noted change in the nature of this dependence occurring at the preparation temperature of the composite [18].

III. Material and Test Specimen

3.1 Materials

Four different material systems were studied in this research effort. All are non-oxide composites that rely on a dense matrix for strength, stiffness, and oxidation protection. Fracture toughness is imparted through weak fiber-matrix interfaces that allow fiber-matrix debonding and fiber pullout to occur. Two of the CMCs were manufactured by ATK COI Ceramics, Inc. (COIC), San Diego, California, using polymer infiltration and pyrolosis (PIP). The remaining two CMCs were manufactured by Hyper-Therm High-Temperature Composites (HTC), Inc., Huntington Beach, California, through chemical vapor infiltration (CVI). COIC manufactured the two PIP-derived CMCs: SiC/SiNC (Hi-Nicalon™/SiNC – trade name S200H); and C/SiC (HexTow® IM7/SiC – trade name S400). Hyper-Therm HTC manufactured the two CVI-derived CMCs: C/SiC-B_4C (T300/HYPR-SiC™); and SiC/SiC-B_4C (Hi-Nicalon™/HYPR-SiC™). All four CMCs are summarized in Table 1 and are described in further detail in the following sections.

Table 1: Summary of CMCs

Trade Name	S200H (SiC/SiNC)	S400 (C/SiC)	HYPR-SiC (C/SiC)	HYPR-SiC (SiC/SiC)
Manufacturer	COIC, Inc.	COIC, Inc.	Hyper-Therm HTC	Hyper-Therm HTC
Processing	PIP	PIP	CVI	CVI
Fiber	Hi-Nicalon™ Si-C Low O Fiber	IM7 PAN based C	T300-1K C	Hi-Nicalon™ Si-C Low O Fiber
Fiber Coating	BN + Si_3N_4	BN +Si_3N_4	Pyrolitic Carbon + B_4C	Pyrolitic Carbon + B_4C
Matrix	SiNC	SiC + oxidation inhibitors	SiC	SiC
Filler	Si_3N_4	SiC	B_4C	B_4C
Exterior Coating	none	SiC	HYPR-Coat 1300™ SiC-based glaze	none
# Plies/Layup	8 [0/90]2S	8 [0]	24 [0/90]	9 [0/90]
Weave	8HSW	5HSW	Plain	5HSW

3.1.1 SiC/SiNC (Hi-Nicalon™/SiNC)

The COIC S200H composite is an amorphous silicon nitrocarbide matrix reinforced by Hi-Nicalon™ silicon carbide fibers. Hi-Nicalon is the trade name for the SiC fiber manufactured by Nippon Carbon Co., Ltd., Tokyo, Japan. The Hi- designation indicates significantly reduced oxygen content from the original Nicalon SiC fiber, resulting in increased fiber density, modulus, expansion, and conductivity [19]. Table 2 summarizes the fiber properties [19].

Table 2: Summary of Hi-Nicalon™ fiber properties

Elemental Composition (% by weight)	Fiber Diameter (μm)	Fibers Per Tow	Density (g/cm^3)	R.T. Tensile Strength (MPa)	R.T. Tensile Modulus (GPa)
62 Si + 37 C + 0.5 O	14	500	2.74	3,000	220

The Hi-Nicalon™ fibers are woven into an 8HSW fabric and are coated with BN+Si_3N_4 using chemical vapor infiltration. The fiber coating promotes fiber-matrix debonding, thus providing the CMC with increased fracture toughness. Once coated, the fabrics are infiltrated with a preceramic polymer resin with added submicron SiC and Si_3N_4 filler constituents, then run through rollers to form a prepreg. The prepreg sheets are cut to size then green-formed using a vacuum bag in an autoclave. Once consolidated, the green-formed ceramics are pyrolyzed and densified using the PIP process. The PIP process involves submerging the green-formed ceramic in a preceramic SiNC polymer bath under vacuum to fill shrinkage cracks or voids, then firing at a temperature consistent with use temperature, converting the preceramic polymer into a ceramic SiNC matrix. This PIP process is repeated incrementally to reduce matrix porosity until desired density is achieved [20]. A schematic of the PIP process is shown in Figure 7.

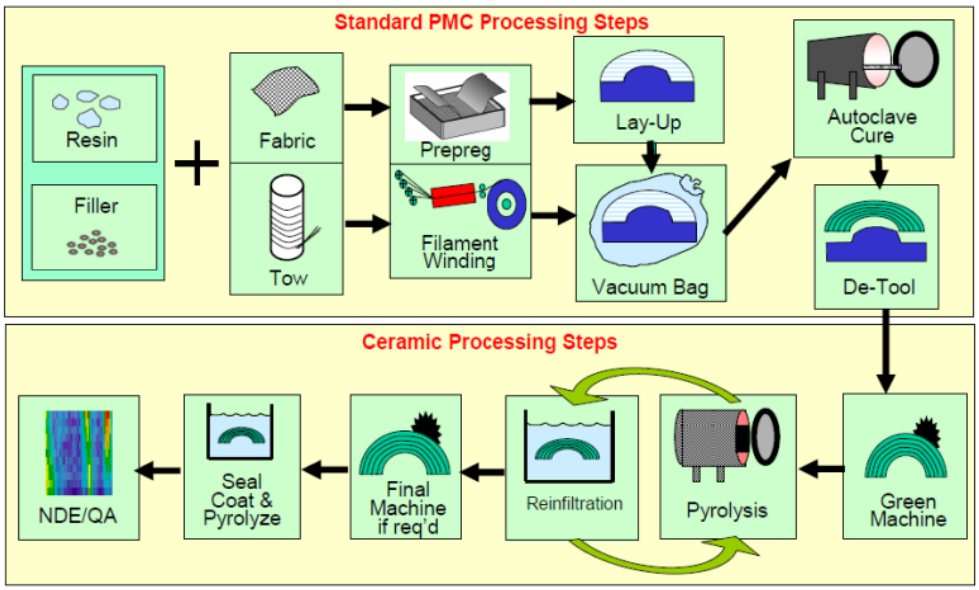

Figure 7: Non-oxide PIP CMC fabrication process [21]

The SiC/SiNC composite was supplied in a form of ~2.25-mm thick panels comprised of 8 0°/90° 8HSW woven plies symmetric about the composite structural mid-plane. Table 3 lists the physical properties of the Hi-Nicalon™/SiNC composite as reported by COIC [22].

Table 3: Reported physical properties of Hi-Nicalon™/SiNC composite

Thickness (mm)	Density (g/cm^3)	Fiber Volume (%)	Matrix Volume (%)	Open Porosity (%)
2.25	2.37	Not reported	Not reported	1.19

3.1.2 C/SiC (HexTow® IM7/SiC)

The COIC S400 CMC is a crystalline silicon carbide matrix reinforced by HexTow® IM7 carbon fibers. HexTow® IM7 is the trade name for the continuous, intermediate modulus, polyacrylonitrile (PAN) based carbon fiber manufactured

by Hexcel Corporation, Stamford, Connecticut. Table 4 summarizes the fiber properties [23].

Table 4: Summary of HexTow® IM7 fiber properties

Elemental Composition (% by weight)	Fiber Diameter (μm)	Fibers Per Tow	Density (g/cm^3)	R.T. Tensile Strength (MPa)	R.T. Tensile Modulus (GPa)
95 C	5.2	6,000	1.78	5,515	276

The HexTow® fibers are woven into a 5HSW fabric and are coated with $BN+Si_3N_4$ using chemical vapor infiltration. The fiber coating promotes fiber-matrix debonding, thus providing the CMC with increased fracture toughness. Once fabrics are coated, the C/SiC CMC is processed via PIP in the same manner as the SiC/SiC CMC described above, with the following variations: 1.) the primary matrix includes only SiC; 2.) the PIP-derived matrix includes a boron-containing oxidation inhibitor; 3.) an additional, higher-temperature pyrolysis converts the amorphous SiC matrix to a crystalline SiC matrix after the final PIP cycle; and 4.) the CMC exterior is seal-coated with PIP-derived SiC.

The C/SiC composite was supplied in a form of ~2.82-mm thick panels comprised of 8 0° 5HSW woven plies. Table 5 lists the physical properties of the HexTow® IM7/SiC composite as reported by COIC [22].

Table 5: Reported physical properties of HexTow® IM7/SiC composite

Thickness (mm)	Density (g/cm^3)	Fiber Volume (%)	Matrix Volume (%)	Open Porosity (%)
2.82	2.1	45.7	49.4	4.9

3.1.3 C/SiC-B_4C (T300/HYPR-SiC™)

The Hyper-Therm HTC T300/HYPR-SiC™ composite is a layered silicon carbide and boron carbide matrix (trade name HYPR-SiC™) reinforced by T300-1K fibers. T300-1K is the trade name for the baseline, 1,000 filament/tow, PAN-based carbon fiber manufactured by Toray Carbon Fibers America, Santa Ana, California. Table 6 summarizes the fiber properties [24, 25, 26].

Table 6: Summary of T300-1K fiber properties

Elemental Composition (% by weight)	Fiber Diameter (μm)	Fibers Per Tow	Density (g/cm^3)	R.T. Tensile Strength (MPa)	R.T. Tensile Modulus (GPa)
93 C + <50ppm Na+K	7	1,000	1.76	3,530	230

The T300 fibers are woven into a plain weave (PW) fabric and are coated with pyrolitic carbon and boron carbide via chemical vapor infiltration. This fiber-matrix interface provides improved CMC fracture toughness by promoting fiber-matrix debonding. The coating is applied to the cut and layed-up fabrics as they are held together and hung with graphite tooling in a CVI reactor. Once coated, the preform is placed in a different CVI reactor wherein the layered, multi-constituent HYPR-SiC™ matrix is deposited and densified. In both fiber-coating and matrix deposition, the CVI process entails introduction of reactant gases onto the heated fabric or preform through either diffusion or forced convection. The HYPR-SiC™ matrix requires multiple CVI runs, alternating the reactive gases with each run to accomplish the layered SiC-B_4C matrix. When desired CMC density was achieved, HYPR-Coat 1300™ glaze, a SiC-based exterior coating, was applied for overall oxidation protection. The utilization of boron carbide in the

matrix and the fiber-matrix interface, and the application of an exterior coating provide critical oxidation inhibiting properties for the CMC [11]. An increased ability to resist oxidation is necessitated by the inherently porous CVI matrix and thus increased vulnerability to oxidation of the carbon fibers and non-oxide matrix.

The C/SiC-B_4C composite was supplied in a form of ~3.01-mm thick panels comprised of 24 0°/90° PW woven plies. Table 7 lists the physical properties of the T300/HYPR-SiC™ composite.

Table 7: Reported physical properties of T300/HYPR-SiC™ composite

Thickness (mm)	Density (g/cm^3)	Fiber Volume (%)	Matrix Volume Ratio (SiC:B_4C)	Ply Thickness (mm)
3.01	Not reported	45.8	5:1	0.117

3.1.4 SiC/SiC-B_4C (Hi-Nicalon™/HYPR-SiC™)

The Hyper-Therm HTC Hi-Nicalon™/HYPR-SiC™ composite is a layered silicon carbide and boron carbide matrix reinforced by Hi-Nicalon™ silicon carbide fibers – fibers are described in Section 3.1.1 (p.23) and summarized in Table 2 (p. 23). The Hi-Nicalon™ fibers are woven into a 5HSW fabric and are coated with pyrolitic carbon and boron carbide via chemical vapor infiltration. Like with the T300/HYPR-SiC™ and other non-oxide CMCs, the fiber-matrix interface provides improved CMC fracture toughness by promoting fiber-matrix debonding. The fiber coating is applied through the same CVI process as described for the T300/HYPR-SiC™ material, and is followed by again the same CVI process for

deposition and densification of the multi-constituent, layered SiC-B_4C matrix until desired density is achieved. Once again, the boron carbide utilized in the matrix and the fiber-matrix interface of this CMC provides critical oxidation inhibiting properties that are necessitated by the inherently porous and oxidation-susceptible non-oxide CVI matrix.

The SiC/SiC-B_4C composite was supplied in a form of ~2.79-mm thick panels comprised of 9 0°/90° 5HSW woven plies. Table 8 lists the physical properties of the Hi-Nicalon™/HYPR-SiC™ composite.

Table 8: Reported physical properties of Hi-Nicalon™/HYPR-SiC™ composite

Thickness (mm)	Density (g/cm^3)	Fiber Volume (%)	Matrix Volume Ratio (SiC:B_4C)	Ply Thickness (mm)
2.79	Not reported	34.1	5:1	0.310

3.2 Test Specimen Geometry

The CMCs for this research were provided by the Structural Materials Division, Composites Branch, Air Force Research Lab (AFRL) Materials & Manufacturing Directorate at Wright Patterson Air Force Base, Ohio. All materials were provided in a form of 4 inch x 4 inch square plates. Six plates of each material system were used for the purposes of this research. The COIC CMCs were fabricated in a form of 12 inch x 12 inch square panels, which were then cut into nine 4 inch x 4 inch square plates. All six plates of each COIC CMC were cut from the same mother panel of the respective material system. Definitive

information regarding the same was not provided by the manufacturer for the Hyper-Therm CMCs. Five of six panels per material system were subjected to various time-temperature histories, then all panels were machined into test specimens. Using diamond grinding under water, each panel was cut into six dogbone-shaped test specimens according to the cutting plan in Figure 8.

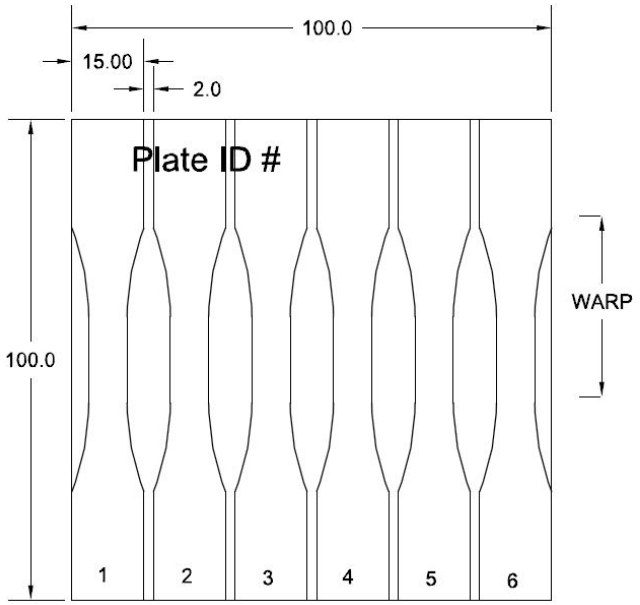

Figure 8: Cutting plan. All dimensions in mm.

Specimens with variable cross section are typically used for determination of tensile strength and elastic modulus. Especially in the case of high-strength composites, specimens with a variable cross section provide a more uniform state of stress within the gage section and thus more consistent results than those with constant cross section [27]. The reduced cross section area of the gage section as compared to the grip sections causes the maximum stress, and consequently specimen failure, to occur within the gage section. In determining dogbone geometry, the most critical design feature is the radius for tapering from

the wider tab/grip area to the narrower gage section. Undesirable stress concentrations occur in this area of varying cross section, so determining a taper radius that minimizes these stress concentrations is of primary concern. Finite element analysis supports selection of a 50 mm radius. Because specimen length for this research was pre-determined by the size of delivered panels, the gage and grip section lengths were fed by required radius and overall length constraints, with additional consideration for extensometer size and grip area. The dogbone-shaped specimen geometry selected for this research is indicated in Figure 9.

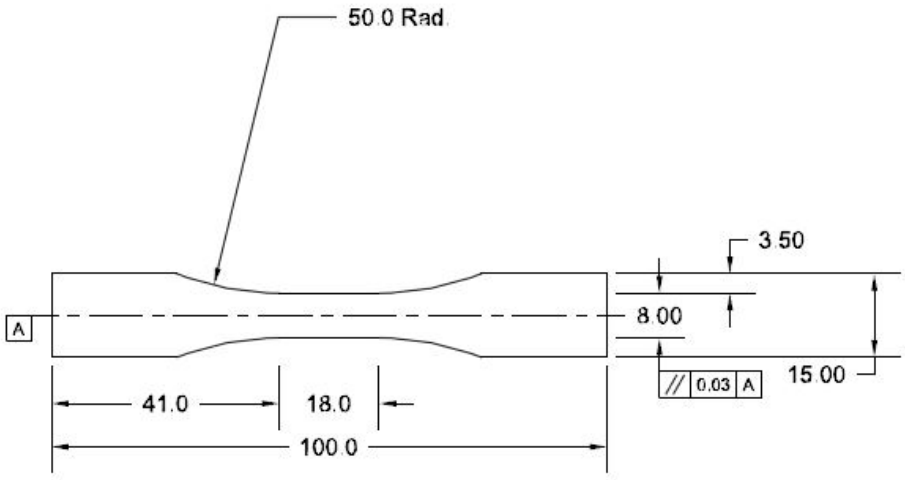

Figure 9: Dogbone specimen geometry. All dimensions in mm.

IV. Experimental Procedures

4.1 Mechanical Testing Equipment

Uniaxial, monotonic tensile tests were performed using an MTS Systems Corporation model 810 Material Test System servohydraulic load frame equipped with: 15 kN (3.3 kip) capacity MTS model 661.19E-03 force transducer; 25 kN (5.5 kip) capacity MTS model 609.02A-01 alignment fixture; and 25 kN (5.5 kip) dynamic load capacity MTS model 647.02B hydraulic wedge grips surfaced with Surfalloy grip texture to prevent slippage. The MTS FlexTest 40 digital controller with MTS FlexTest 40 Station Manager and MultiPurpose TestWare (MPT) application was used for input signal generation and data collection. Strain measurements were taken using an MTS model 632.13E-20 axial extensometer with standard elastic attachment kit. The testing station is pictured in Figure 10.

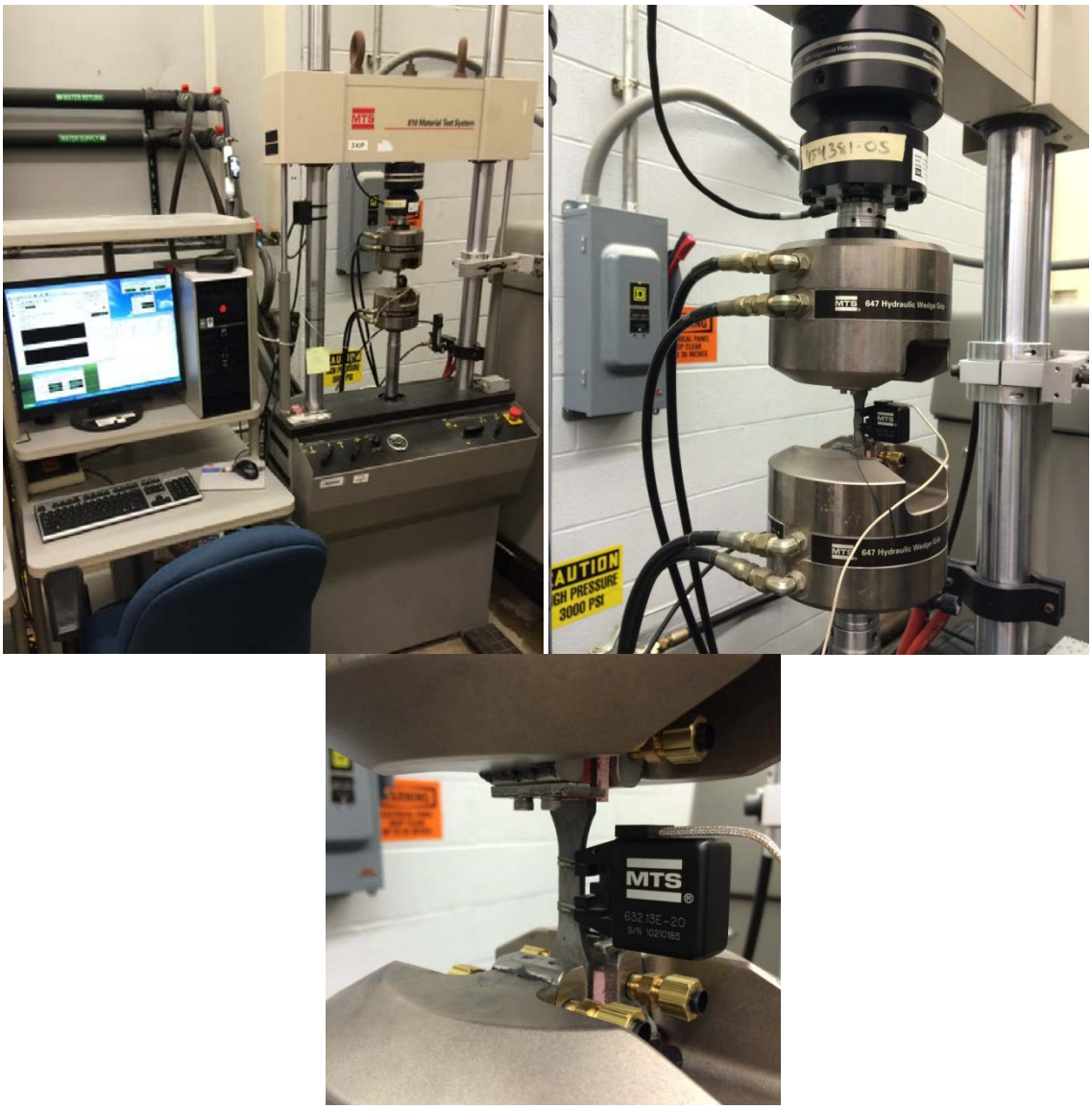

Figure 10: Testing station (top-left); load frame with alignment fixture, force transducer, hydraulic wedge grips, and loaded specimen (top-right); loaded specimen with elastically attached axial extensometer (bottom)

4.2 Test Preparation

Every plate was weighed with an Ohaus Pioneer Precision Balance model PA3102, 3100g x 0.01g digital scale. Weights were measured and recorded before and after being dried in a Jeio Tech model OV-11 Lab Companion vacuum for 24 hours at 120°C. To prevent potential cross-contamination of the

boron-containing HYPR-SiC™ matrix material with the SiC and SiNC matrix composites, all plates of the two COIC CMCs were dried separately from the Hyper-Therm CMCs. Once dried, the length, width, and thickness of each plate was measured using a Mitutoyo 0.01 mm resolution digital caliper and recorded. The dry density of each panel was calculated using the recorded weight and dimension measurements. A detailed description of dimension measurement and density calculation procedures with accompanying data is included in Appendix A.

4.2.1 Thermal Exposure

After density data were recorded, thermal exposures were begun. Plates of all four CMCs were subjected to various prescribed time-temperature histories. A Barnstead International, ThermoLyne model 46200 high performance 1700°C furnace was utilized for thermal exposures. The furnace was controlled externally by computer and programmed to heat 10°C/minute until reaching prescribed temperature. Exposure temperature and hold time for each plate is indicated in Table 9. Following the prescribed exposure time at temperature, the furnace was cooled at 10°C/minute or slower until furnace temperature reached approximately 60°C. All heat treatments were accomplished in air. Like with the drying procedure, COIC plates were exposed separately from Hyper-Therm plates to avoid material cross-contamination. Upon exposure completion, plates were removed from the cooled furnace for additional cooling. Once cool to touch,

plates were weighed and measured as before. Weights and dimensions were recorded and are shown in Appendix A.

Table 9: Prescribed Time-Temperature Exposures

Material	*Panel*	*Plate*	*Temperature (°C)*	*Time (h)*
Hi-Nicalon™/SiNC	172151-1	11101	1300	10
		11103	1300	20
		11104	1300	40
		11105	1300	100
		11106	1200	100
C/SiC	172799-1	12011	1300	10
		12019	1300	20
		12018	1300	40
		12015	1300	100
		12016	1200	100
C/HYPR-SiC™		11117	1300	10
		11124	1300	20
		11125	1300	40
		11121	1300	100
		11122	1200	100
Hi-Nicalon™/HYPR-SiC™		11133	1400	10
		11135	1400	20
		11136	1400	40
		11137	1400	100
		11139	1300	100

All plates exhibited visible physical changes as a result of heat treatment. Both COIC materials – Hi-Nicalon™/SiNC and C/SiC – exhibited discoloration characterized by a general, nearly uniform whitening of the plate surfaces (Figure 11 and Figure 12). All Hyper-Therm C/HYPR-SiC™ plates exhibited surface blistering ranging from mild to severe in nature (Figure 13). The blistering appeared to affect only the HYPR-Coat 1300™ glaze on every exposed plate. The Hyper-Therm Hi-Nicalon™/HYPR-SiC™ plates exhibited discoloration characterized by a change from matte to glossy black surface color with non-

uniform patches of greenish-blue (Figure 14). In addition to the examples below, images of all virgin and heat-treated plates are included in Appendix B.

Figure 11: Example of Hi-Nicalon™/SiNC plate discoloration due to heat treatment – virgin plate (left); exposed plate (right).

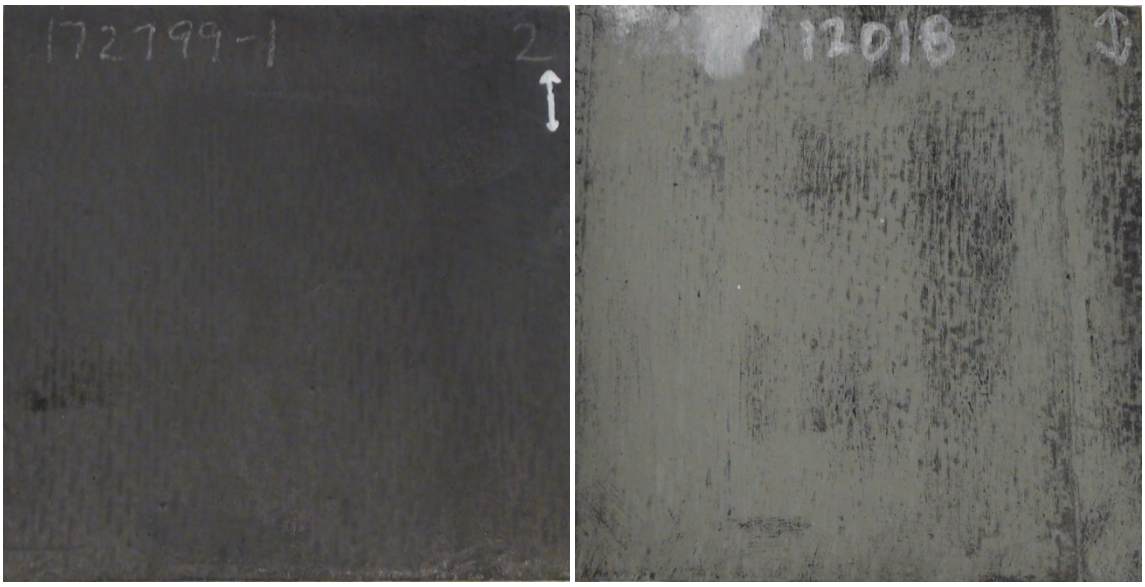

Figure 12: Example of HexTow® IM7/SiC plate discoloration due to heat treatment – virgin plate (left); exposed plate (right).

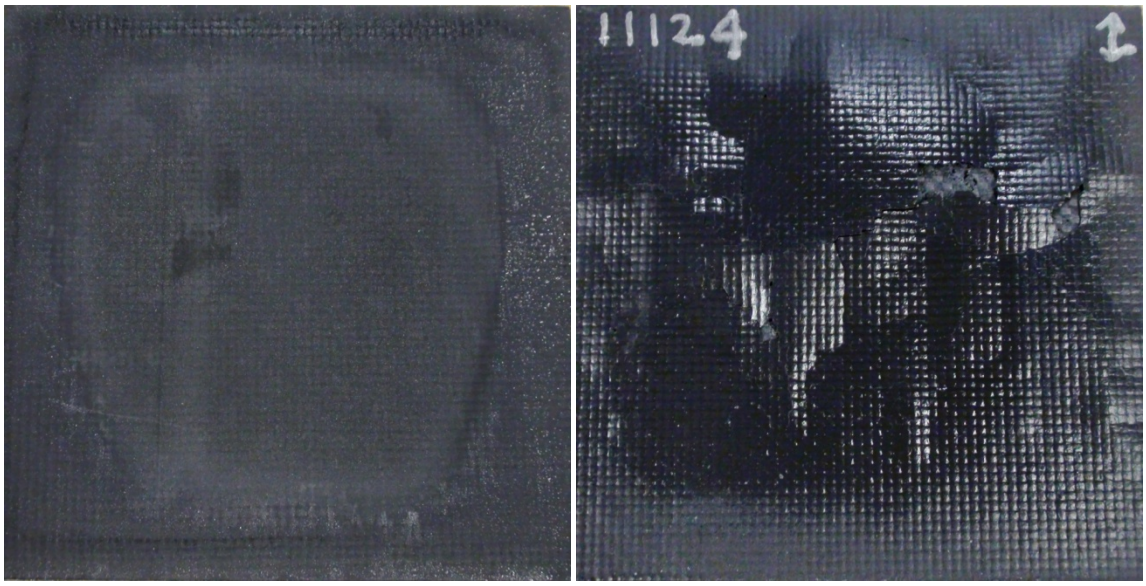

Figure 13: Example of T300/HYPR-SiC™ surface blistering and glossy appearance due to heat treatment – virgin plate (left); exposed plate (right).

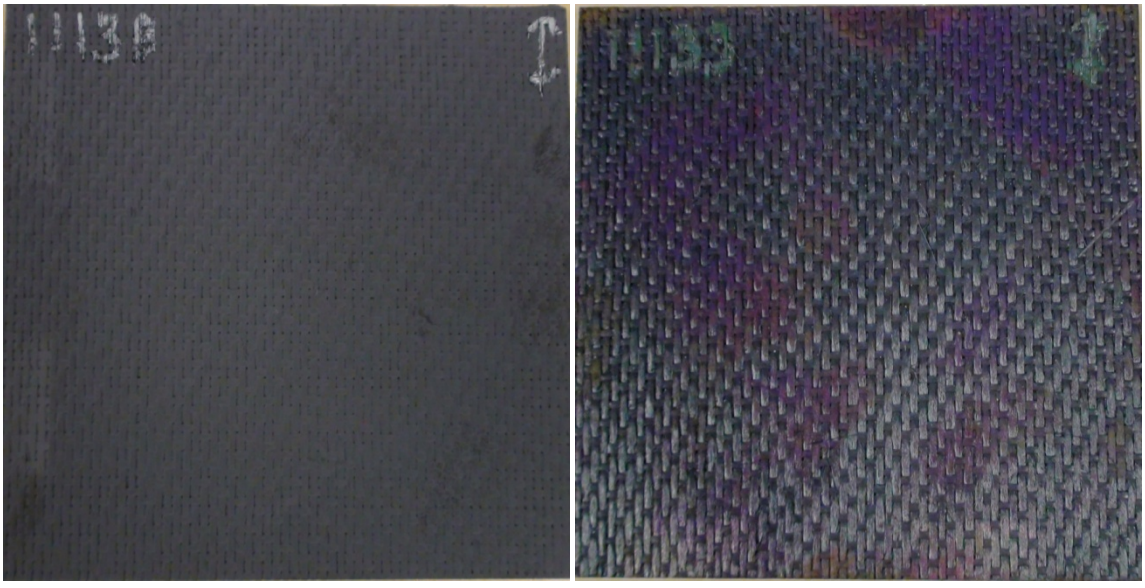

Figure 14: Example of Hi-Nicalon™/HYPR-SiC™ plate discoloration due to heat treatment – virgin plate (left); exposed plate (right).

4.2.2 Specimen Preparation

Following heat treatment, every plate was machined into six dog bone shaped specimens as described and indicated in Section 3.2, Figure 8 and Figure 9. Optical microscopy was performed on the machined specimens in order to identify and document any defects. Examination of Hi-Nicalon™/SiNC specimens revealed areas of matrix porosity and slight fraying along specimen edges (Figure 15). Examination of HexTow® IM7/SiC specimens revealed matrix porosity and minor spalling along specimen edges (Figure 16). Examination of T300/HYPR-SiC™ specimens revealed randomly distributed voids, debonding, delamination, and chipped-off glaze from blisters developed during heat treatment (Figure 17). Examination of Hi-Nicalon™/HYPR-SiC™ specimens revealed matrix voids and fraying along specimen edges (Figure 18).

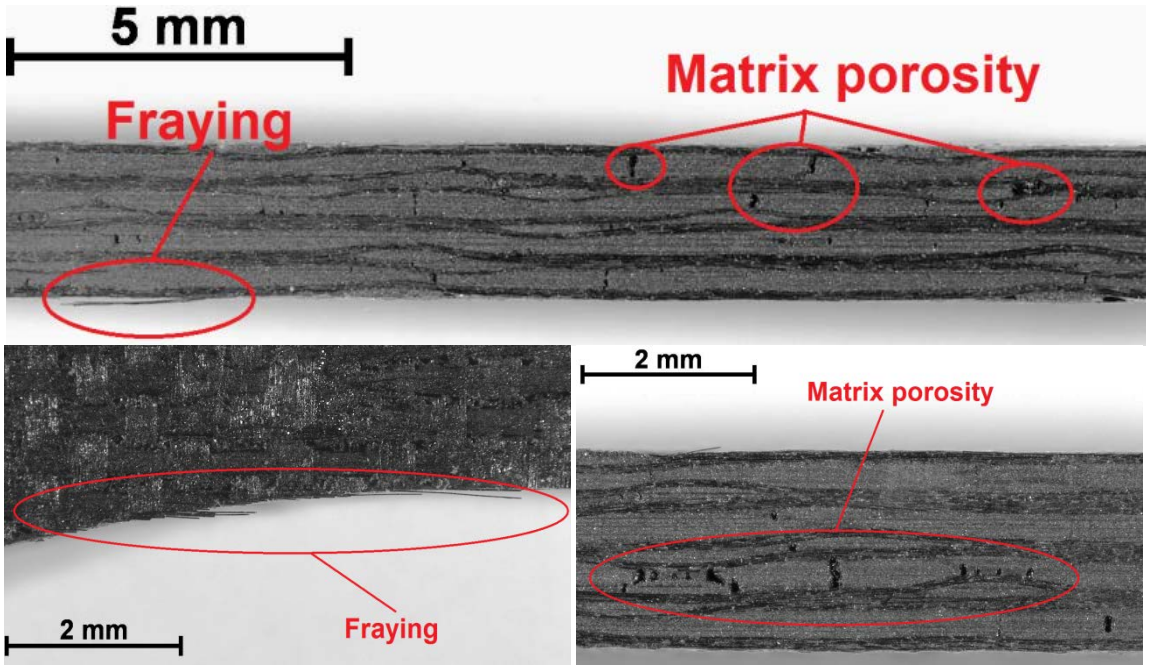

Figure 15: Pre-test optical micrographs of Hi-Nicalon™/SiNC test specimens showing fraying and matrix porosity

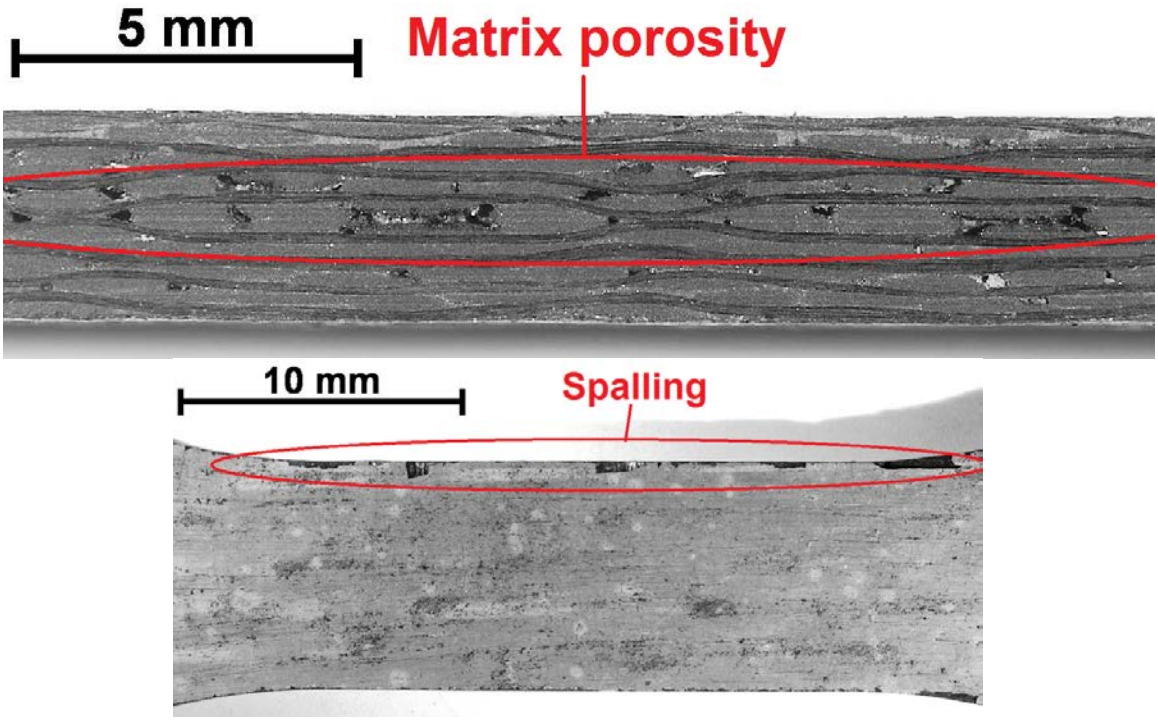

Figure 16: Pre-test optical micrographs of HexTow® IM7/SiC test specimens showing matrix porosity and spalling

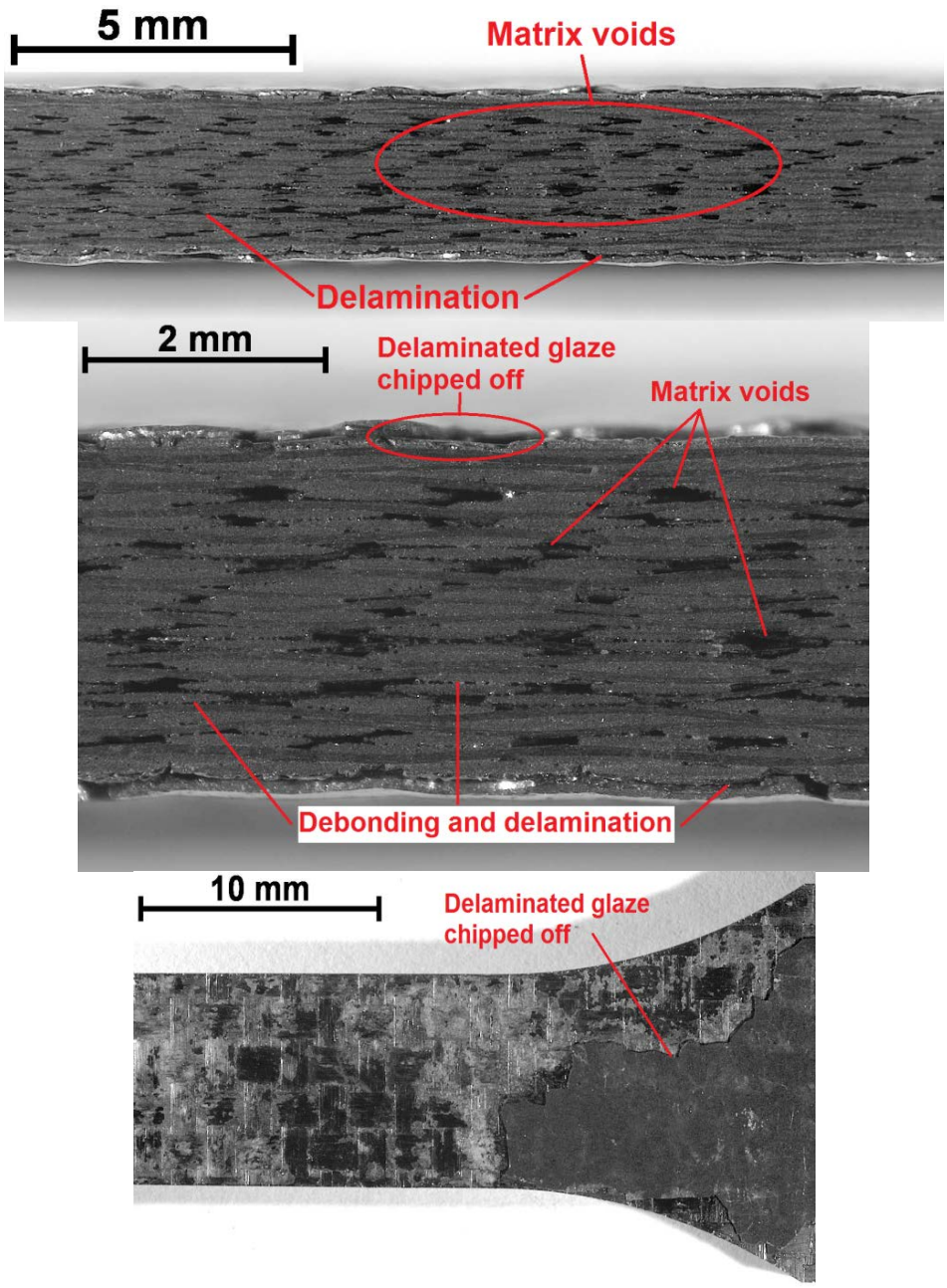

Figure 17: Pre-test optical micrographs of T300/HYPR-SiC™ test specimens showing matrix voids, debonding, and delamination

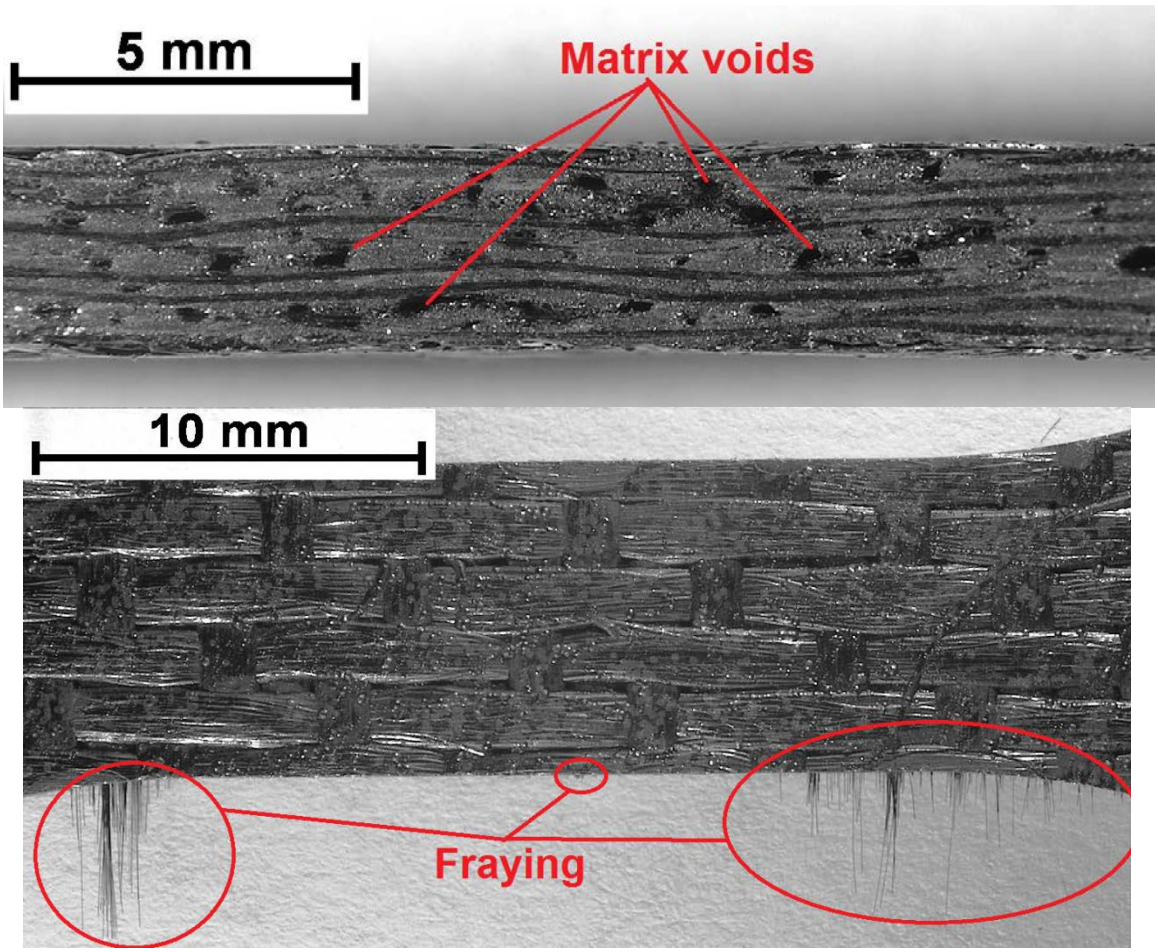

Figure 18: Pre-test optical micrographs of Hi-Nicalon™/HYPR-SiC™ test specimens showing matrix voids and fraying

It was noted that for all material systems, both virgin and heat-treated specimens exhibited the characteristics described above, with the exception of fraying in the Hi-Nicalon™/HYPR-SiC™ composite. Virgin specimens of Hi-Nicalon™/HYPR-SiC™ did not exhibit fraying. Further, for all CMCs, the degree to which defects occurred generally increased from virgin to exposed materials.

After microscopy, every test specimen was fitted with 0.25-inch thick fiberglass tabs to protect the specimen from the rough Surfalloy grips and to provide a more uniform grip pressure application. The tabs were attached to the

grip section using M-Bond 200 cyanoacrylate adhesive. Specimen identification and orientation were indicated on the tabs as can be seen in Figure 19.

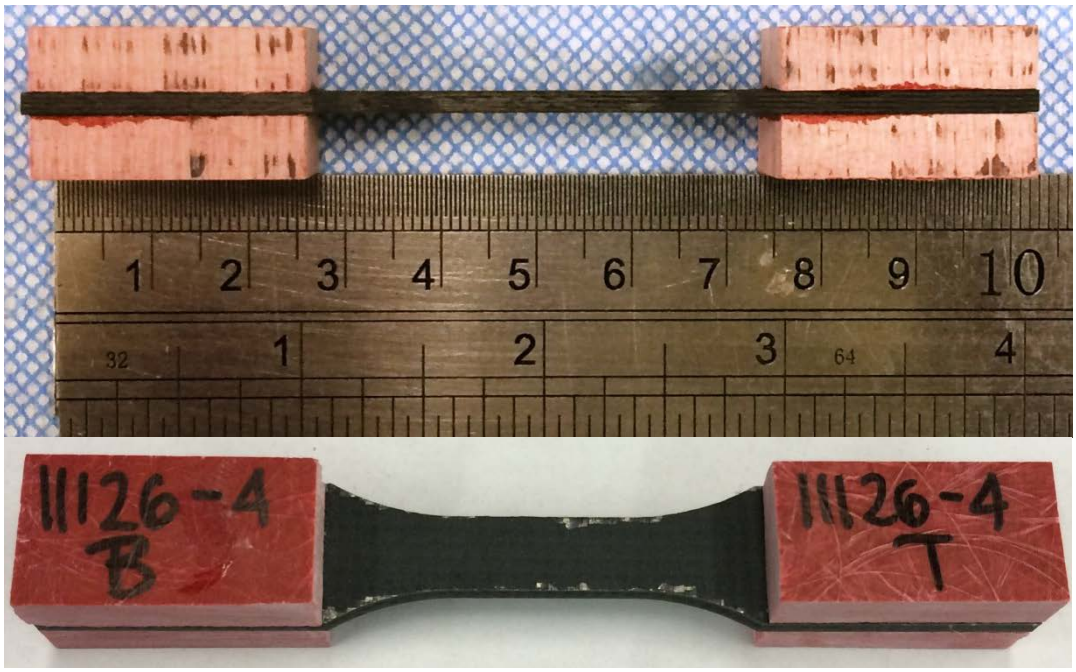

Figure 19: Test-ready specimen – edge view (top) and face-up (bottom)

Before being tested, gage section width and thickness were measured using a Mitutoyo 0.01 mm resolution digital caliper and recorded. Gage cross section area was then determined for use in stress calculations. The resulting specimen dimensions are reported in Appendix D.

4.3 Mechanical Testing Procedure

Prior to beginning a series of tests, the servo-hydraulic MTS system was warmed up. Warm up was accomplished by running a sine wave function in displacement control with 1.0 Hz frequency and 0.25-inch amplitude for at least 15 minutes. Additionally, the machine was subjected to a square wave

displacement-controlled procedure with 0.25-inch amplitude and progressive increase from 1.0 to 5.0 Hz frequency, then holding at 5.0 Hz for approximately 10 minutes. The sine waveform procedure served to warm the hydraulic fluid while the square waveform served to accomplish cleaning of the servo valve through the imparted aggressive opening and closing motion.

After the warm-up sequence, the MultiPurpose TestWare (MPT) application was opened within the MTS FlexTest 40 Station Manager. The test procedure was composed and selected for use. A uniaxial, monotonic tension to failure procedure was utilized in all tests conducted for this research. The procedure was run in displacement control at a constant rate of 0.05 mm/s and was manually terminated upon specimen failure. Time, displacement command, displacement, strain, and force were recorded at approximately 20.0 Hz.

Following procedure selection, the specimen was loaded into the hydraulic grips, ensuring specimen alignment with the test axis. Once aligned, the specimen was held in place, the top grip was closed while in displacement control mode, and the load cell auto-zeroed. Control mode was then switched from displacement to force control. Next, the actuator was raised to the desired gripping location and the bottom grip was closed while simultaneously zeroing force control. Grip pressure ranged from 5.0 to 7.5 MPa for all tests. The variation in grip pressure is a result of: 1.) grip replacement after first 25 specimens tested, and 2.) evidence of grip slippage during the first Hi-Nicalon™/HYPR-SiC™ tests, which necessitated a gripping pressure increase.

After the specimen was gripped in place, the extensometer was mounted on the edge of specimen gage section using elastics. The specimen edge surface provided enough roughness and the elastics enough tension for extensometer knife edges to be sufficiently held in place without surface treatment or notching. Once the extensometer was mounted, the locking pin was removed and strain reading was tared to ensure zero initial strain measurement.

Manual control mode was relinquished and the test procedure was initiated. The procedure was run and manually terminated upon specimen failure. Upon specimen failure the extensometer was detached, actuator lowered, and the broken specimen was removed. All tests were performed at room temperature in laboratory air.

4.4 Microstructural Characterization

After all tests were complete, data were processed, and strength and elastic modulus values were calculated for each specimen. The strength and modulus values, along with visual observation of fractured specimens, were used to select a representative sample of specimens for microstructural analysis. Four time-temperature exposure histories for each material are represented in the selection. The sample selection for each of the four material systems includes the four specimens subjected to the following exposures: 1.) the as-received virgin material; 2.) exposure at which the first significant change in strength occurred; 3.) maximum exposure duration at 100°C over operating temperature;

and 4.) exposure at operating temperature. The specimens selected are indicated in Table 10.

Table 10: Specimen selection for microscopy

Material	*Exposure Time (h)*	*Temperature (°C)*	*Plate*	*Specimen*
Hi-Nicalon™/SiNC	0	N/A	11107	3
	10	1300	11101	6
	100	1300	11105	6
	100	1200	11106	4
C/SiC	0	N/A	12012	6
	40	1300	12018	2
	100	1300	12015	3
	100	1200	12016	3
C/HYPR-SiC™	0	N/A	11126	4
	40	1300	11125	4
	100	1300	11121	5
	100	1200	11122	5
Hi-Nicalon™/ HYPR-SiC™	0	N/A	11138	3
	10	1400	11133	2
	100	1400	11137	6
	100	1300	11139	1

Microstructural analysis was conducted on selected fractured specimens using both an optical microscope and scanning electron microscope (SEM). Resulting micrographs were analyzed for characterization of the dominant damage mechanisms and identification of microstructural changes caused by prior heat treatment.

4.4.1 Optical Microscope

Optical microscopy was conducted first. Top and bottom fracture surfaces were examined and imaged in four orientations: 1.) face up; 2.) face down; 3.) left edge up; 4.) right edge up. A Zeiss Discovery.V12 stereo optical microscope with

Zeiss PlanApo S 0.63x FWD 81-mm lens and Zeiss AxioCam HRc digital camera was used to image the specimens (Figure 20). Image processing was carried out with AxioVision 4.8 software. Optical images of all fractured specimens can be seen in Appendices F – I.

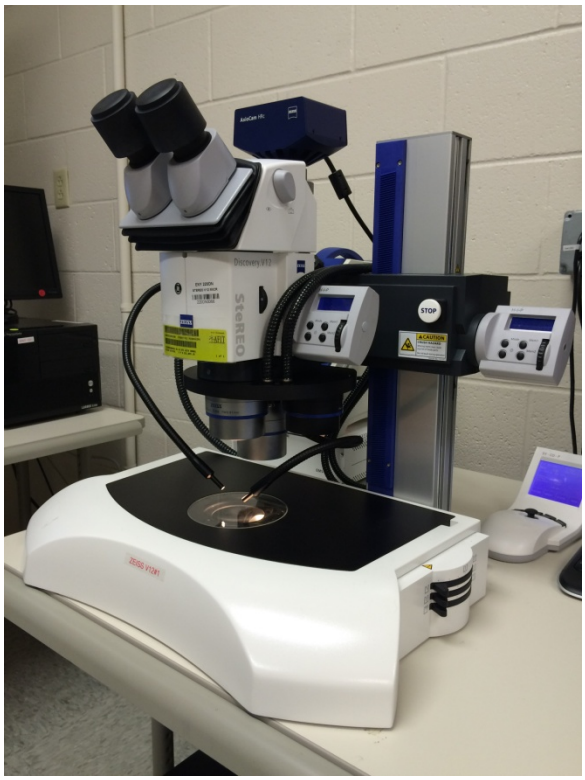

Figure 20: Zeiss Discovery V.12 stereo optical microscope

4.4.2 Scanning Electron Microscope

Next, higher magnification imaging was conducted using an FEI Quanta 450 scanning electron microscope (SEM), shown in Figure 21. Either the top or bottom fracture surface of each selected specimen was examined under the SEM. The specimens were cut perpendicular to loading direction approximately 7 mm below the fracture surface using an MTI Corporation CNC-400 precision cutting saw with IsoMet 20HC wafering blade. To avoid specimen contamination,

no lubricant was used during cutting. The specimens did not require carbon coating for SEM microscopy and were mounted onto an SEM specimen stage using carbon tape.

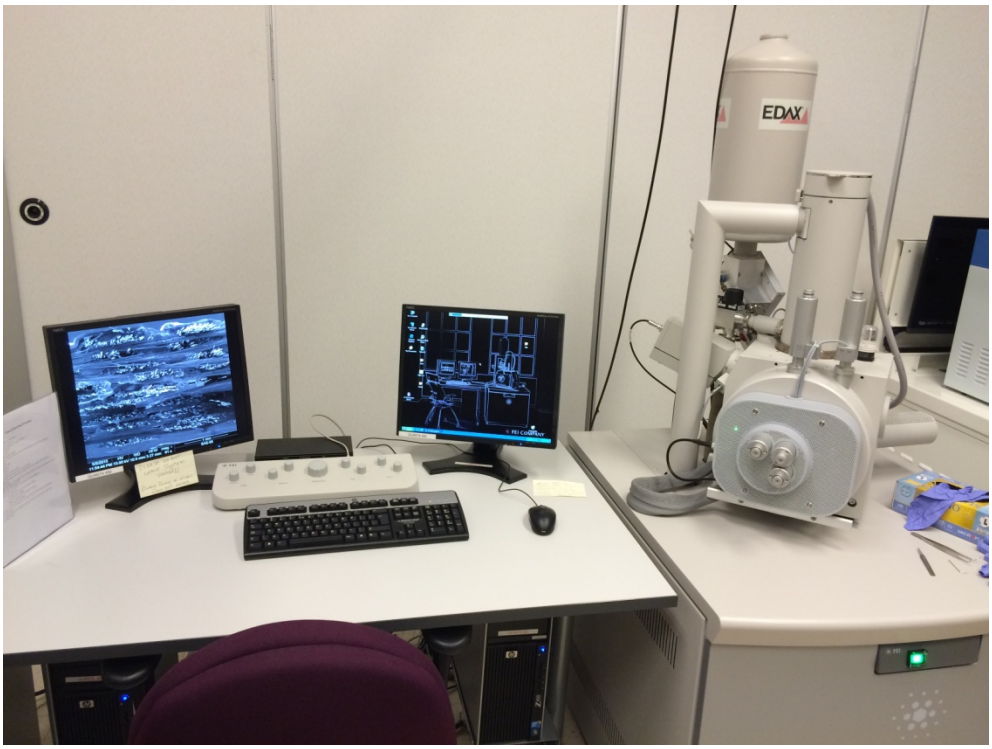

Figure 21: FEI Quanta 450 scanning electron microscope

V. Results and Discussion

5.1 Effect of Heat Treatment on Composite Density

Composite density for all plates was calculated before and after prescribed heat treatments. To ensure measurement of a true dry density, all plates were vacuum-dried prior to initial density measurement. Density was then measured again following heat treatment and allowing composite plates to cool. Percent change in density for all material systems is illustrated in Figure 22.

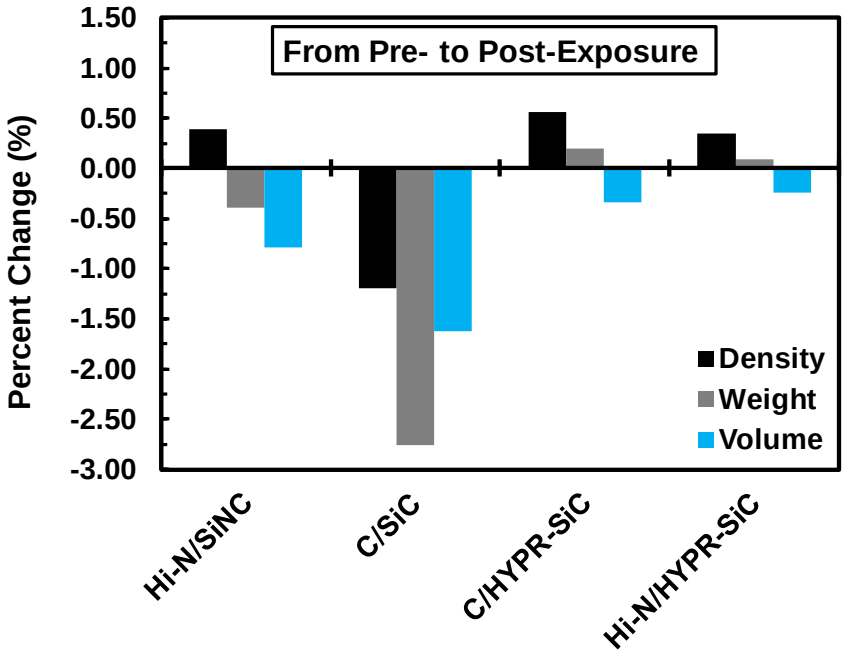

Figure 22: Percent change in composite plate density due to heat treatments for all materials are shown with relation to percent change in weight and volume.

With the exception of the C/SiC composite, all CMCs exhibited a slight increase in density from before to after heat treatment. As indicated by Figure 22, the density increase can be attributed in most part to a reduction in volume for the

three relevant CMCs. On the other hand, the C/SiC composite exhibited a decrease in density, which can be attributed to a significant decrease in weight. All values graphed in Figure 22 are the calculated averages of all five exposures for each material system and are shown in Table 11.

Table 11: Average density, weight, and volume of CMCs measured before and after heat treatment

	Average Density (g/mm^3)			*Average Weight (g)*			*Average Volume (mm^3)*		
Material	***Pre-exposure***	***Post-exposure***	***Percent Change***	***Pre-exposure***	***Post-exposure***	***Percent Change***	***Pre-exposure***	***Post-exposure***	***Percent Change***
Hi-N/SiNC	2.28E-03	2.29E-03	0.392	52.9	52.7	-0.397	2.32E+04	2.30E+04	-0.792
C/SiC	1.99E-03	1.97E-03	-1.195	61.4	59.7	-2.762	3.08E+04	3.03E+04	-1.622
C/HYPR-SiC	1.87E-03	1.88E-03	0.559	58.7	58.8	0.198	3.13E+04	3.12E+04	-0.339
Hi-N/HYPR-SiC	2.41E-03	2.42E-03	0.347	76.1	76.1	0.095	3.16E+04	3.15E+04	-0.247

5.2 Effect of Heat Treatment on Composite Tensile Properties

For purposes of establishing baseline tensile properties, the as-received, un-treated CMCs were tested in addition to the heat-treated CMCs. The four material systems studied in this effort have also been studied to a limited extent by the Air Force Research Laboratory (AFRL). As-received CMC ultimate tensile strength (UTS) and elastic modulus (E) determined through this research as well as those determined by AFRL are reported in Table 12 [28]. Results match reasonably well given consideration that CMCs tested between the two efforts were manufactured in different batches and will thus inherently have slight variances in properties. However, the high values of standard deviation and coefficient of variation (COV) must be noted and examined.

Table 12: Summary of tensile properties of un-treated CMCs as reported in this and prior research

Material	*AFRL UTS (MPa)*	*Report UTS (MPa)*	*Standard Deviation*	*COV (%)*	*AFRL Modulus (GPa)*	*Report Modulus (GPa)*	*Standard Deviation*	*COV (%)*
Hi-N/SiNC	531	546	10.6	1.97	147	133	9.90	7.07
C/SiC	345	284	43.1	13.7	94	98	2.83	2.95
C/HYPR-SiC™	433	326	75.7	19.9	135	98	26.2	22.5
Hi-N/HYPR-SiC™	390	396	4.24	1.08	233	252	13.4	5.54

The C/SiC UTS results show a standard deviation of 43.1 and COV of 13.7% between the two test programs. The standard deviation and COV for UTS of the six virgin C/SiC CMC specimens tested for this research are 11.4 and 4.02%, respectively. Between the two test programs, the C/HYPR-SiC™ UTS shows a standard deviation of 75.7 and COV of 19.9%; values of E have a standard deviation of 26.2 and COV of 22.5%. The standard deviation and COV for the six virgin C/HYPR-SiC™ CMC specimens tested for this research are 12.9 and 3.6% (for UTS), and 4.49 and 4.57% (for E), respectively. Standard deviation and COV values for tensile testing performed in the AFRL test program were not available. There is a clear disparity between results obtained in this research and the AFRL test program in the two cases discussed above. The standard deviation and COV for UTS and elastic modulus values obtained through this research indicate that although there is a disparity between the two test programs, the values obtained through this research are adequately precise. Further, CMCs for each test program were processed in different batches. Attribution to composite anomalies resulting from different processing batches is reasonable and sufficient explanation for the discrepancy in tensile properties of the C/SiC and C/HYPR-SiC™ CMCs tested in each program.

Stress-strain graphs were created for all tests conducted during this research. The complete set of graphs can be found in Appendix E. Further, stress-strain, ultimate tensile strength, elastic modulus, and strain at UTS data were composed in various ways to enable assessment of changes in tensile behavior among exposure times and between material systems. These results are presented and discussed in the following sections.

5.2.1 Effect of Heat Treatment on Tensile Properties of Hi-Nicalon™/SiNC (Hi-N/SiNC)

A representative sample of stress-strain curves for the Hi-Nicalon™/SiNC (Hi-N/SiNC) material system is shown in Figure 23. One as-received specimen as well as one specimen from each prescribed time-temperature history is represented in the chart. There is a noticeable decrease in UTS from the as-received to the heat-treated material. Among the heat-treated material there exists only slight variation of UTS. Additionally, prior heat treatment appears to have no significant effect on elastic modulus.

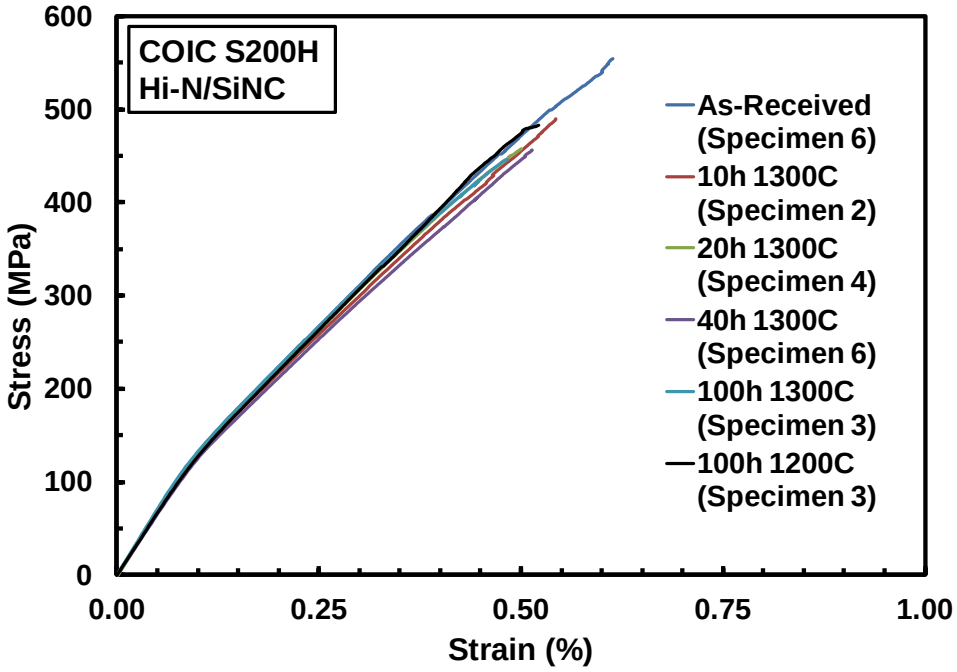

Figure 23: Representative stress-strain curves for Hi-Nicalon™/SiNC CMC including all prescribed heat treatments and as-received material

Figure 24 shows elastic modulus versus UTS for all tests of the Hi-Nicalon™/SiNC CMC. Figure 24 reinforces the noted drop in UTS from virgin to heat-treated material, and the nearly constant elastic modulus with varied time-temperature history.

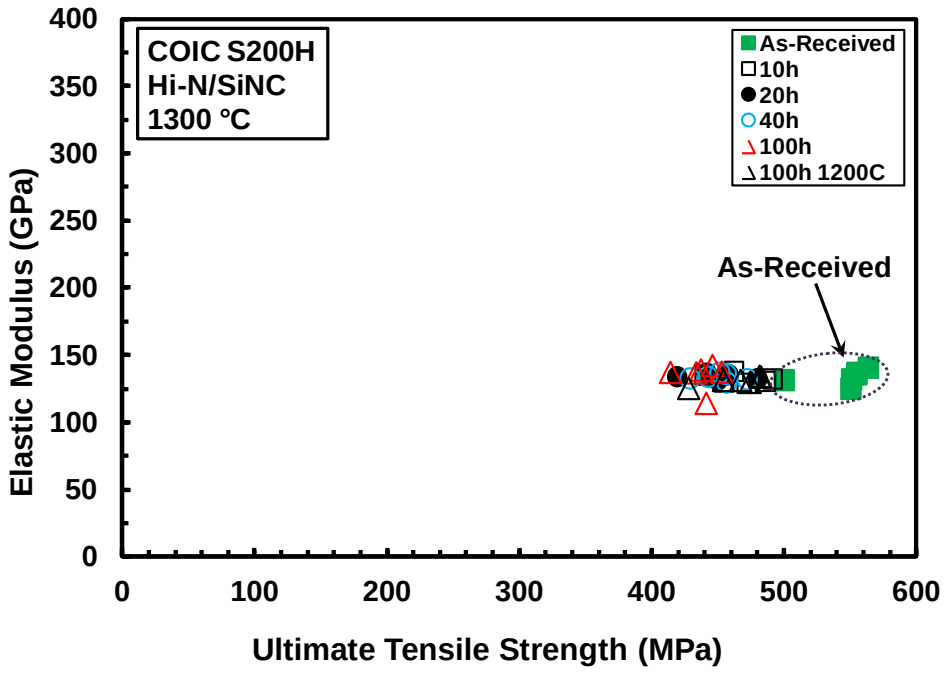

Figure 24: Elastic modulus versus UTS as a function of time-temperature history for Hi-Nicalon™/SiNC

Ultimate tensile strength, elastic modulus, and strain at UTS values for all Hi-Nicalon™/SiNC specimens exposed to different time-temperature histories are shown in Table 13, Table 14, and Table 15, respectively.

Table 13: Effect of prior heat treatment on tensile strength of Hi-Nicalon™/SiNC composite

Exposure Time (h)	*Exposure Temp (°C)*	*Individual Specimen UTS (MPa)*						*Average UTS (MPa)*	*Standard Deviation*	*COV (%)*
		1	*2*	*3*	*4*	*5*	*6*			
0	N/A	550	500	551	563	555	555	546	22.9	4.20
10	1300	462	491	486	454	440	471	467	19.5	4.17
20	1300	480	419	450	458	455	441	450	20.0	4.45
40	1300	472	451	442	456	429	456	451	14.6	3.24
100	1300	433	453	446	414	441	437	437	13.3	3.04
100	1200	474	481	482	467	428	454	464	20.8	4.48

Table 14: Effect of prior heat treatment on elastic modulus (E) of Hi-Nicalon™/SiNC composite

Exposure Time (h)	*Exposure Temp (°C)*	*Individual Specimen E (GPa)*						*Average E (GPa)*	*Standard Deviation*	*COV (%)*
		1	*2*	*3*	*4*	*5*	*6*			
0	N/A	125	131	132	140	137	135	133	5.45	4.09
10	1300	138	132	130	130	135	129	132	3.42	2.59
20	1300	132	134	131	135	135	136	134	1.93	1.44
40	1300	132	137	134	136	132	129	133	2.65	1.99
100	1300	137	137	142	137	114	139	134	10.1	7.56
100	1200	129	134	133	131	125	131	131	3.25	2.49

Table 15: Effect of prior heat treatment on strain at UTS of Hi-Nicalon™/SiNC composite

Exposure Time (h)	*Exposure Temp (°C)*	*Individual Specimen Strain at UTS (%)*						*Average Strain at UTS (%)*	*Standard Deviation*	*COV (%)*
		1	*2*	*3*	*4*	*5*	*6*			
0	N/A	0.713	0.547	0.738	0.615	0.563	0.614	0.632	0.078	12.4
10	1300	0.496	0.530	0.576	0.526	0.511	0.554	0.532	0.029	5.43
20	1300	0.585	0.461	0.493	0.512	0.432	0.561	0.507	0.058	11.5
40	1300	0.562	0.519	0.557	0.531	0.447	0.508	0.521	0.042	8.07
100	1300	0.435	0.518	0.483	0.493	0.508	0.473	0.485	0.029	6.05
100	1200	0.550	0.556	0.522	0.564	0.448	0.464	0.517	0.050	9.62

5.2.2 Effect of Prior Heat Treatment on Tensile Properties of HexTow®IM7/SiC (C/SiC)

A representative sample of stress-strain curves for the C/SiC material system is shown in Figure 25. This material system exhibits a noticeable effect on tensile properties due to prior exposure history. When subjected to exposure at 100°C above manufacturer recommended operating temperature (i.e. over-temp), the material tensile properties degrade with time exposed. There is a reduction in strength and modulus, and a mild increase in strain at UTS. Additionally, when

exposed for 100 hours to recommended operating temperature conditions, the material exhibits noticeable degradation of tensile properties, though less pronounced than the same duration exposure at over-temp.

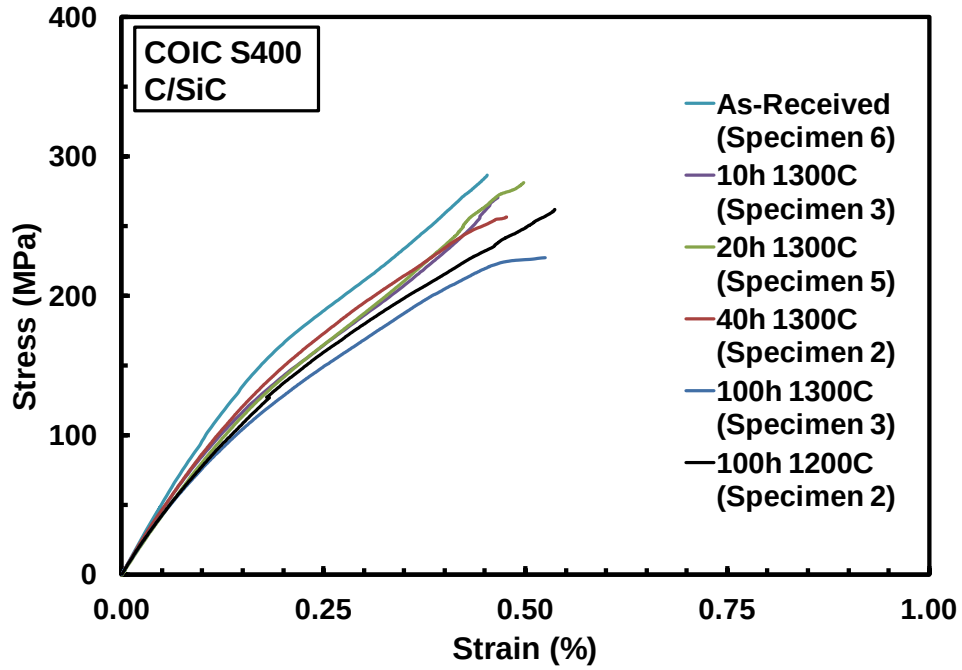

Figure 25: Representative stress-strain curves for C/SiC CMC including all prescribed heat treatments and as-received material

Elastic modulus versus UTS for all tested C/SiC specimens is shown in Figure 26. The gradual reduction in strength with exposure time is visible, especially with both 100-hour exposure durations. A very slight but gradual reduction in elastic modulus with exposure time can also be seen.

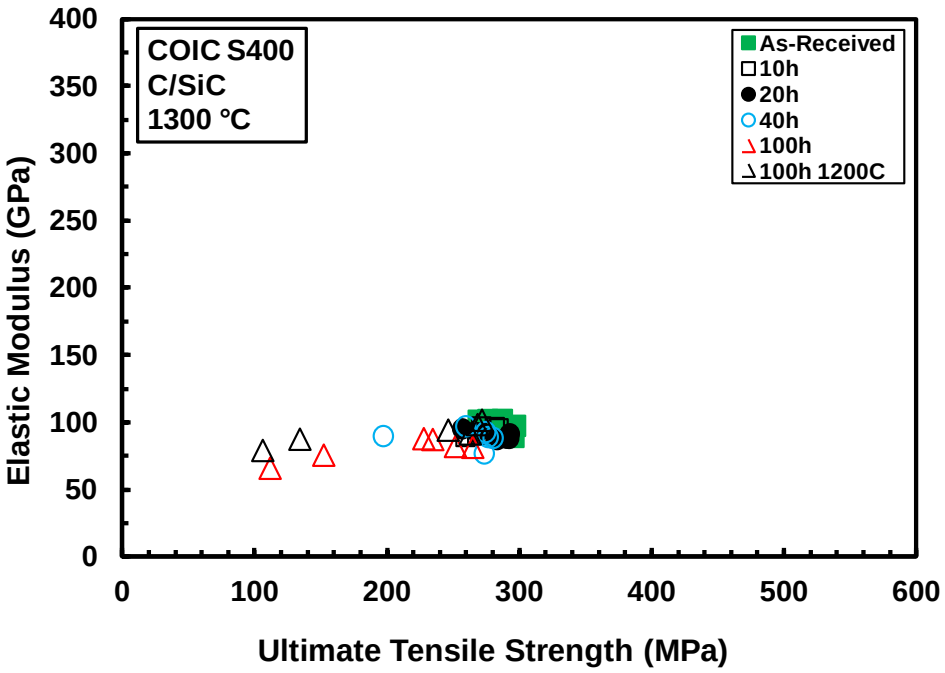

Figure 26: Elastic modulus versus UTS as a function of time-temperature history for HexTow® IM7/SiC

Ultimate tensile strength, elastic modulus, and strain at UTS values for all C/SiC specimens exposed to different time-temperature histories are shown in Table 16, Table 17, and Table 18, respectively.

Table 16: Effect of prior heat treatment on tensile strength of C/SiC composite

Exposure Time (h)	*Exposure Temp (°C)*	*Individual Specimen UTS (MPa)*						*Average UTS (MPa)*	*Standard Deviation*	*COV (%)*
		1	*2*	*3*	*4*	*5*	*6*			
0	N/A	277	276	269	297	296	287	284	11.4	4.02
10	1300	281	284	271	259	270	268	272	9.10	3.36
20	1300	256	268	292	292	283	290	280	14.9	5.31
40	1300	274	259	197	280	273	276	260	31.7	12.2
100	1300	111	251	227	264	234	152	207	61.0	29.5
100	1200	134	263	246	271	268	106	215	74.5	34.7

Table 17: Effect of prior heat treatment on elastic modulus (E) of C/SiC composite

Exposure Time (h)	*Exposure Temp (°C)*	*Individual Specimen E (GPa)*						*Average E (GPa)*	*Standard Deviation*	*COV (%)*
		1	*2*	*3*	*4*	*5*	*6*			
0	N/A	96	101	101	97	89	102	98	4.90	5.02
10	1300	96	95	96	89	91	91	93	3.01	3.23
20	1300	95	92	88	91	87	88	90	3.10	3.43
40	1300	93	97	90	88	77	89	89	6.74	7.60
100	1300	66	82	88	81	87	75	80	8.20	10.3
100	1200	87	91	94	101	98	79	92	8.00	8.80

Table 18: Effect of prior heat treatment on strain at UTS of C/SiC composite

Exposure Time (h)	*Exposure Temp (°C)*	*Individual Specimen Strain at UTS (%)*						*Average Strain at UTS (%)*	*Standard Deviation*	*COV (%)*
		1	*2*	*3*	*4*	*5*	*6*			
0	N/A	0.631	0.492	0.461	0.593	0.455	0.452	0.514	0.078	15.2
10	1300	0.532	0.588	0.466	0.598	0.552	0.594	0.555	0.051	9.15
20	1300	0.447	0.461	0.626	0.652	0.489	0.595	0.545	0.090	16.5
40	1300	0.534	0.455	0.584	0.542	0.692	0.593	0.567	0.078	13.8
100	1300	0.750	0.638	0.525	0.634	0.438	0.370	0.559	0.142	25.3
100	1200	0.412	0.536	0.760	0.528	0.609	0.275	0.520	0.166	31.9

5.2.3 Effect of Heat Treatment on Tensile Properties of T300/SiC-B_4C (C/HYPR-SiC™)

A representative sample of stress-strain curves for the C/HYPR-SiC™ material system is shown in Figure 27. The material exhibits only very slight variation in tensile properties between as-received material and 10, 20, and 40 hour exposures at over-temperature. However, there is a noticeable drop in UTS for the materials with a 100-hour exposure history at either over-temp or recommended operating temperature.

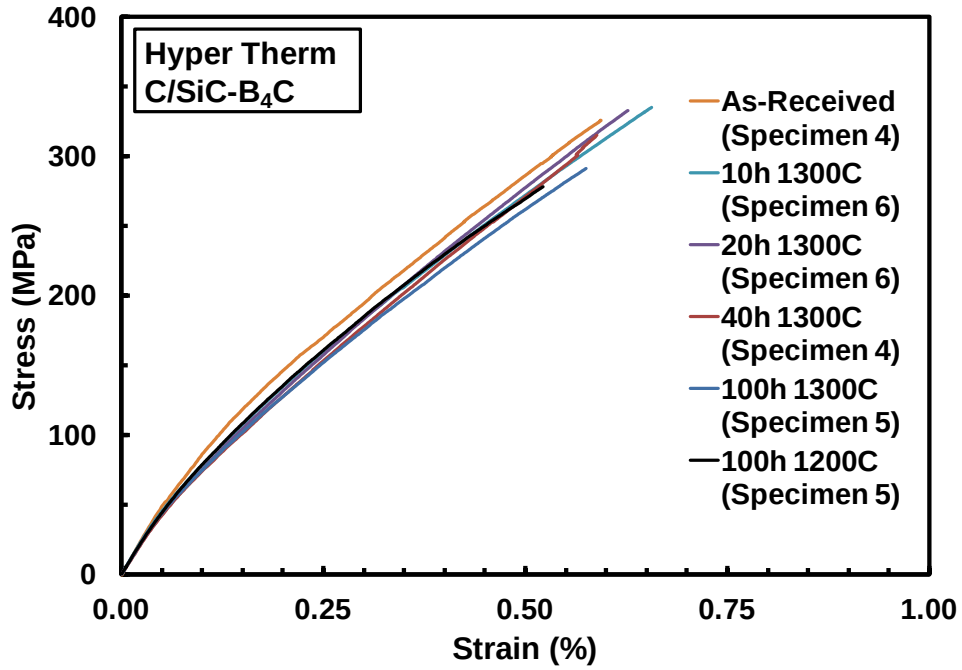

Figure 27: Representative stress-strain curves for C/HYPR-SiC™ CMC including all prescribed heat treatments and as-received material

The graph of elastic modulus versus UTS as a function of time-temperature history (Figure 28) shows tight grouping of all as-received and 10, 20, and 40-hour exposed specimens. Material strength decreases significantly with exposure time of 100 hours, whether at operating temperature or 100°C over-temperature. Elastic modulus is nearly constant with time-temperature history. Ultimate tensile strength, elastic modulus, and strain at UTS values for all C/HYPR-SiC™ specimens exposed to different time-temperature histories are shown in Table 19, Table 20, and Table 21, respectively.

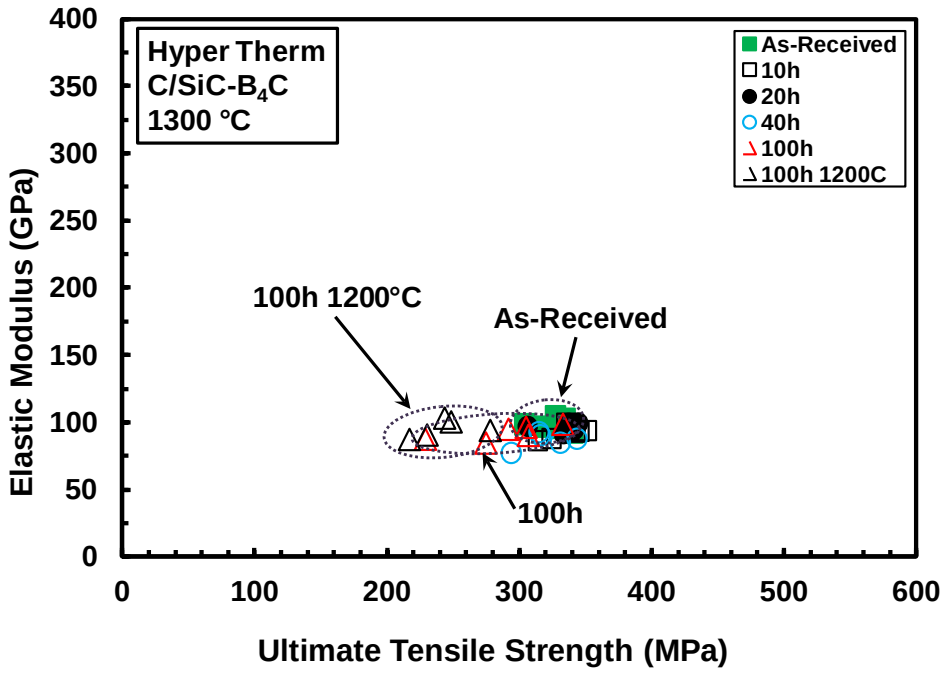

Figure 28: Elastic modulus versus UTS as a function of time-temperature history for C/HYPR-SiC™

Table 19: Effect of prior heat treatment on tensile strength of C/HYPR-SiC™ composite

Exposure Time (h)	*Exposure Temp (°C)*	*Individual Specimen UTS (MPa)*						*Average UTS (MPa)*	*Standard Deviation*	*COV (%)*
		1	*2*	*3*	*4*	*5*	*6*			
0	N/A	334	319	340	327	330	304	326	12.9	3.96
10	1300	314	342	345	351	324	335	335	14.0	4.18
20	1300	337	306	336	344	341	333	333	13.8	4.13
40	1300	294	331	N/A	316	343	315	319	16.9	5.28
100	1300	274	229	306	333	291	305	290	35.5	12.3
100	1200	230	N/A	217	243	278	248	243	37.5	15.4

Table 20: Effect of prior heat treatment on elastic modulus (E) of C/HYPR-SiC™ composite

Exposure Time (h)	*Exposure Temp (°C)*	*Individual Specimen E (GPa)*						*Average E (GPa)*	*Standard Deviation*	*COV (%)*
		1	*2*	*3*	*4*	*5*	*6*			
0	N/A	102	97	92	104	96	98	98	4.49	4.57
10	1300	86	92	93	94	88	99	92	4.63	5.03
20	1300	99	97	94	99	94	91	96	3.14	3.28
40	1300	77	85	N/A	90	88	92	86	5.98	6.93
100	1300	84	87	90	98	95	96	92	5.40	5.90
100	1200	90	N/A	87	103	94	100	95	7.00	7.00

Table 21: Effect of prior heat treatment on strain at UTS of C/HYPR-SiC™ composite

Exposure Time (h)	*Exposure Temp (°C)*	*Individual Specimen Strain at UTS (%)*						*Average Strain at UTS (%)*	*Standard Deviation*	*COV (%)*
		1	*2*	*3*	*4*	*5*	*6*			
0	N/A	0.685	0.586	0.662	0.592	0.680	0.598	0.634	0.047	7.35
10	1300	0.625	0.612	0.704	0.689	0.679	0.656	0.661	0.037	5.53
20	1300	0.609	0.578	0.649	0.610	0.631	0.627	0.618	0.024	3.93
40	1300	0.629	0.630	N/A	0.588	0.685	0.635	0.633	0.031	4.9
100	1300	0.552	0.457	0.587	0.636	0.575	0.603	0.568	0.061	10.8
100	1200	0.462	N/A	0.398	0.405	0.529	0.418	0.442	0.058	13.2

5.2.4 Effect of Heat Treatment on Tensile Properties of Hi-Nicalon™/SiC-B_4C (Hi-N/HYPR-SiC™)

A representative sample of stress-strain curves for the Hi-Nicalon™/HYPR-SiC™ material system is shown in Figure 29. There is a marked difference between the as-received and heat-treated materials, characterized by degradation in tensile properties with subjection to prior heat treatment. Material subjected to prior heat treatment exhibits a significant decrease in UTS as well

as a decrease in elastic modulus. The as-received material exhibits a distinctly near bi-linear stress-strain behavior whereas heat-treated material shows a linear-elastic region followed by highly non-linear behavior. The proportional limit decreases significantly with prior time-temperature exposure.

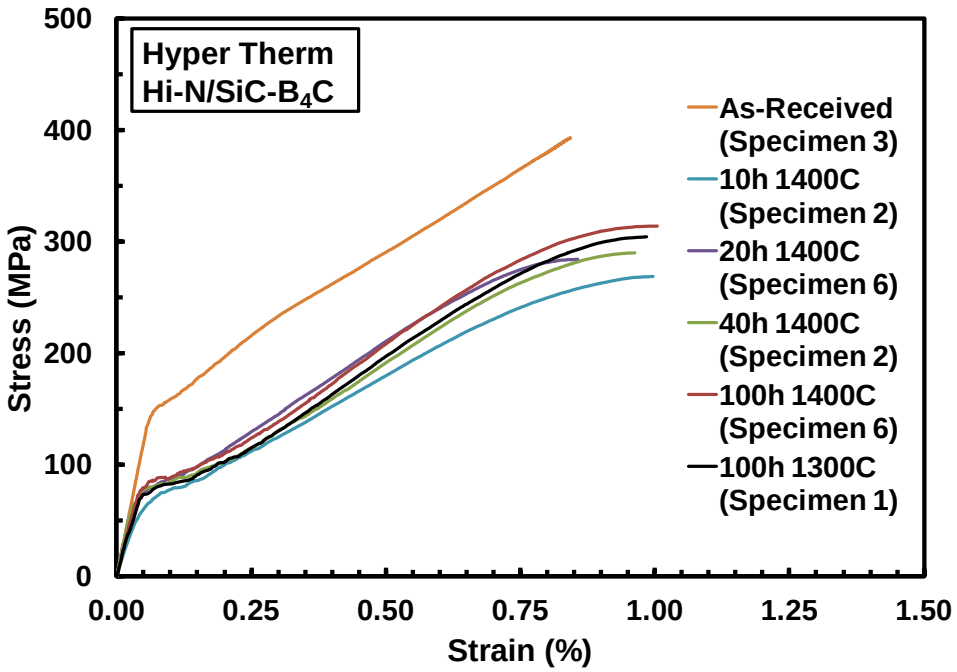

Figure 29: Representative stress-strain curves for Hi-Nicalon™/HYPR-SiC™ CMC including all prescribed heat treatments and as-received material

As indicated in Figure 30, UTS drops significantly with only 10 hours prior exposure at over-temperature. Interestingly, the material exhibits a slight increase in UTS with increased prior exposure time up to 100 hours. The same pattern is exhibited with regards to elastic modulus – significant decrease from as-received material to prior 10-hour exposure at over-temp, followed by a gradual but slight increase in modulus up to 100 hours exposure time at over-temp. Additionally, material exposed to 100°C over-temp for 100 hours

performed slightly better than that exposed to recommended operating temperature for the same amount of time.

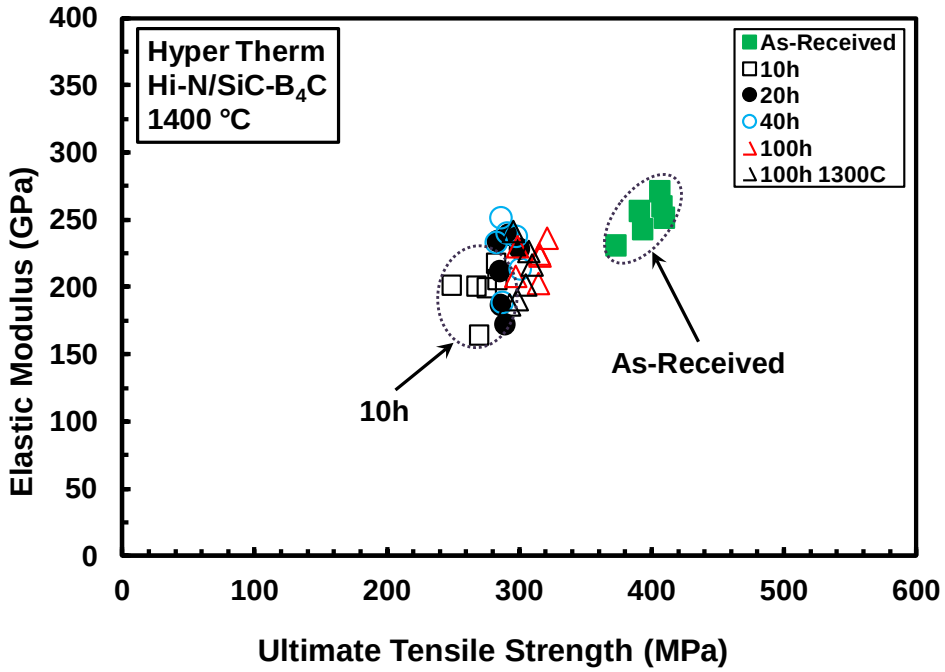

Figure 30: Elastic modulus versus UTS as a function of time-temperature history for Hi-Nicalon™/HYPR-SiC™

Ultimate tensile strength, elastic modulus, and strain at UTS values for all Hi-Nicalon™/HYPR-SiC™ specimens exposed to different time-temperature histories are shown in Table 22, Table 23, and Table 24, respectively.

Table 22: Effect of prior heat treatment on tensile strength of Hi-Nicalon™/HYPR-SiC™ composite

Exposure Time (h)	*Exposure Temp (°C)*	*Individual Specimen UTS (MPa)*						*Average UTS (MPa)*	*Standard Deviation*	*COV (%)*
		1	*2*	*3*	*4*	*5*	*6*			
0	N/A	407	406	393	409	373	390	396	14.1	3.55
10	1400	282	269	249	267	283	275	271	12.7	4.69
20	1400	291	285	300	289	283	285	289	6.10	2.11
40	1400	300	290	286	282	297	287	290	7.04	2.42
100	1400	321	297	315	298	315	314	310	9.91	3.20
100	1300	304	298	292	307	295	309	301	6.84	2.27

Table 23: Effect of prior heat treatment on elastic modulus (E) of Hi-Nicalon™/HYPR-SiC™ composite

Exposure Time (h)	*Exposure Temp (°C)*	*Individual Specimen E (GPa)*						*Average E (GPa)*	*Standard Deviation*	*COV (%)*
		1	*2*	*3*	*4*	*5*	*6*			
0	N/A	260	271	243	251	231	256	252	14.0	5.55
10	1400	217	164	201	200	205	199	198	17.9	9.04
20	1400	239	186	228	172	234	212	212	27.2	12.8
40	1400	213	240	251	233	237	188	227	22.7	10.0
100	1400	236	208	224	230	223	202	220	12.9	5.87
100	1300	201	190	186	226	241	216	210	21.3	10.2

Table 24: Effect of prior heat treatment on strain at UTS of Hi-Nicalon™/HYPR-SiC™ composite

Exposure Time (h)	*Exposure Temp (°C)*	*Individual Specimen Strain at UTS (%)*						*Average Strain at UTS (%)*	*Standard Deviation*	*COV (%)*
		1	*2*	*3*	*4*	*5*	*6*			
0	N/A	0.841	0.779	0.844	0.873	0.836	0.797	0.828	0.034	4.15
10	1300	0.954	0.996	0.733	0.963	0.939	0.929	0.919	0.094	10.2
20	1300	0.981	0.922	1.03	0.985	0.830	0.856	0.934	0.078	8.38
40	1300	0.963	0.963	0.938	0.941	0.914	0.931	0.942	0.019	2.01
100	1300	1.08	1.04	1.02	0.960	1.10	1.00	1.03	0.050	4.82
100	1200	0.985	0.910	1.11	1.04	0.918	0.972	0.989	0.075	7.61

5.2.5 Comparison of Results for Different Material Systems

Tensile performance between all four material systems is compared in the following section. Comparisons between subsets of like materials are also considered.

First, Figure 31 illustrates strength retention as a function of exposure time for all four CMCs. There is a clear trend of strength degradation over time with all material systems. The Hyper-Therm C/HYPR-SiC™ composite performed best overall in strength retention, exhibiting an unexpected yet slight (~3%) increase

after 10 hour exposure at over-temp, followed by a very gradual and relatively small (~10%) decrease in strength with increasing prior exposure time. As discussed in the previous section, the Hi-Nicalon™/HYPR-SiC™ CMC exhibits a very drastic (> 30%) reduction in strength with a relatively short time-temperature history, followed by a very gradual and slight re-gaining of strength (~10%) with increased exposure time. The Hi-Nicalon™/SiNC material system performed the most predictably, exhibiting a gradual decrease and leveling-out of strength retention with increasing prior exposure time at over-temp. The COIC C/SiC CMC exhibited a small decrease followed by a small increase in retained strength from virgin material to 10-hour, and from 10-hour to 20-hour exposure times, respectively. After 20 hours prior exposure at over-temp, there was a significant (~26%) and linear decrease with increasing prior exposure time up to 100 hours.

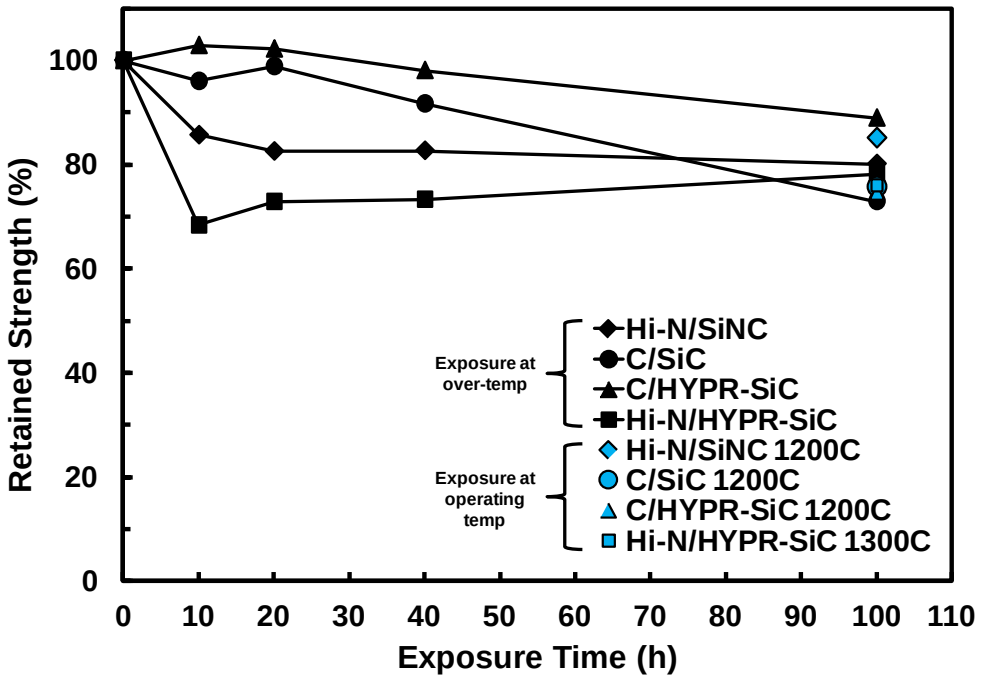

Figure 31: Comparison of retained strength with time-temperature history for all CMCs

Trends in retained strength for 100-hour exposure times at recommended operating temperature also varied between material systems. Both COIC materials (Hi-Nicalon™/SiNC and C/SiC) exhibited slightly greater strength retention after 100-hour heat treatments at operating temperature as compared to 100 hours at over-temp. On the other hand, strength retention of the C/HYPR-SiC™ and Hi-Nicalon™/HYPR-SiC™ CMCs after 100-hour exposure times at operating temperature was less than that for a history of 100 hours at over-temp (Figure 31and Figure 32).

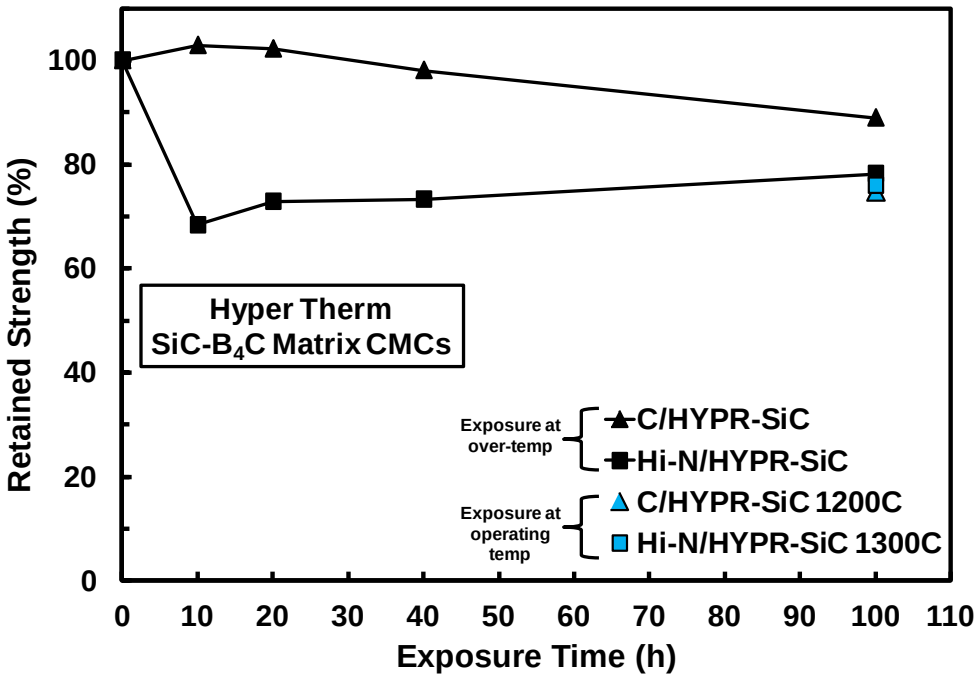

Figure 32: Strength retention of HYPR-SiC™ matrix CMCs

Further, Figure 32 compares strength retention for only the HYPR-SiC™ layered matrix composites. Unexpectedly, the carbon fiber-reinforced CMC had greater strength retention than that of the Hi-Nicalon™ SiC fiber-reinforced CMC over the range of time-temperature histories. Carbon-reinforced composites are typified by susceptibility to oxidation and thereby performance degradation when exposed to high temperatures. However, this study shows superior strength retention of the carbon fiber-reinforced CMC over the Hi-Nicalon™-reinforced CMC with the same matrix. It must be noted that there is a 100°C difference in recommended operating temperature of the two HYPR-SiC™ matrix composites. It is possible that the oxidation inhibition properties of the layered SiC-B_4C matrix become considerably degraded when exposed to 1400°C as compared to 1300°C. However, after prior heat treatment for 100 h at 1300°C, the Hi-

Nicalon™/HYPR-SiC™ composite still performs significantly worse in tensile strength retention than the C/HYPR-SiC™ composite subjected to the same time-temperature history. This suggests that a factor other than the difference in recommended operating temperature is contributing to the drastically lower retention of tensile strength after prior heat treatment of the Hi-Nicalon™/HYPR-SiC™ composite. Other possible contributing factors include manufacturing defects and quality of matrix densification during CMC fabrication (e.g. poor matrix infiltration with many voids versus good matrix infiltration with few voids). These potential causes were further investigated via optical and SEM microscopy and will be discussed later in this chapter.

Retained tensile strength of the two CMCs reinforced with Hi-Nicalon™ fibers is illustrated in Figure 33. Both materials exhibit an overall decrease in strength with prior high-temperature exposure. The Hi-Nicalon™/SiNC composite shows a more predictable, graceful, and progressive degradation than the Hi-Nicalon/HYPR-SiC™ CMC. The Hi-Nicalon™/HYPR-SiC™ composite behaves rather unpredictably with increased exposure time at over-temp: large loss of tensile strength (~32%) after 10 h exposure, followed by a gradual increase with increased exposure time. The unexpected increase over time in tensile strength retention of the Hi-Nicalon™/HYPR-SiC™ CMC may be due to changes in composite microstructure with prolonged exposures.

Although degradation behavior with increased exposure time at 100°C over-temp varies between the two Hi-Nicalon™ fiber-reinforced CMCs, both exhibit approximately the same amount of retained tensile strength (~80%) after 100 h

exposure at over-temp. Further, the Hi-Nicalon™/SiNC CMC shows a noticeable increase in tensile strength when exposed for 100 h at operating temperature versus 100°C over-temperature, while the Hi-Nicalon/HYPR-SiC™ CMC shows a slight drop in retained tensile strength.

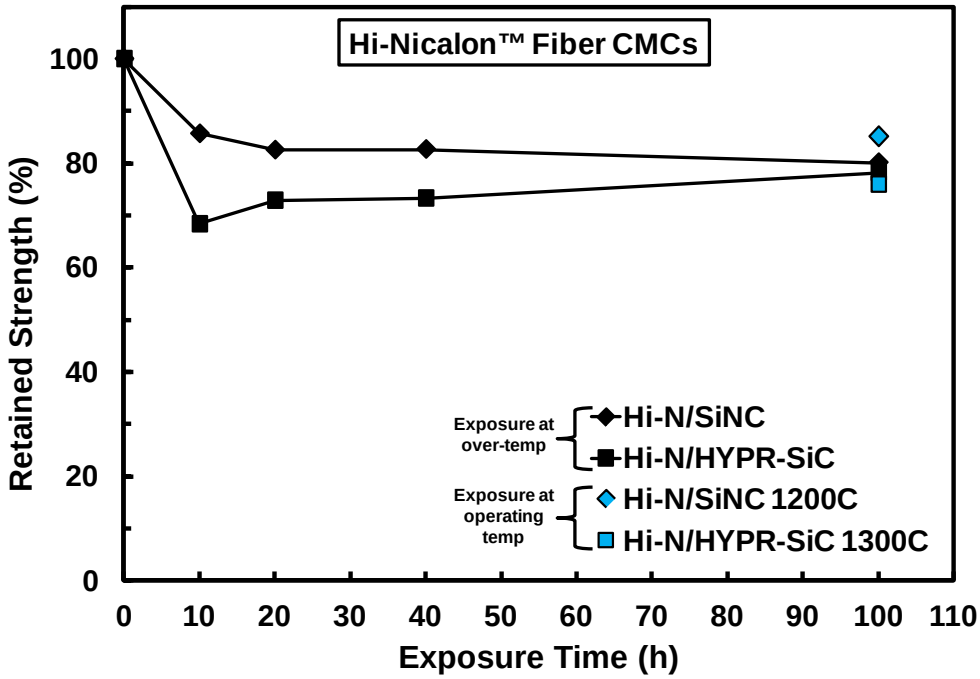

Figure 33: Strength retention of Hi-Nicalon™ fiber-reinforced CMCs

Next, change in elastic modulus with exposure time is compared between all material systems (Figure 34). The Hi-Nicalon™/HYPR-SiC™ CMC exhibits significant changes and an overall decrease of elastic modulus with increased exposure time whereas the other three material systems show negligible change. Similar to behavior in strength retention, Hi-Nicalon™/HYPR-SiC™ exhibits a significant decrease in elastic modulus after a relatively short heat treatment, followed by a gradual increase with increased exposure time, and a final decrease from 40 h to 100 h prior exposure at 100°C over-temp.

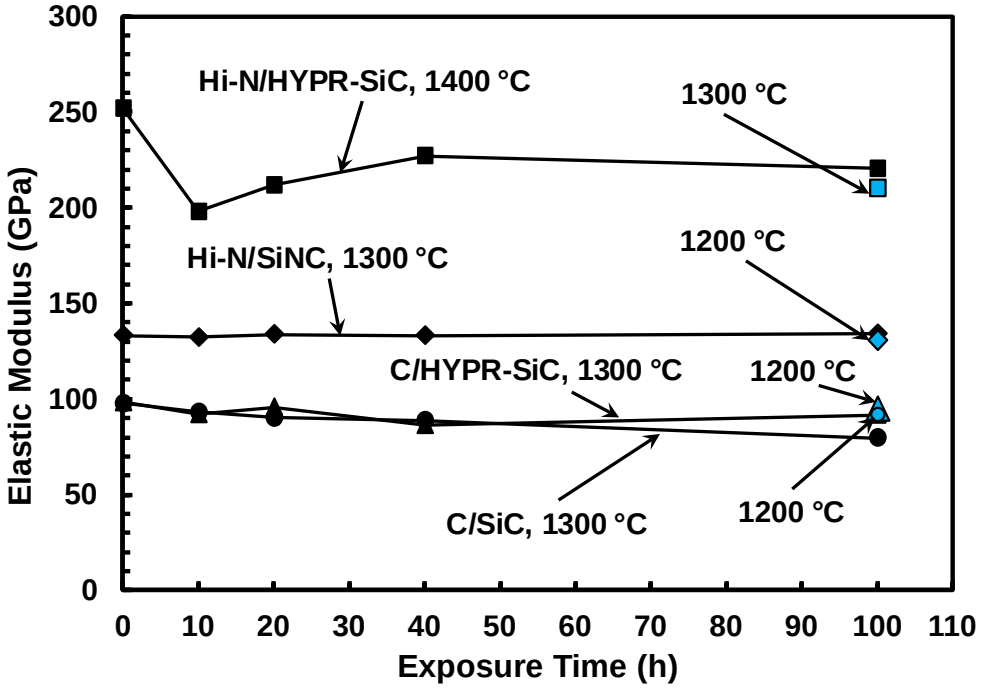

Figure 34: Comparison of elastic modulus versus exposure time for all CMCs

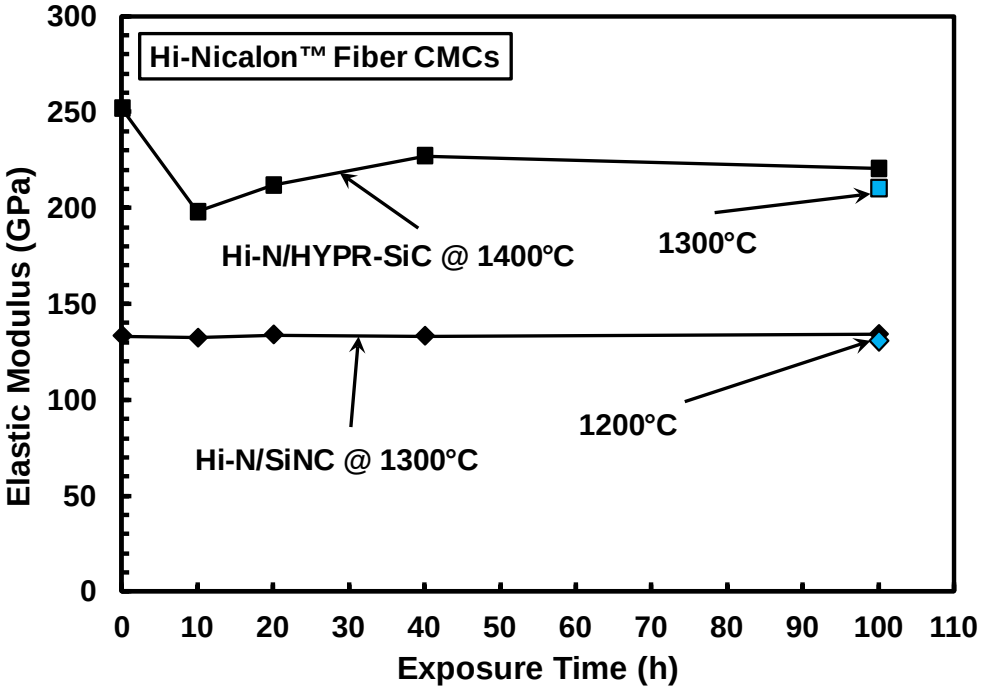

Figure 35: Comparison of elastic modulus versus exposure time for Hi-Nicalon™ fiber-reinforced CMCs

Figure 35 shows a comparison between the two Hi-Nicalon™ fiber-reinforced CMCs. Because tensile properties of [0°/90°] CMCs are dominated by those of the fiber, these results along with the strength retention results shed light on the ability of the different matrices to protect the Hi-Nicalon™ fibers from oxidation and degradation at very high temperatures. The results indicate that the Hi-Nicalon™/SiNC composite is more thermally stable, which can be attributed to better oxidation inhibiting capabilities of the SiNC matrix over that of the HYPR-SiC™ matrix. Better oxidation inhibition is likely due to the density and/or the material properties of the matrix. A more dense (thus less porous) matrix results in better protection of the fibers and the fiber-matrix interface, allowing the desirable properties of the CMC to be preserved when exposed to harsh environments. Also, matrix materials themselves respond differently at very high temperatures, some performing better than others with regards to oxidation, fracture toughness, etc. Differences in matrix behavior after prior heat treatment was examined via optical and SEM microscopy and will be discussed later in this chapter.

Figure 36 and Figure 37 illustrate elastic modulus versus UTS for HYPR-SiC™ matrix CMCs and Hi-Nicalon™ fiber-reinforced CMCs, respectively. Data points for every tested specimen of the relevant material systems are included in these charts. As discussed before, the Hi-Nicalon™/HYPR-SiC™ CMC exhibits a significant decrease in UTS with increasing exposure time, and the C/HYPR-SiC™ also shows a decrease, though less pronounced. This is shown graphically by the overall tighter grouping of the C/HYPR-SiC™ data points as compared to

those of Hi-Nicalon™/HYPR-SiC™. Additionally, the more horizontally level appearance of the C/HYPR-SiC™ data points versus the more vertically spread Hi-Nicalon™/HYPR-SiC™ data points indicate less vulnerability to elastic modulus degradation of the C/HYPR-SiC™ CMC when subjected to prior high temperature exposure.

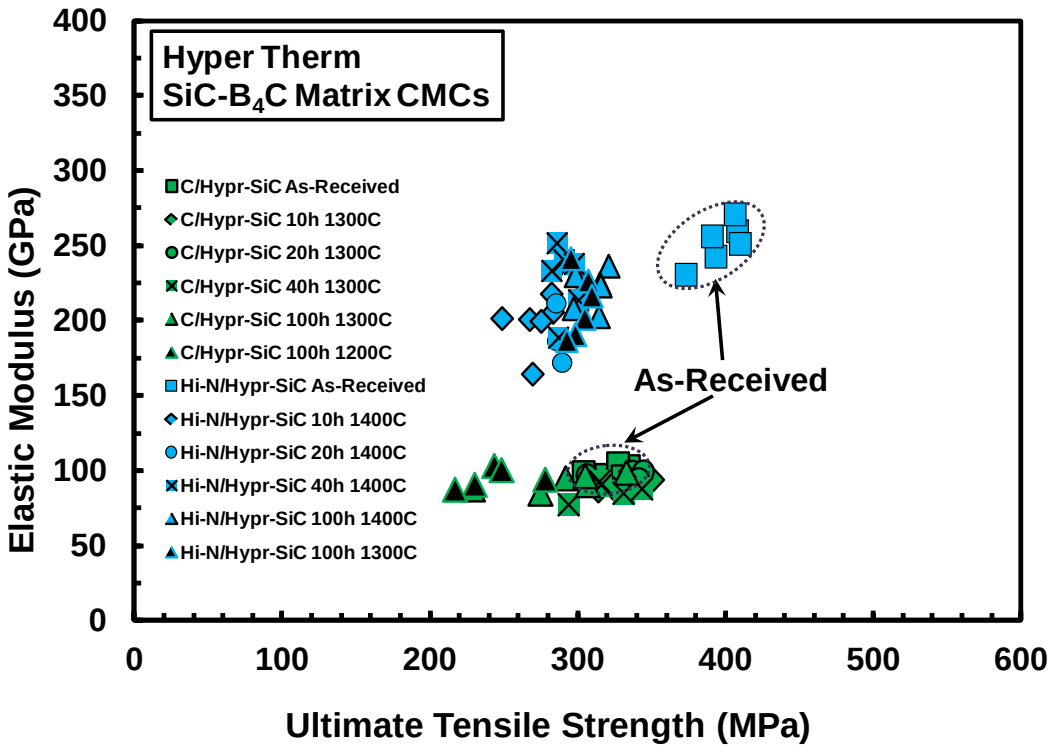

Figure 36: Ashby plot of elastic modulus versus UTS for HYPR-SiC™ matrix CMCs

Figure 37 shows similar behavior when comparing the two CMCs reinforced by Hi-Nicalon™ SiC fibers. The Hi-Nicalon™/HYPR-SiC™ material system shows less stability with respect to both strength and elastic modulus when subjected to prior high temperature exposure. On the other hand, the

Hi-Nicalon™/SiNC exhibits far more stable behavior with a gradual decrease in UTS and nearly constant elastic modulus as exposure time increases.

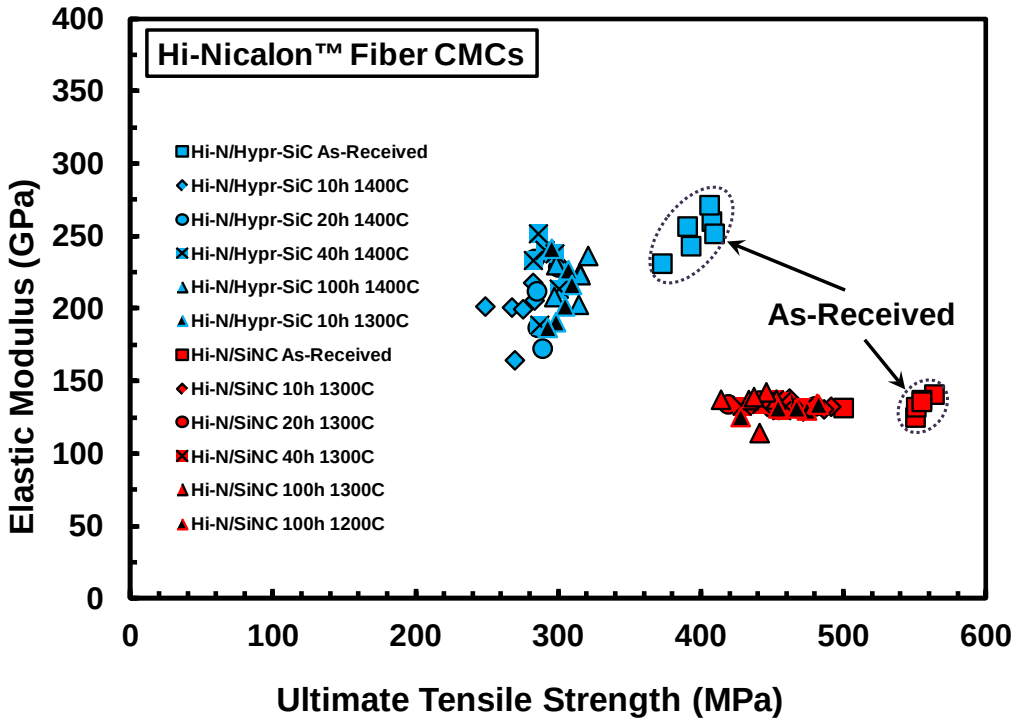

Figure 37: Ashby plot of elastic modulus versus UTS for Hi-Nicalon™ fiber-reinforced CMCs

5.3 Effect of Heat Treatment on Composite Microstructure – Optical Microscopy

Microstructural analysis was conducted on selected fractured specimens using both an optical microscope and scanning electron microscope (SEM). The strength and modulus values, along with visual examination of fractured specimens, were used to select a representative sample of specimens for microstructural analysis. Four time-temperature exposure histories for each material are represented in the selection (Section 4.4, Table 10). The sample selection for each of the four material systems includes: 1.) as-received virgin

material; 2.) exposure at which the first significant change in strength occurred; 3.) maximum exposure time (100 h) at 100°C over operating temperature; and 4.) 100 h exposure at operating temperature. Additional optical micrographs for each CMC are located in Appendices F–I.

5.3.1 Hi-Nicalon™/SiNC Composite

Optical micrographs of the fracture surfaces obtained in tension tests of the Hi-Nicalon™/SiNC specimens are shown in Figure 38: (a) as-received; (b) 10 h at 1300°C; (c) 100 h at 1300°C; (d) 100h at 1200°C. Fracture surfaces of the as-received specimen and specimen with prior heat treatment for 10 h at 1300°C exhibit considerable fiber pullout, revealing excellent crack deflection and graceful failure. The jagged appearance of the fracture surfaces indicates failure of plies at different locations. The fracture surface of the specimen heat treated for 100 h at 1200°C is less jagged, though the appearance still indicates some crack deflection and fiber pullout. The fracture surface of the specimen heat treated for 100 h at 1300°C is considerably more planar with very little fiber pullout. Crack deflection is minimal with all plies failing nearly in concert. Prior heat treatment significantly degraded the crack deflection capability of the composite. Degradation became more pronounced with increased exposure time. Exposure for 100 h at 100°C over operating temperature significantly diminished desired composite failure behavior compared to the 100 h exposure at operating temperature. These observations are consistent with the strength retention results presented in Section 5.2.

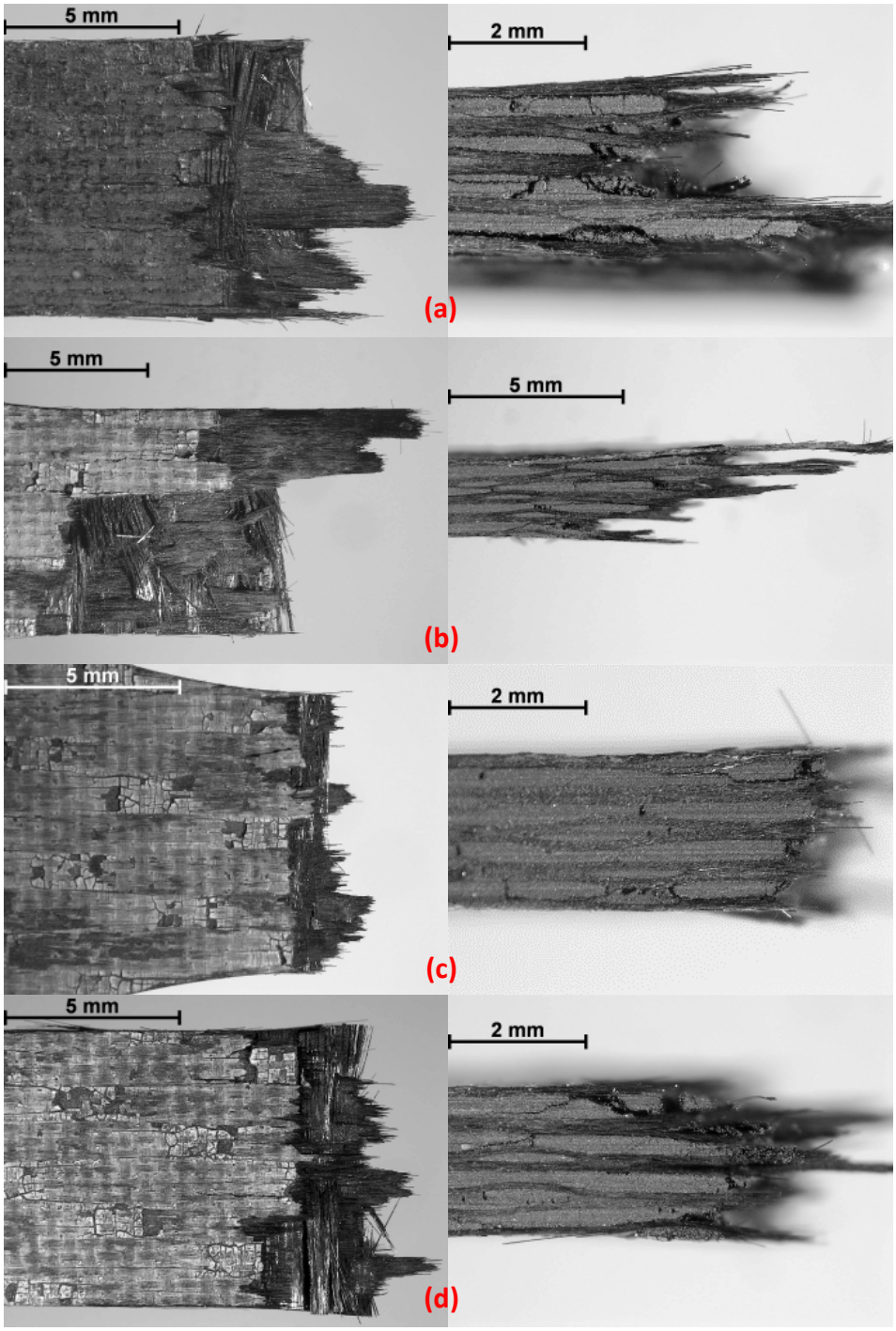

Figure 38: Fracture surfaces obtained in tensile tests of Hi-Nicalon™/SiNC specimens (left: face-up; right: edge-on) – (a) virgin specimen; and specimens with prior heat treatments at (b) 1300°C for 10 h; (c) 1300°C for 100 h; (d) 1200°C for 100 h

5.3.2 HexTow® IM7/SiC (C/SiC) Composite

Optical micrographs of the fracture surfaces obtained in tension tests of the C/SiC specimens are shown in Figure 39: (a) as-received; (b) 40 h at 1300°C; (c) 100 h at 1300°C; (d) 100h at 1200°C. The fracture surface of the as-received specimen and the specimen with prior heat treatment for 40 h at 1300°C are jagged and stepwise, indicative of individual ply failure at different locations. Both specimens display moderate fiber pullout. Though slight, the degree of fiber pullout decreased with the increase in exposure duration.

The fracture surface of the specimen heat treated for 100 h at 1300°C exhibits delamination and pullout of a single ply, saddled by two areas of planar fracture. Poor crack deflection is indicated by the planar fracture surfaces as well as the readily visible crack growth parallel to the loading direction on either side of the pulled-out ply. The specimen heat treated for 100 h at 1200°C also exhibits two main regions where multiple plies have failed almost in concert. Crack growth parallel to the loading direction is visible, though crack deflection appears slightly better than the specimen exposed for 100 h at 1300°C.

These observations are consistent with strength retention results presented in Section 5.2, which indicate: 92% strength retained after heat treatment for 40 h at 1300°C; 19% drop from 40 to 100 h exposure at 1300°C; and near consistent results between 100 h at 1300°C and 100 h at 1200°C exposures.

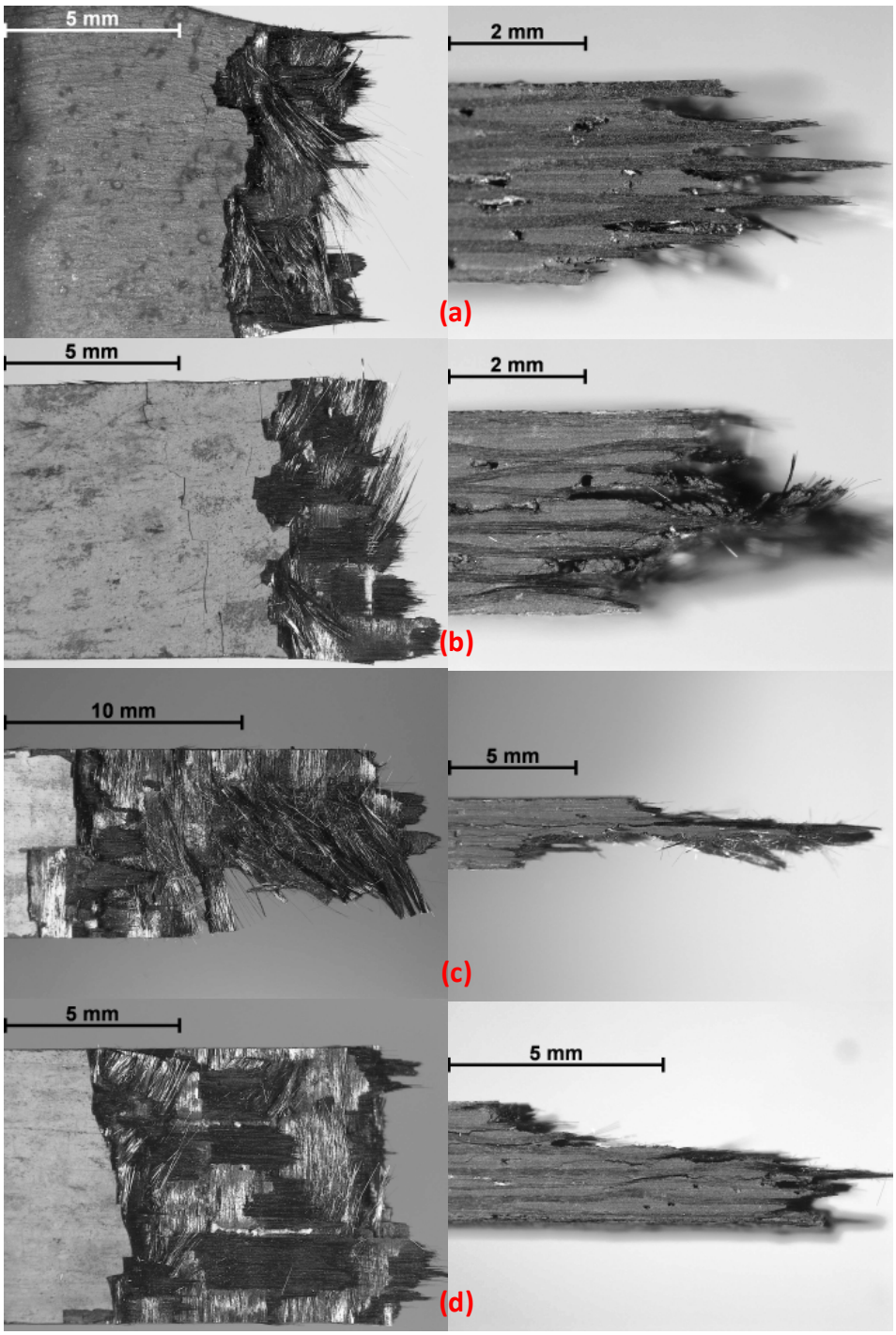

Figure 39: Fracture surfaces obtained in tensile tests of C/SiC specimens (left: face-up; right: edge-on) – (a) virgin specimen; and specimens with prior heat treatments at (b) 1300°C for 40 h; (c) 1300°C for 100 h; (d) 1200°C for 100 h

5.3.3 T300/SiC-B_4C (C/HYPR-SiC™) Composite

Optical micrographs of the fracture surfaces obtained in tension tests of the C/HYPR-SiC™ specimens are shown in Figure 40: (a) as-received; (b) 40 h at 1300°C; (c) 100 h at 1300°C; (d) 100h at 1200°C. All fracture surfaces exhibit distinct and separate regions of nearly planar fracture. These regions are distinguished by groups of plies that failed almost in concert, with each group having failed at a different time. Among the plies that failed in concert, crack deflection was generally poor. However, better crack deflection is evident in the transition from one group of failed plies to the next.

The as-received specimen exhibits more groupings of failed plies compared to the other specimens. This indicates slightly better crack deflection performance and thus more graceful failure of the virgin composite. The fracture surface of the specimen exposed for 100 h at 1200°C is the most planar of all specimens, characterized by minimal crack deflection and brittle fracture of two distinctly planar regions. Interestingly so, this specimen exhibits a more brittle fracture behavior than the specimen exposed for the same duration at 100°C higher temperature. Note the large void in the specimen (Figure 40d) from which a large crack has grown. Additionally, Figure 40(b) indicates ply delamination as a major component of the fracture surface. Poor matrix densification is likely a key factor in the overall poor and inconsistent failure behavior of this composite. The above observations are consistent with results presented in Section 5.2 regarding progression of composite degradation with time-temperature history.

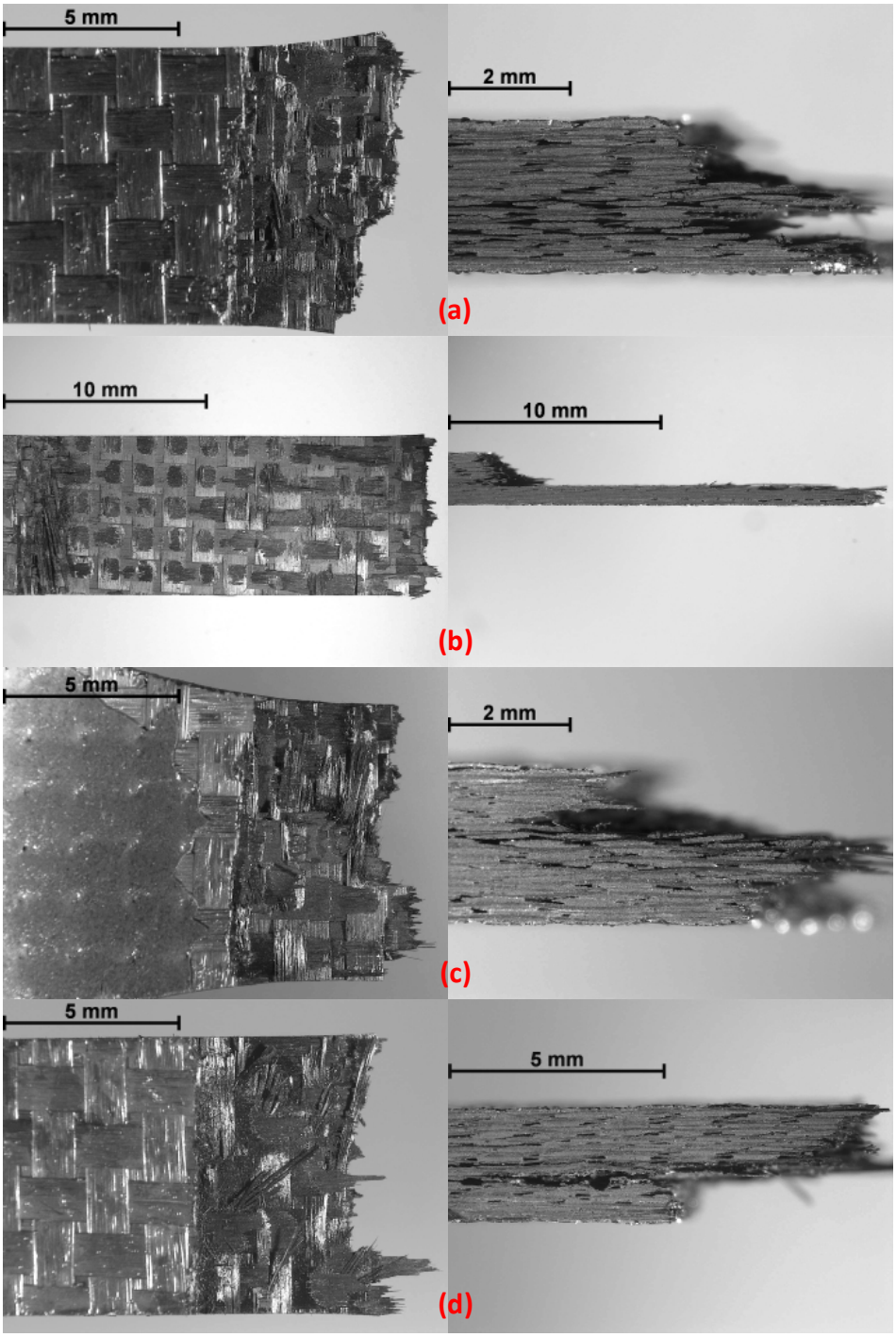

Figure 40: Fracture surfaces obtained in tensile tests of C/HYPR-SiC™ specimens (left: face-up; right: edge-on) – (a) virgin specimen; and specimens with prior heat treatments at (b) 1300°C for 40 h; (c) 1300°C for 100 h; (d) 1200°C for 100 h

5.3.4 Hi-Nicalon™/SiC-B_4C (Hi-Nicalon™/HYPR-SiC™) Composite

Optical micrographs of the fracture surfaces obtained in tension tests of the Hi-Nicalon™/HYPR-SiC™ specimens are shown in Figure 41: (a) as-received; (b) 10 h at 1400°C; (c) 100 h at 1400°C; (d) 100h at 1300°C. The fracture surface of the as-received specimen exhibits failure of plies at different times as well as considerable fiber pullout. The specimen had good crack deflection. The specimen heat treated for 10 h at 1400°C exhibits significant fiber pullout with planar matrix fracture. The fiber pullout is more brushy than the as-received specimen. The pulled-out fibers vary in length from less than 2 mm to greater than 10 mm. It is evidenced that crack propagation occurred with great ease across the matrix, in some places traveling directly through and fracturing the reinforcing fibers in-plane, while in other areas appearing to travel around the fibers. This crack growth behavior resulted in a very planar and brittle fracture of the matrix. The planar matrix fracture indicates that the extent of fiber pullout in this specimen has little correlation with good crack deflection behavior.

The fracture surface of the specimen heat treated at 1400°C for 100 h exhibits a combination of planar fracture with some fiber pullout. Planar fracture and fiber pullout are less pronounced than the specimen exposed for 10 h at 1400°C. Further, the more varied location of ply failure indicates that crack deflection in the specimen exposed for 100 h at 1400°C is improved over that of the specimen exposed for 10 h.

The fracture surface of the specimen exposed for 100 h at 1300°C is characterized by two distinct regions of nearly planar fracture and minimal fiber

pullout. Readily seen in Figure 41(d) are two cracks that grew nearly unobstructed, perpendicular to the direction of loading and across the entire specimen thickness. Again, as evidenced by the more varied location of ply failure, the specimen with prior heat treatment for 100 h at 1400°C exhibited better crack deflection and a more graceful failure than the specimen heat treated for 100 h at 1300°C.

The observations above indicate that just 10 hours of heat treatment at 1400°C impart a significant degradation of desired composite behavior. Further, increased duration exposure at 1400°C resulted in slightly better damage tolerance, while heat treatment for 100 h at 1300°C resulted in more brittle composite behavior than that of the specimen exposed for 100 h at 100°C higher temperature. These observations are consistent with the results presented in Section 5.2. It is plausible that inconsistencies in the fabrication of this composite are responsible for the somewhat anomalous behavior.

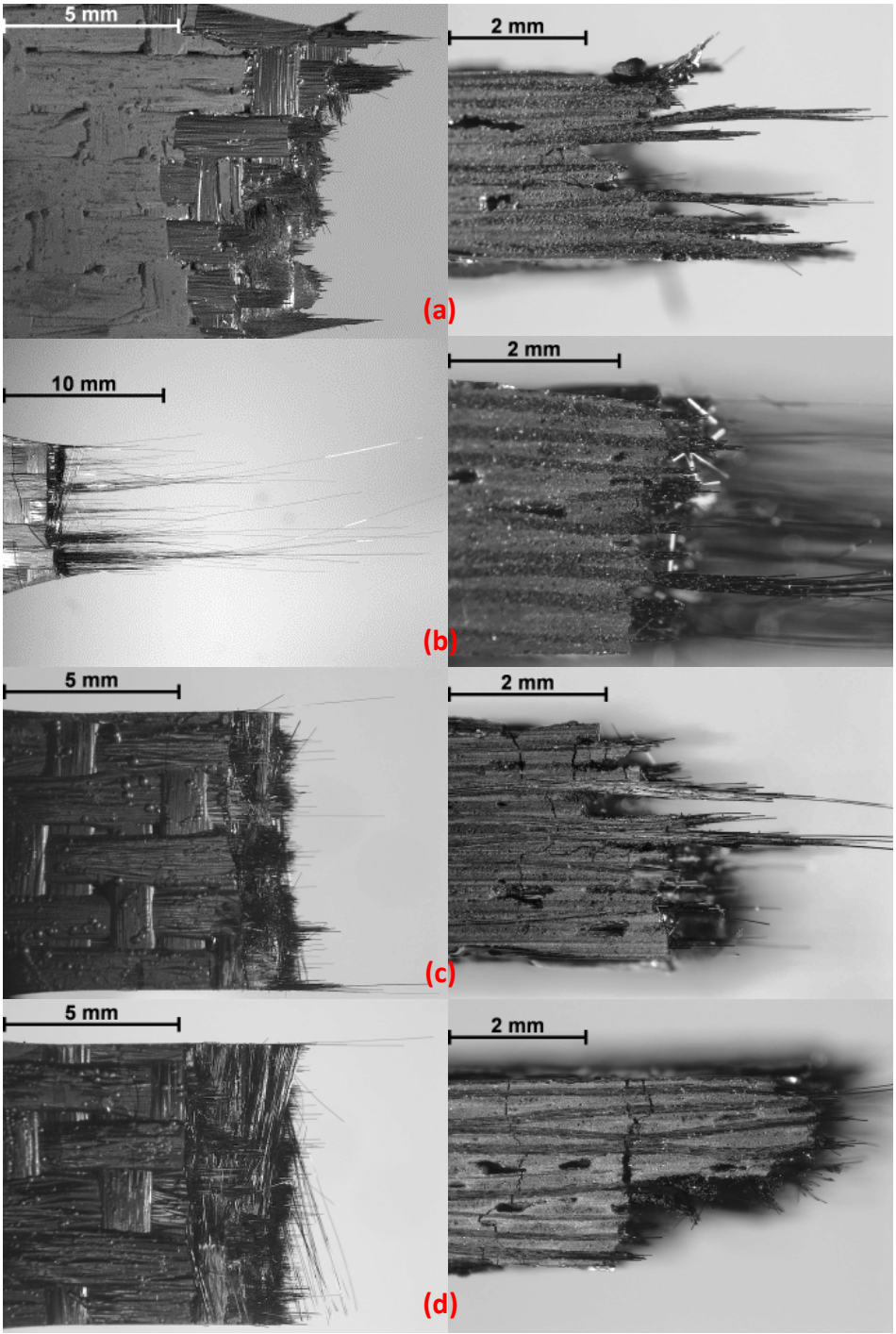

Figure 41: Fracture surfaces obtained in tensile tests of Hi-Nicalon™/HYPR-SiC™ specimens (left: face-up; right: edge-on) – (a) virgin specimen; and specimens with prior heat treatments at (b) 1400°C for 10 h; (c) 1400°C for 100 h; (d) 1300°C for 100 h

5.4 Effect of Heat Treatment on Composite Microstructure – Scanning Electron Microscopy

To further understand the effect of prior heat treatment on composite microstructure, the fracture surfaces discussed in the previous section were subsequently examined under a scanning electron microscope (SEM). The specimens did not require carbon coating and were attached to an SEM specimen stage with carbon tape. Additional SEM micrographs for each CMC are located in Appendices J–M.

5.4.1 Hi-Nicalon™/SiNC Composite – SEM Examination

SEM micrographs of fracture surfaces obtained in tension tests of the Hi-Nicalon™/SiNC specimens are shown in Figure 42: (a) as-received; (b) 10 h at 1300°C; (c) 100 h at 1300°C; (d) 100 h at 1200°C. The fracture surfaces examined under SEM reveal microstructural characteristics consistent with the observations made during optical microscopy. The fracture surface of the as-received specimen is dominated by fibrous fracture. Pullout of individual fibers as well as pullout of fiber bundles is readily visible. The fracture surface of the specimen that was heat treated for 10 h at 1300°C consists of bundles of fibers that have pulled out with significantly fewer instances of individual fiber pullout. The fiber bundles fractured at different times, resulting in significant pullout of the bundles. This behavior is indicated by the distinct cavities seen in Figure 42(b). The specimen exposed for 100 h at 1300°C has a fracture surface dominated by planar fracture. Coordinated fracture of fiber bundles is evidenced by the more

level appearance of the fracture surface. Finally, the fracture surface of the specimen that was subjected to heat treatment for 100 hours at 1200°C exhibits a combination of pullout and planar fracture. Pullout occurred mostly in bundles of fibers with very little pullout of individual fibers. As with the specimen heat treated for 10 h at 1300°C, the distinctly different depths of fiber bundle pullout indicates bundle failure at different times.

Overall, failure of the Hi-Nicalon™/SiNC composite progressed from graceful to more brittle failure with increase in duration of prior heat treatment at 100°C over-temp. When subjected to heat treatment at operating temperature for 100 hours, the composite failure mode was more graceful than the same duration exposure at over-temp, and was even comparable to the specimen exposed for 10 h at over-temp. This suggests that degradation of desired composite failure mechanisms is significant for the Hi-Nicalon™/SiNC CMC when subjected to prior heat treatment at 100°C above operating temperature. Higher magnification micrographs in Figure 43 clearly show this progression from graceful, fibrous failure to a more brittle failure, as well as the better retention of desired composite behavior when exposed at operating temperature as opposed to 100°C over-temp.

Figure 44 shows an additional micrograph of the fracture surface of the specimen subjected to prior heat treatment for 100 h at over-temp. Coordinated fiber failure, strong fiber-matrix bonding, and a dense, well-infiltrated matrix are readily visible. Recall that a dense matrix and a fiber-matrix interface conducive to fiber-debonding are key components to the desired graceful failure mechanism

of non-oxide CMCs. Although the dense matrix is present, when exposed to 100°C over-temperature for a significant duration, the Hi-Nicalon™/SiNC composite exhibited a substantial degradation in the fiber-matrix debonding mechanism. In other words, the fiber-matrix interface was strengthened with prior heat treatment, thus diminishing the desired fiber-matrix debonding and fiber pullout behavior that is conducive to graceful composite failure.

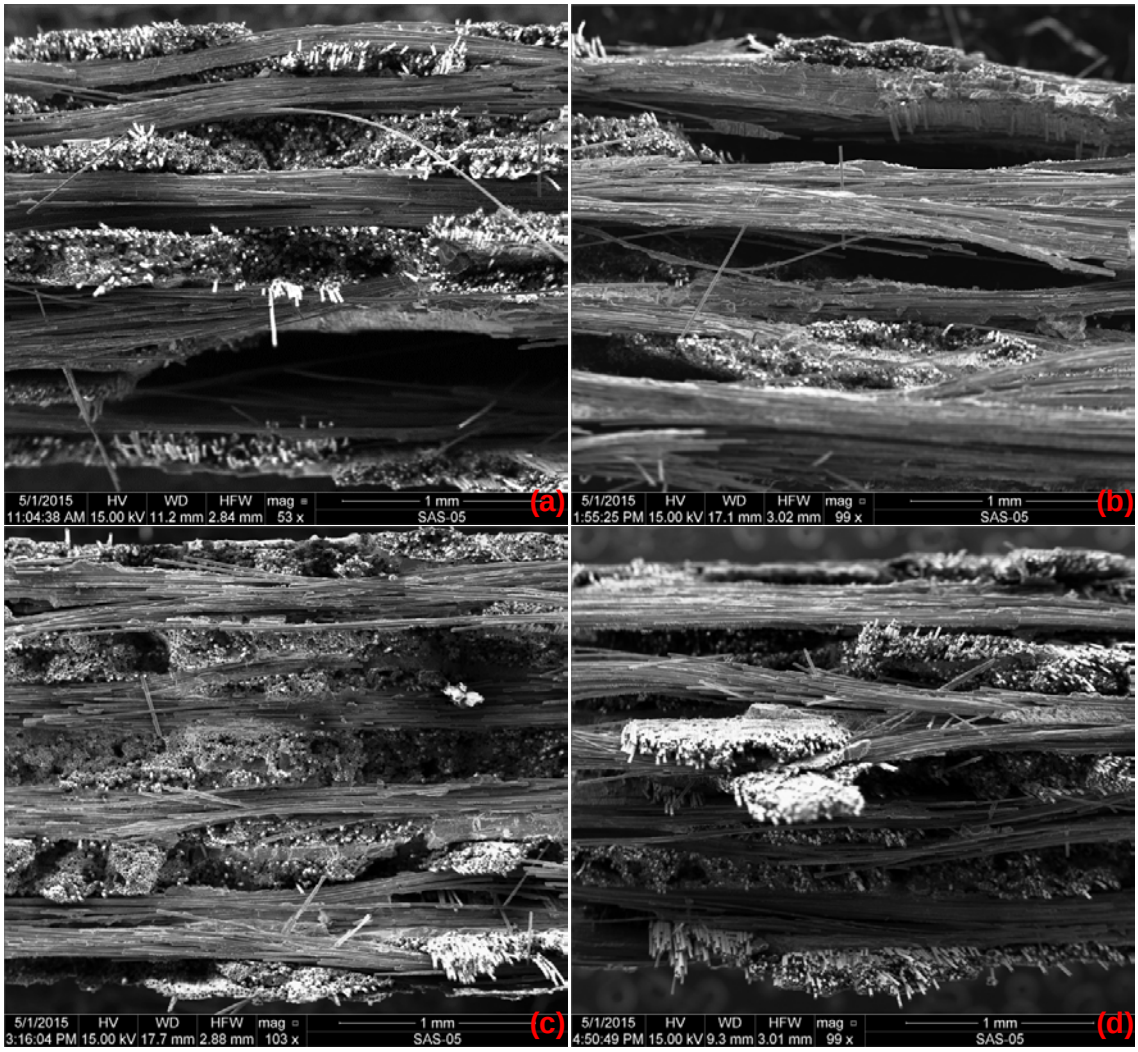

Figure 42: SEM micrographs of fracture surfaces obtained in tensile tests of Hi-Nicalon™/SiNC – (a) virgin specimen; and specimens exposed for (b) 10 h at 1300°C; (c) 100 h at 1300°C; and (d) 100 h at 1200°C

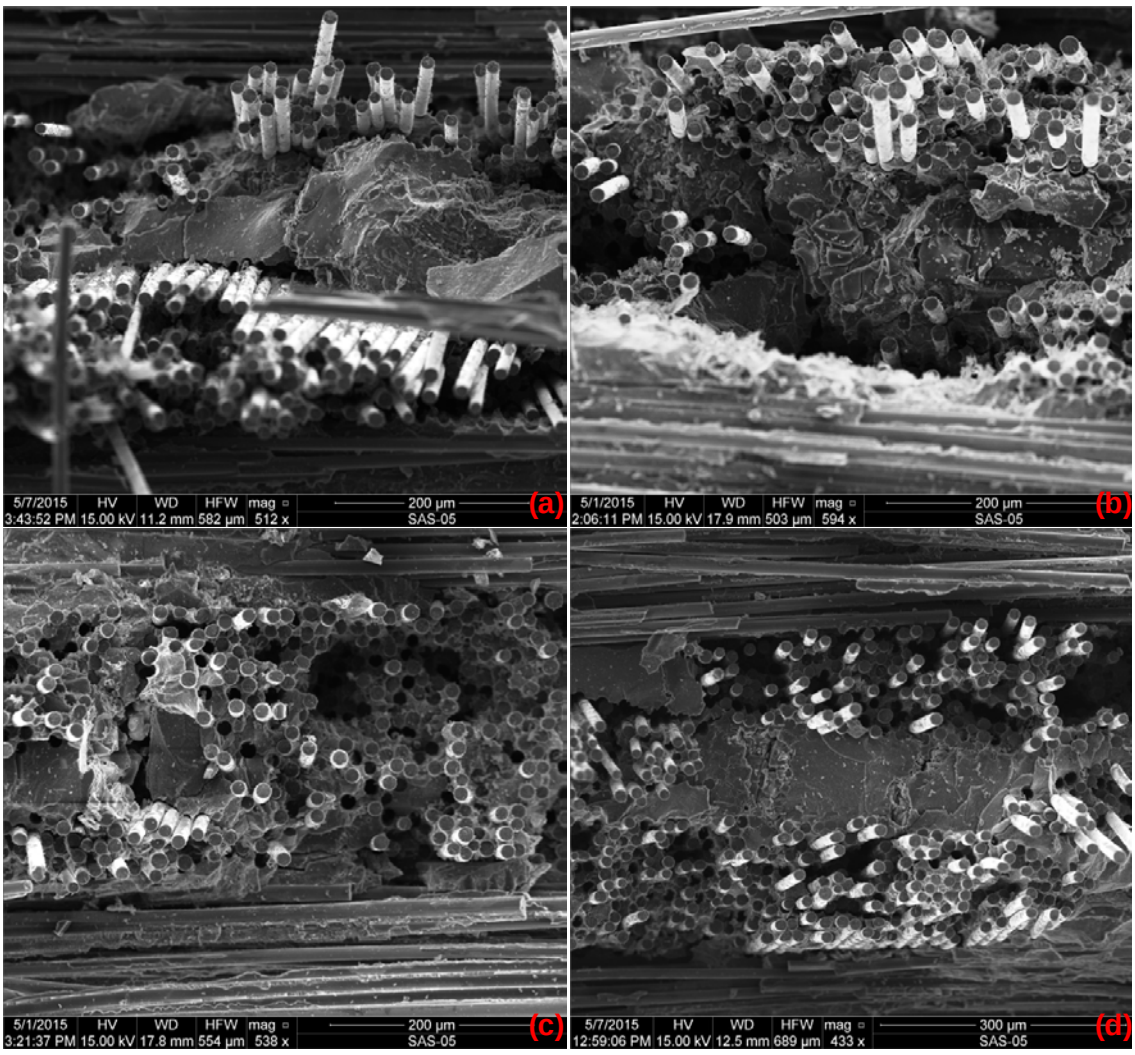

Figure 43: Higher magnification SEM micrographs of fracture surfaces obtained in tensile tests of Hi-Nicalon™/SiNC. Correlation of exposure duration and temperature to degree of planar fracture is visible. (a) virgin specimen; (b) 10 h at 1300°C; (c) 100 h at 1300°C; and (d) 100 h at 1200°C

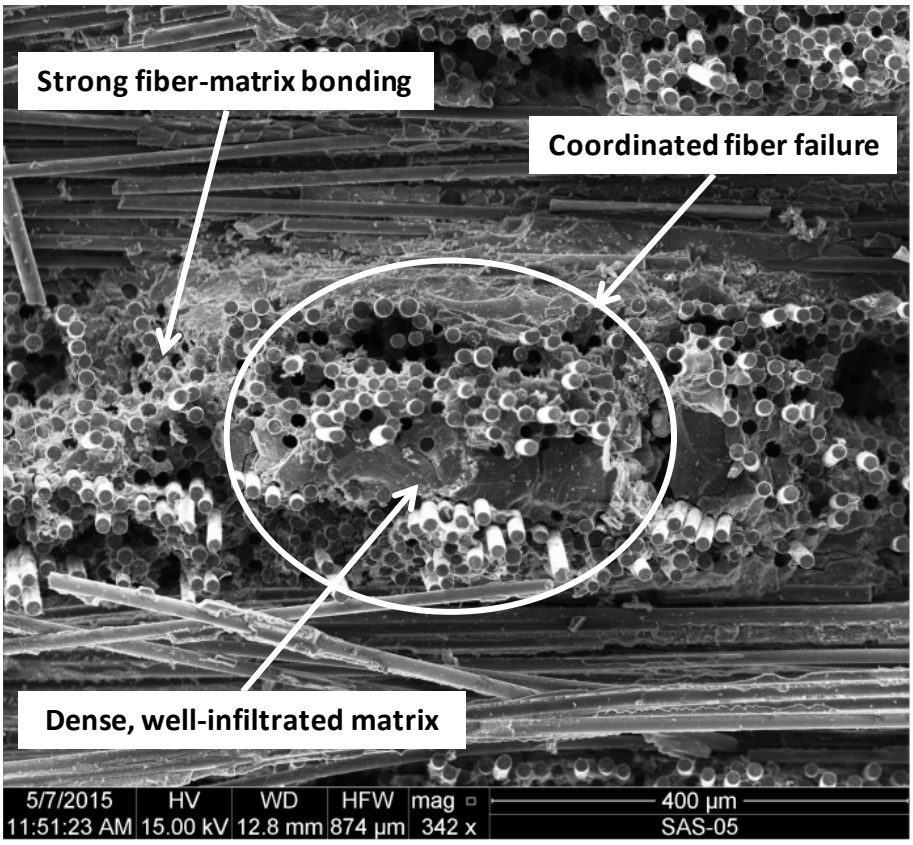

Figure 44: Higher magnification SEM micrograph of fracture surface obtained in tensile test of Hi-Nicalon™/SiNC specimen heat treated for 100 h at 1300°C. Coordinated fiber fracture, strong fiber-matrix bonding, and a dense, well-infiltrated matrix are visible.

5.4.2 HexTow® IM7/SiC (C/SiC) Composite – SEM Examination

SEM micrographs of fracture surfaces obtained in tension tests of the C/SiC specimens are shown in Figure 45: (a) as-received; (b) 40 h at 1300°C; (c) 100 h at 1300°C; (d) 100 h at 1200°C. All specimens are characterized by stepwise fracture surfaces. At this lower magnification, it is readily seen that the number of levels and depth of each level on the fracture surface varies from exposure to exposure. The virgin specimen and the specimen exposed to prior heat treatment for 40 h at 1300°C each exhibit numerous different levels, indicative of a less

coordinated and more graceful failure of the composite. On the other hand, both specimens heat treated for 100 h (at 1300°C and 1200°C) exhibit fracture surfaces with roughly 2-3 distinct levels. These levels are distinguished by significant changes in depth. The fewer distinct levels, or planes of fracture, indicate a more concerted and thus more brittle failure of the composite after a long-duration heat treatment. Higher magnification micrographs in Figure 46 allow further investigation of the variation in failure mechanisms between different time-temperature histories.

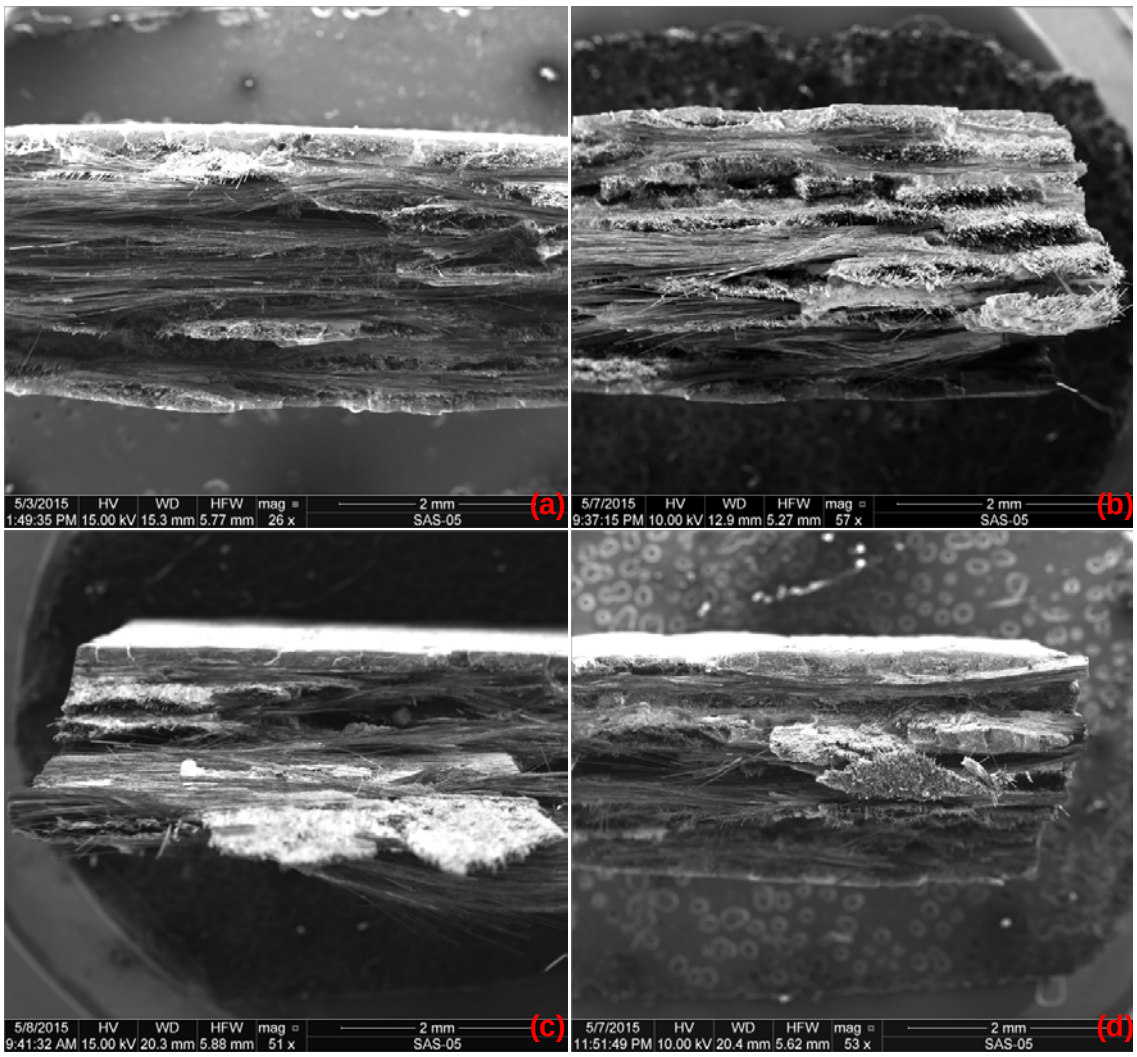

Figure 45: SEM micrographs of fracture surfaces obtained in tensile tests of C/SiC – (a) virgin specimen; and specimens exposed for (b) 40 h at 1300°C; (c) 100 h at 1300°C; and (d) 100 h at 1200°C

Figure 46(a) and Figure 46(b) show the fracture surface of the virgin specimen and the specimen that was heat treated for 40 h at 1300°C, respectively. As noted above, the fracture surface of both specimens exhibits failure on several different planes perpendicular to the loading direction. There are clear matrix rich areas as well as distinct regions of fiber bundle pullout and pullout of individual fibers. Fiber-matrix bonding is slightly more pronounced in

the 40 h specimen. Individual fiber and fiber bundle pullout in conjunction with the multiple different planes of failure indicate excellent crack deflection of the composite and a graceful failure mode. These conclusions are consistent with those presented in Section 5.3.2 for optical microscopy.

Figure 46(c) and Figure 46(d) show the fracture surface of the specimens heat treated for 100 h at 1300°C and 1200°C, respectively. Though similar to the previous two specimens in that failure was not restricted to one plane, these two fracture surfaces exhibit some distinct differences. Both specimens exhibit aggressive fiber-matrix bonding and pullout of large clumps of bonded fibers. The fiber bundles are dominated by coordinated fiber fracture, with negligible pullout of individual fibers. The degree of fiber-matrix bonding and the prevalence of planar fracture are greater in the specimen exposed at operating temperature (1200°C) than in the specimen exposed at 100°C over-temp. Additionally, while the planes of the 1200°C specimen fracture surface do vary in depth, there is a notably abrupt change in depth exhibited by the 1300°C specimen. This abrupt change is indicative of unobstructed crack growth in the longitudinal direction and ply delamination. This observation is consistent with conclusions made in Section 5.3.2, and provides explanation for the slightly (~3%) higher strength retention of the specimen exposed at 1200°C despite the more aggressive fiber-matrix bonding and more pronounced planar fracture.

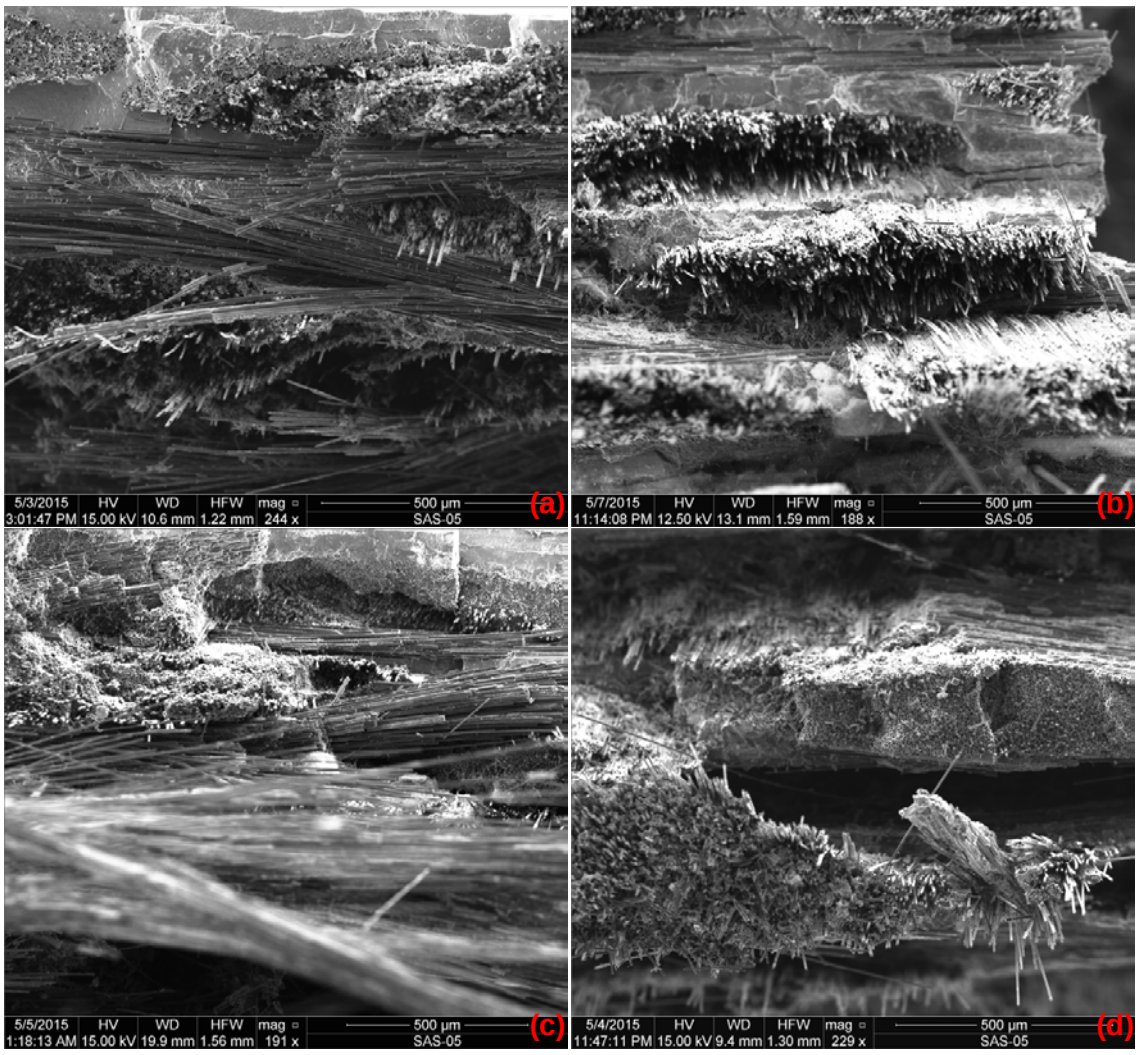

Figure 46: Higher magnification SEM micrographs of fracture surfaces obtained in tensile tests of C/SiC. Progression of fiber-matrix bonding and coordinated fiber fracture is visible. (a) virgin specimen; (b) 40 h at 1300°C; (c) 100 h at 1300°C; and (d) 100 h at 1200°C

A higher magnification micrograph (Figure 47) of the C/SiC composite shows good matrix infiltration into the woven fabric, similar to the Hi-Nicalon™/SiNC composite – the other PIP-processed CMC examined in this research. Good matrix infiltration produces a highly dense composite. Because non-oxide CMCs rely on a highly dense matrix to help prevent fiber oxidation, a weak fiber-matrix interface is key in providing crack deflection and fiber pullout mechanisms for the

composite. With these mechanisms present and functioning, the composite will fail gracefully. As substantiated by the strength retention results presented in Section 5.2, the damage mechanisms necessary for graceful composite failure were degraded with prior heat treatment at temperatures consistent with as well as above recommended operating temperature.

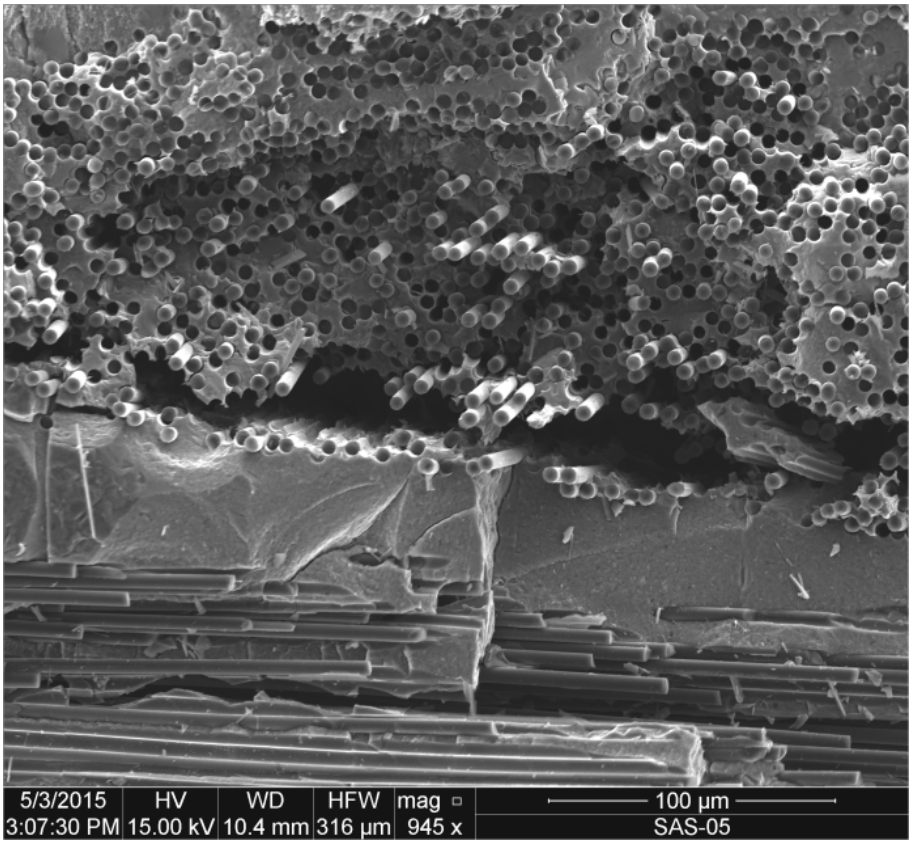

Figure 47: Higher magnification SEM micrograph of fracture surface obtained in tensile test of C/SiC virgin specimen. The PIP-produced composite exhibits a dense, well-infiltrated matrix.

5.4.3 T300/SiC-B_4C (C/HYPR-SiC™) Composite – SEM Examination

SEM micrographs of fracture surfaces obtained in tension tests of the C/HYPR-SiC™ specimens are shown in Figure 48: (a) as-received; (b) 40 h at 1300°C; (c) 100 h at 1300°C; (d) 100 h at 1200°C. The stepwise fracture surface

of the virgin specimen indicates that failure of different plies of the composite occurred as distinct events. Pullout of fiber bundles is prevalent. The fiber bundles exhibit nearly planar fracture surfaces with very little evidence of individual fiber pullout. The fracture surface of the specimen that was heat treated for 40 h at 1300°C indicates a more concerted failure of plies with isolated occurrences of fiber bundle pullout. Again, the fiber bundles exhibit a nearly planar fracture surface with very little evidence of individual fiber pullout. The specimen that was subjected to prior heat treatment for 100 h at 1300°C has a fracture surface dominated planar fracture. The plies of the composite failed nearly in concert, indicating a more brittle failure mode. The fracture surface of the specimen that was subjected to heat treatment for 100 h at 1200°C exhibits a combination of nearly planar fracture and fiber bundle pullout.

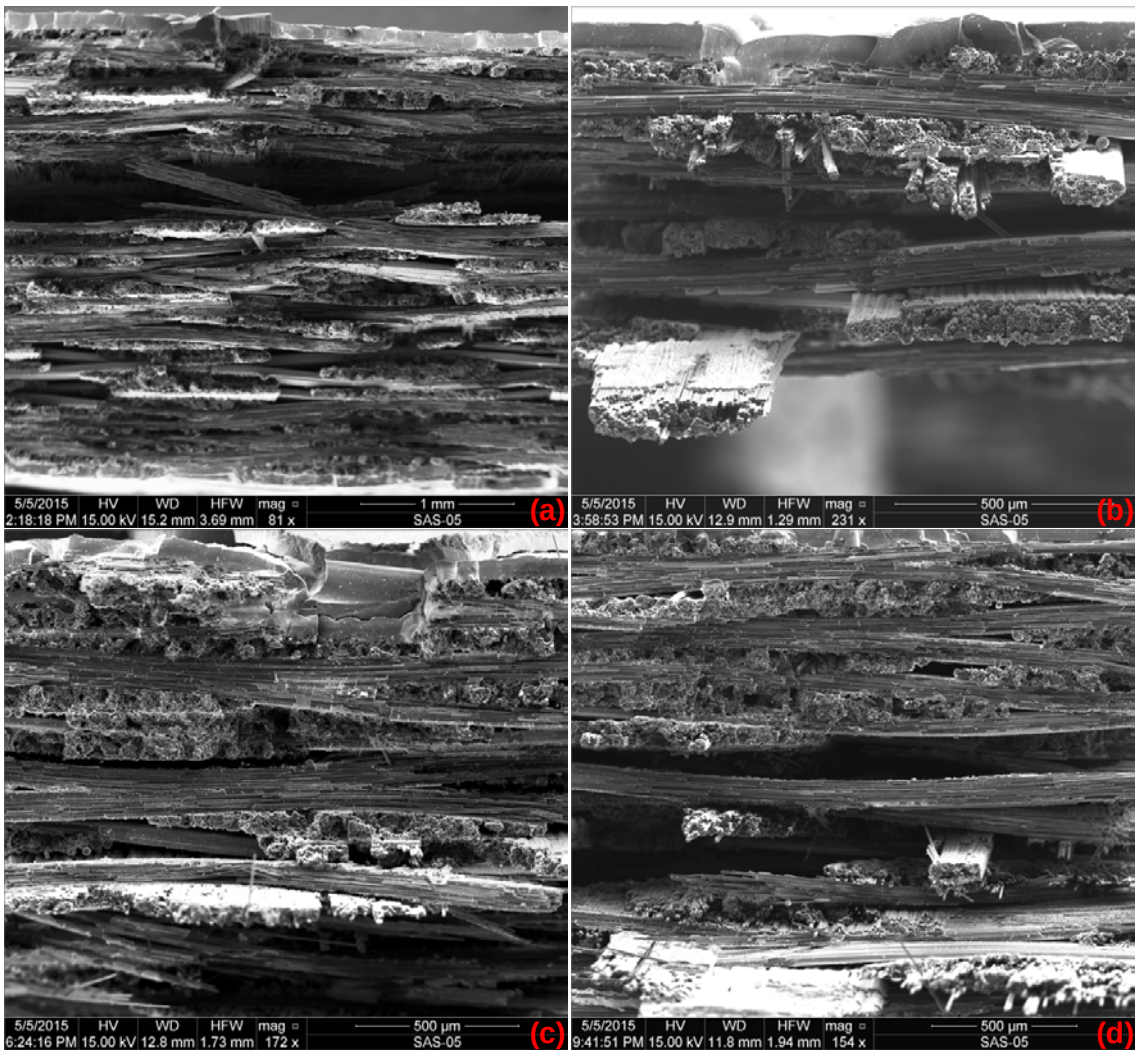

Figure 48: SEM micrographs of fracture surfaces obtained in tensile tests of C/HYPR-SiC™ – (a) virgin specimen; and specimens exposed for (b) 40 h at 1300°C; (c) 100 h at 1300°C; and (d) 100 h at 1200°C

Higher magnification micrographs are shown in Figure 49. Note that the correlation of prior heat treatment duration and temperature to degree of planar fracture is readily visible. As is consistent with strength results presented in Section 5.2, the toughening mechanisms of the composite are degraded with increased durations of exposure at 100°C over-temp. Planar fracture is least prevalent in the virgin specimen and most prevalent in the specimen subjected to

heat treatment for 100 h at over-temp. As mentioned above and as indicated by Figure 48 and Figure 49, the specimen that was heat treated for 100 h at operating temperature exhibited more fiber bundle pullout and less planar fracture than the specimen exposed for 100 h at over-temp. However, it must be noted that this observation is inconsistent with strength retention results in Section 5.2. The specimen subjected to heat treatment at recommended operating temperature retained 10% less strength than the specimen exposed for the same duration at 100°C over-temperature (79% versus 89%). This anomalous behavior was hypothesized earlier to be a consequence of poor matrix infiltration during composite fabrication.

As can be seen in Figure 50(b), SEM microscopy reveals that the 1200°C composite indeed exhibits areas of poor matrix infiltration. Poor matrix infiltration results in a matrix that is less dense than desirable and is riddled with voids. Voids in the matrix are irregular in shape and introduce stress concentrations within the matrix where they would not otherwise occur. These stress concentrations can result in premature matrix cracking and in turn, premature composite failure. The earlier hypothesis made regarding the anomalous decrease in strength of the composite exposed at operating temperature is further substantiated by examination of the microstructure at higher magnification (Figure 50). The images reveal matrix voids that are larger and more pervasive in that specimen when compared to the specimen exposed for 100 h at over-temp (Figure 50a).

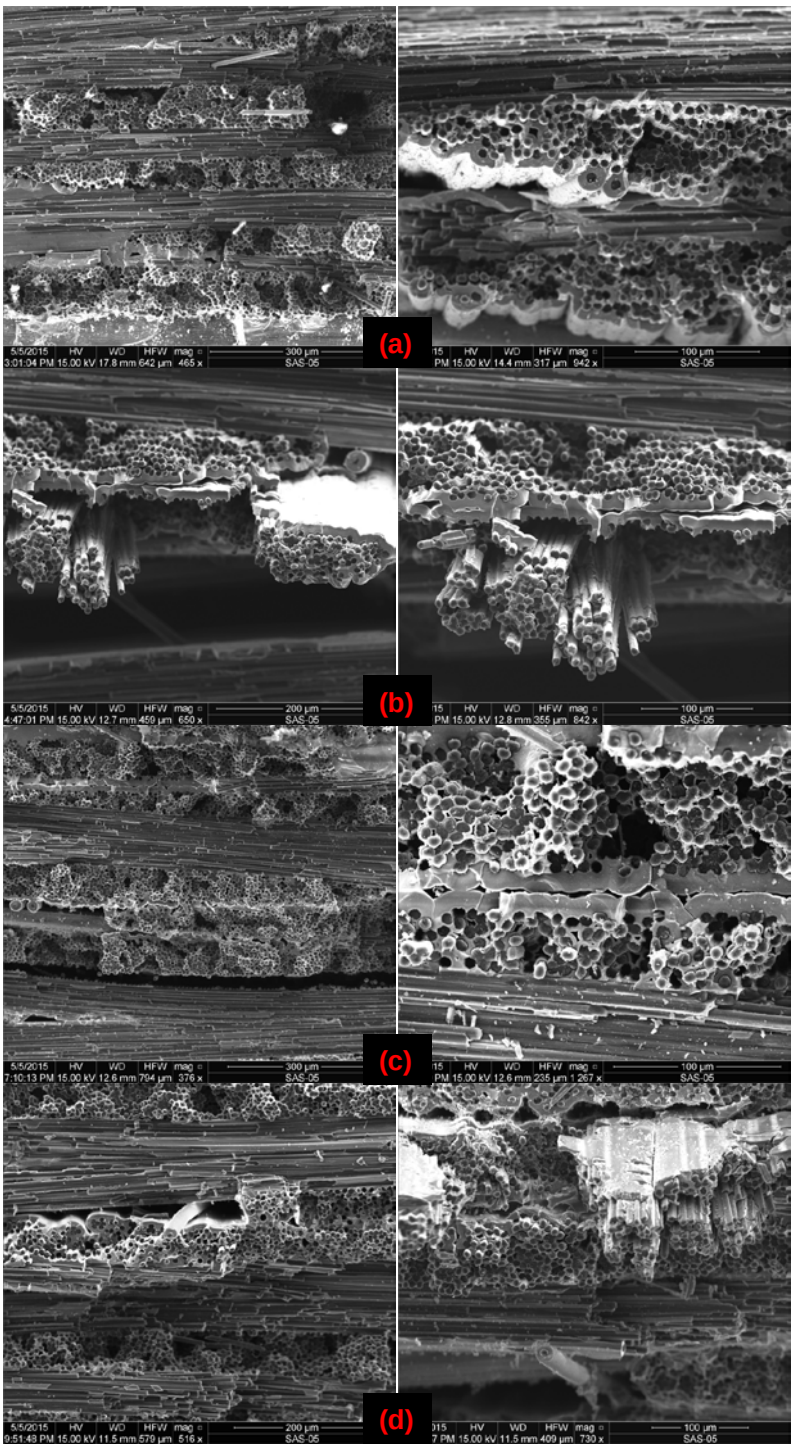

Figure 49: Higher magnification SEM micrographs of fracture surfaces obtained in tensile tests of C/HYPR-SiC™. Correlation of exposure duration and temperature to degree of planar fracture is visible. (a) virgin specimen; (b) 40 h at 1300°C; (c) 100 h at 1300°C; and (d) 100 h at 1200°C

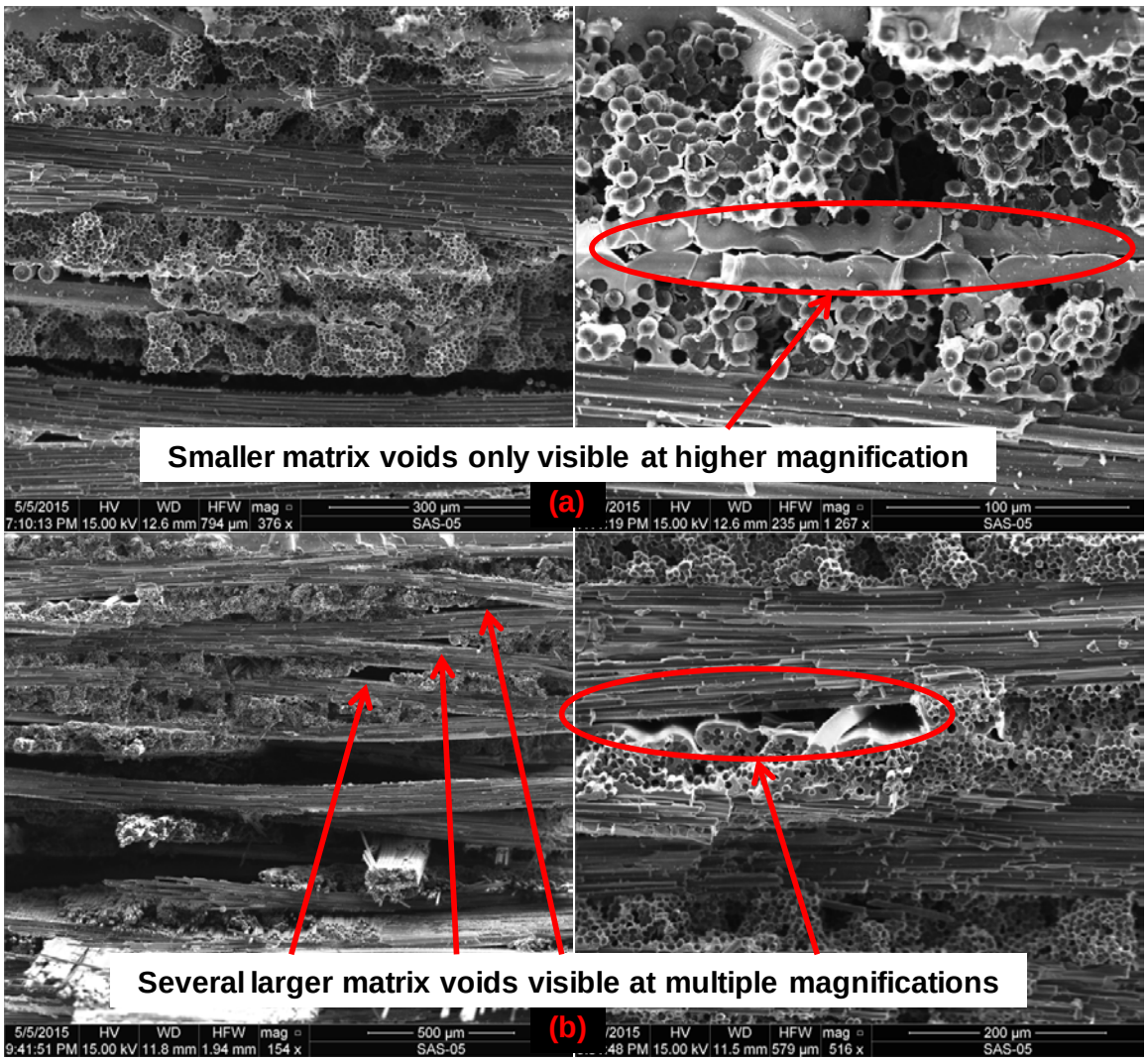

Figure 50: SEM micrographs indicating the difference in prevalence of matrix voids between two C/HYPR-SiC™ specimens – (a) 100 h at 1300°C and (b) 100 h at 1200°C.

5.4.4 Hi-Nicalon™/SiC-B_4C (Hi-Nicalon™/HYPR-SiC™) Composite – SEM Examination

SEM micrographs of fracture surfaces obtained in tension tests of the Hi-Nicalon™/HYPR-SiC™ specimens are shown in Figure 51: (a) as-received; (b) 10 h at 1400°C; (c) 100 h at 1400°C; (d) 100 h at 1300°C. It must first be noted that all fracture surfaces exhibit one stark similarity: fiber bundles are

encased with a thick layer of matrix material. This characteristic is equally prevalent among all specimens and does not vary in degree.

The virgin specimen exhibits a stepwise and non-planar fracture surface. Failure at different locations on every ply is evident. Pullout of fiber bundles and individual fibers dominates the fracture surface. The fracture surface indicates desired composite behavior and graceful failure of the specimen. The fracture surface of the specimen that was heat treated for 10 h at 1400°C exhibits a far more planar fracture. Pullout of individual fibers is also readily visible, though not dominant. The white string-like materials are fibers that have pulled-out to a significant length. At the base from which fibers have pulled-out there is a very planar fracture surface. As is readily seen in Figure 51(b), some of the pulled-out fibers are uncharacteristically long while others are more normal in length, and yet there are other fibers that have not been pulled out at all but rather fractured in-plane with the surrounding matrix (Figure 52). This specimen fractured in a brittle fashion, dominated by planar fracture of the composite matrix. Fiber pullout appears to be secondary and of little significance to the brittle failure mode, as the fracture is evidenced to have propagated through the matrix, then around and also directly through the fibers.

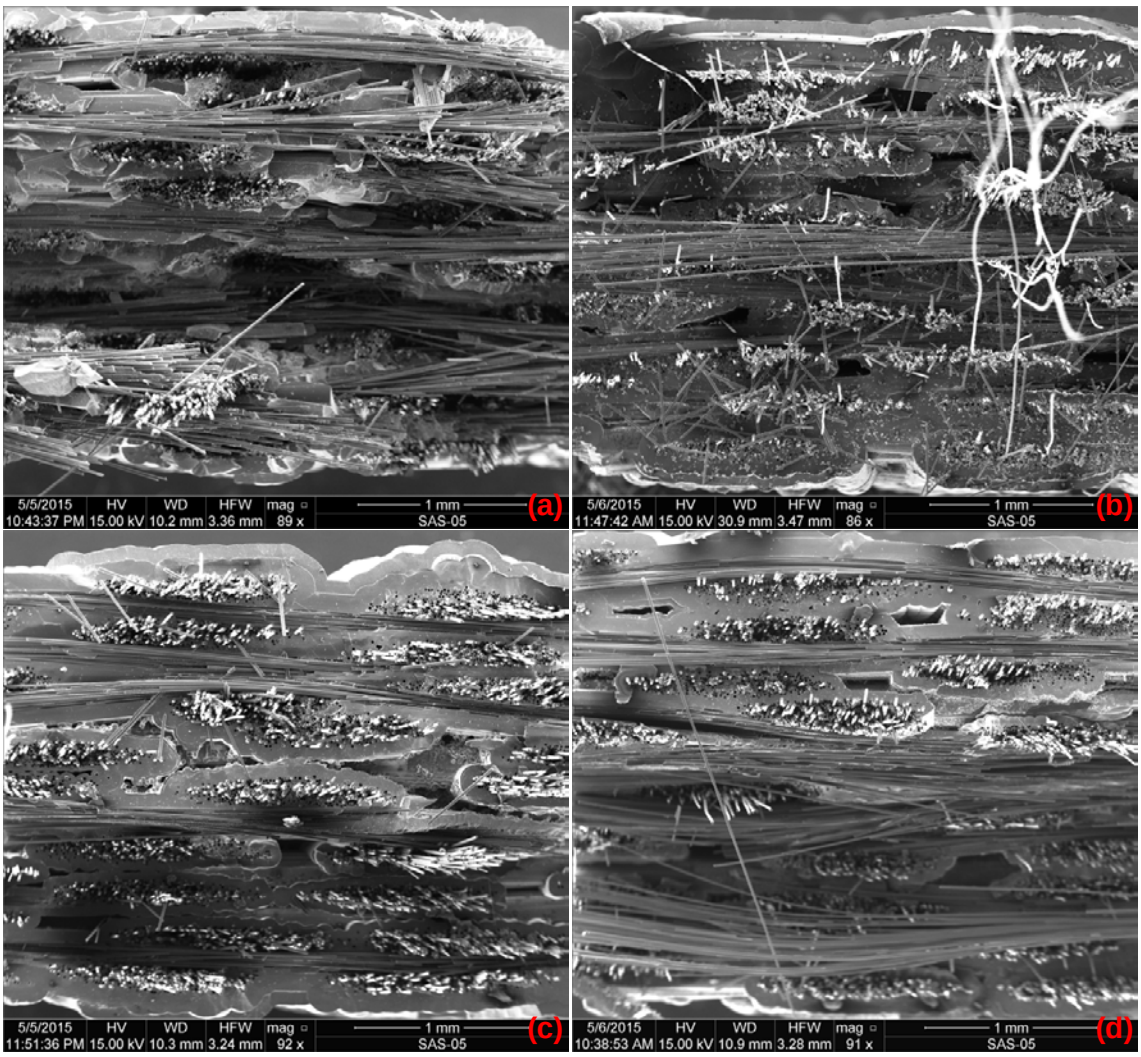

Figure 51: SEM micrographs of fracture surfaces obtained in tensile tests of Hi-Nicalon™/HYPR-SiC™ – (a) virgin specimen; and specimens exposed for (b) 10 h at 1400°C; (c) 100 h at 1400°C; and (d) 100 h at 1300°C

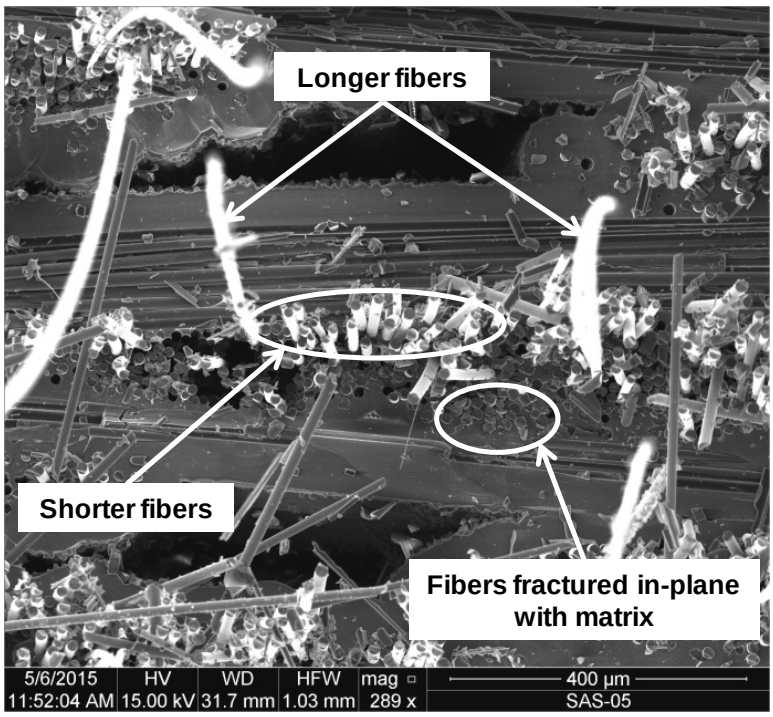

Figure 52: Higher magnification SEM micrograph of Hi-Nicalon™/HYPR-SiC™ specimen heat treated for 10 h at 1400°C. Planar matrix fracture and variation in fiber failure behavior is readily visible.

The fracture surface of the specimen exposed for 100 h at 1400°C (Figure 51c) is dominated by planar fracture of matrix rich regions and pullout of fiber bundles that are surrounded by these regions. Pullout of individual fibers is visible but not prevalent. Further, the fracture surface consists of at least 2-3 planar regions, each located at different depths along the longitudinal axis of the specimen. The specimen exhibited undesirable composite behavior, fracturing in a brittle failure mode. The specimen subjected to prior heat treatment for 100 h at 1300°C exhibits a fracture surface very similar to that of the specimen exposed for 100 h at 1400°C. Matrix rich regions exhibit planar fracture, and fiber bundles that are surrounded by the matrix rich regions exhibit bundle pullout, with minimal pullout of individual fibers.

The above observations are consistent with those of the optical microscopy as well as the results presented in Section 5.2. The strength retention results presented indicate a drastic decrease in composite performance after just 10 hours of prior heat treatment at 100°C over-temperature. Following the drastic decrease, strength retention remained nearly constant for increased exposure times from 20 to 100 h at over-temp, as well as for 100 h at operating temperature.

A possible explanation for this behavior is embrittlement of the Hi-Nicalon™ fibers in conjunction with strengthening of the fiber-matrix interface caused by exposure to temperatures at 1400°C for a duration of 10 hours or more, or to 1300°C for a longer, 100 hour duration. A strong fiber-matrix interface hinders the desired fiber-matrix debonding and fiber pullout from occurring, and when fibers have become embrittled, instead of deflecting a growing crack and providing a mechanism for load transfer, the fibers will easily fracture, allowing the crack to propagate straight through them. Higher magnification micrographs in Figure 53 show fracture surfaces of an as-received and a heat treated specimen for comparison. The desired fiber pullout and graceful composite failure is exhibited by the virgin specimen on the left. The image on the right illustrates behavior indicative of a strong fiber-matrix interface, fiber embrittlement, and a more planar fracture that occurs as a result of prior heat treatment of the Hi-Nicalon™/ HYPR-SiC™ CMC.

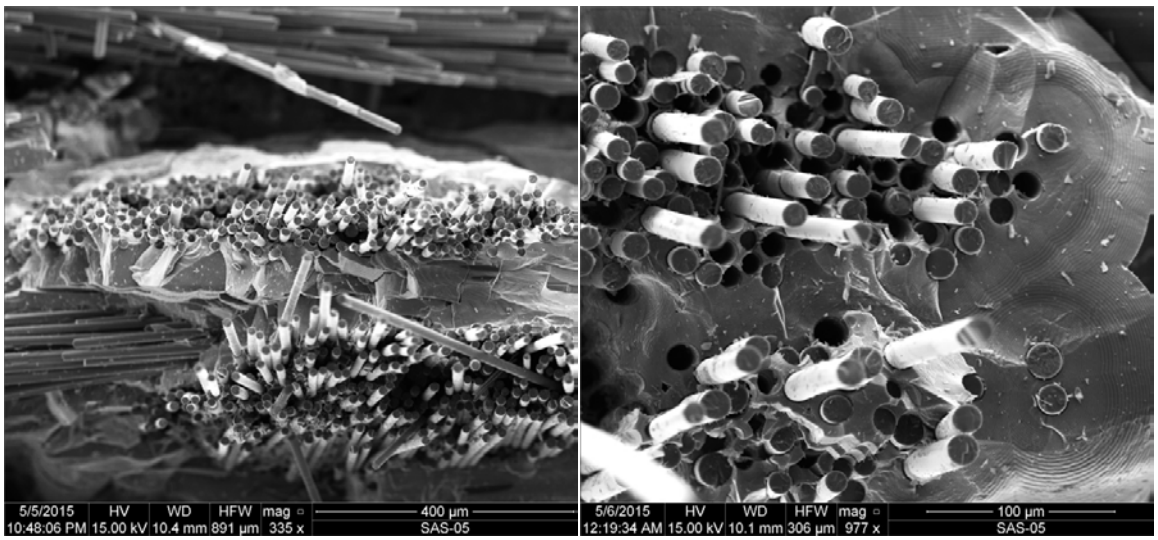

Figure 53: Higher magnification SEM micrographs of fracture surfaces of two Hi-Nicalon™/HYPR-SiC™ specimens – as-received (left); and heat treated for 100 h at 1400°C (right). A shift from fiber-dominated (left) to matrix-dominated fracture (right) is readily visible.

VI. Conclusions and Recommendations

This research effort investigated the effect of different time-temperature histories on the tensile behavior of four non-oxide ceramic matrix composites: Hi-Nicalon™/SiNC; C/SiC; C/SiC-B_4C; and Hi-Nicalon™/SiC-B_4C. The first two composites listed were manufactured via PIP and the last two were manufactured via CVI. The SiC-B_4C matrix material (trade name HYPR-SiC™) consists of alternating layers of SiC and B_4C produced with alternating CVI runs. Every material system was subjected to 5 prescribed time-temperature histories. The Hi-Nicalon™/SiNC, C/SiC, and C/SiC-B_4C CMCs were heat treated in laboratory air for 10 h, 20 h, 40 h, and 100 h at 1300°C and for 100 h at 1200°C. The Hi-Nicalon™/SiC-B_4C composite was heat treated in laboratory air for 10 h, 20 h, 40 h, and 100 h at 1400°C and for 100 h at 1300°C. Room-temperature tensile properties of heat treated materials were measured by conducting uniaxial monotonic tension tests to failure. Virgin material was also tested to establish baseline properties. The effects of prior heat treatment on tensile properties and stress-strain behavior were then evaluated.

Prior heat treatment caused an overall decrease in tensile strength of all composites. The C/HYPR-SiC™ composite performed best in overall strength retention with an 11% loss of tensile strength following heat treatment at over-temp (1300°C) for 100 h. A more significant loss of about 21% of tensile strength occurred after prior heat treatment for 100 h at operating temperature (1200°C). This anomalous exhibition of significant loss of tensile strength after heat treatment at a temperature 100°C lower is attributed to poor matrix infiltration

during CVI processing, resulting in a prevalence of matrix voids that contribute to unwanted stress concentrations and premature crack growth and fracture.

Heat treatment at both operating temperature (1300°C) and over-temp (1400°C) caused a dramatic loss of tensile strength of the Hi-Nicalon™/HYPR-SiC™ composite – 32% after only 10 h exposure at over-temp. The poor strength retention is attributed to strengthening of the fiber-matrix interface and embrittlement of the Hi-Nicalon™ fibers caused by the high-temperature exposures. The strong interface and embrittled fibers are conducive to a brittle fracture mode and thus degraded tensile performance of the composite.

Heat treatment at over-temp (1300°C) of the C/SiC CMC caused a moderate loss of retained tensile strength up to and including 40 h exposure duration (~92% retained tensile strength with 40 h exposure). Heat treatments of the C/SiC composite at both operating temperature (1200°C) and over-temp for 100 h caused a dramatic loss of about 25% of tensile strength. Poor strength retention after 100 h exposure times is attributed to aggressive fiber-matrix bonding and decreased fiber-matrix debonding as a result of the heat treatments.

Heat treatment at over-temp (1300°C) caused a gradual loss of tensile strength of the Hi-Nicalon™/SiNC composite with increased exposure times from 10 h (14% loss) to 20 h (17% loss). Beyond 20 h exposure time the Hi-Nicalon™/SiNC composite exhibited good thermal stability with a nearly constant 83% retention of tensile strength. The composite exhibited a nominal increase in retained tensile strength from heat treatment at over-temp for 100 h to operating temperature (1200°C) for 100 h.

With the exception of the Hi-Nicalon™/HYPR-SiC™ composite, all CMCs exhibited nearly constant elastic modulus over the range of time-temperature histories. Similar to strength retention performance, elastic modulus of the Hi-Nicalon™/HYPR-SiC™ composite decreased dramatically by about 50 GPa after only 10 h prior heat treatment at over-temp. This significant decrease is attributed to severe degradation of crack deflecting mechanisms when exposed to 1300°C or higher – e.g. strengthening of the fiber-matrix interface (diminished capability for fiber debonding and pullout) and fiber embrittlement.

First and foremost, repeatability of the results presented in this research should be established in future efforts. Particular emphasis should be placed on materials that exhibited unexpected or anomalous behavior. Hi-Nicalon™/HYPR-SiC™ is of great interest in this regard. It is recommended to further evaluate CMC tensile performance after prior exposure to operating temperature conditions for additional time durations – 10 h, 20 h, and 40 h. This will provide a better comparison of performance after exposure to operating temperature versus over-temperature environments.

Additionally, evaluation of composite performance when subjected to various environments (e.g. steam and combustion environments) should be established in future efforts. Tensile, fatigue, and creep testing of the materials while subjected to these environments is recommended. Also recommended is further microstructural characterization of the virgin and heat treated materials studied in this research. In addition to further examination using an SEM, a transmitting electron microscope (TEM), and/or Auger electron spectroscopy (AES) could be

used to more thoroughly asses material degradation of fibers, matrix, and fiber-matrix interface.

Appendix A: Plate Measurement and Density Calculation Procedures

Dimensions of all plates were measured using a Mitutoyo 0.01 mm resolution digital caliper. Length and width were measured in two locations, and thickness was measured in four locations (Plate dimension measurement locations).

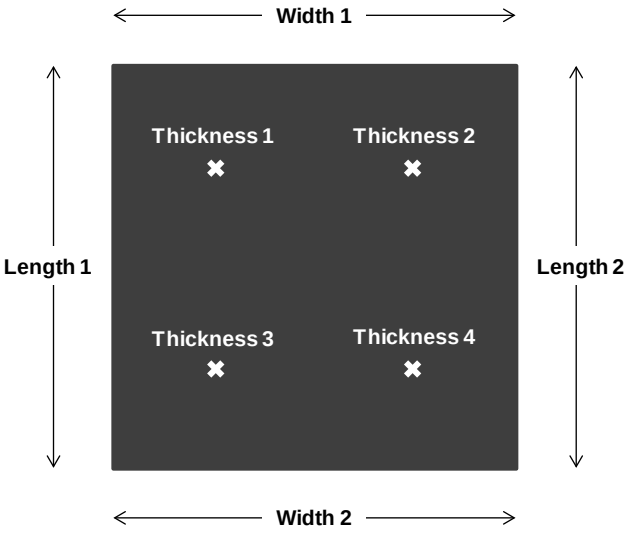

Figure A.1: Plate dimension measurement locations

Weights were measured with an Ohaus Pioneer Precision Balance model PA3102, 3100g x 0.01g digital scale. Weights were measured and recorded before and after plates were dried in the vacuum oven, and after subjection to the prescribed high temperature exposure. Plate dimensions were measured after drying and after prescribed high temperature exposure.

The measured values were used to calculate the mean length, width, and thickness for every plate. These values were multiplied to estimate plate volume. Plate mass was divided by volume to produce an estimated density for each

plate. This procedure was performed prior to and following all heat treatments. The measured and calculated values are presented in the following tables.

Table A.1: Plate measurements prior to heat treatment

		Length (mm)		*Width (mm)*		*Thickness (mm)*				*Weight (g)*	
Material	*Plate*	*1*	*2*	*1*	*2*	*1*	*2*	*3*	*4*	*Pre-Drying*	*Post-Drying*
Hi-Nicalon™/SiNC	11101	101.50	101.33	101.55	101.46	2.39	2.32	2.26	2.35	54.11	53.92
	11103	101.53	101.43	101.45	101.62	2.22	2.21	2.25	2.23	52.42	52.13
	11104	101.50	101.48	101.48	101.44	2.20	2.25	2.39	2.30	54.07	53.79
	11105	101.63	101.55	101.56	101.46	2.22	2.24	2.23	2.26	53.25	52.99
	11106	101.49	101.53	101.50	101.51	2.15	2.17	2.19	2.21	52.11	51.81
HexTow® IM7/SiC	12011	101.65	101.55	101.57	101.52	3.02	3.10	3.18	3.13	62.40	62.21
(C/SiC)	12019	101.66	101.57	101.56	101.52	2.99	2.95	2.95	2.93	62.14	61.98
	12018	101.80	101.76	101.70	101.55	2.89	2.94	2.95	2.95	60.96	60.76
	12015	101.63	101.61	101.51	101.53	3.01	3.01	2.96	2.98	61.51	61.32
	12016	101.69	101.61	101.56	101.60	2.94	2.93	2.91	2.95	60.96	60.75
T300/HYPR-SiC™	11117	102.84	102.37	102.96	102.33	3.06	3.00	3.08	3.03	60.53	60.30
(C/HYPR-SiC™)	11124	102.53	102.68	102.37	103.02	2.96	2.99	2.97	2.94	58.05	57.84
	11125	103.28	102.29	103.20	102.65	2.90	2.93	2.89	2.90	57.84	57.70
	11121	102.44	102.52	102.32	102.98	3.02	3.01	2.95	2.91	59.05	58.84
	11122	102.38	103.02	102.44	102.38	2.99	2.94	3.01	2.96	58.76	58.62
Hi-Nicalon™/HYPR-SiC™	11133	102.26	102.35	102.19	102.64	3.09	3.05	3.06	3.04	76.45	76.44
	11135	102.36	102.15	102.24	102.95	2.98	3.01	3.01	3.00	74.83	74.82
	11136	102.22	102.00	102.20	102.83	3.01	3.03	2.97	3.02	76.79	76.79
	11137	102.21	102.74	101.62	102.52	3.03	2.98	3.02	2.98	75.97	75.97
	11139	102.22	102.50	102.29	102.92	3.01	2.99	3.01	3.02	76.26	76.27

Table A.2: Calculated plate dimension averages and density prior to heat treatment

Material	*Plate*	*Mean Length (mm)*	*Mean Width (mm)*	*Mean Thickness (mm)*	*Dry Density (g/mm^3)*	*Dry Weight (g)*
Hi-Nicalon™/SiNC	11101	101.42	101.51	2.33	0.00225	53.92
	11103	101.48	101.54	2.23	0.00227	52.13
	11104	101.49	101.46	2.29	0.00229	53.79
	11105	101.59	101.51	2.24	0.00230	52.99
	11106	101.51	101.51	2.18	0.00231	51.81
HexTow® IM7/SiC	12011	101.60	101.55	3.11	0.00194	62.21
(C/SiC)	12019	101.62	101.54	2.96	0.00203	61.98
	12018	101.78	101.63	2.93	0.00200	60.76
	12015	101.62	101.52	2.99	0.00199	61.32
	12016	101.65	101.58	2.93	0.00201	60.75
T300/HYPR-SiC™	11117	102.61	102.65	3.04	0.00188	60.30
(C/HYPR-SiC™)	11124	102.61	102.70	2.97	0.00185	57.84
	11125	102.79	102.93	2.91	0.00188	57.70
	11121	102.48	102.65	2.97	0.00188	58.84
	11122	102.70	102.41	2.98	0.00187	58.62
Hi-Nicalon™/HYPR-SiC™	11133	102.31	102.42	3.06	0.00238	76.44
	11135	102.26	102.60	3.00	0.00238	74.82
	11136	102.11	102.52	3.01	0.00244	76.79
	11137	102.48	102.07	3.00	0.00242	75.97
	11139	102.36	102.61	3.01	0.00241	76.27

Table A.3: Plate measurements after heat treatment

		Length (mm)		*Width (mm)*		*Thickness (mm)*				*Weight (g)*	
Material	*Plate*	*1*	*2*	*1*	*2*	*1*	*2*	*3*	*4*	*Post-Drying*	*Post-Exposure*
Hi-Nicalon™/SiNC	11101	101.40	101.43	101.41	101.38	2.30	2.35	2.25	2.25	53.92	53.68
	11103	101.42	101.37	101.38	101.50	2.17	2.19	2.22	2.19	52.13	51.89
	11104	101.43	101.51	101.35	101.44	2.24	2.24	2.40	2.30	53.79	53.57
	11105	101.31	101.32	101.25	101.32	2.21	2.24	2.24	2.25	52.99	52.83
	11106	101.50	101.50	101.52	101.52	2.16	2.17	2.18	2.21	51.81	51.62
HexTow® IM7/SiC	12011	101.71	101.58	101.61	101.52	2.97	2.98	2.98	2.93	62.21	61.73
(C/SiC)	12019	101.55	101.50	101.51	101.50	2.94	2.95	2.95	2.92	61.98	60.68
	12018	101.75	101.62	101.68	101.56	2.94	2.95	2.93	2.93	60.76	59.20
	12015	101.66	101.55	101.43	101.46	2.96	2.95	2.94	2.92	61.32	58.77
	12016	101.67	101.63	101.57	101.42	2.93	2.87	2.89	2.91	60.75	58.16
T300/HYPR-SiC™	11117	102.74	102.37	102.99	102.29	3.01*	2.89*	2.92*	2.95*	60.30	60.45
(C/HYPR-SiC™)	11124	102.54	102.68	102.40	103.02	3.00*	2.91*	2.94*	2.84*	57.84	58.00
	11125	103.25	102.28	103.19	102.64	2.90*	2.97*	2.99*	2.82*	57.70	57.55
	11121	102.47	102.50	102.35	103.07	2.98*	3.00*	2.98*	2.94*	58.84	59.14
	11122	102.40	103.04	102.47	102.45	3.01*	3.12*	3.06*	3.00*	58.62	58.74
Hi-Nicalon™/HYPR-SiC™	11133	102.27	102.33	102.15	102.65	3.10	3.06	3.04	3.07	76.44	76.48
	11135	102.30	102.10	102.15	102.90	3.00	2.98	2.95	3.01	74.82	74.88
	11136	102.15	101.93	102.10	102.75	3.01	3.01	2.98	2.99	76.79	76.84
	11137	102.15	102.70	101.52	102.47	2.97	3.02	2.97	3.01	75.97	76.07
	11139	102.26	102.45	102.19	102.88	3.01	3.03	3.00	3.01	76.27	76.38

* Plate blistering occurred during exposure. To avoid blistered regions, thickness measurements had to be taken in locations not completely consistent with those taken prior to exposure.

Table A.4: Calculated plate dimension averages and density after heat treatment

Material	*Plate*	*Mean Length (mm)*	*Mean Width (mm)*	*Mean Thickness (mm)*	*Density (g/mm^3)*	*Weight (g)*
Hi-Nicalon™/SiNC	11101	101.42	101.40	2.29	0.0023	53.68
	11103	101.40	101.44	2.19	0.0023	51.89
	11104	101.47	101.40	2.30	0.0023	53.57
	11105	101.32	101.29	2.24	0.0023	52.83
	11106	101.50	101.52	2.18	0.0023	51.62
HexTow® IM7/SiC	12011	101.65	101.57	2.97	0.0020	61.73
(C/SiC)	12019	101.53	101.51	2.94	0.0020	60.68
	12018	101.69	101.62	2.94	0.0020	59.20
	12015	101.61	101.45	2.94	0.0019	58.77
	12016	101.65	101.50	2.90	0.0019	58.16
T300/HYPR-SiC™	11117	102.56	102.64	2.94*	0.0020	60.45
(C/HYPR-SiC™)	11124	102.61	102.71	2.92*	0.0019	58.00
	11125	102.77	102.92	2.92*	0.0019	57.55
	11121	102.49	102.71	2.98*	0.0019	59.14
	11122	102.72	102.46	3.05*	0.0018	58.74
Hi-Nicalon™/HYPR-SiC™	11133	102.30	102.40	3.07	0.0024	76.48
	11135	102.20	102.53	2.99	0.0024	74.88
	11136	102.04	102.43	3.00	0.0025	76.84
	11137	102.43	102.00	2.99	0.0024	76.07
	11139	102.36	102.54	3.01	0.0024	76.38

* Plate blistering occurred during exposure. To avoid blistered regions, thickness measurements had to be taken in locations not completely consistent with those taken prior to exposure.

Appendix B: Pre- and Post-Exposure Plate Images

Figure B.1: Hi-Nicalon™/SiNC –
Virgin plate 11107 (left);
10h 1300°C exposure plate 11101 (right).
Exposed plate exhibits discoloration.

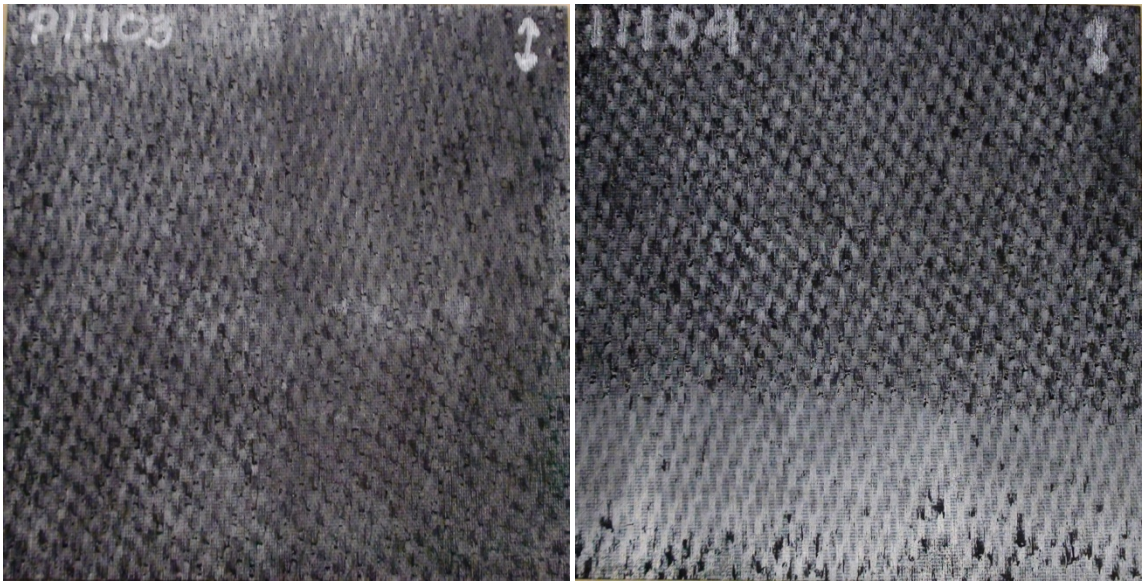

Figure B.2: Hi-Nicalon™/SiNC –
20h 1300°C exposure plate 11103 (left);
40h 1300°C exposure plate 11104 (right).
Exposed plates exhibit discoloration.

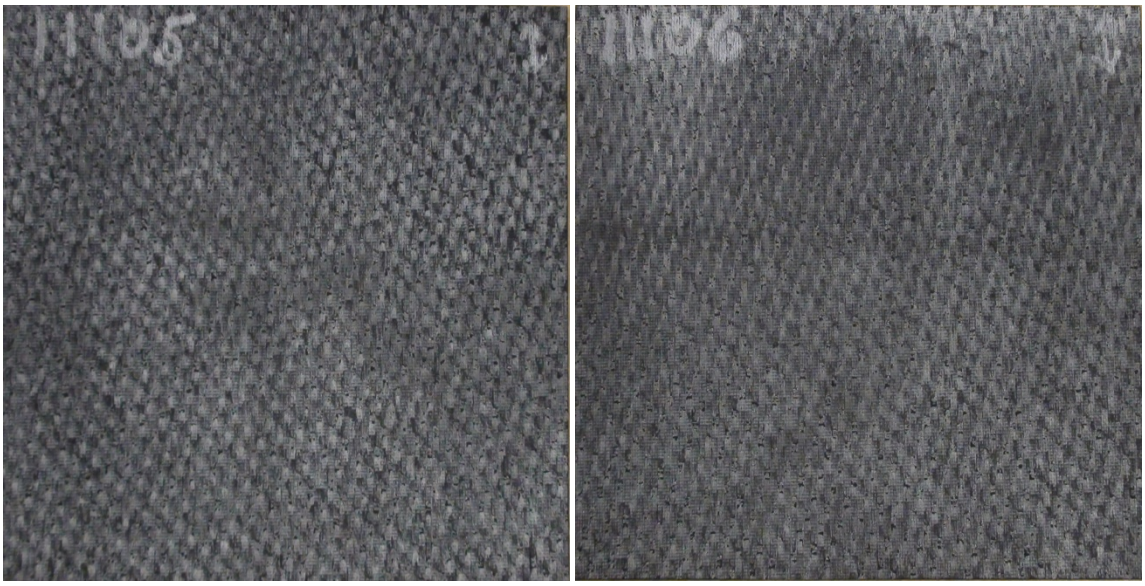

Figure B.3: Hi-Nicalon™/SiNC –
100h 1300°C exposure plate 11105 (left);
100h 1200°C exposure plate 11106 (right).
Exposed plates exhibit discoloration.

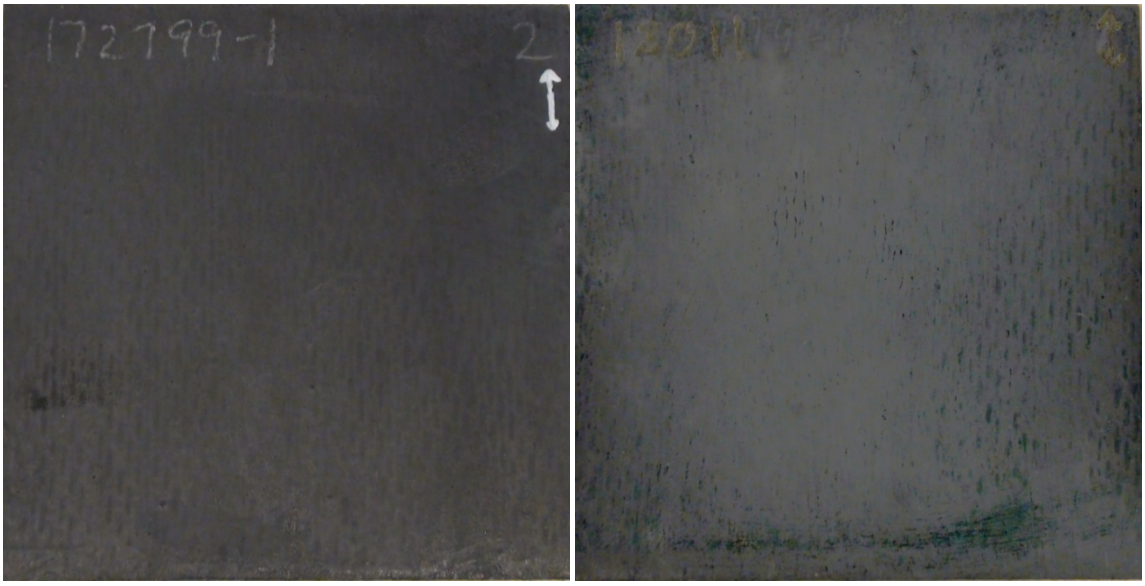

Figure B.4: HexTow® IM7/SiC –
Virgin plate 12012 (left);
10h 1300°C exposure plate 12011 (right).
Exposed plate exhibits discoloration.

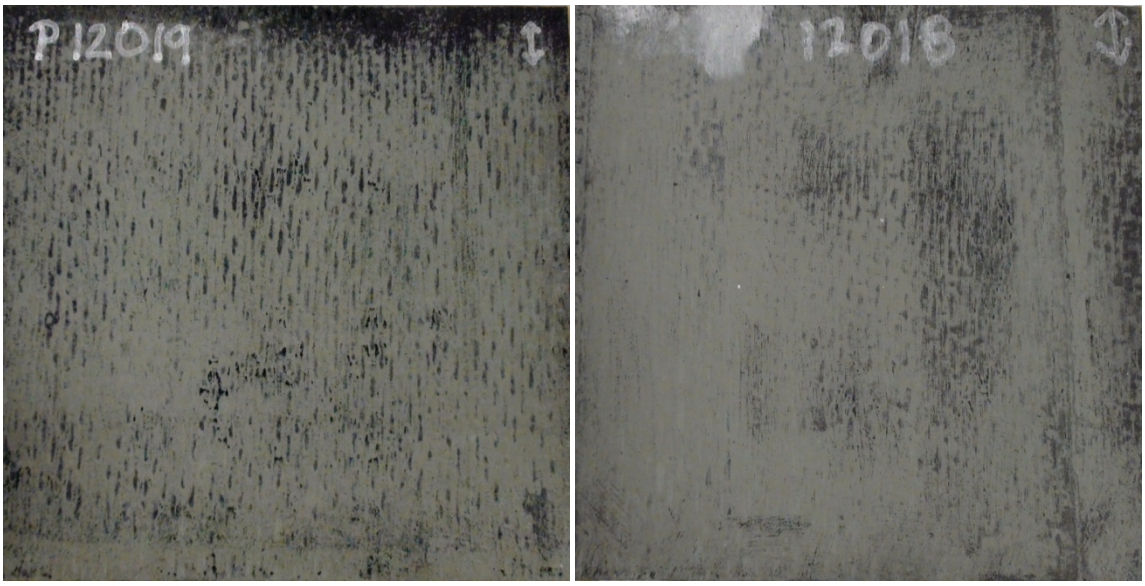

Figure B. 5: HexTow® IM7/SiC –
20h 1300°C exposure plate 12019 (left);
40h 1300°C exposure plate 12018 (right).
Exposed plates exhibit discoloration.

Figure B.6: HexTow® IM7/SiC –
100h 1300°C exposure plate 12015 (left);
100h 1200°C exposure plate 12016 (right).
Exposed plates exhibit discoloration.

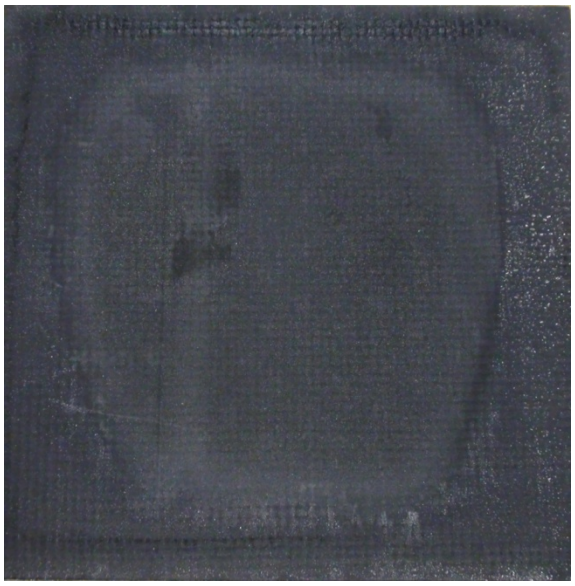

Figure B.7: T300/HYPR-SiC™ – Virgin plate 11126
Plate exhibits large center region of discoloration and a matte appearance

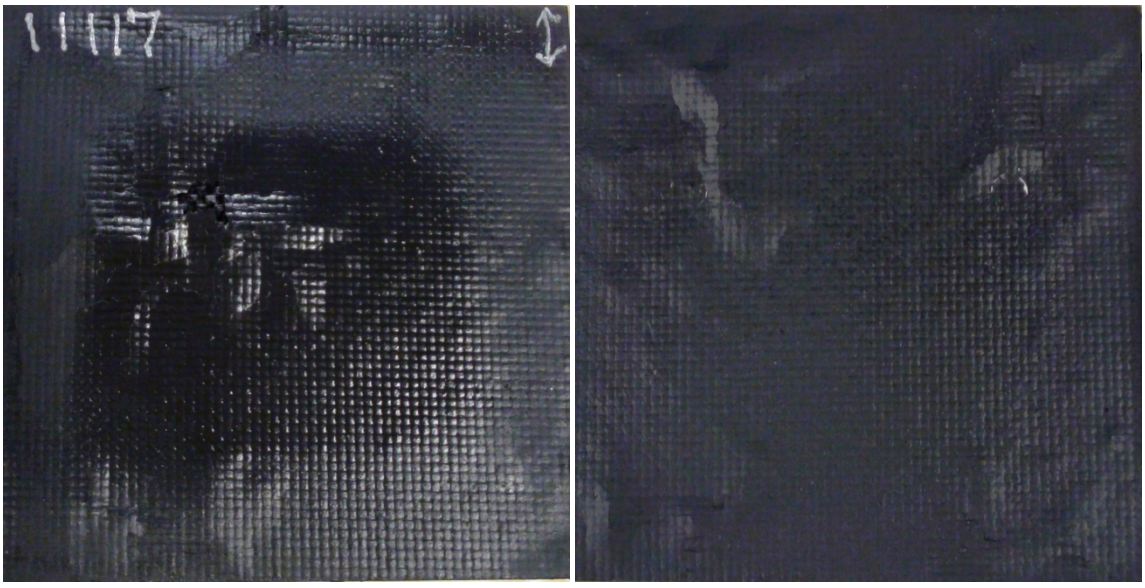

Figure B.8: T300/HYPR-SiC™ –
10h 1300°C exposure plate 11117 top face (left) and bottom face (right)
Plate exhibits severe blistering and a glossy appearance.

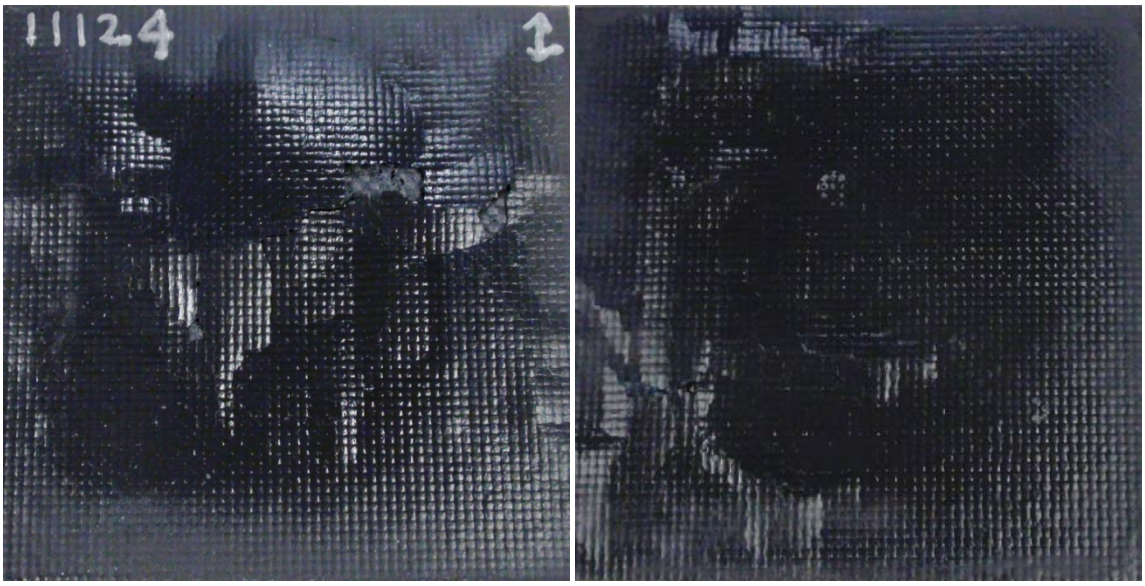

Figure B.9: T300/HYPR-SiC™ –
20h 1300°C exposure plate 11124 top face (left) and bottom face (right)
Plate exhibits severe blistering and a glossy appearance.

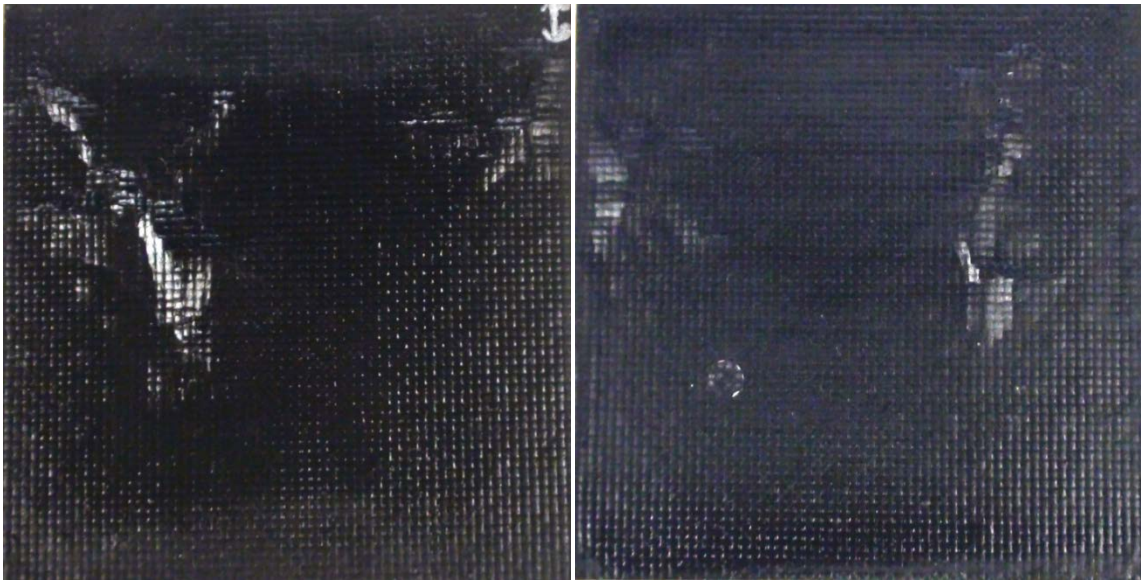

Figure B.10: T300/HYPR-SiC™ –
40h 1300°C exposure plate 11125 top face (left) and bottom face (right)
Plate exhibits moderate blistering and a glossy appearance.

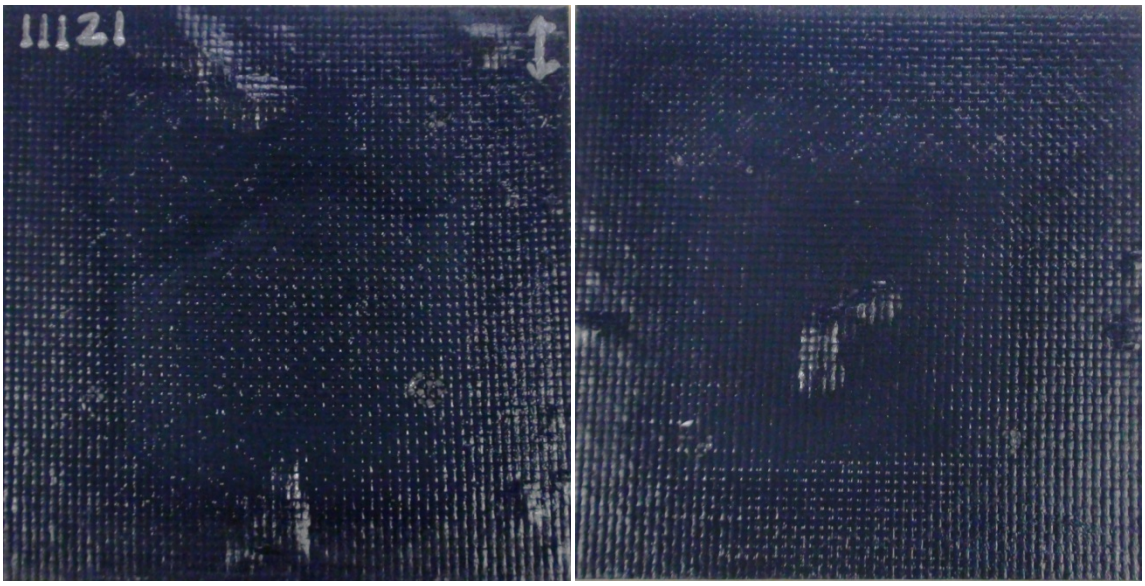

Figure B.11: T300/HYPR-SiC™ –
100h 1300°C exposure plate 11121 top face (left) and bottom face (right)
Plate exhibits mild blistering and a glossy appearance.

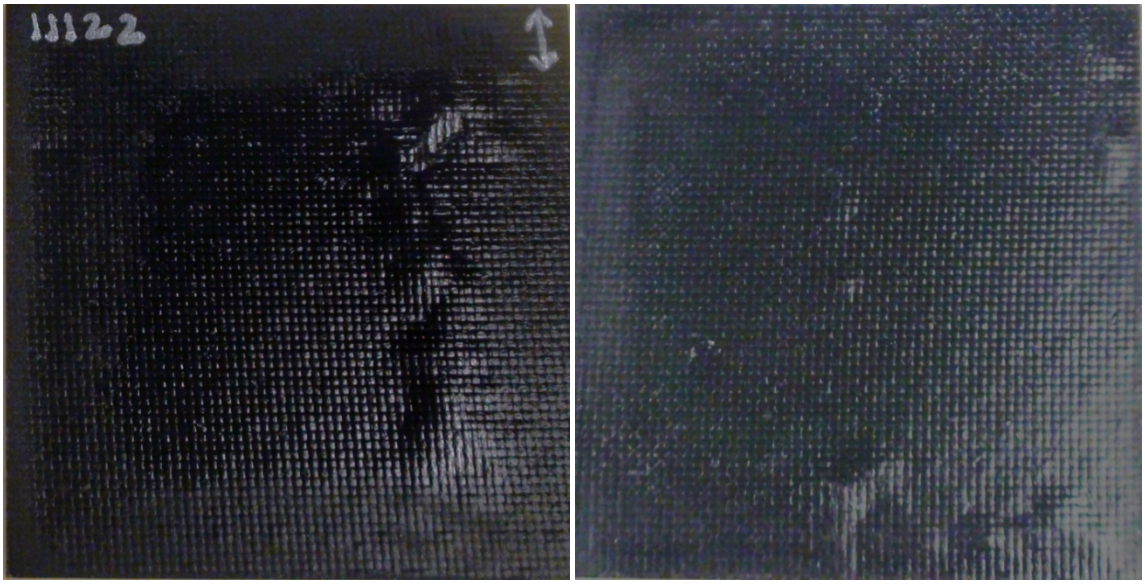

Figure B.12: T300/HYPR-SiC™ –
100h 1200°C exposure plate 11122 top face (left) and bottom face (right)
Plate exhibits mild blistering and a glossy appearance.

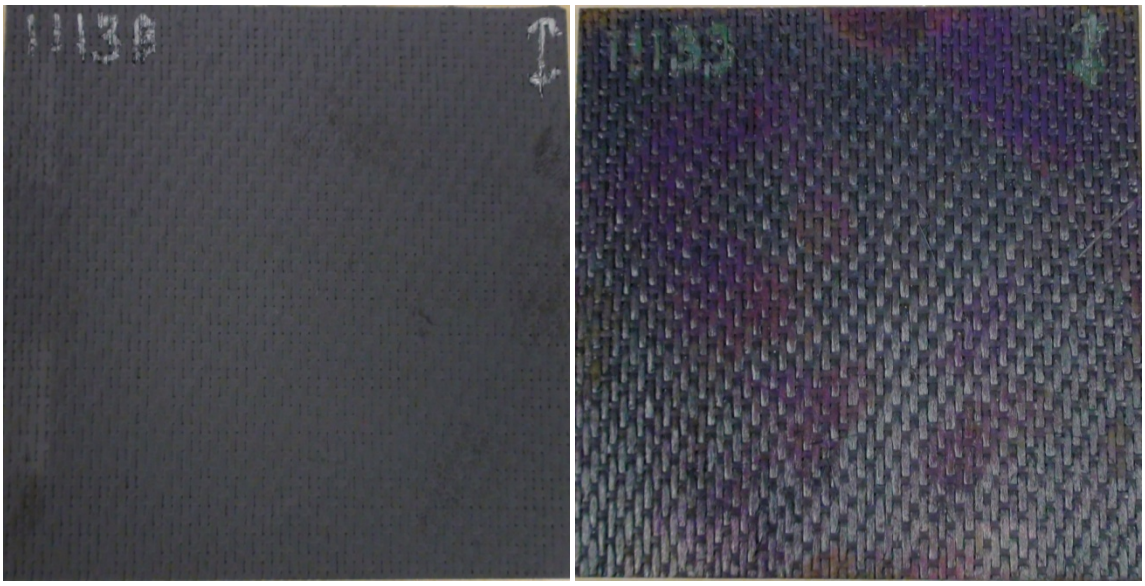

Figure B.13: Hi-Nicalon™/HYPR-SiC™ –
Virgin plate 11138 (left);
10h 1400°C exposure plate 11133 (right).
Exposed plate exhibits greenish-blue discoloration.

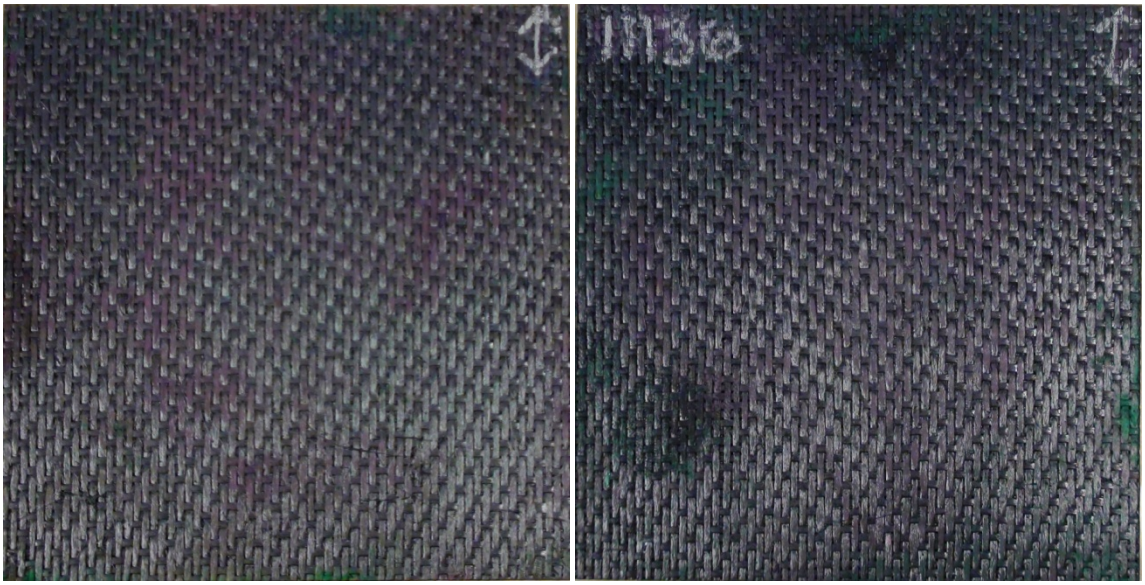

Figure B.14: Hi-Nicalon™/HYPR-SiC™ –
20h 1400°C exposure plate 11135 (left);
40h 1400°C exposure plate 11136 (right).
Exposed plates exhibit greenish-blue discoloration.

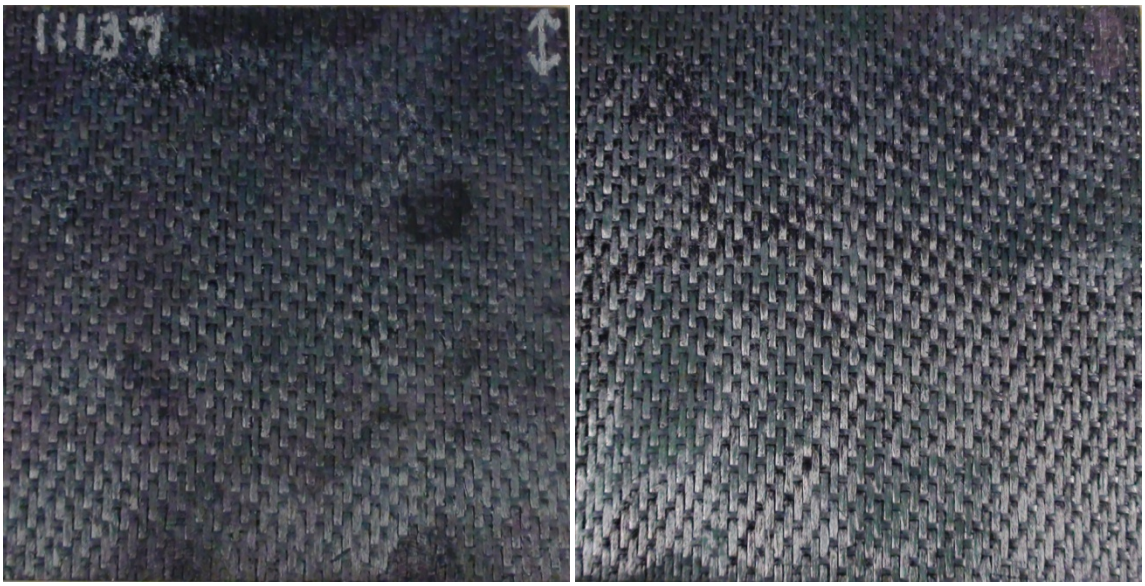

Figure B.15: Hi-Nicalon™/HYPR-SiC™ –
100h 1400°C exposure plate 11137 (left);
100h 1300°C exposure plate 11139 (right).
Exposed plates exhibit greenish-blue discoloration.

Appendix C: Diagrams of Blistered T300/HYPR-SiC™ (C/HYPR-SiC™) Plates

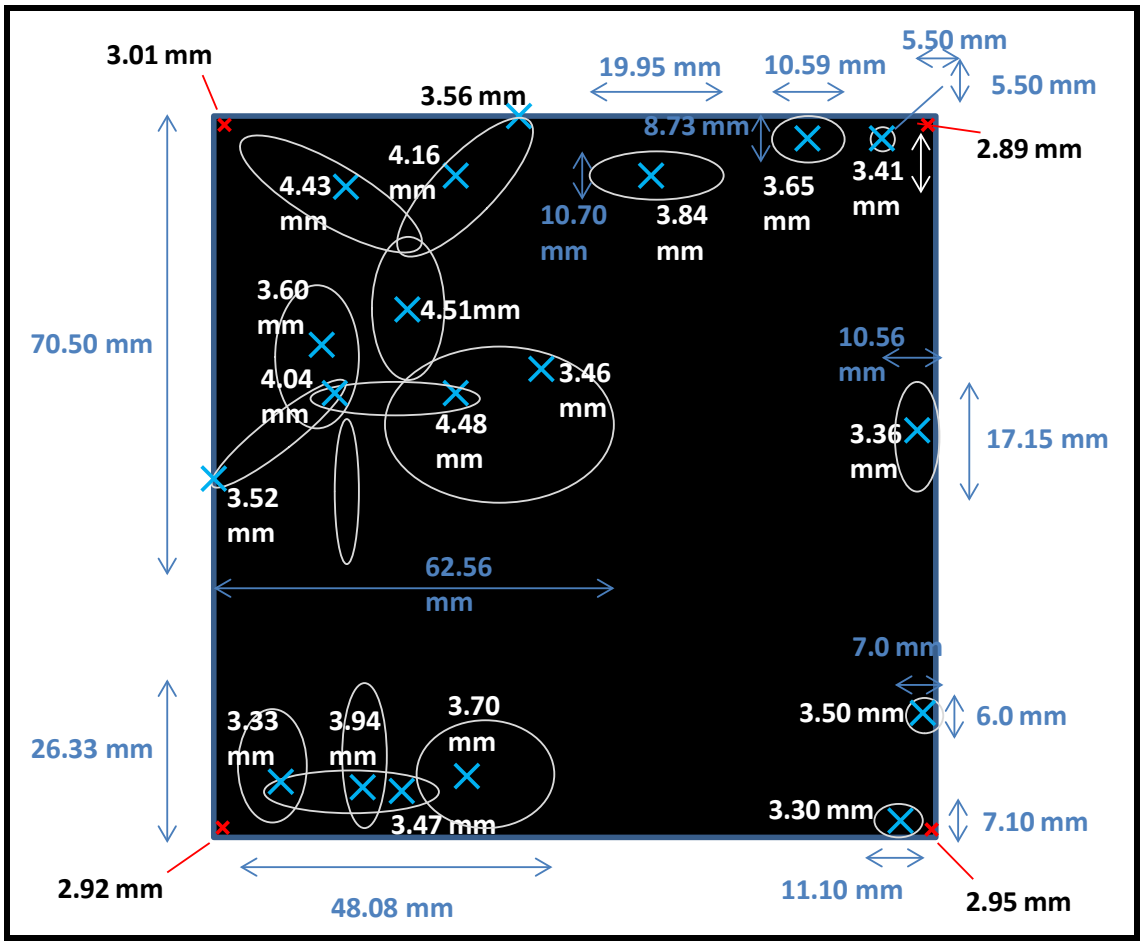

Figure C.1: Diagram of blistered C/HYPR-SiC™ plate after 10 h 1300°C exposure – plate 11117, face up

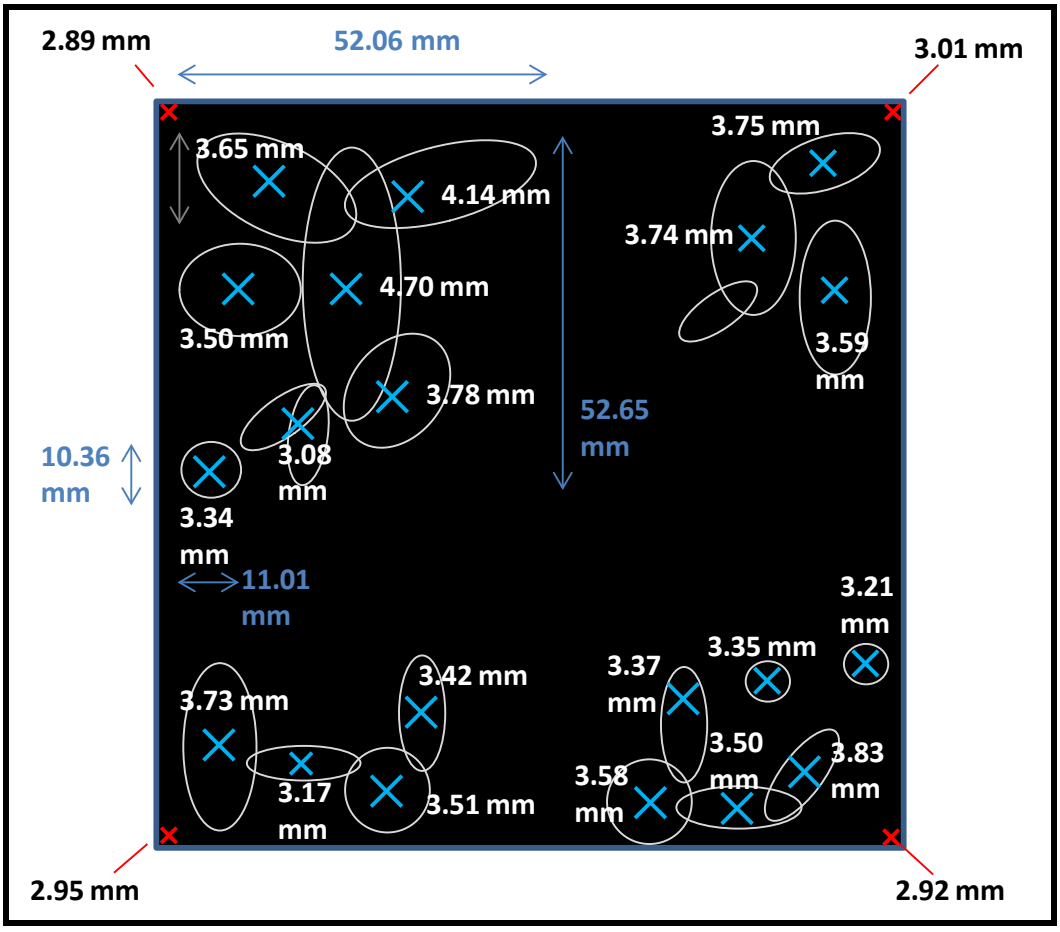

Figure C.2: Diagram of blistered C/HYPR-SiC™ plate after 10 h 1300°C exposure – plate 11117, face down

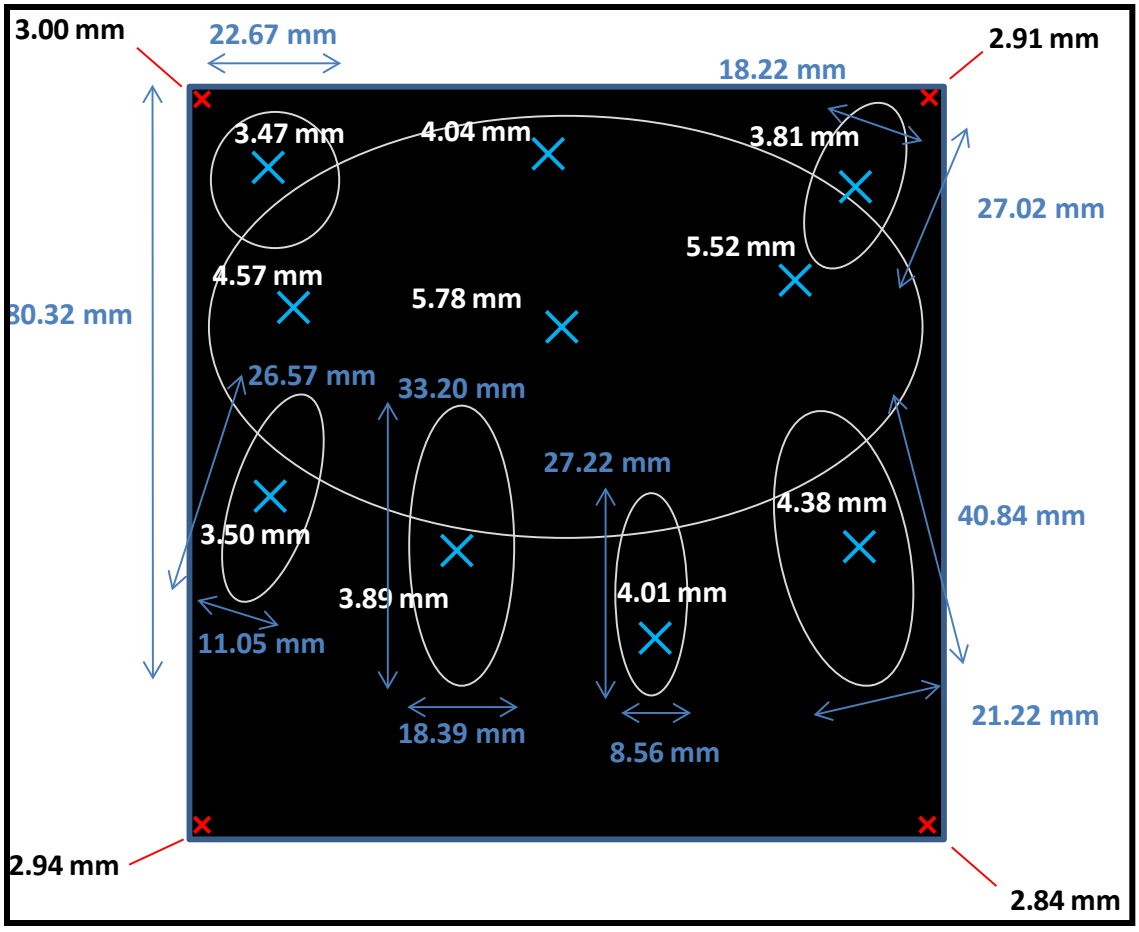

Figure C. 3: Diagram of blistered C/HYPR-SiC™ plate after 20 h 1300°C exposure – plate 11124, face up

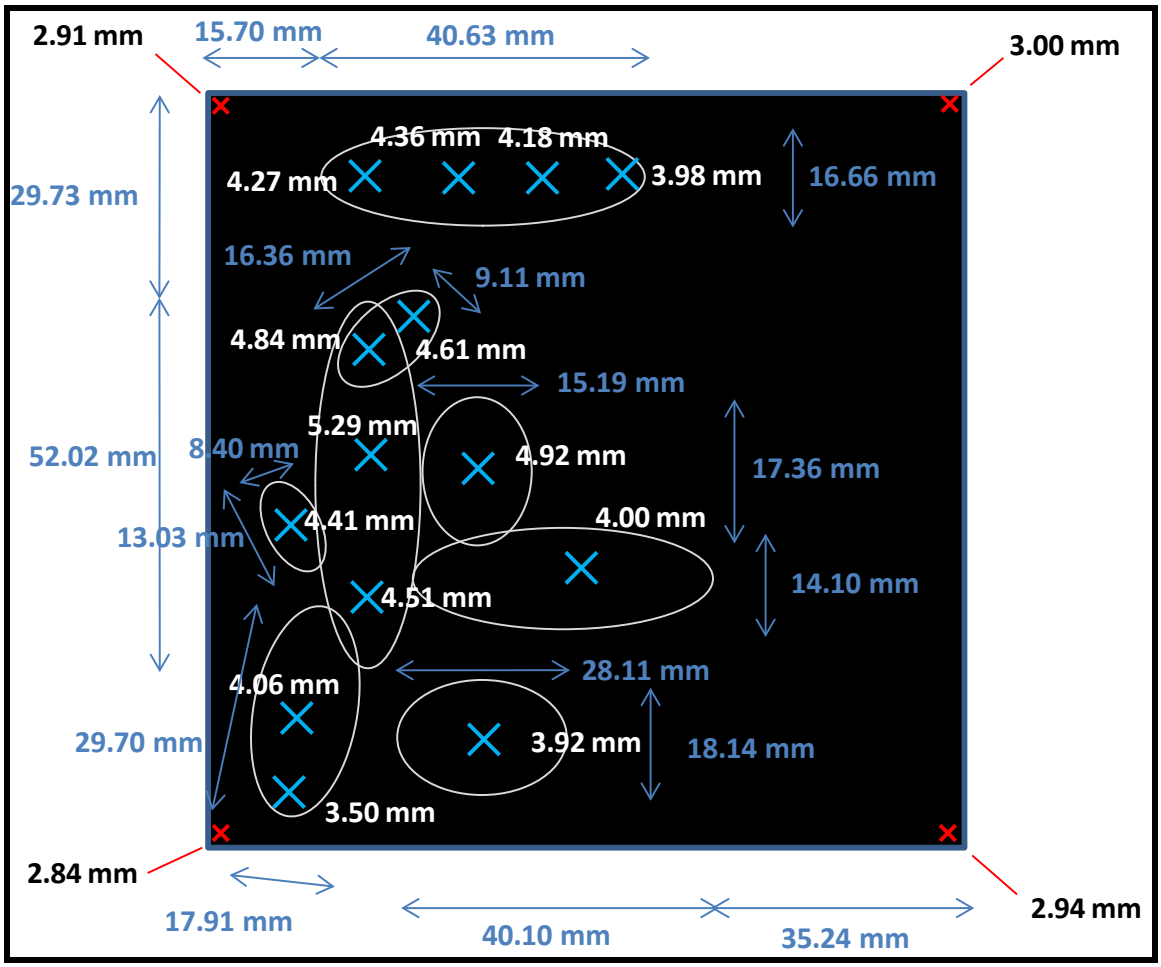

Figure C.4: Diagram of blistered C/HYPR-SiC™ plate after 20 h 1300°C exposure – plate 11124, face down

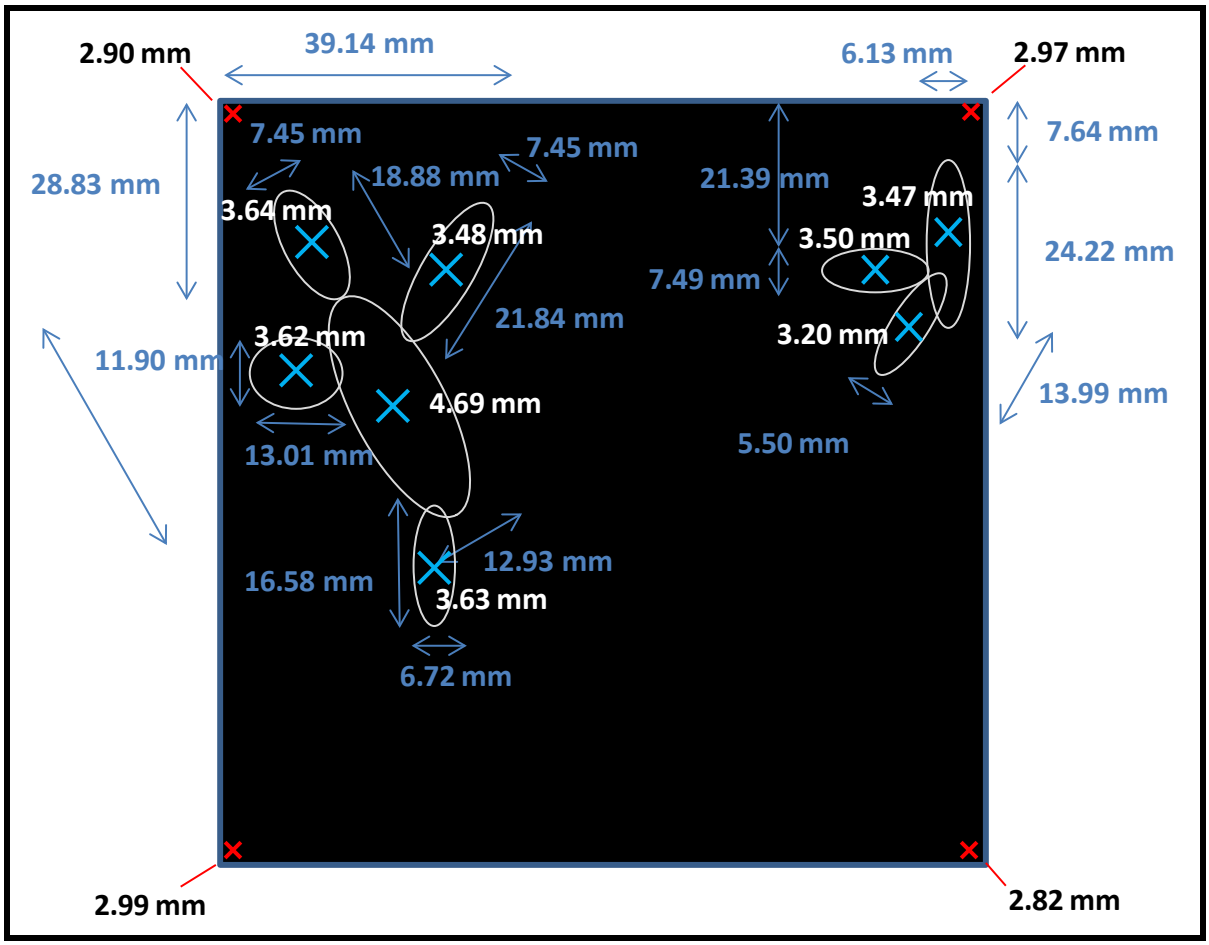

Figure C.5: Diagram of blistered C/HYPR-SiC™ plate after 40 h 1300°C exposure – plate 11125, face up

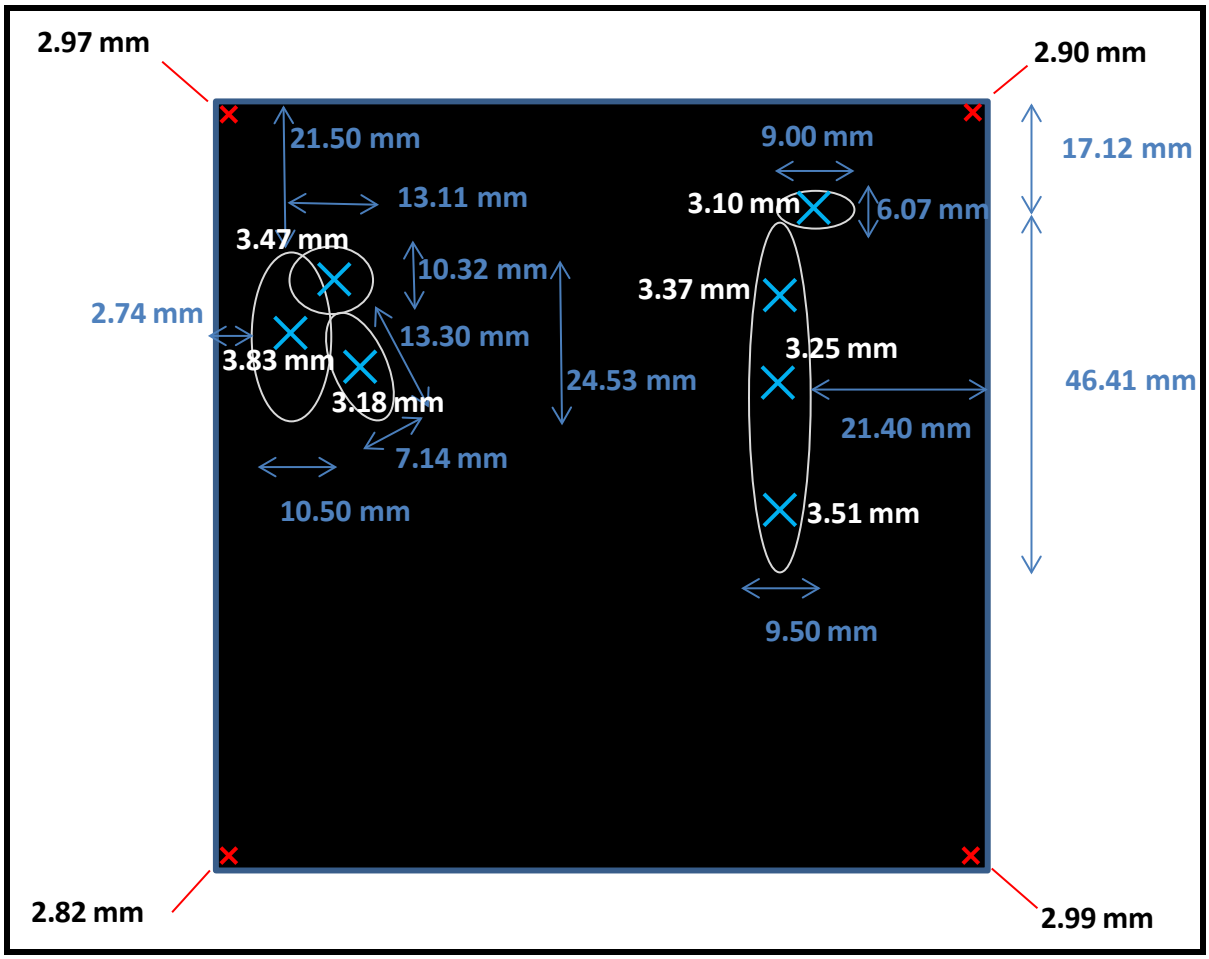

Figure C.6: Diagram of blistered C/HYPR-SiC™ plate after 40 h 1300°C exposure – plate 11125, face down

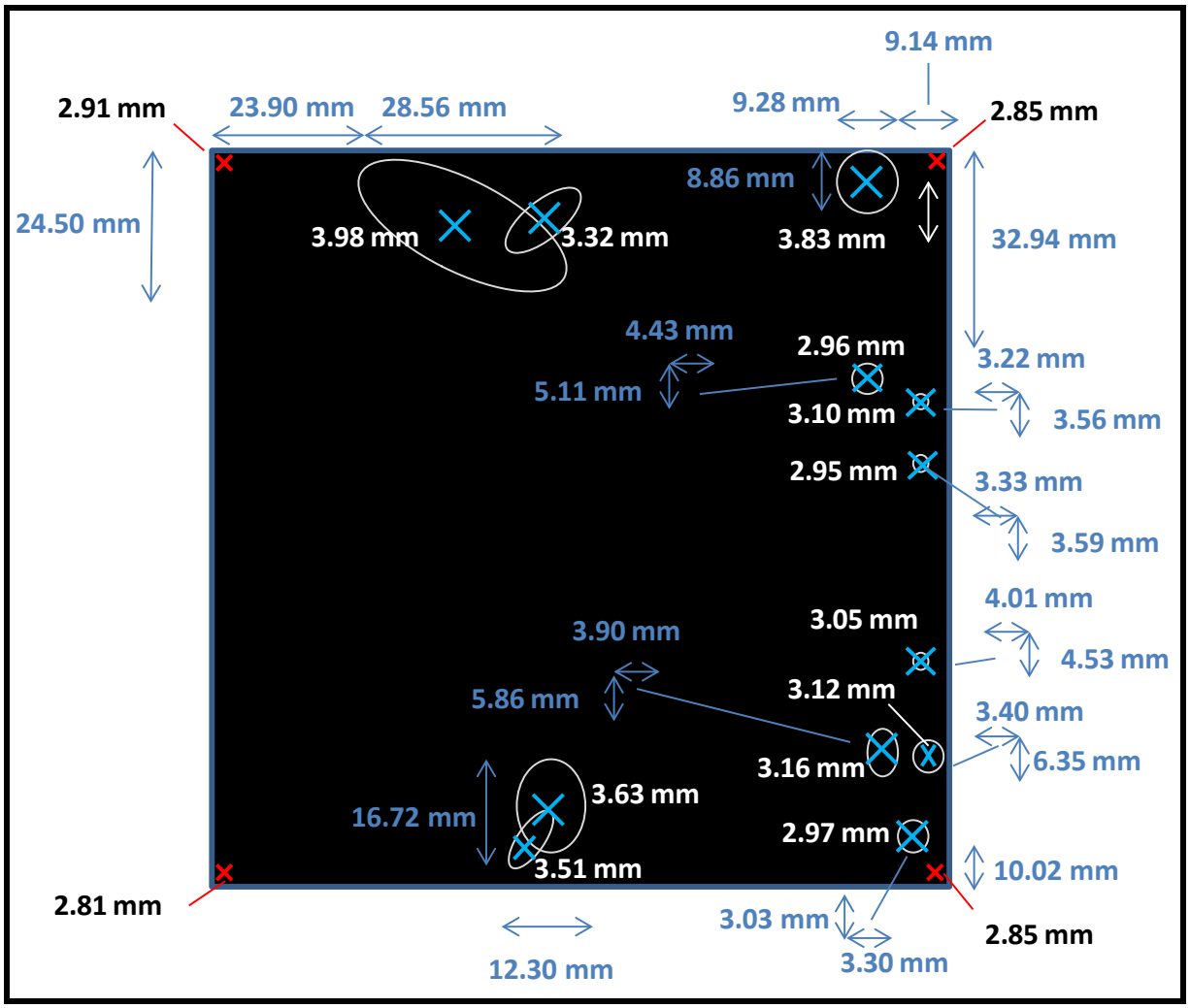

Figure C.7: Diagram of blistered C/HYPR-SiC™ plate after 100 h 1300°C exposure – plate 11121, face up

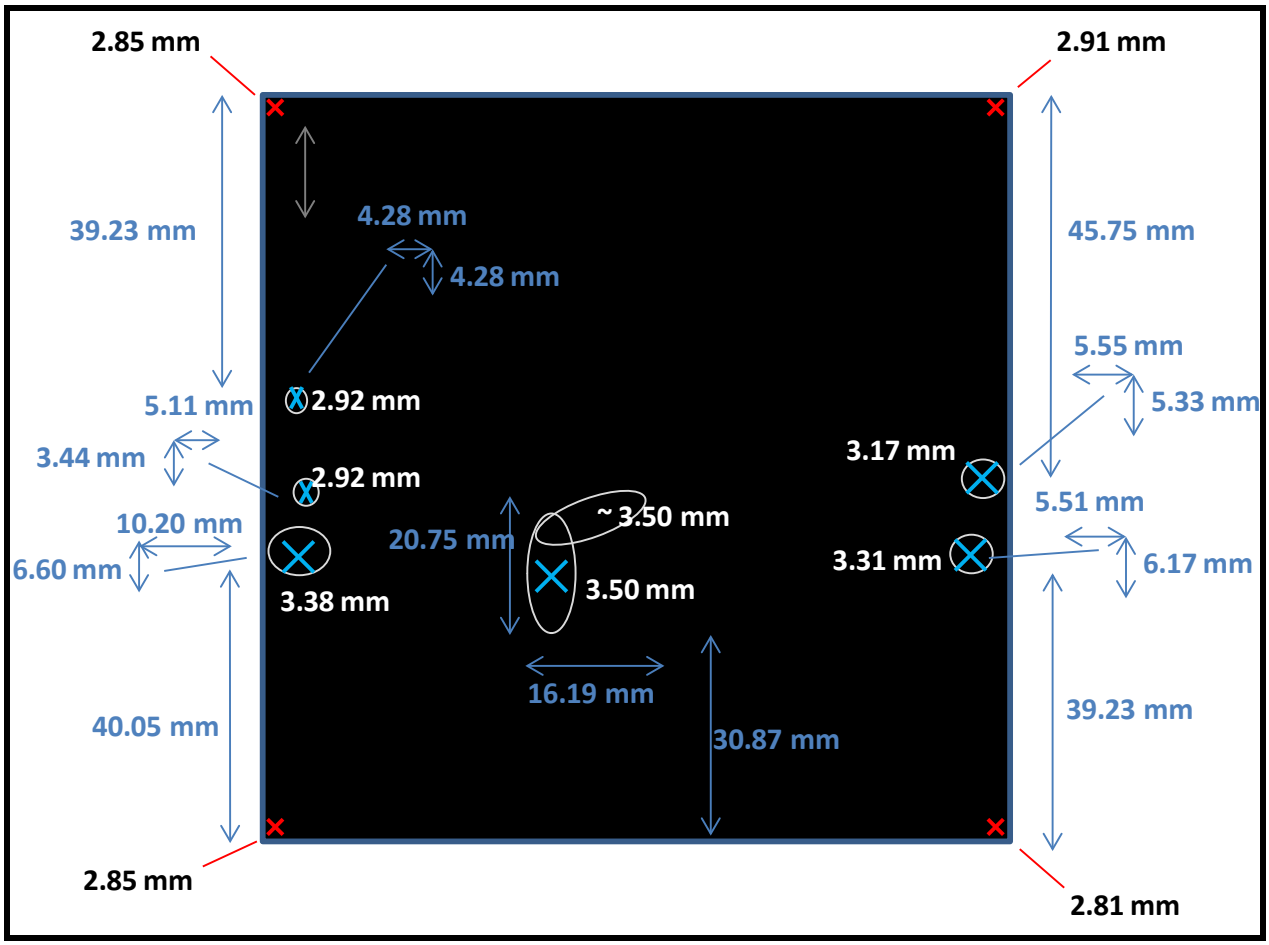

Figure C.8: Diagram of blistered C/HYPR-SiC™ plate after 100 h 1300°C exposure – plate 11121, face down

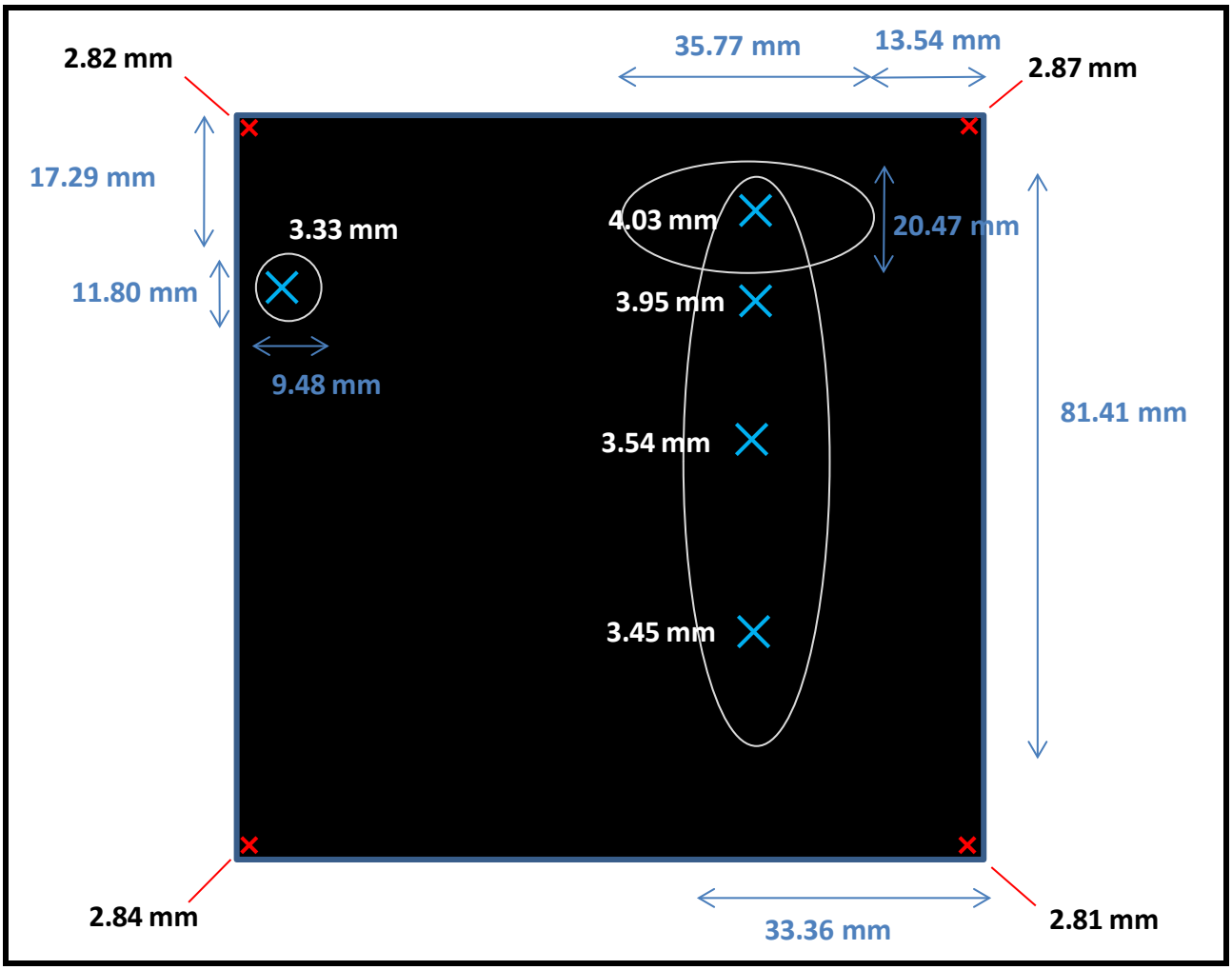

Figure C.9: Diagram of blistered C/HYPR-SiC™ plate after 100 h 1200°C exposure – plate 11122, face up

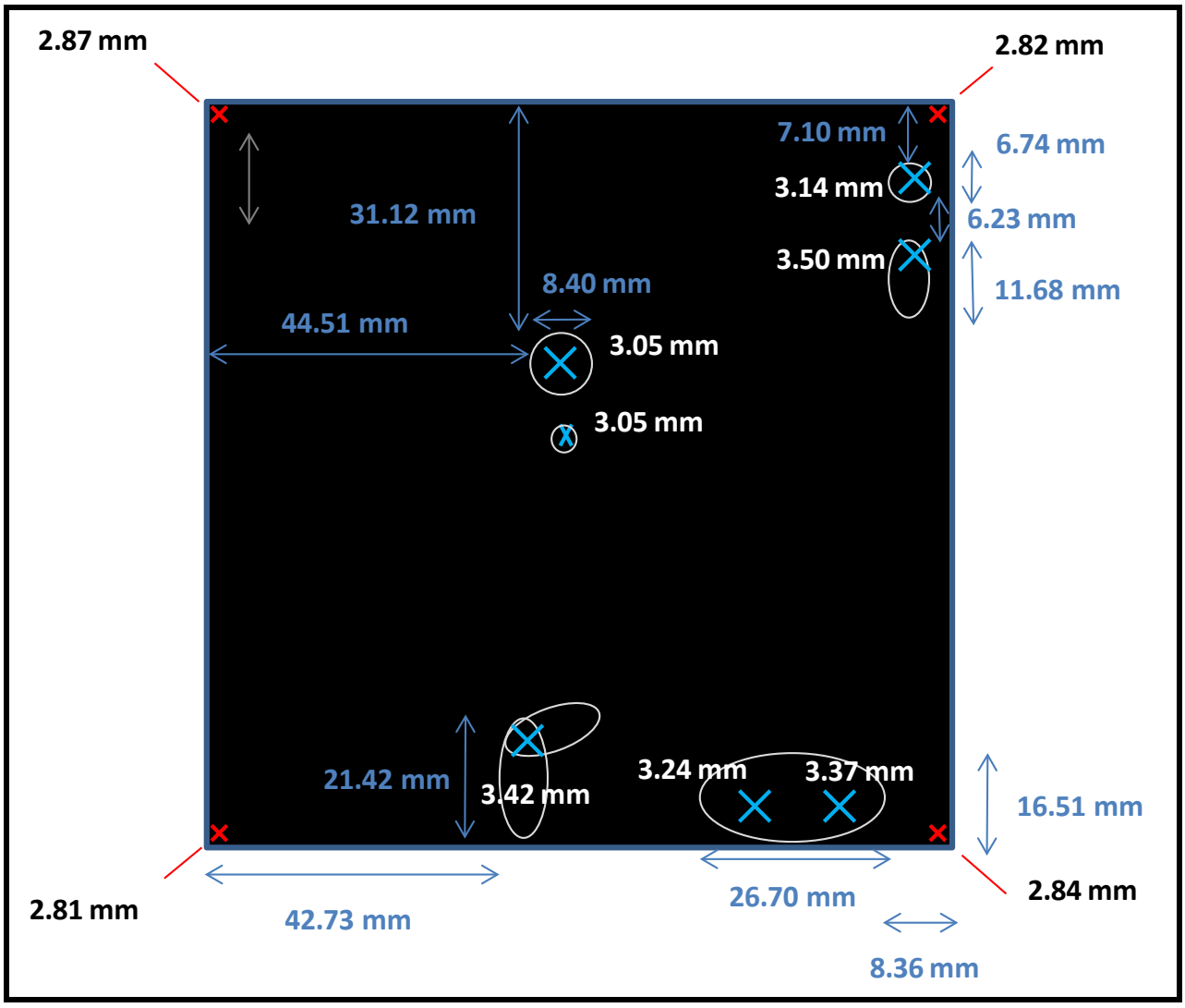

Figure C.10: Diagram of blistered C/HYPR-SiC™ plate after 100 h 1200°C exposure – plate 11122, face down

Appendix D: Specimen Cross-Section Area Dimensions

Table D.1: Hi-Nicalon™/SiNC Specimen Cross Section Dimensions

Plate	*Specimen*	*Gage Thickness (mm)*	*Gage Width (mm)*	*Cross-section Area (mm^2)*
11107	1	2.15	8.00	17.20
11107	2	2.15	8.00	17.20
11107	3	2.19	8.00	17.52
11107	4	2.19	8.00	17.52
11107	5	2.17	7.97	17.29
11107	6	2.14	8.02	17.16
11101	1	2.18	7.97	17.37
11101	2	2.19	7.88	17.26
11101	3	2.22	8.01	17.78
11101	4	2.25	7.62	17.15
11101	5	2.23	7.99	17.82
11101	6	2.24	7.98	17.88
11103	1	2.18	7.99	17.42
11103	2	2.2	8.00	17.60
11103	3	2.2	8.00	17.60
11103	4	2.18	7.98	17.40
11103	5	2.2	8.00	17.60
11103	6	2.15	8.01	17.22
11104	1	2.15	7.99	17.18
11104	2	2.19	7.98	17.48
11104	3	2.22	7.97	17.69
11104	4	2.23	8.00	17.84
11104	5	2.21	7.97	17.61
11104	6	2.21	7.97	17.61
11105	1	2.19	7.96	17.43
11105	2	2.21	8.02	17.72
11105	3	2.17	7.97	17.29
11105	4	2.22	7.99	17.74
11105	5	2.22	7.98	17.72
11105	6	2.21	7.90	17.46
11106	1	2.15	7.57	16.28
11106	2	2.15	7.99	17.18
11106	3	2.13	7.96	16.95
11106	4	2.15	7.99	17.18
11106	5	2.17	7.54	16.36
11106	6	2.18	7.97	17.37

Table D.2: HexTow® IM7 C/SiC Specimen Cross Section Dimensions

Plate	*Specimen*	*Gage Thickness (mm)*	*Gage Width (mm)*	*Cross-section Area (mm^2)*
12012	1	2.88	7.97	22.95
12012	2	2.85	7.94	22.63
12012	3	2.87	7.89	22.64
12012	4	2.86	7.98	22.82
12012	5	2.89	7.98	23.06
12012	6	2.89	7.95	22.98
12011	1	2.92	8.01	23.39
12011	2	2.93	7.99	23.41
12011	3	2.88	7.96	22.92
12011	4	2.90	8.40	24.36
12011	5	2.92	7.90	23.07
12011	6	2.89	7.98	23.06
12019	1	2.91	7.97	23.19
12019	2	2.91	7.96	23.16
12019	3	2.93	7.99	23.41
12019	4	2.89	7.97	23.03
12019	5	2.92	7.99	23.33
12019	6	2.92	7.98	23.30
12018	1	2.90	7.95	23.06
12018	2	2.88	7.94	22.87
12018	3	2.88	7.93	22.84
12018	4	2.87	7.95	22.82
12018	5	2.88	7.95	22.90
12018	6	2.86	7.95	22.74
12015	1	2.90	8.01	23.23
12015	2	2.92	8.01	23.39
12015	3	2.89	8.02	23.18
12015	4	2.92	8.03	23.45
12015	5	2.95	8.02	23.66
12015	6	2.91	8.03	23.37
12016	1	2.92	8.01	23.39
12016	2	2.89	7.99	23.09
12016	3	2.89	7.97	23.03
12016	4	2.82	7.99	22.53
12016	5	2.80	8.00	22.40
12016	6	2.84	7.99	22.69

Table D.3: T300 C/HYPR-SiC™ Specimen Cross Section Dimensions

Plate	*Specimen*	*Gage Thickness (mm)*	*Gage Width (mm)*	*Cross-section Area (mm^2)*
11126	1	2.92	7.95	23.21
11126	2	2.91	7.97	23.19
11126	3	2.95	7.93	23.39
11126	4	2.93	7.92	23.21
11126	5	2.86	7.97	22.79
11126	6	2.94	8.12	23.87
11117	1	2.76	7.95	21.94
11117	2	2.74	7.95	21.78
11117	3	2.83	7.97	22.56
11117	4	2.71	7.95	21.54
11117	5	2.91	7.93	23.08
11117	6	2.75	7.93	21.81
11124	1	2.79	8.00	22.32
11124	2	2.80	7.94	22.23
11124	3	2.75	7.96	21.89
11124	4	2.79	7.99	22.29
11124	5	2.68	7.98	21.39
11124	6	2.70	7.99	21.57
11125	1	2.89	7.94	22.95
11125	2	2.69	7.96	21.41
11125	3	2.77	7.96	22.05
11125	4	2.68	7.93	21.25
11125	5	2.77	7.54	20.89
11125	6	2.85	7.99	22.77
11121	1	2.97	8.02	23.82
11121	2	2.85	8.03	22.89
11121	3	2.91	7.95	23.13
11121	4	2.73	7.95	21.70
11121	5	2.83	7.99	22.61
11121	6	2.93	8.02	23.50
11122	1	2.80	7.97	22.32
11122	2	2.75	7.96	21.89
11122	3	2.78	7.99	22.21
11122	4	2.77	7.97	22.08
11122	5	2.77	7.96	22.05
11122	6	2.93	8.03	23.53

Table D.4: Hi-Nicalon™/HYPR-SiC™ Specimen Cross Section Dimensions

Plate	*Specimen*	*Gage Thickness (mm)*	*Gage Width (mm)*	*Cross-section Area (mm^2)*
11138	1	2.90	7.98	23.14
11138	2	2.87	7.98	22.90
11138	3	2.95	7.98	23.54
11138	4	2.96	7.98	23.62
11138	5	2.99	7.94	23.74
11138	6	3.05	7.82	23.85
11133	1	2.97	8.00	23.76
11133	2	3.02	8.02	24.22
11133	3	2.94	7.89	23.20
11133	4	2.95	7.88	23.25
11133	5	2.97	7.99	23.73
11133	6	2.96	8.00	23.68
11135	1	2.88	7.89	22.72
11135	2	2.89	7.95	22.98
11135	3	2.88	7.96	22.92
11135	4	2.89	7.98	23.06
11135	5	2.92	7.95	23.21
11135	6	2.90	7.99	23.17
11136	1	2.87	7.90	22.67
11136	2	2.96	7.99	23.65
11136	3	2.97	8.00	23.76
11136	4	2.99	7.98	23.86
11136	5	2.95	7.97	23.51
11136	6	3.00	7.99	23.97
11137	1	2.86	7.97	22.79
11137	2	3.00	7.97	23.91
11137	3	2.98	7.99	23.81
11137	4	2.98	7.98	23.78
11137	5	2.97	7.91	23.49
11137	6	2.95	7.95	23.45
11139	1	2.98	8.10	24.14
11139	2	2.95	7.98	23.54
11139	3	3.00	7.98	23.94
11139	4	2.95	7.95	23.45
11139	5	2.97	7.97	23.67
11139	6	2.92	7.98	23.30

Appendix E: Additional Tensile Stress-Strain Curves

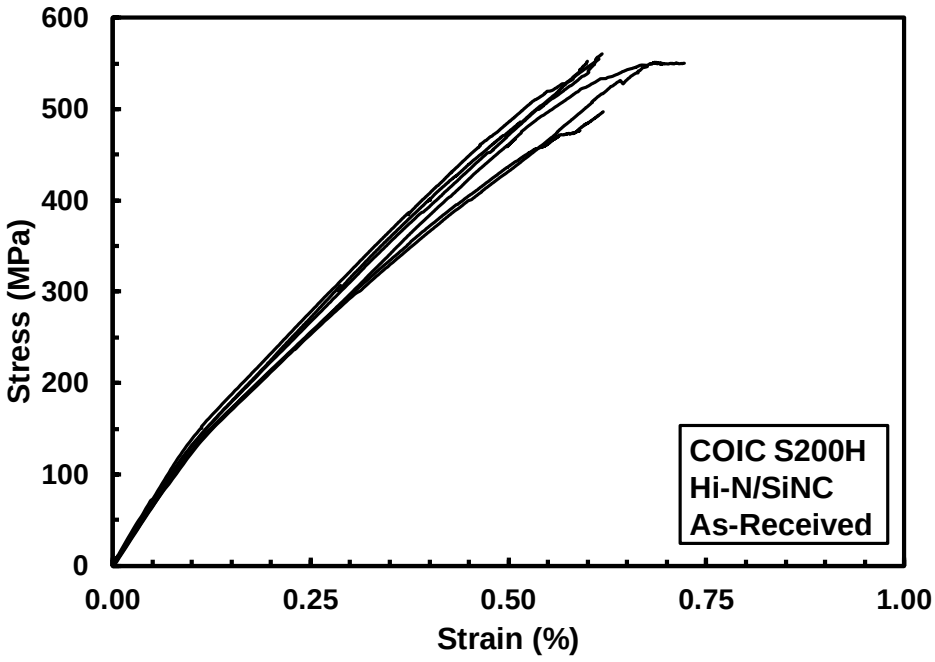

Figure E.1: Tensile stress-strain curves for specimens of as-received Hi-Nicalon™/SiNC composite

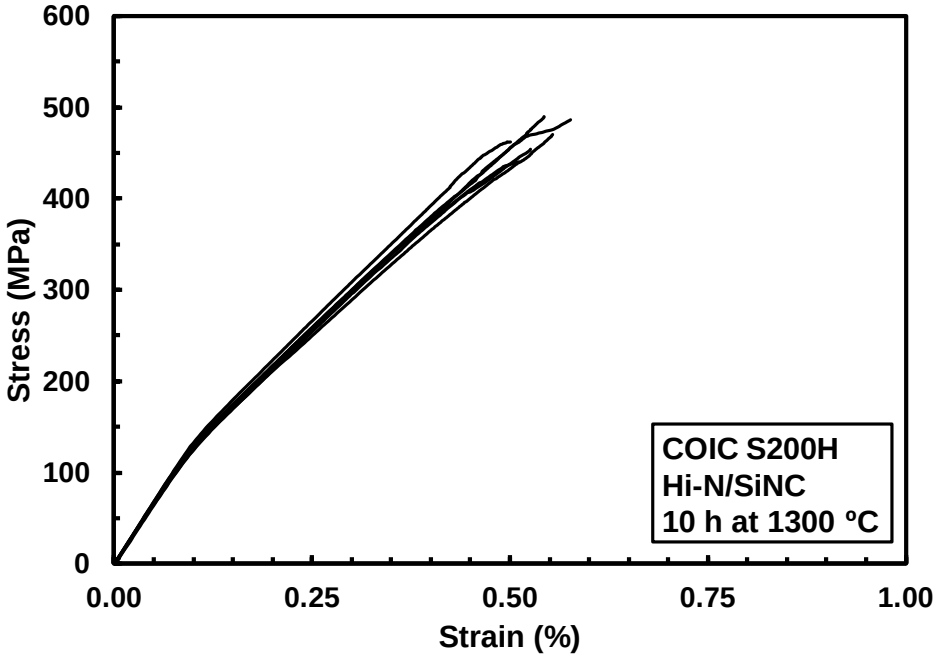

Figure E.2: Tensile stress-strain curves for specimens of Hi-Nicalon™/SiNC composite with prior heat treatment of 10 h at 1300°C

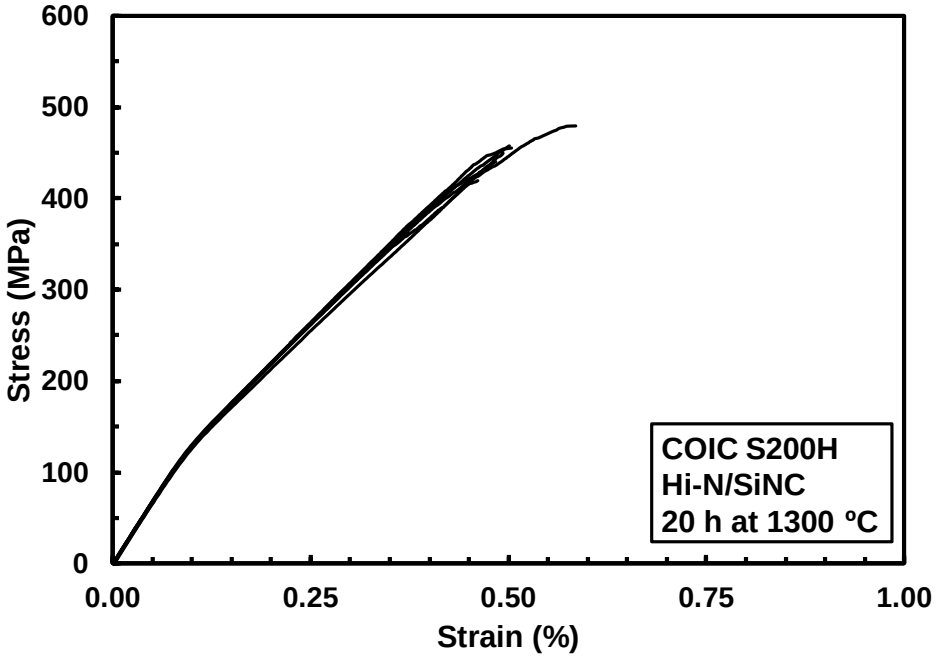

Figure E.3: Tensile stress-strain curves for specimens of Hi-Nicalon™/SiNC composite with prior heat treatment of 20 h at 1300°C

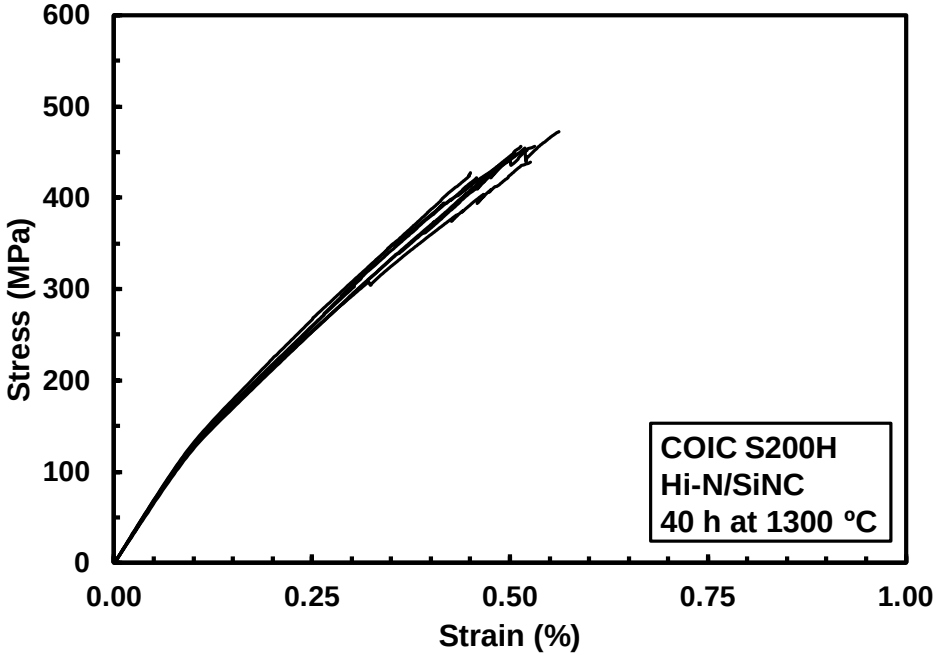

Figure E.4: Tensile stress-strain curves for specimens of Hi-Nicalon™/SiNC composite with prior heat treatment of 40 h at 1300°C

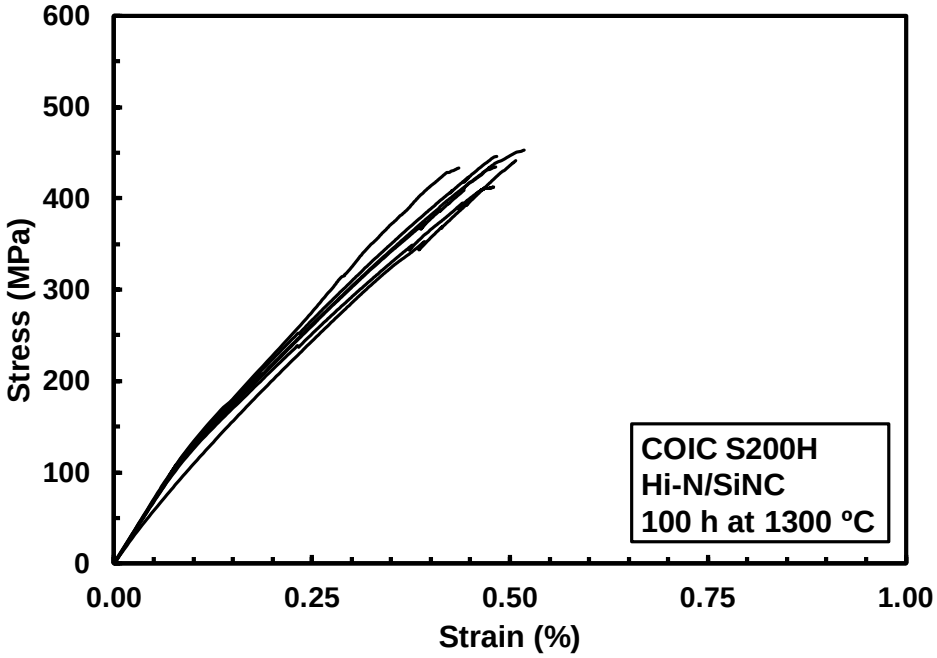

Figure E.5: Tensile stress-strain curves for specimens of Hi-Nicalon™/SiNC composite with prior heat treatment of 100 h at 1300°C

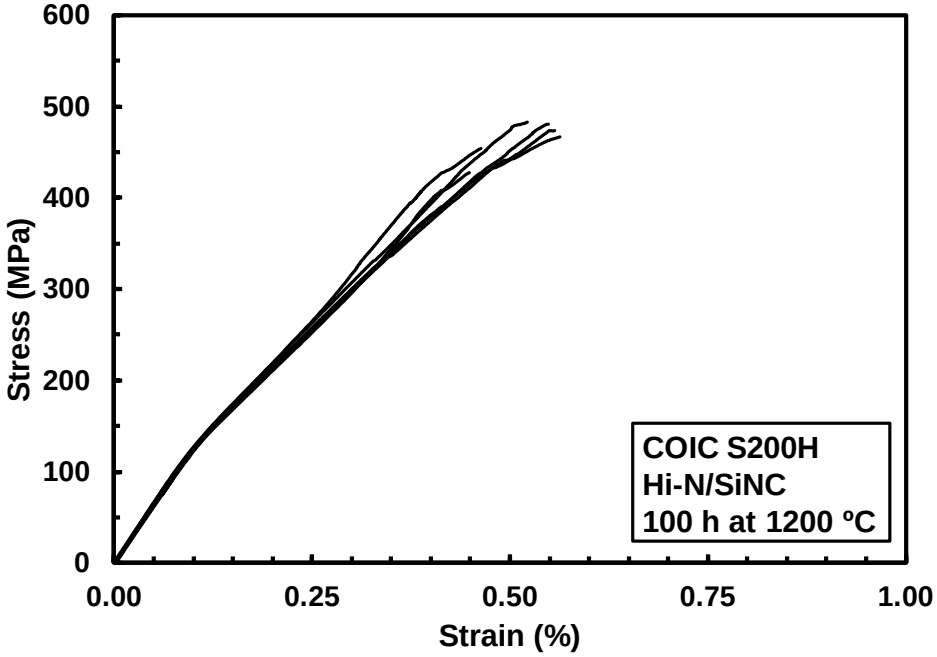

Figure E.6: Tensile stress-strain curves for specimens of Hi-Nicalon™/SiNC composite with prior heat treatment of 100 h at 1200°C

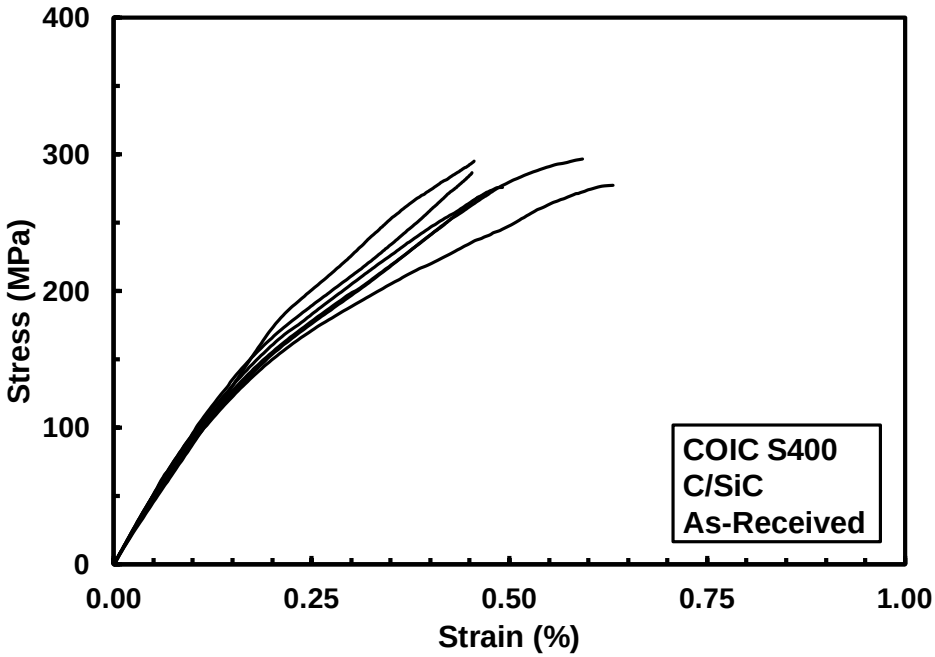

Figure E.7: Tensile stress-strain curves for specimens of as-received HexTow® IM7 C/SiC composite

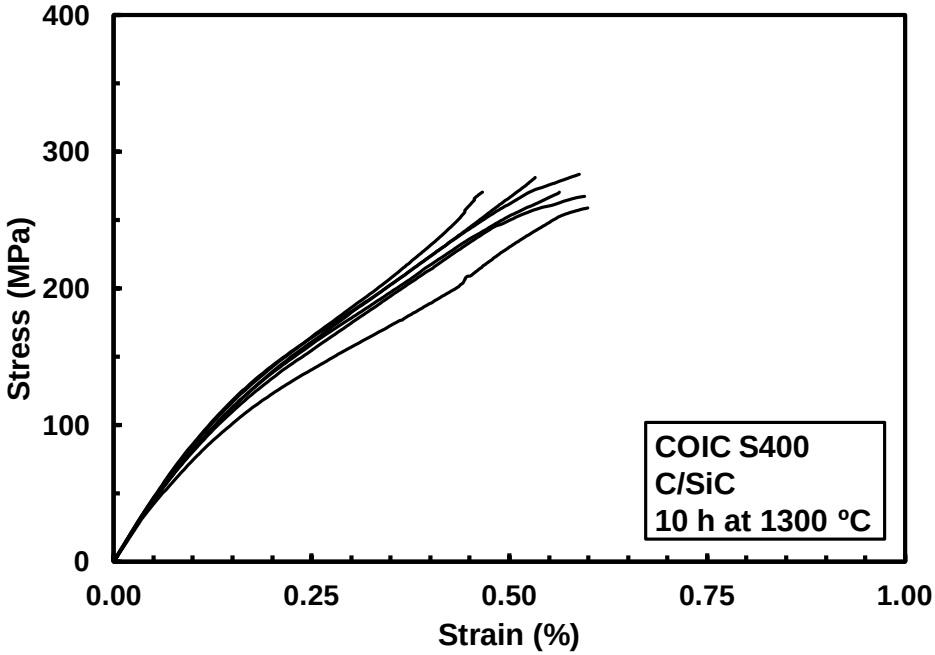

Figure E.8: Tensile stress-strain curves for specimens of HexTow® IM7 C/SiC composite with prior heat treatment of 10 h at 1300°C

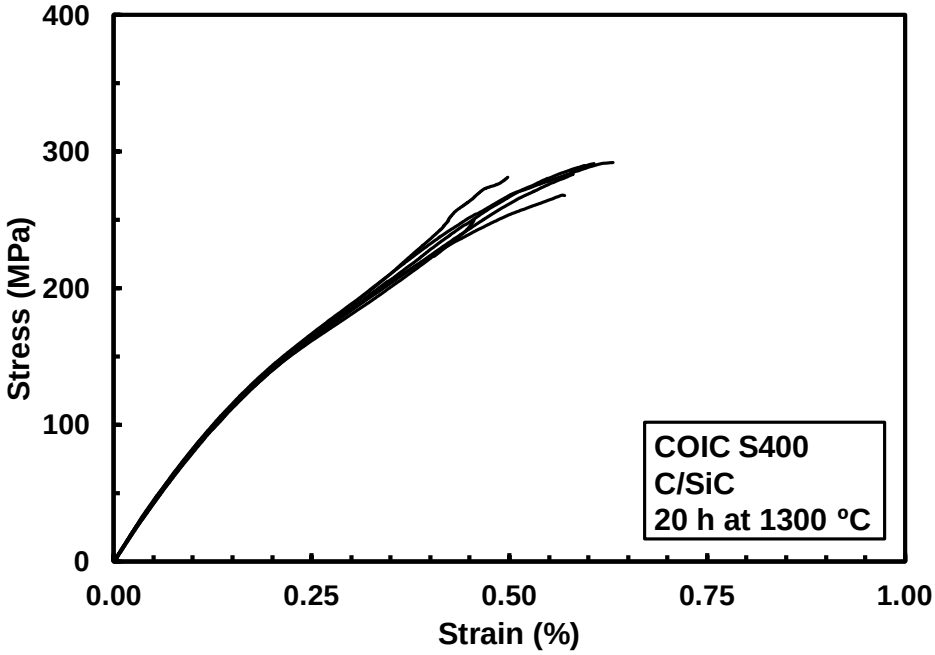

Figure E.9: Tensile stress-strain curves for specimens of HexTow® IM7 C/SiC composite with prior heat treatment of 20 h at 1300°C

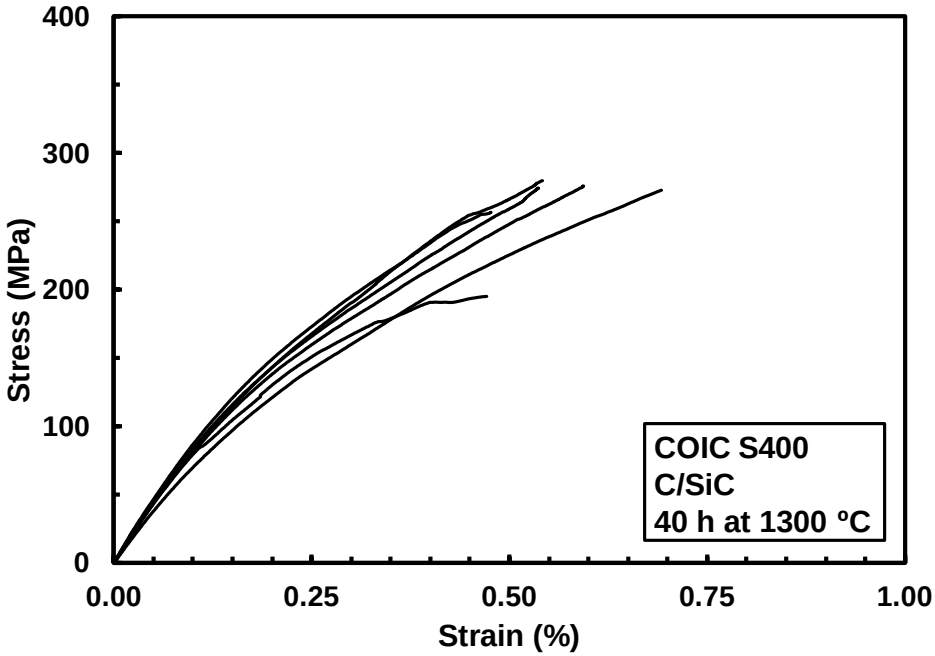

Figure E.10: Tensile stress-strain curves for specimens of HexTow® IM7 C/SiC composite with prior heat treatment of 40 h at 1300°C

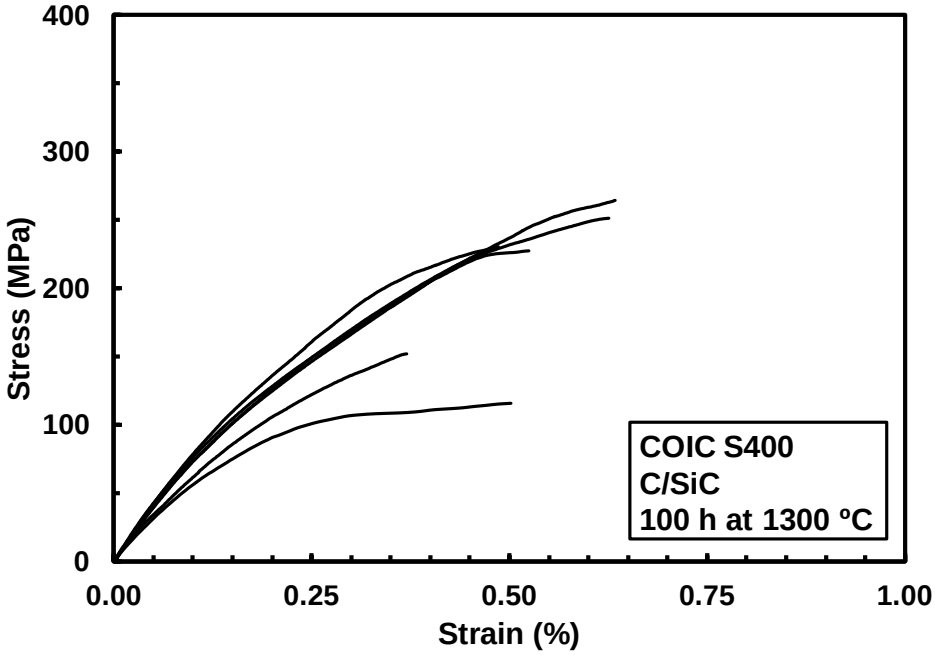

Figure E.11: Tensile stress-strain curves for specimens of HexTow® IM7 C/SiC composite with prior heat treatment of 100 h at 1300°C

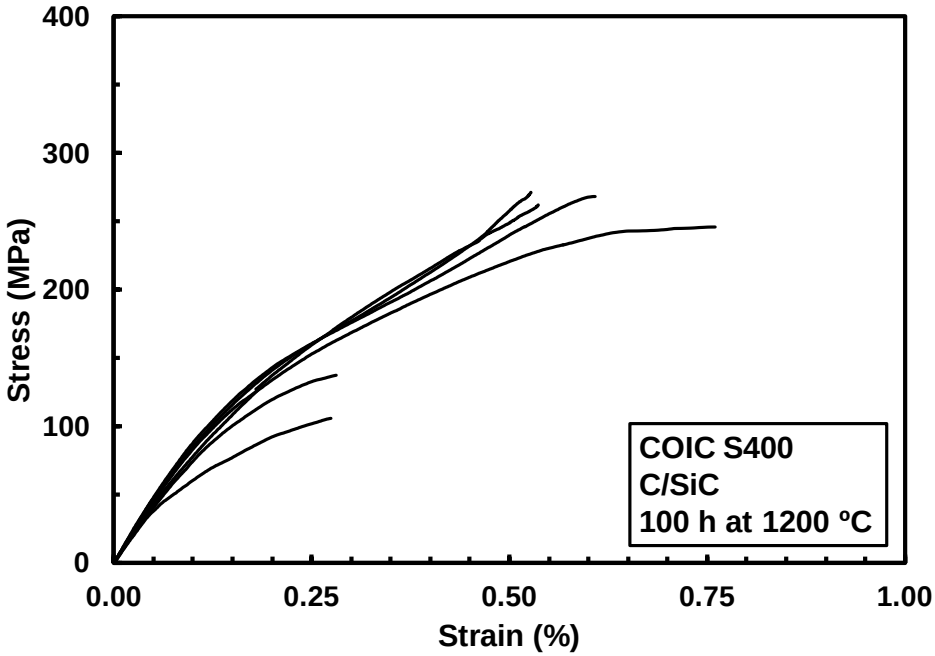

Figure E.12: Tensile stress-strain curves for specimens of HexTow® IM7 C/SiC composite with prior heat treatment of 100 h at 1200°C

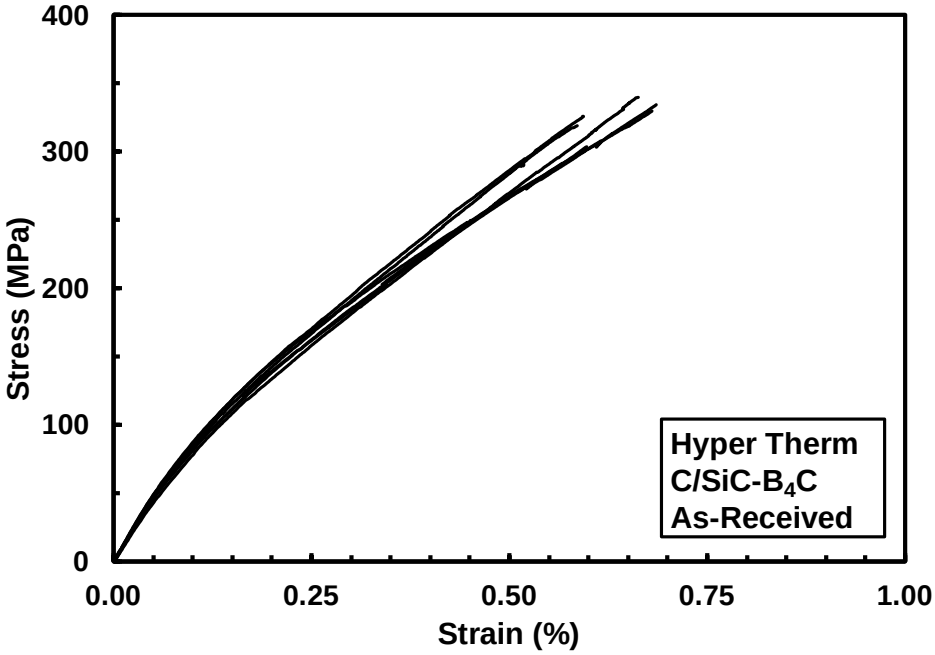

Figure E.13: Tensile stress-strain curves for specimens of as-received T300 C/HYPR-SiC™ composite

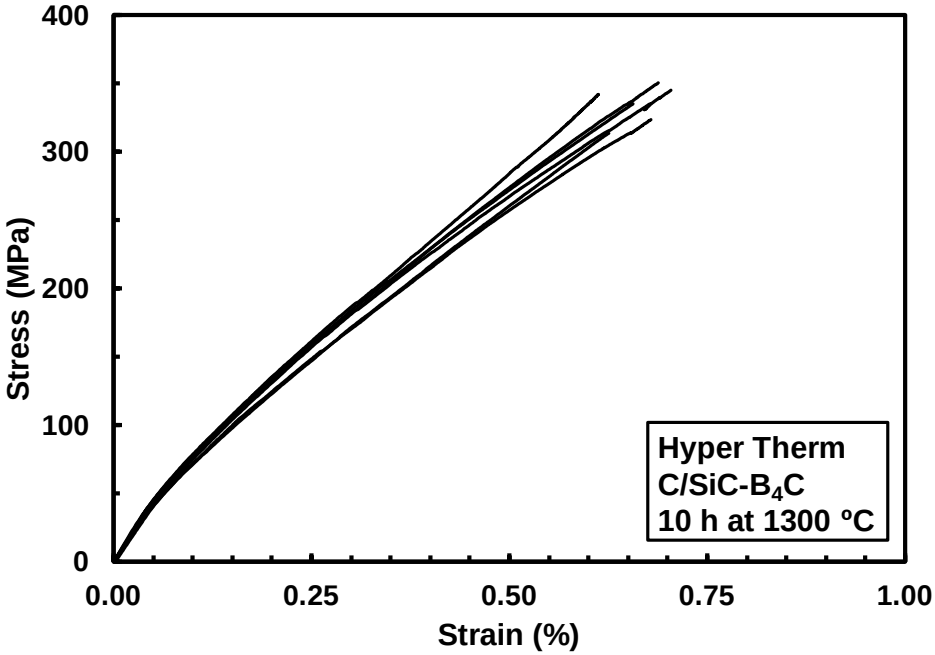

Figure E.14: Tensile stress-strain curves for specimens of T300 C/HYPR-SiC™ composite with prior heat treatment of 10 h at 1300°C

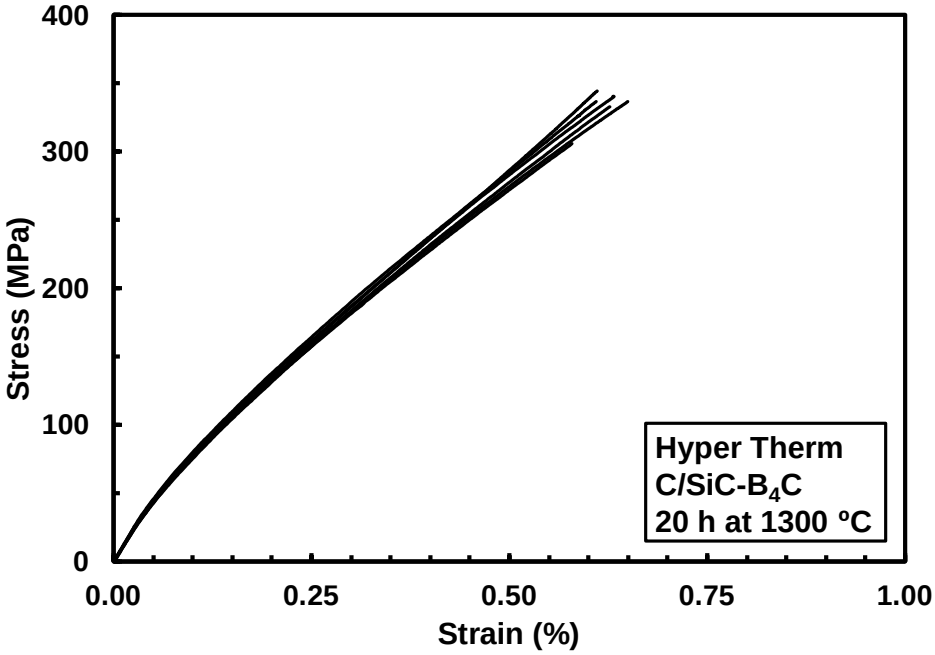

Figure E.15: Tensile stress-strain curves for specimens of T300 C/HYPR-SiC™ composite with prior heat treatment of 20 h at 1300°C

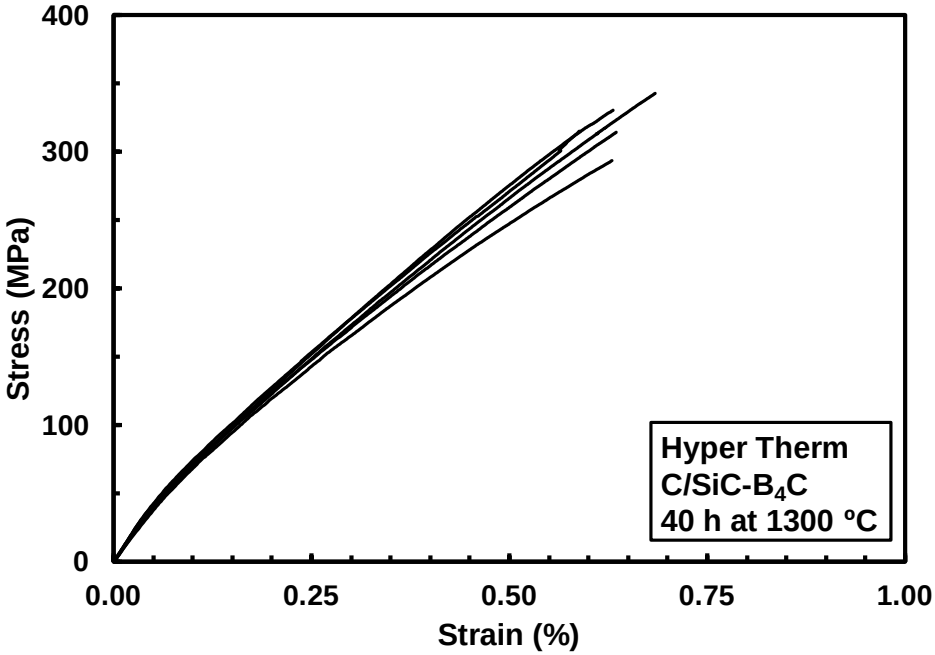

Figure E.16: Tensile stress-strain curves for specimens of T300 C/HYPR-SiC™ composite with prior heat treatment of 40 h at 1300°C

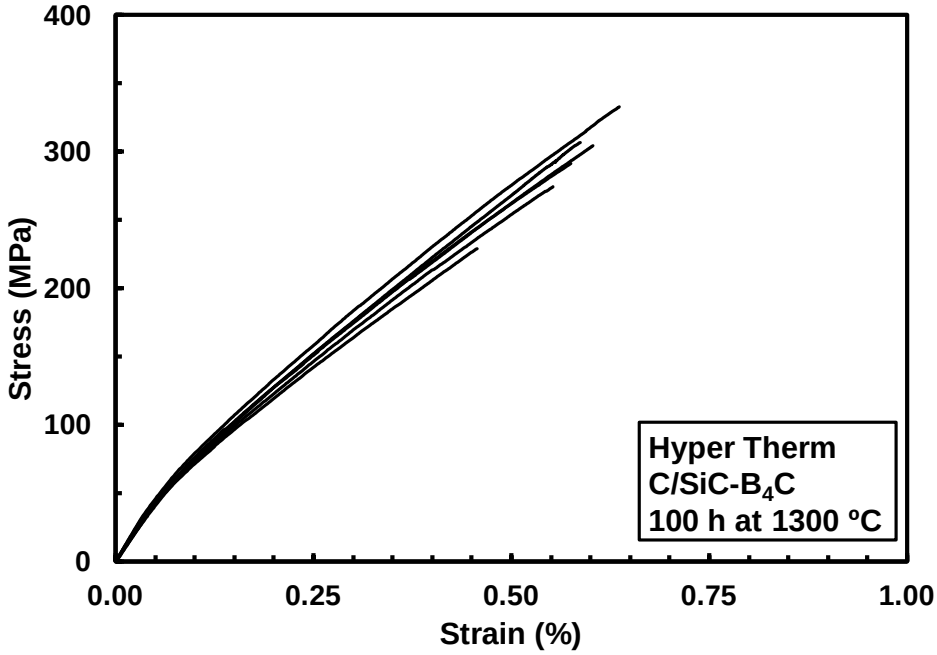

Figure E.17: Tensile stress-strain curves for specimens of T300 C/HYPR-SiC™ composite with prior heat treatment of 100 h at 1300°C

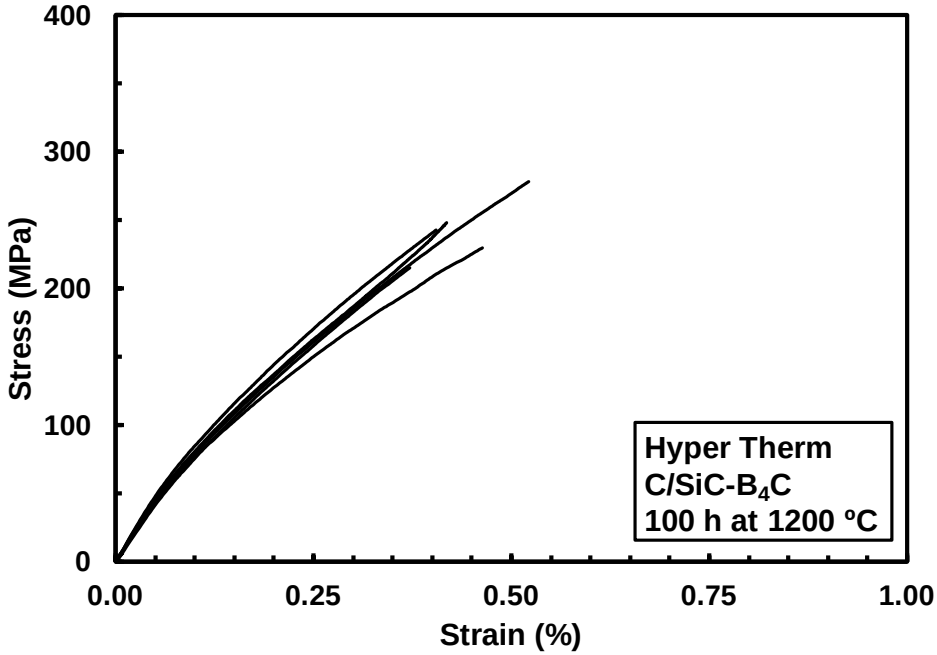

Figure E.18: Tensile stress-strain curves for specimens of T300 C/HYPR-SiC™ composite with prior heat treatment of 100 h at 1200°C

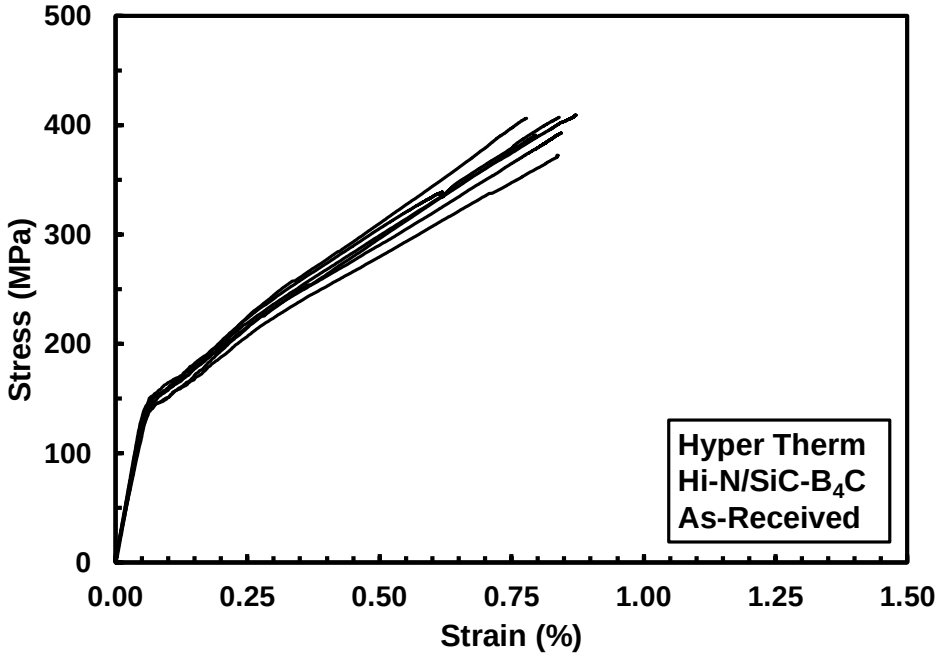

Figure E.19: Tensile stress-strain curves for specimens of as-received Hi-Nicalon™/HYPR-SiC™ composite

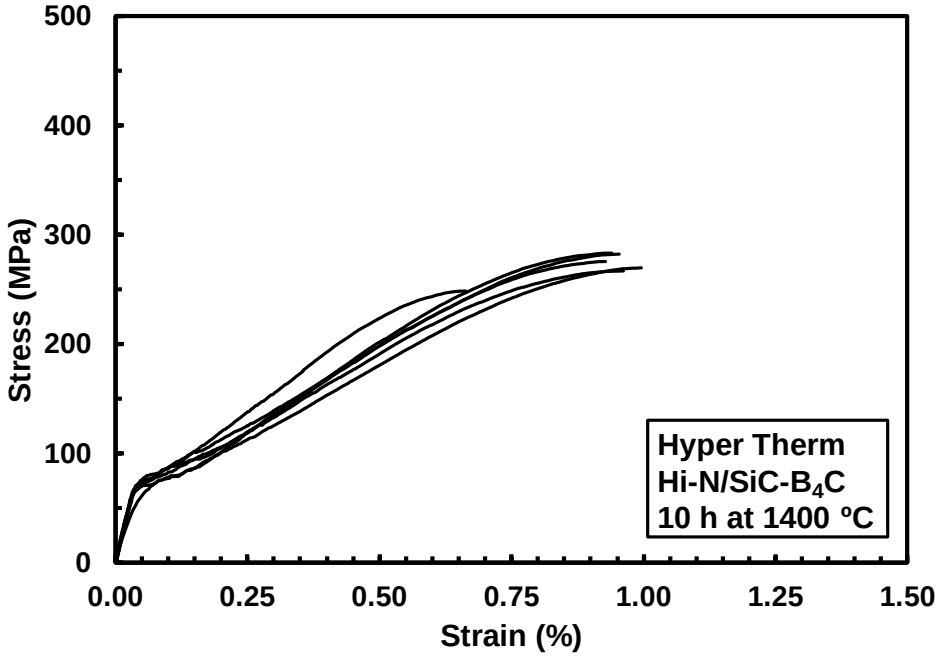

Figure E.20: Tensile stress-strain curves for specimens of Hi-Nicalon™/HYPR-SiC™ composite with prior heat treatment of 10 h at 1400°C

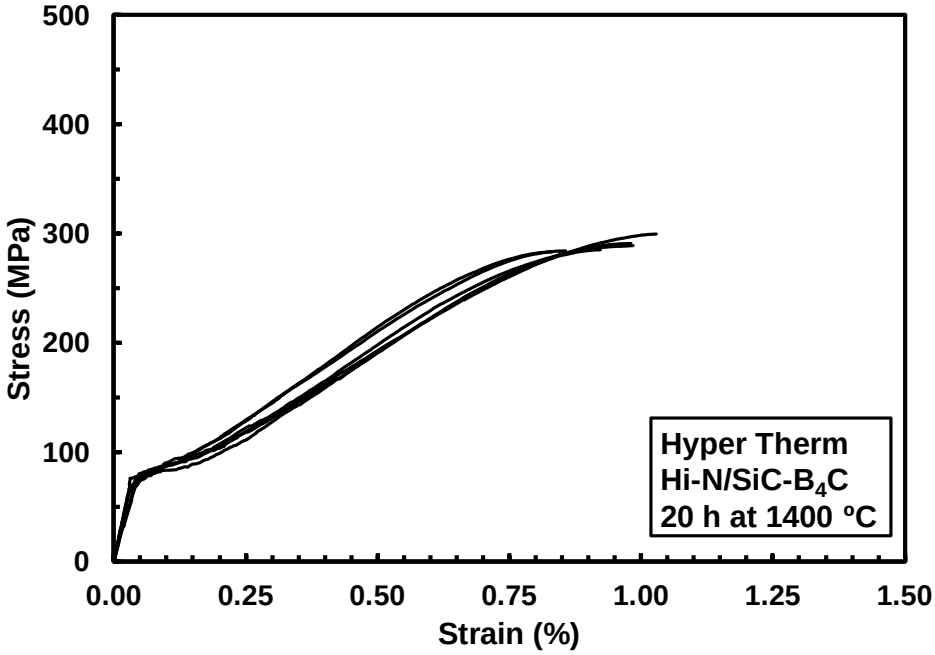

Figure E.21: Tensile stress-strain curves for specimens of Hi-Nicalon™/HYPR-SiC™ composite with prior heat treatment of 20 h at 1400°C

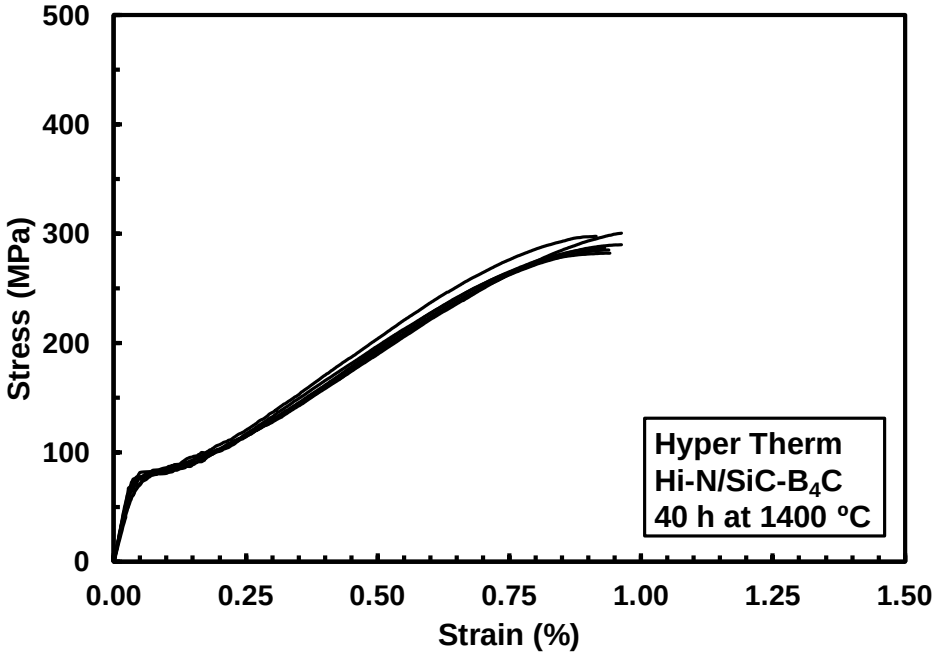

Figure E.22: Tensile stress-strain curves for specimens of Hi-Nicalon™/HYPR-SiC™ composite with prior heat treatment of 40 h at 1400°C

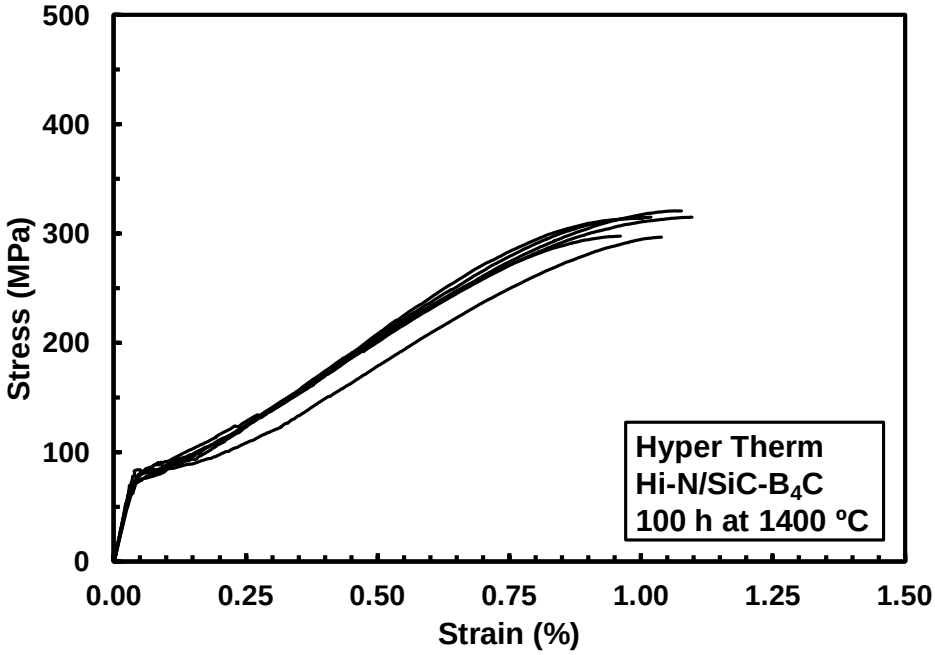

Figure E.23: Tensile stress-strain curves for specimens of Hi-Nicalon™/HYPR-SiC™ composite with prior heat treatment of 100 h at 1400°C

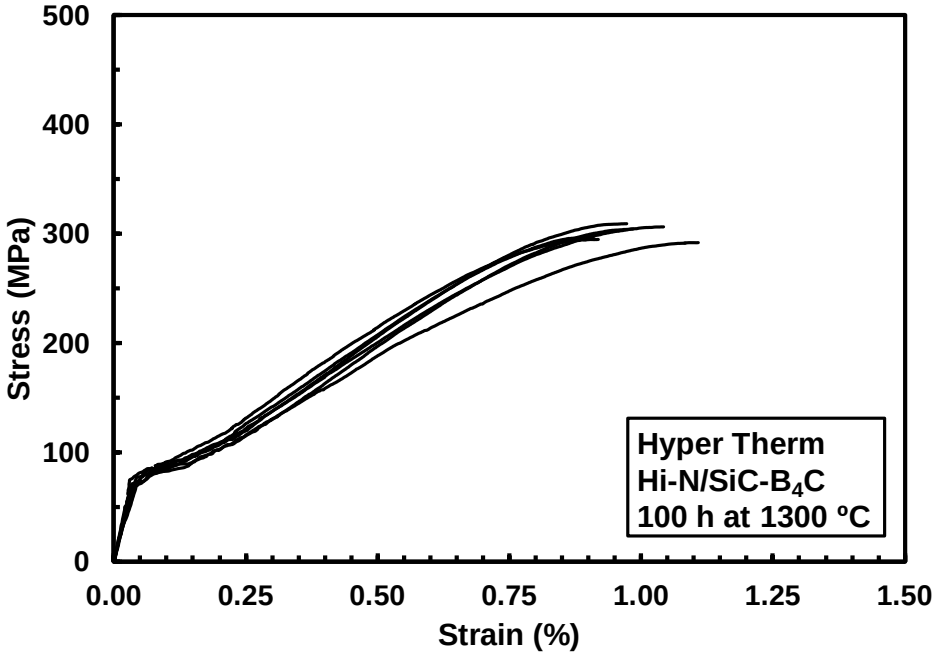

Figure E.24: Tensile stress-strain curves for specimens of Hi-Nicalon™/HYPR-SiC™ composite with prior heat treatment of 100 h at 1300°C

Appendix F: Additional Optical Micrographs of Hi-Nicalon™/SiNC Fracture Surfaces

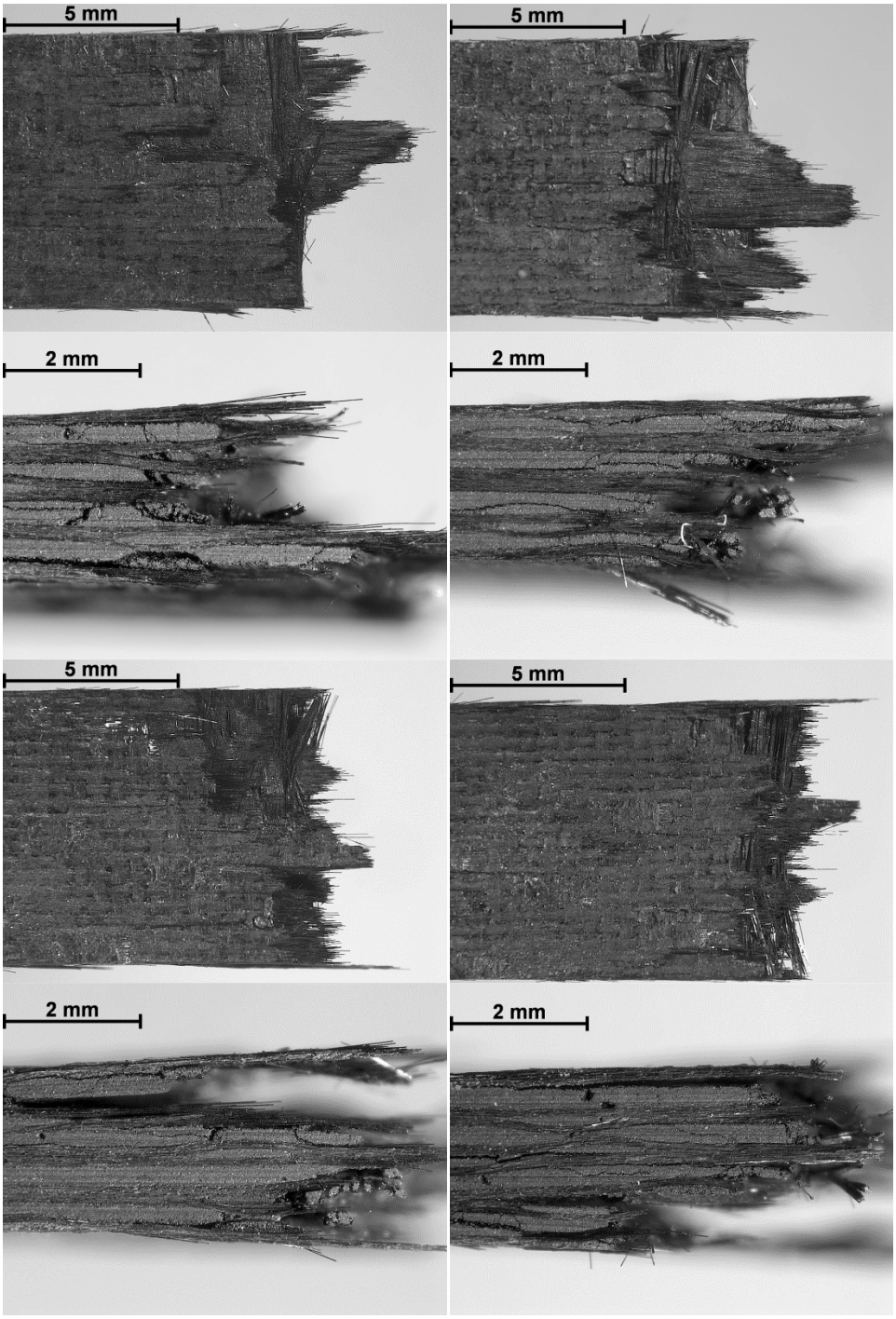

Figure F. 1: Fracture surfaces obtained in tensile test of virgin Hi-Nicalon™/SiNC specimen (Plate 11107, Specimen 3)

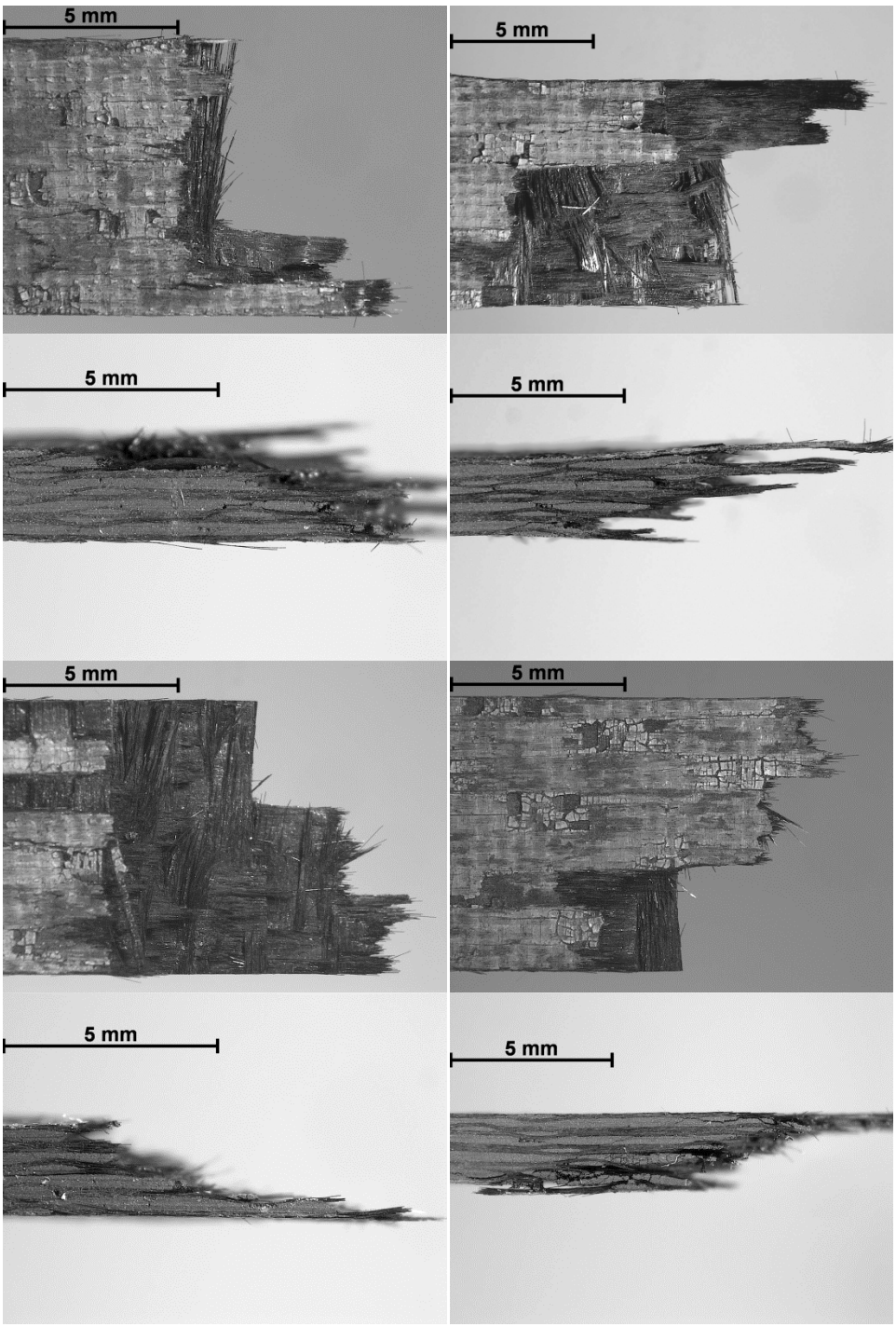

Figure F. 2: Fracture surfaces obtained in tensile test of Hi-Nicalon™/SiNC specimen subjected to prior heat treatment of 10 h at 1300°C (Plate 11101, Specimen 6)

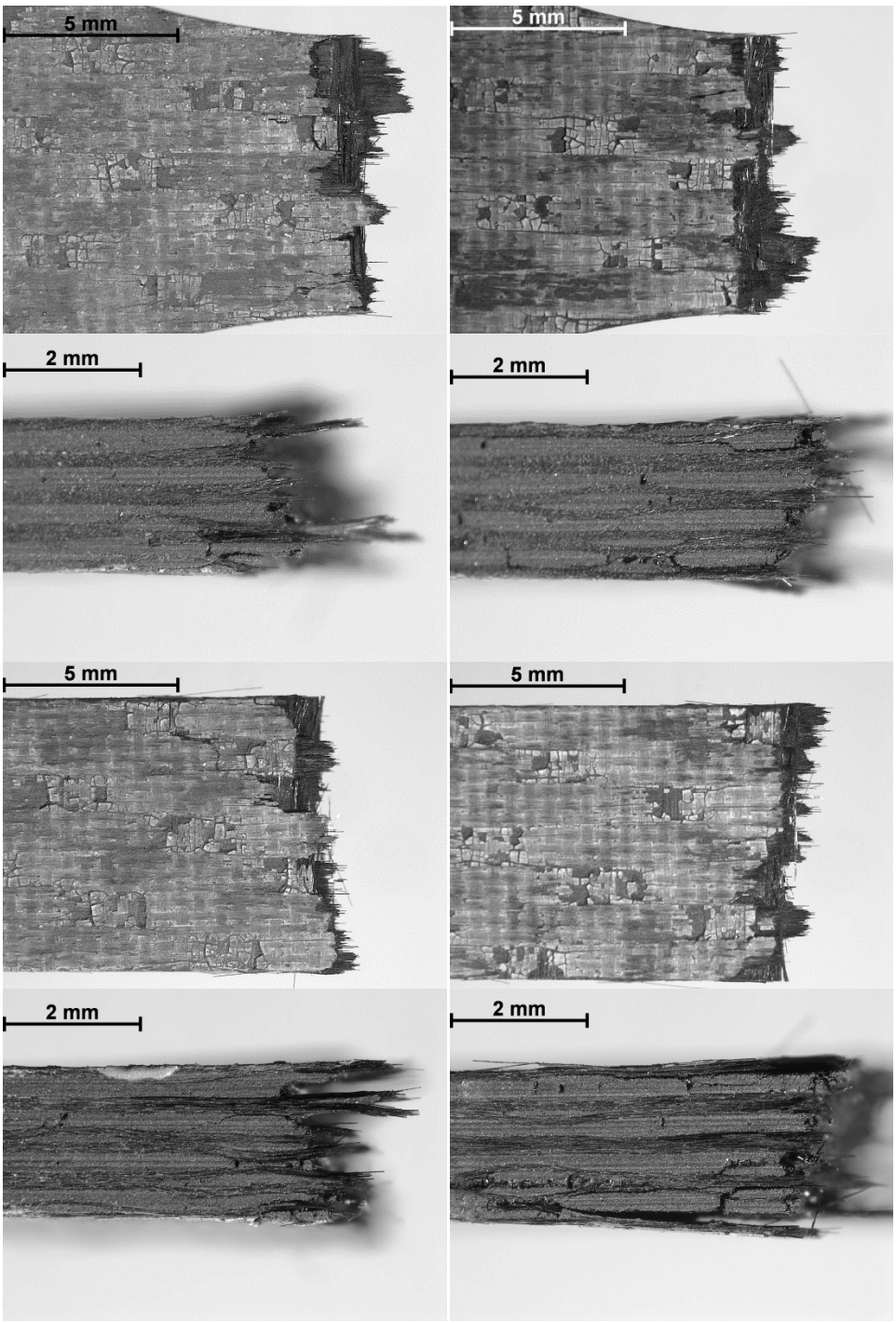

Figure F. 3: Fracture surfaces obtained in tensile test of Hi-Nicalon™/SiNC specimen subjected to prior heat treatment of 100 h at 1300°C (Plate 11105, Specimen 6)

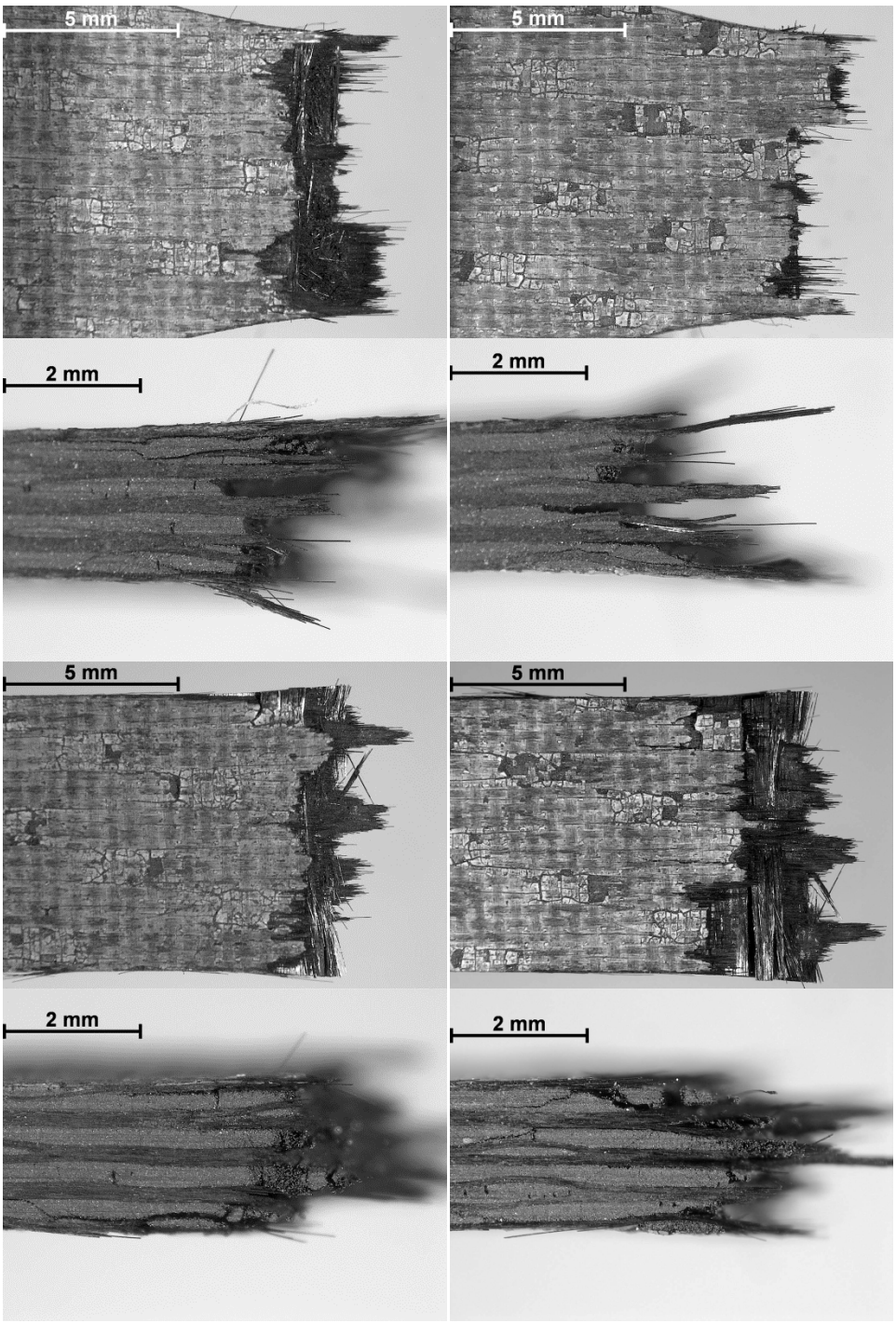

Figure F. 4: Fracture surfaces obtained in tensile test of Hi-Nicalon™/SiNC specimen subjected to prior heat treatment of 100 h at 1200°C (Plate 11106, Specimen 4)

Appendix G: Additional Optical Micrographs of HexTow® IM7 C/SiC Fracture Surfaces

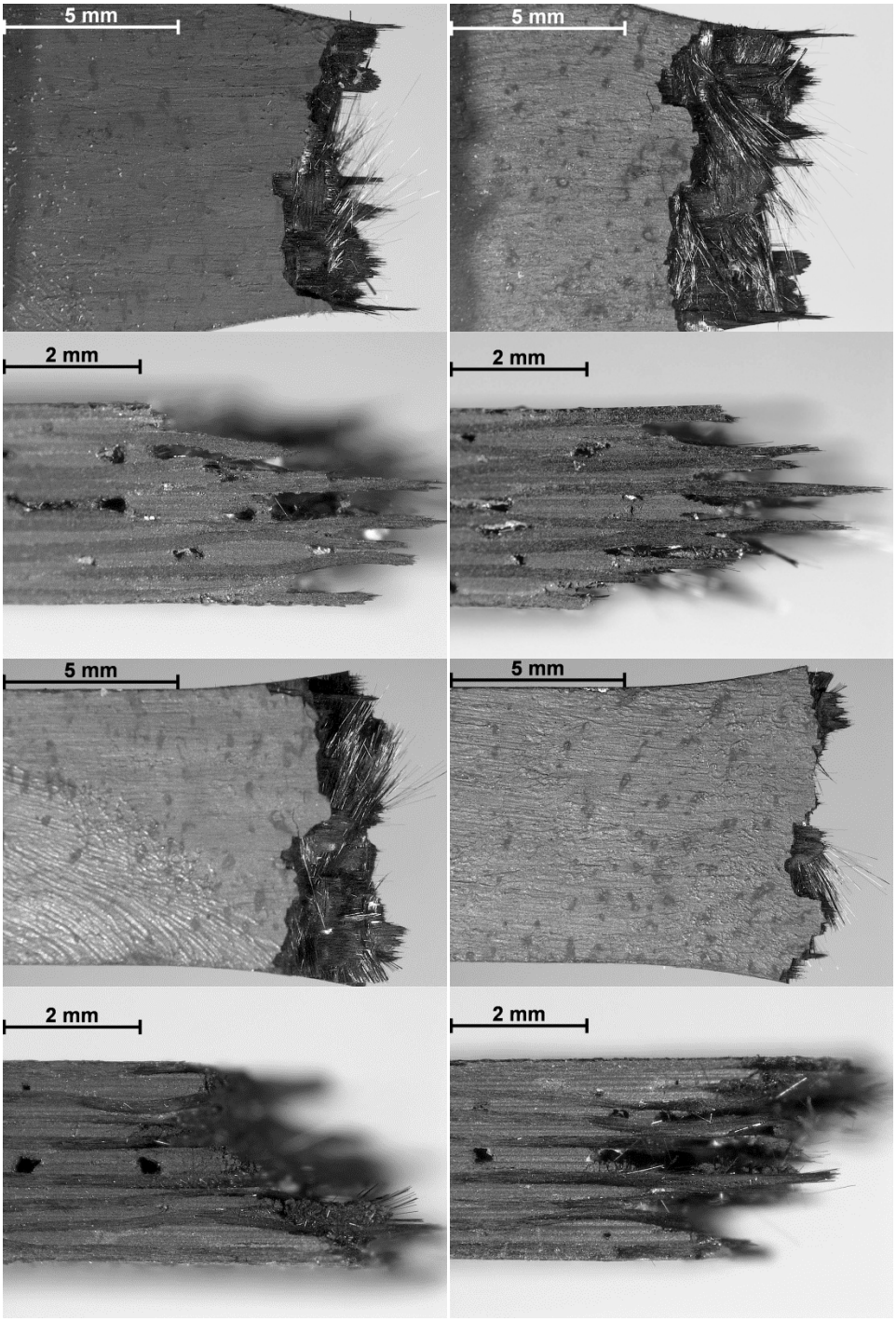

Figure G. 1: Fracture surfaces obtained in tensile test of virgin C/SiC specimen (Plate 12012, Specimen 6)

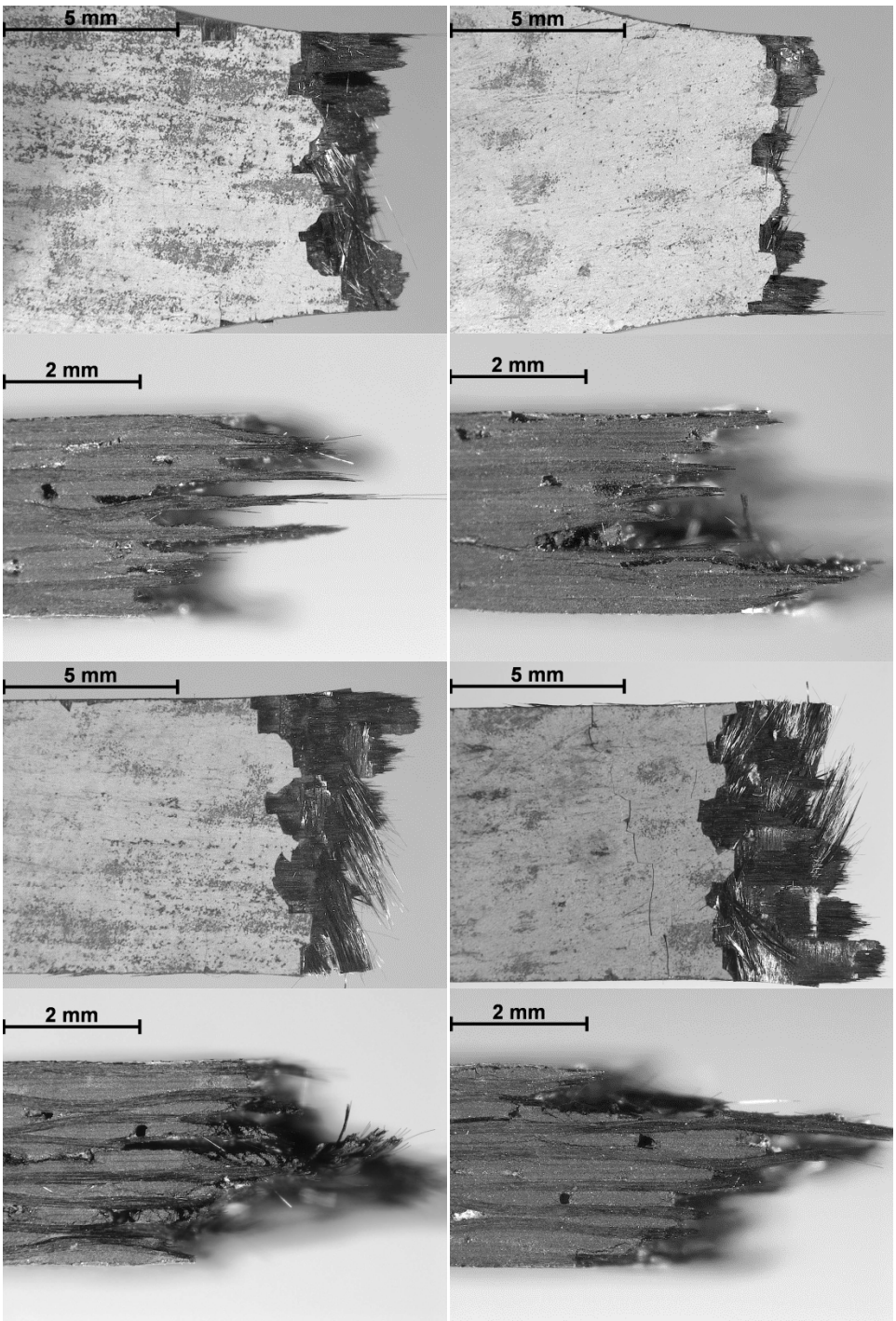

Figure G. 2: Fracture surfaces obtained in tensile test of C/SiC specimen subjected to prior heat treatment of 40 h at 1300°C (Plate 12018, Specimen 2)

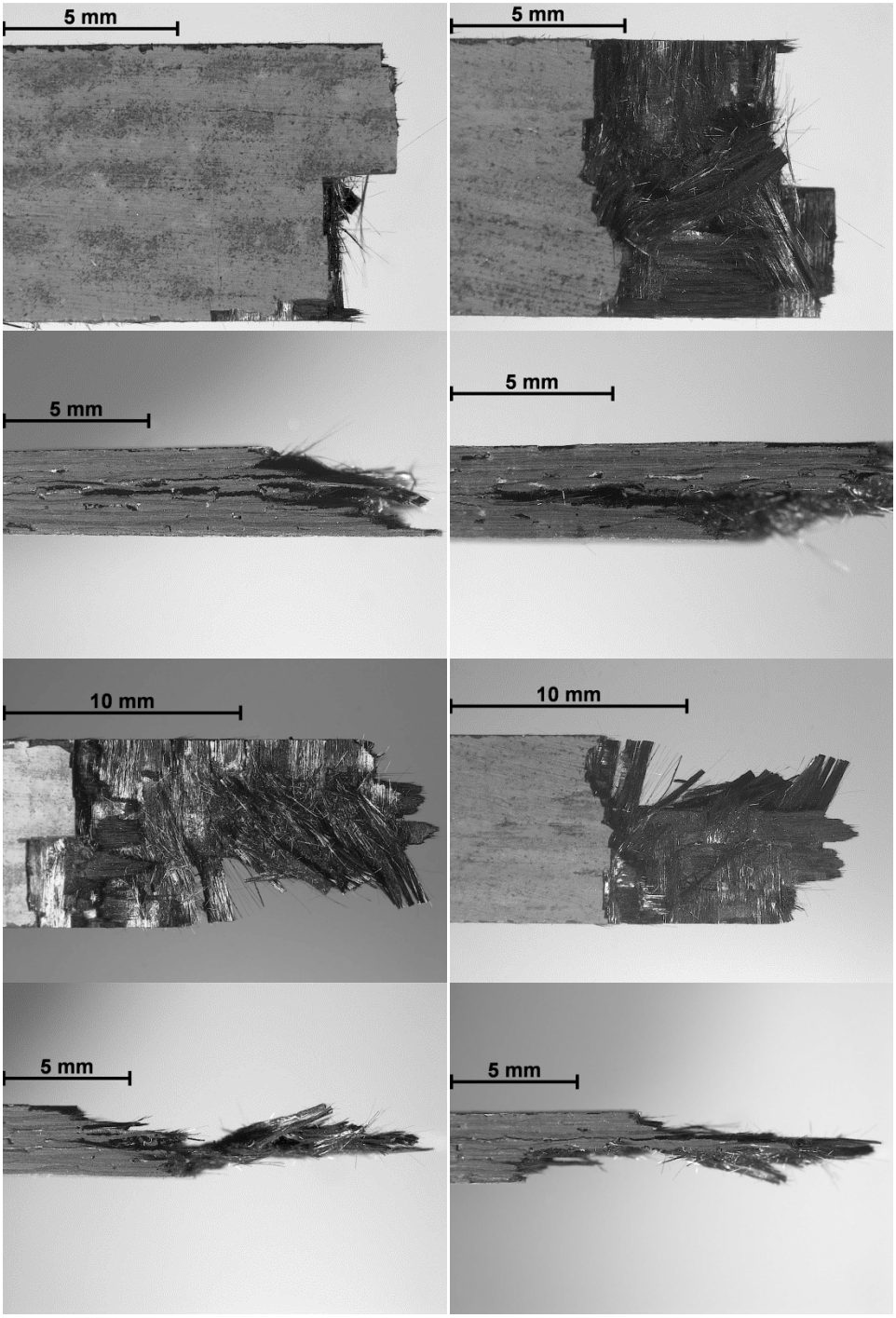

Figure G. 3: Fracture surfaces obtained in tensile test of C/SiC specimen subjected to prior heat treatment of 100 h at 1300°C (Plate 12015, Specimen 3)

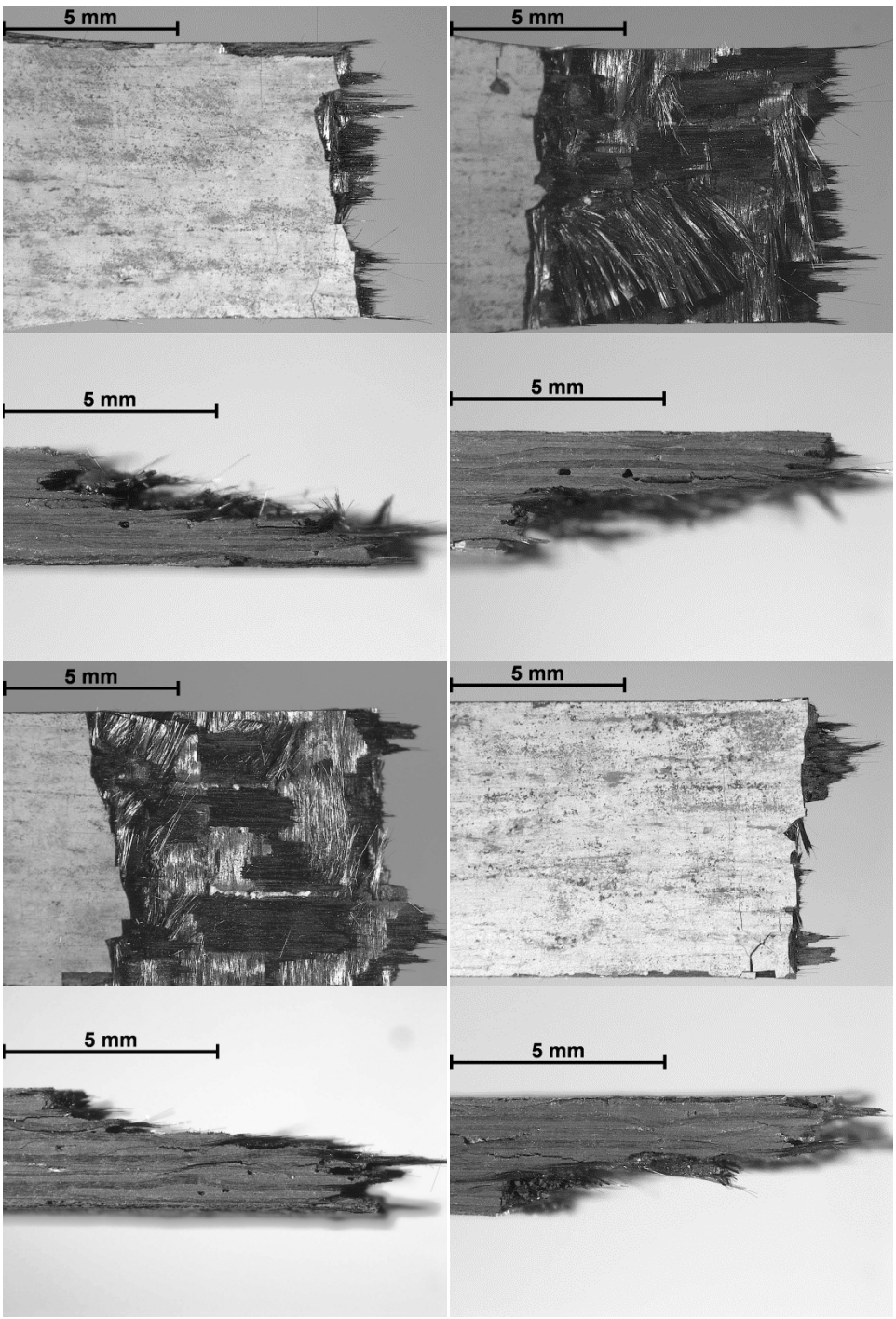

Figure G. 4: Fracture surfaces obtained in tensile test of C/SiC specimen subjected to prior heat treatment of 100 h at 1200°C (Plate 12016, Specimen 3)

Appendix H: Additional Optical Micrographs of T300 C/HYPR-SiC™ Fracture Surfaces

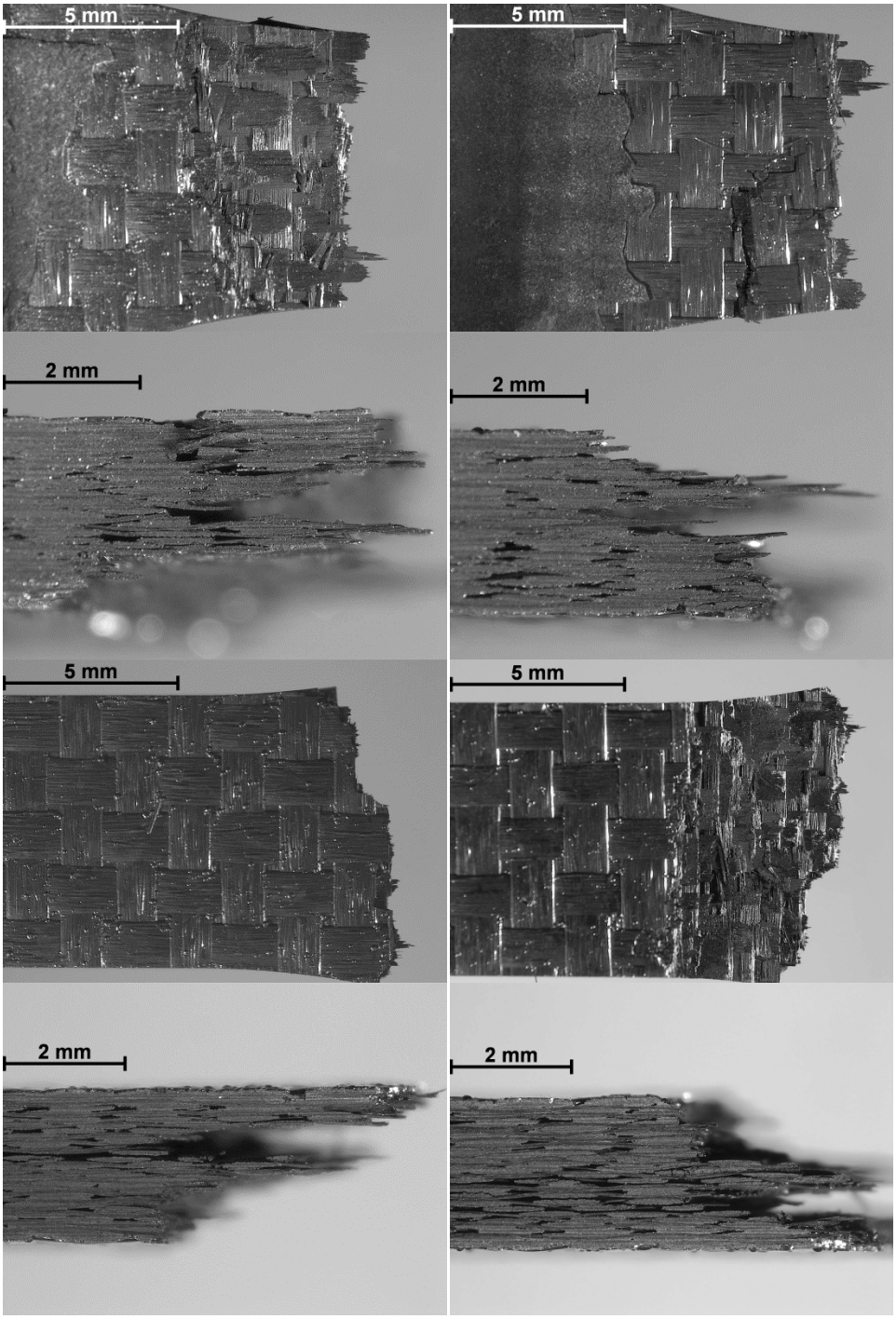

Figure H. 1: Fracture surfaces obtained in tensile test of virgin C/HYPR-SiC™ specimen (Plate 11126, Specimen 4)

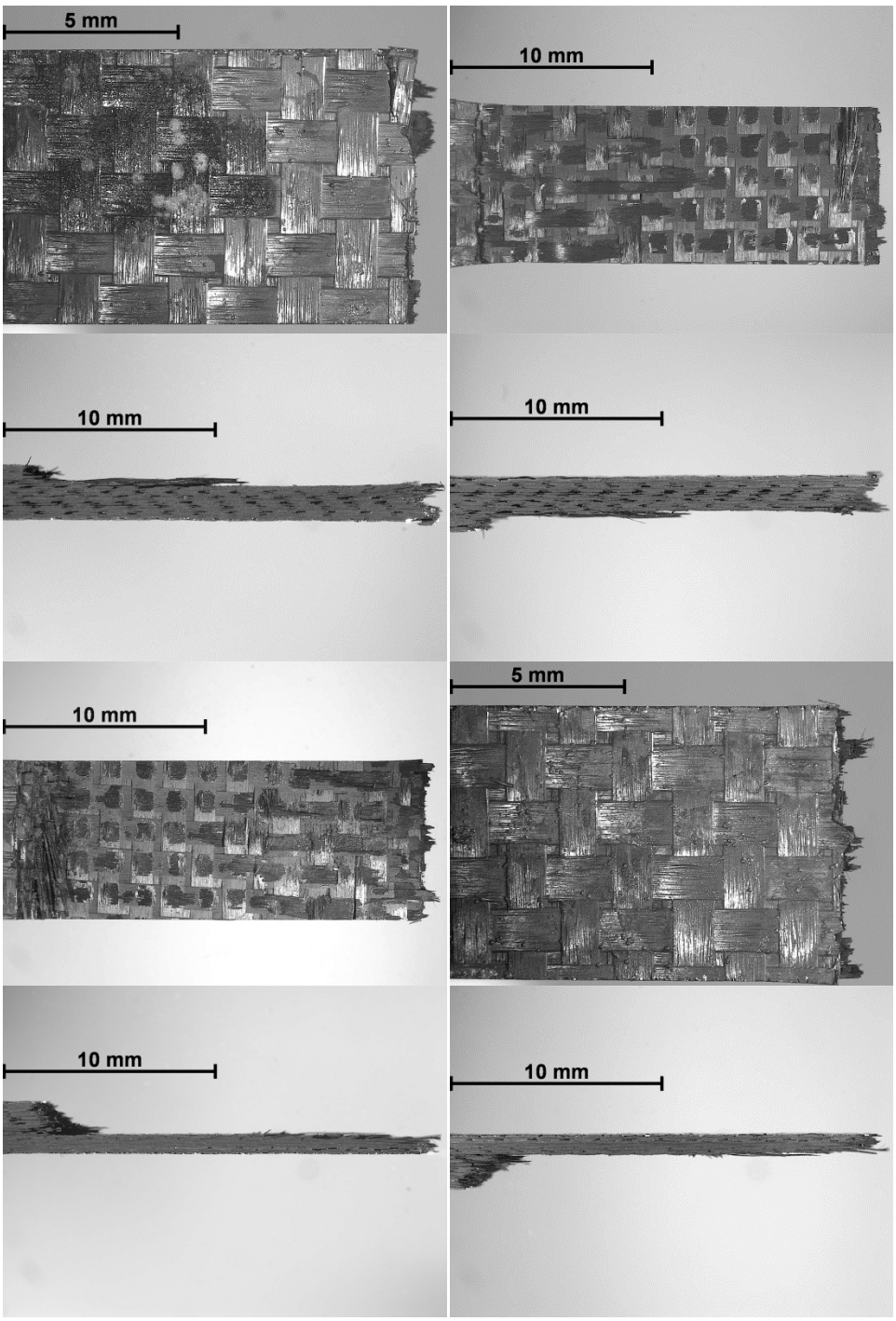

Figure H. 2: Fracture surfaces obtained in tensile test of C/HYPR-SiC™ specimen subjected to prior heat treatment of 40 h at 1300°C (Plate 11125, Specimen 4)

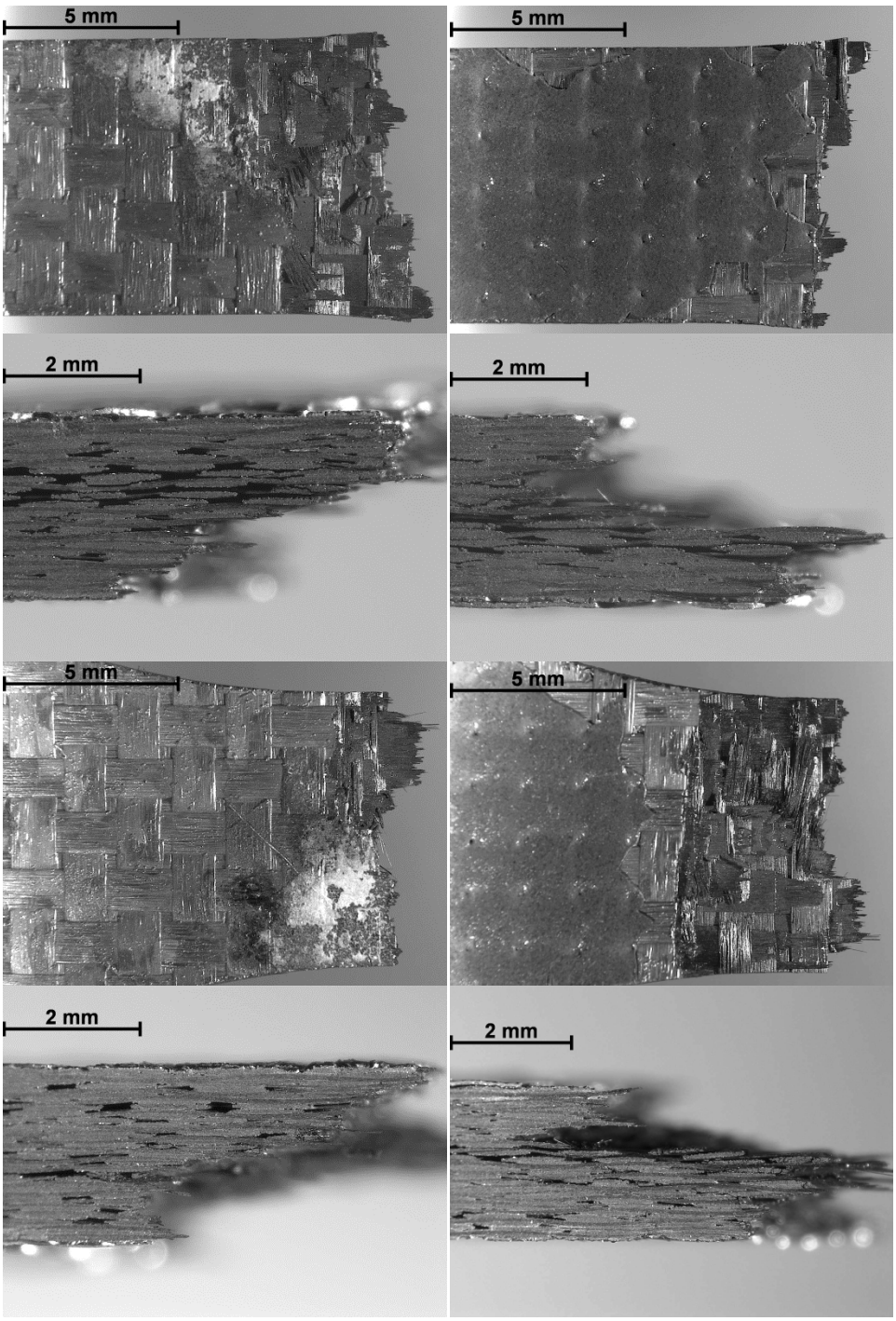

Figure H. 3: Fracture surfaces obtained in tensile test of C/HYPR-SiC™ specimen subjected to prior heat treatment of 100 h at 1300°C (Plate 11121, Specimen 5)

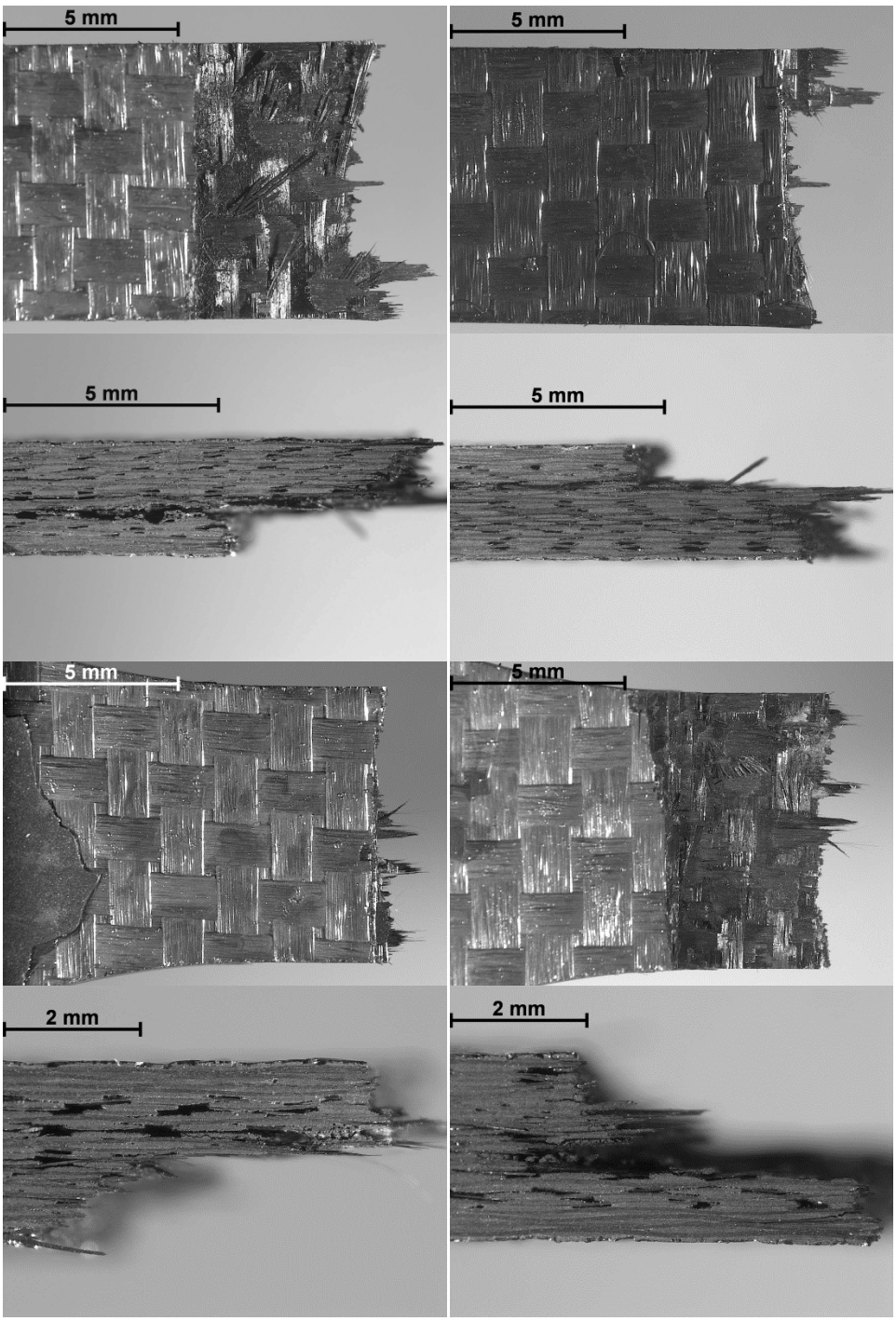

Figure H. 4: Fracture surfaces obtained in tensile test of C/HYPR-SiC™ specimen subjected to prior heat treatment of 100 h at 1200°C (Plate 11122, Specimen 5)

Appendix I: Additional Optical Micrographs of Hi-Nicalon™/HYPR-SiC™ Fracture Surfaces

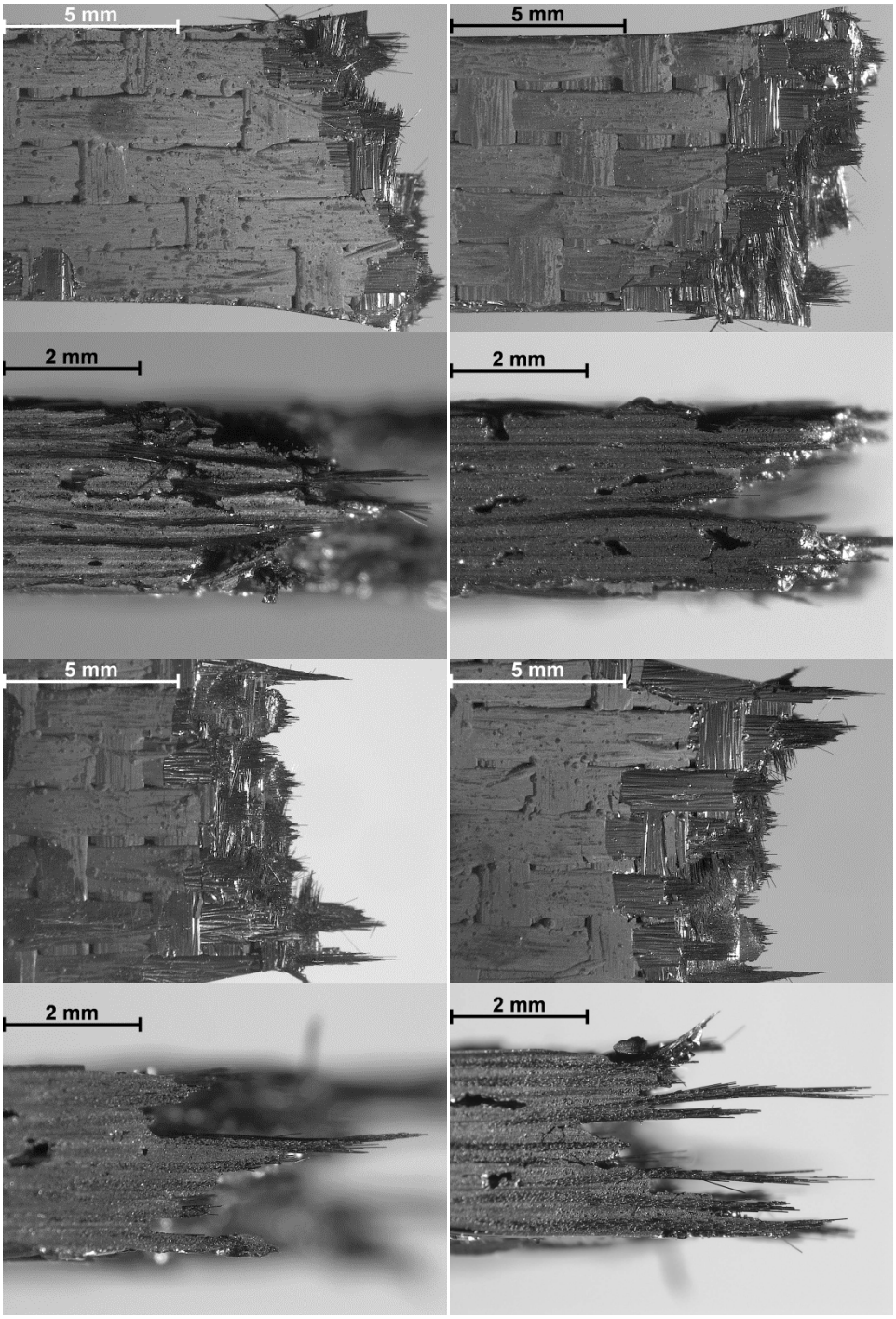

Figure I. 1: Fracture surfaces obtained in tensile test of virgin Hi-Nicalon™/HYPR-SiC™ specimen (Plate 11138, Specimen 3)

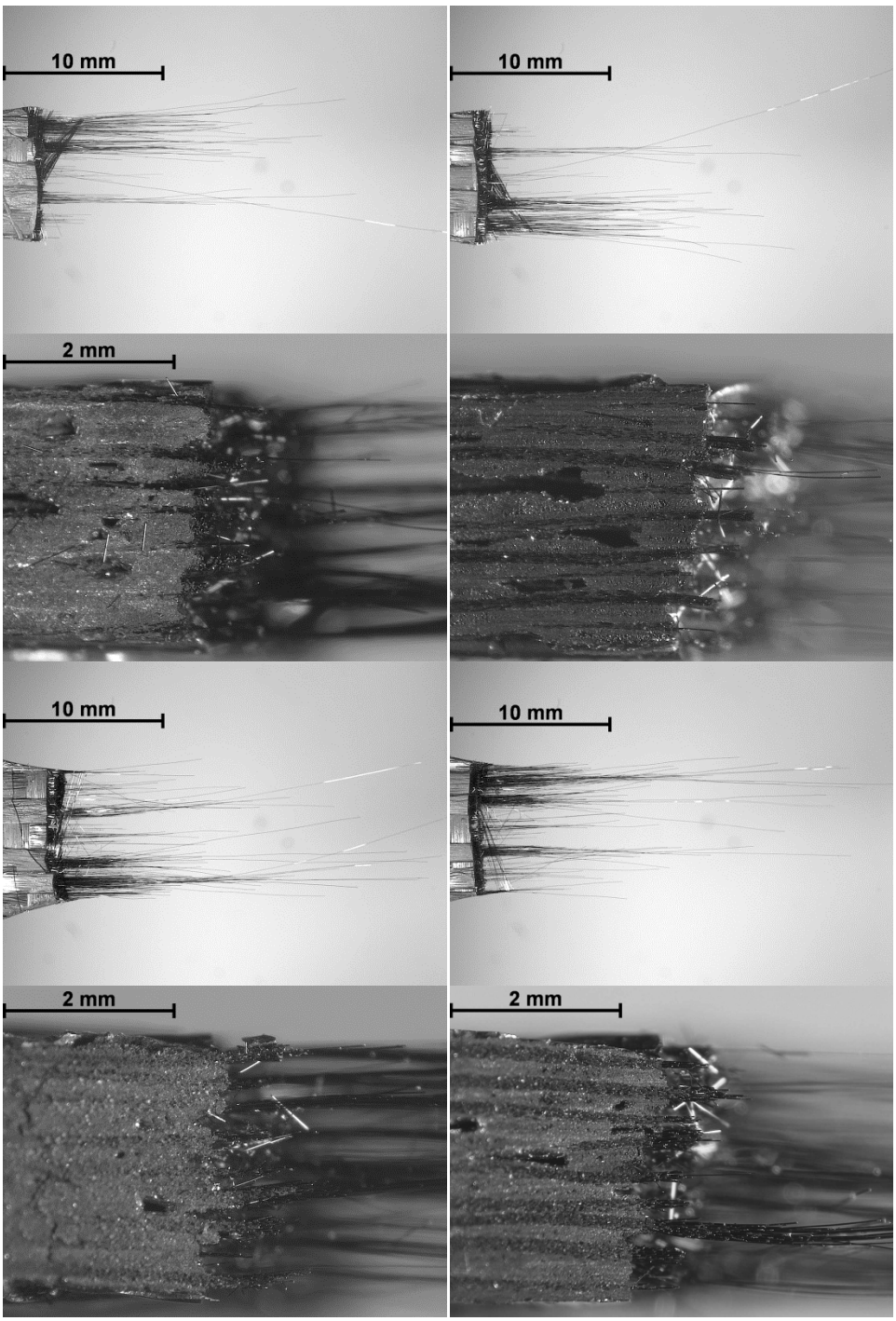

Figure I. 2: Fracture surfaces obtained in tensile test of Hi-Nicalon™/HYPR-SiC™ specimen subjected to prior heat treatment of 10 h at 1400°C (Plate 11133, Specimen 2)

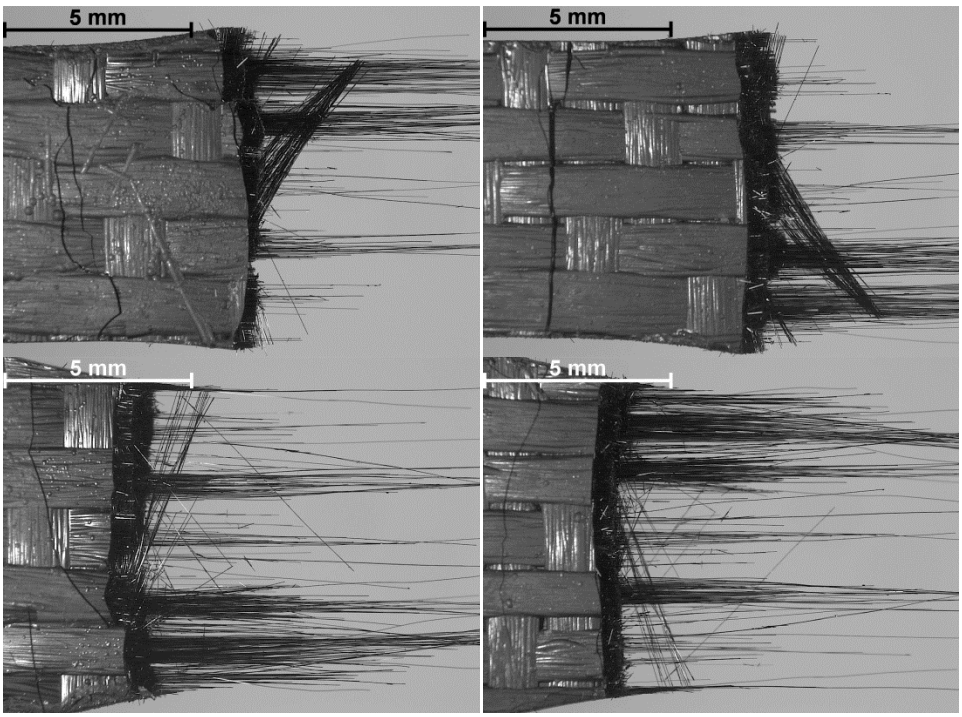

Figure I. 3: Fracture surfaces obtained in tensile test of Hi-Nicalon™/HYPR-SiC™ specimen subjected to prior heat treatment of 10 h at 1400°C (Plate 11133, Specimen 2)

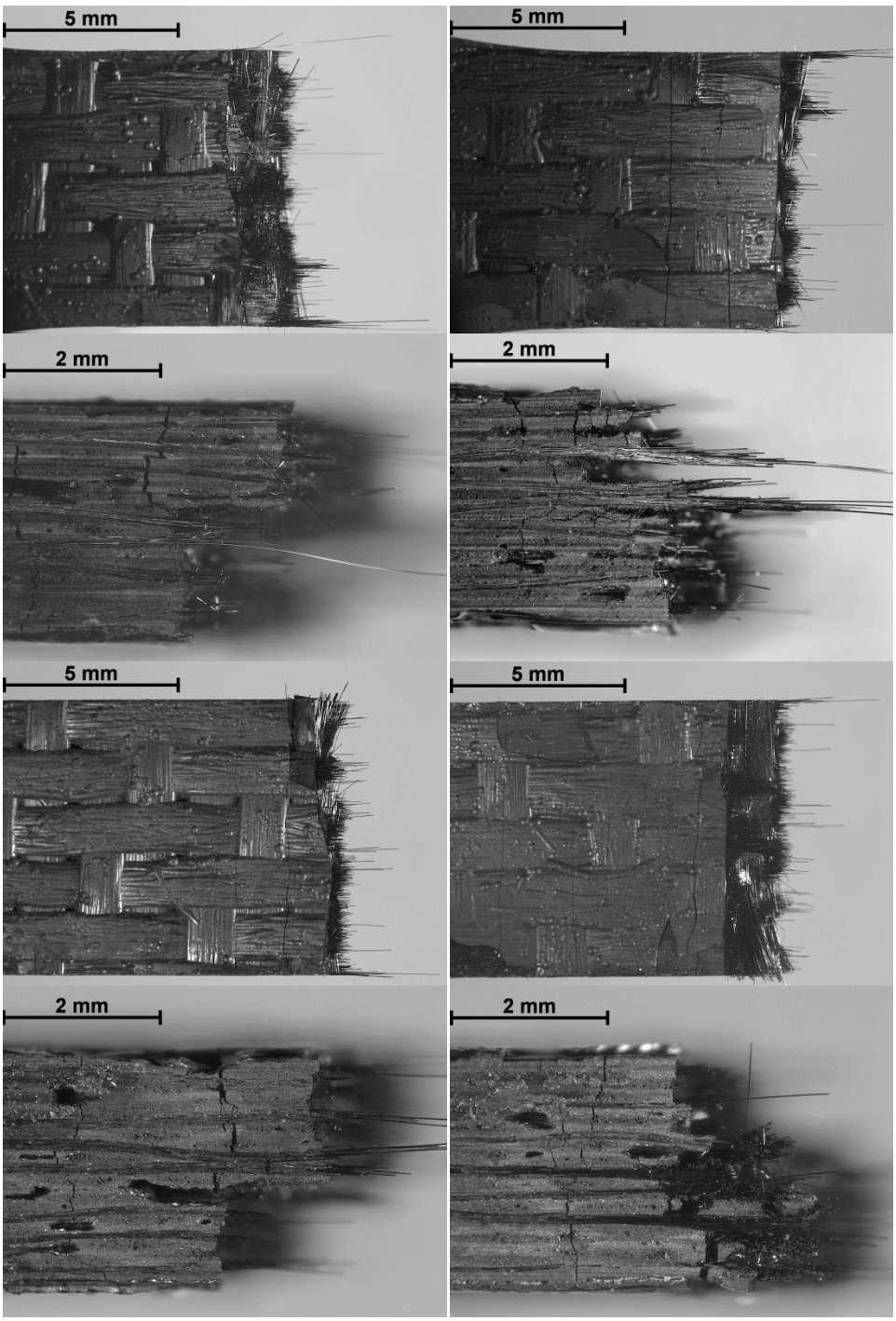

Figure I. 4: Fracture surfaces obtained in tensile test of Hi-Nicalon™/HYPR-SiC™ specimen subjected to prior heat treatment of 100 h at 1400°C (Plate 11137, Specimen 6)

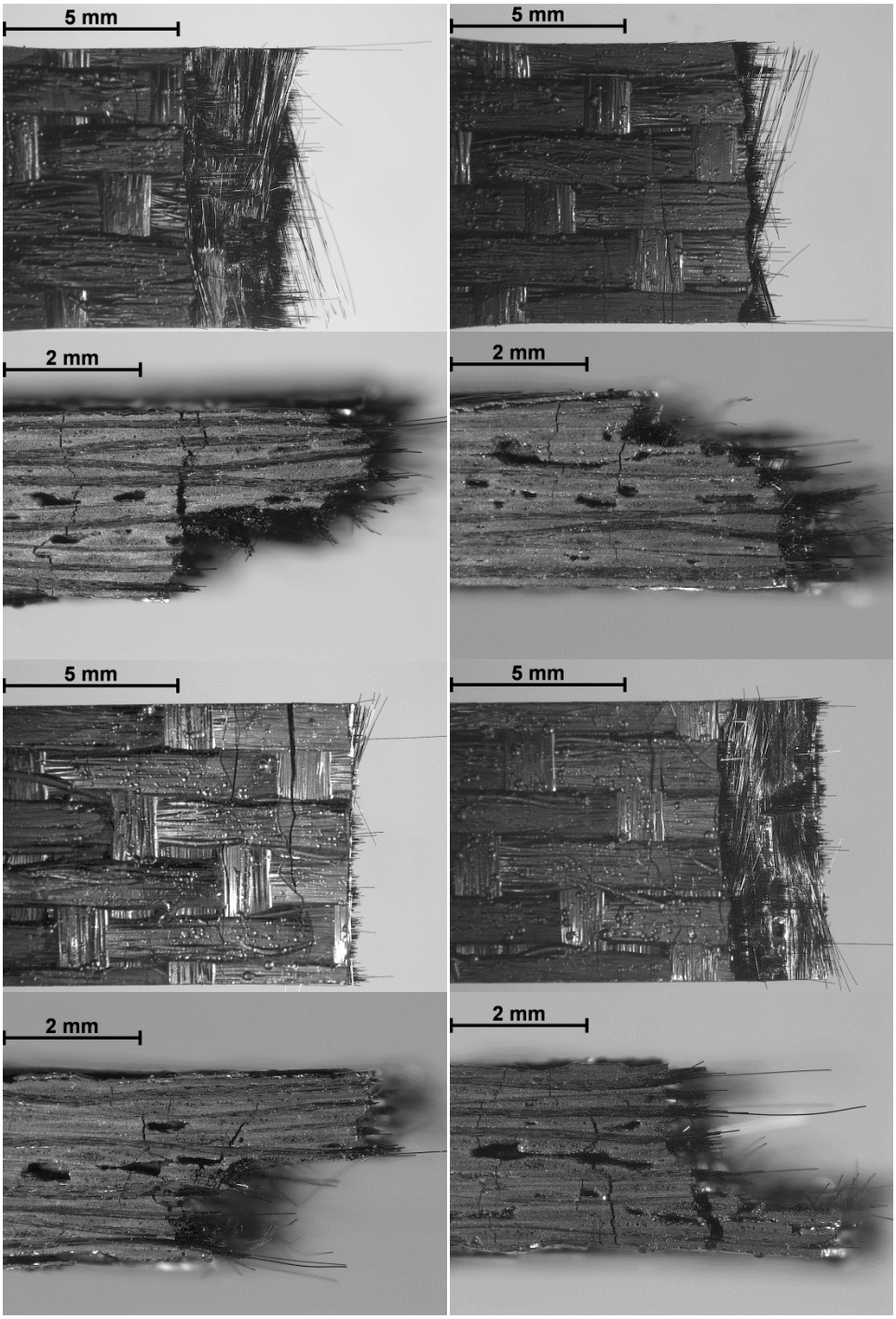

Figure I. 5: Fracture surfaces obtained in tensile test of Hi-Nicalon™/HYPR-SiC™ specimen subjected to prior heat treatment of 100 h at 1300°C (Plate 11139, Specimen 1)

Appendix J: Additional SEM Micrographs of Hi-Nicalon™/SiNC Fracture Surfaces

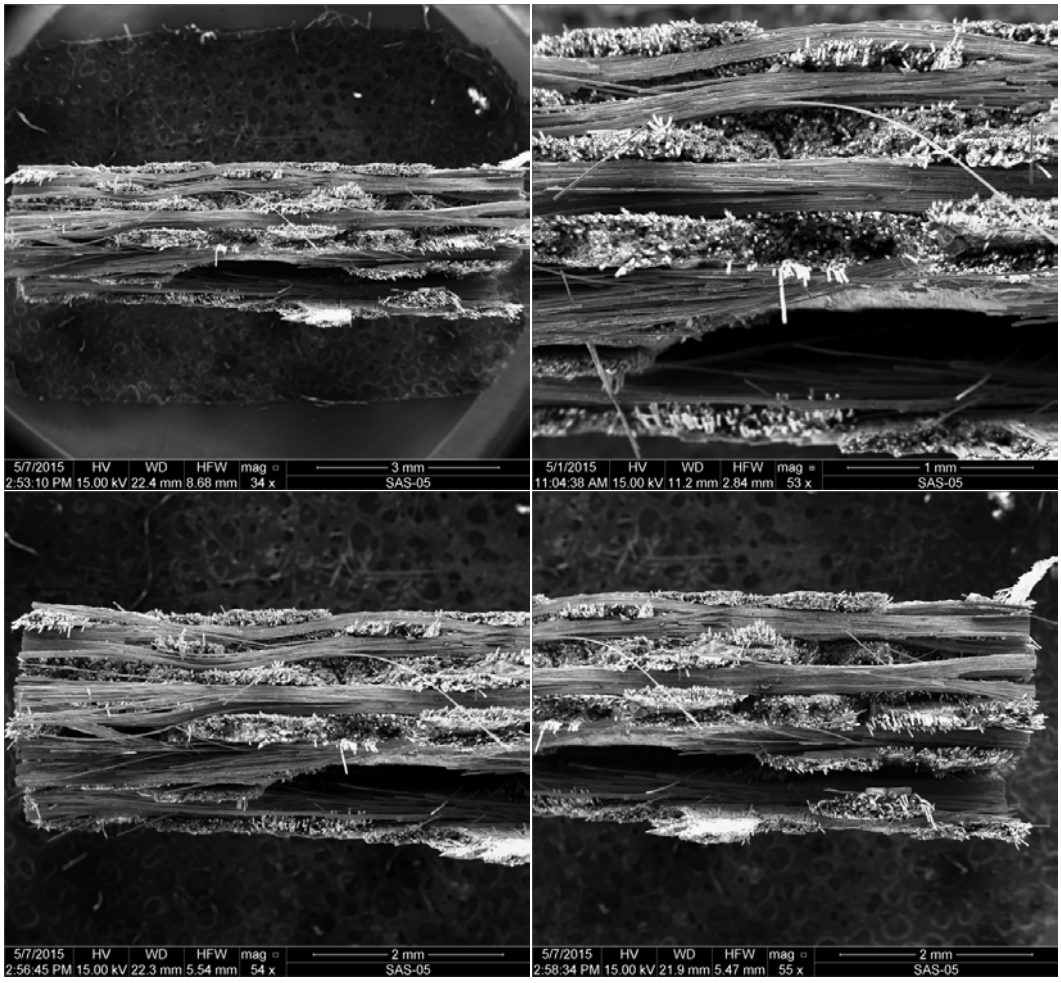

Figure J. 1: SEM micrographs of a fracture surface obtained in tensile test of a virgin Hi-Nicalon™/SiNC specimen (Plate 11107, Specimen 3)

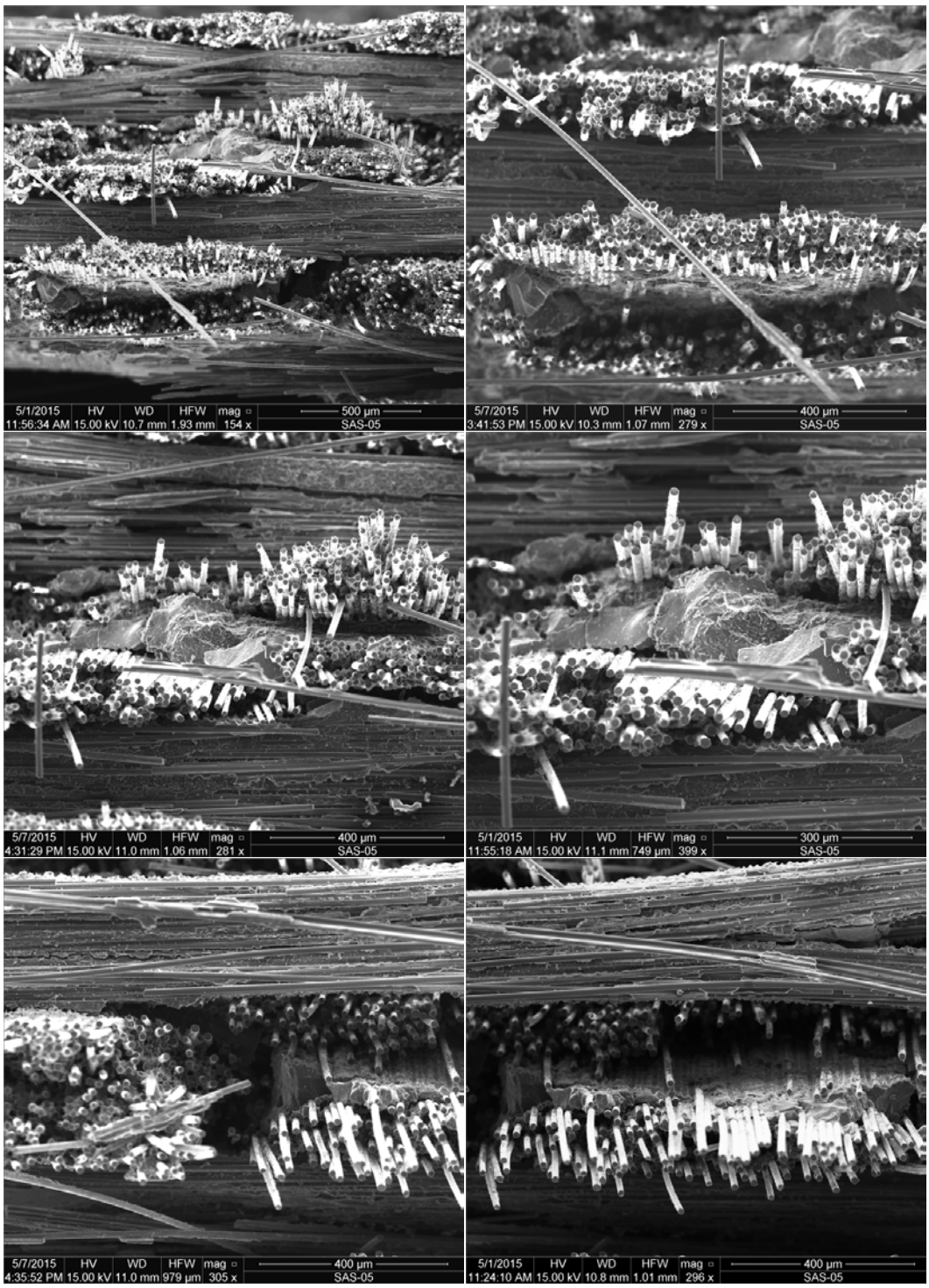

Figure J. 2: SEM micrographs of a fracture surface obtained in tensile test of a virgin Hi-Nicalon™/SiNC specimen (Plate 11107, Specimen 3)

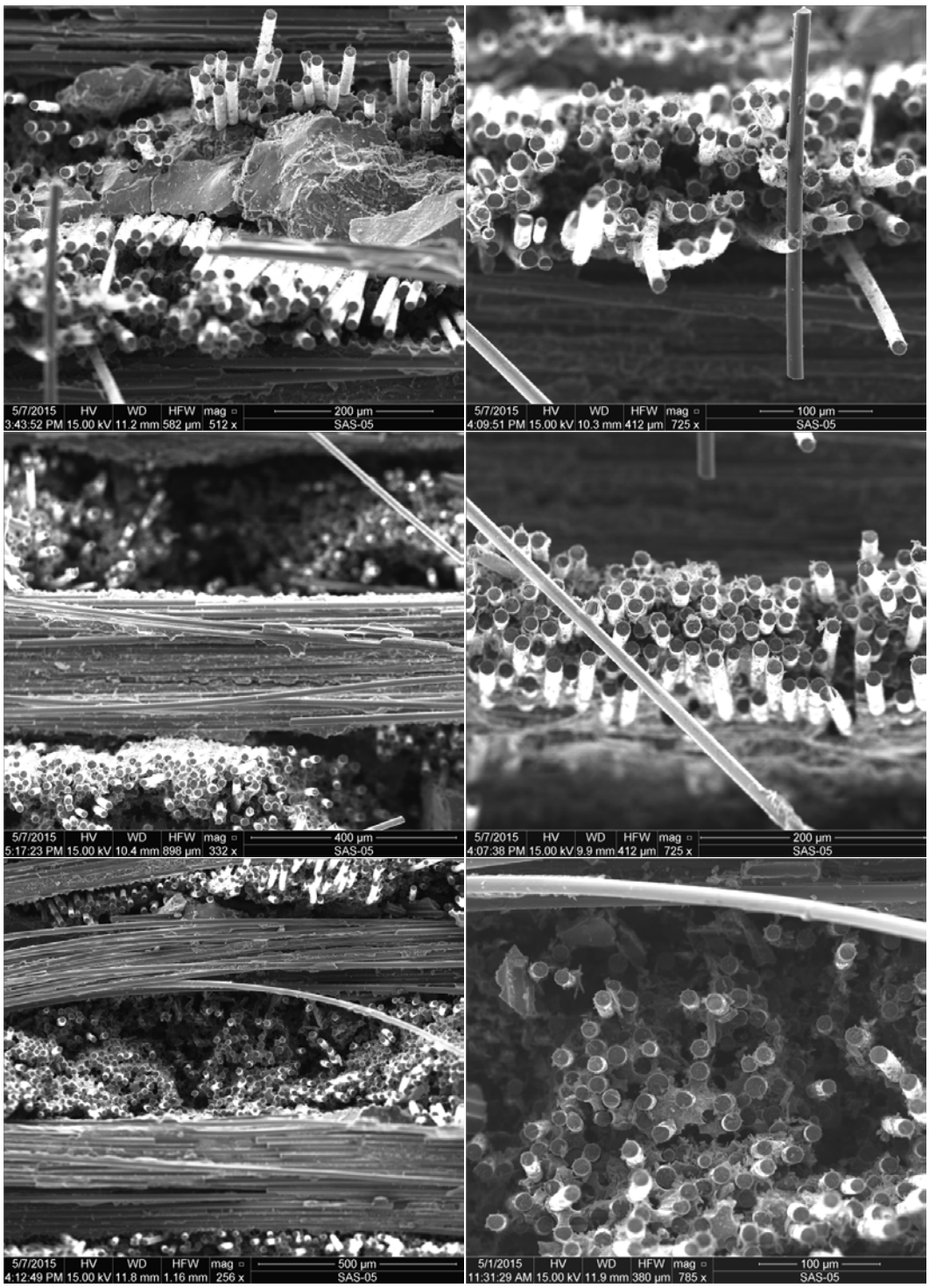

Figure J. 3: SEM micrographs of a fracture surface obtained in tensile test of a virgin Hi-Nicalon™/SiNC specimen (Plate 11107, Specimen 3)

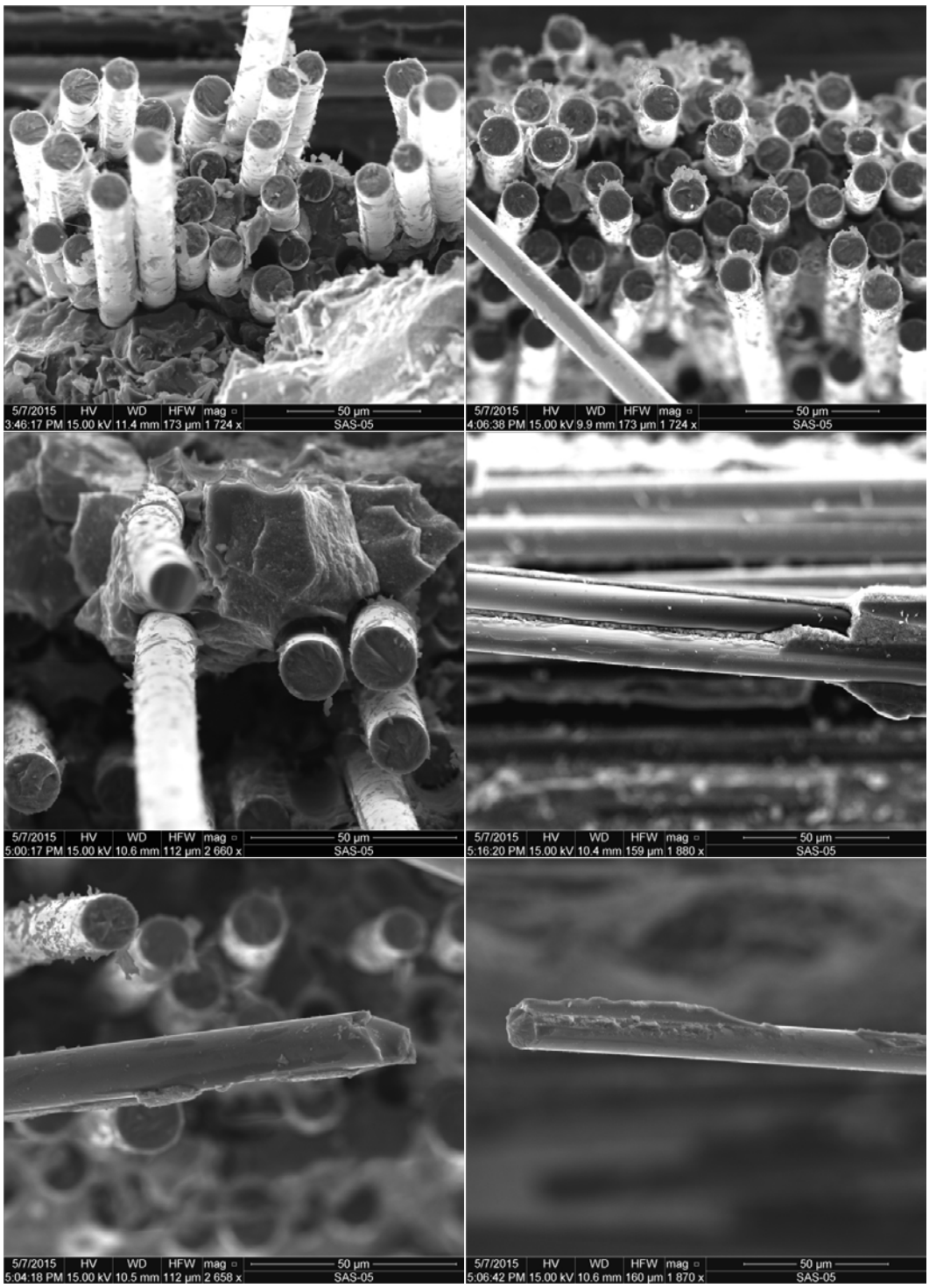

Figure J. 4: SEM micrographs of a fracture surface obtained in tensile test of a virgin Hi-Nicalon™/SiNC specimen (Plate 11107, Specimen 3)

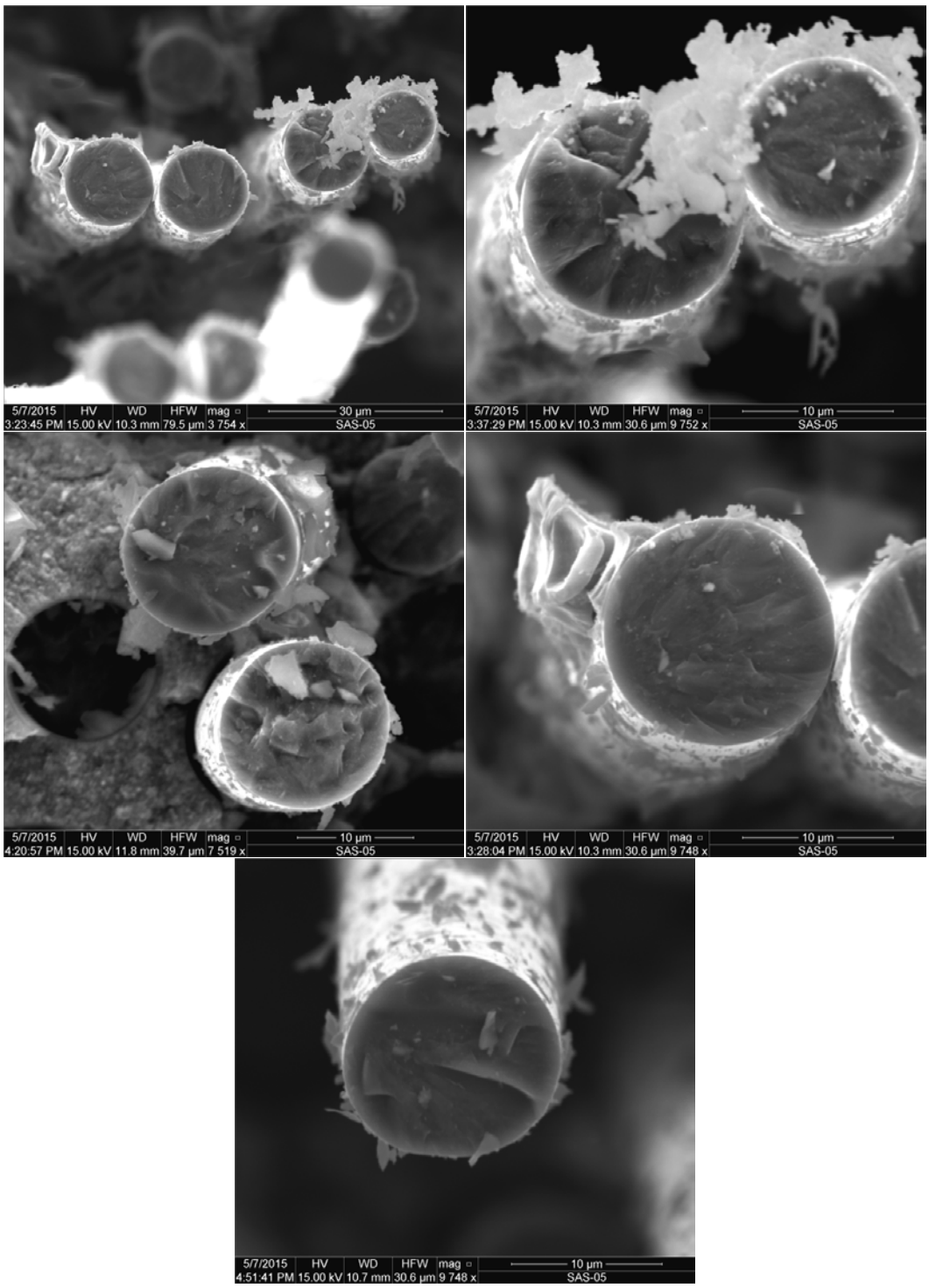

Figure J. 5: SEM micrographs of a fracture surface obtained in tensile test of a virgin Hi-Nicalon™/SiNC specimen (Plate 11107, Specimen 3)

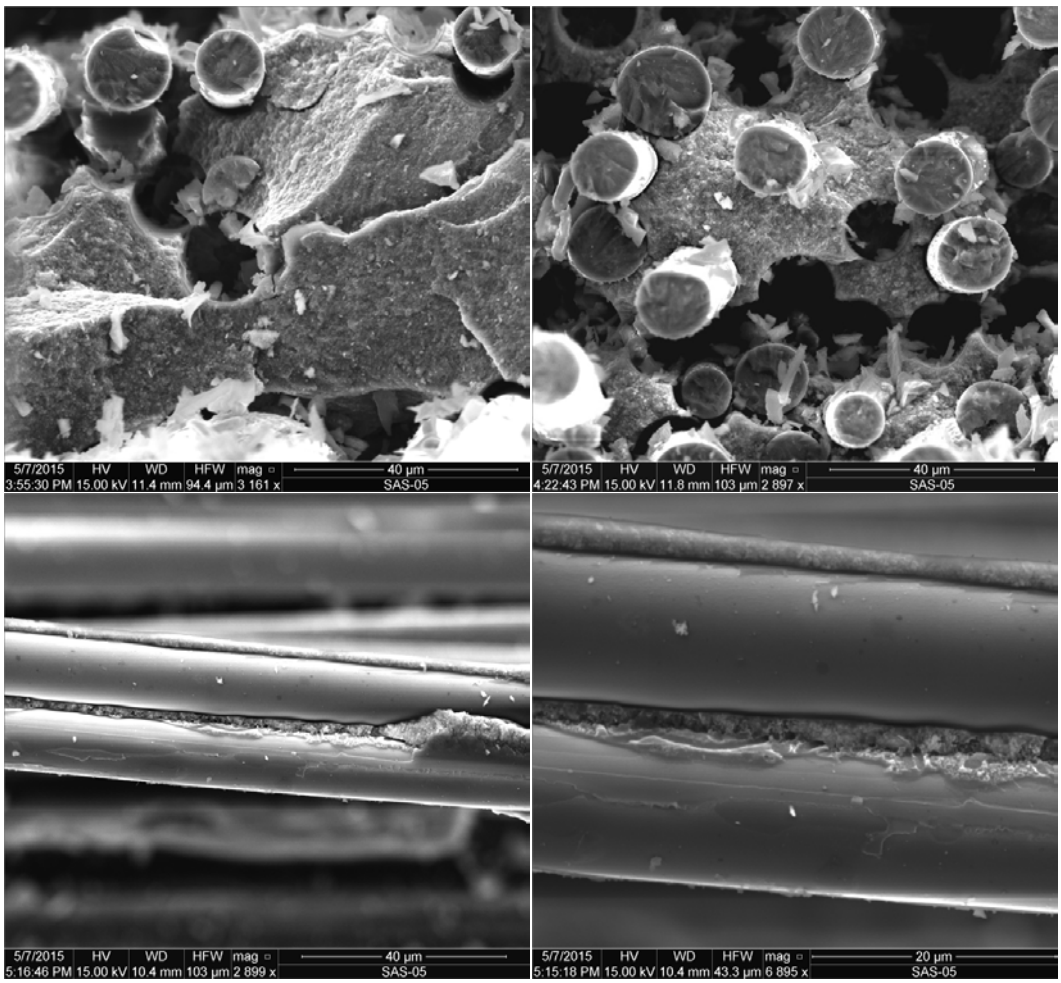

Figure J. 6: SEM micrographs of a fracture surface obtained in tensile test of a virgin Hi-Nicalon™/SiNC specimen (Plate 11107, Specimen 3)

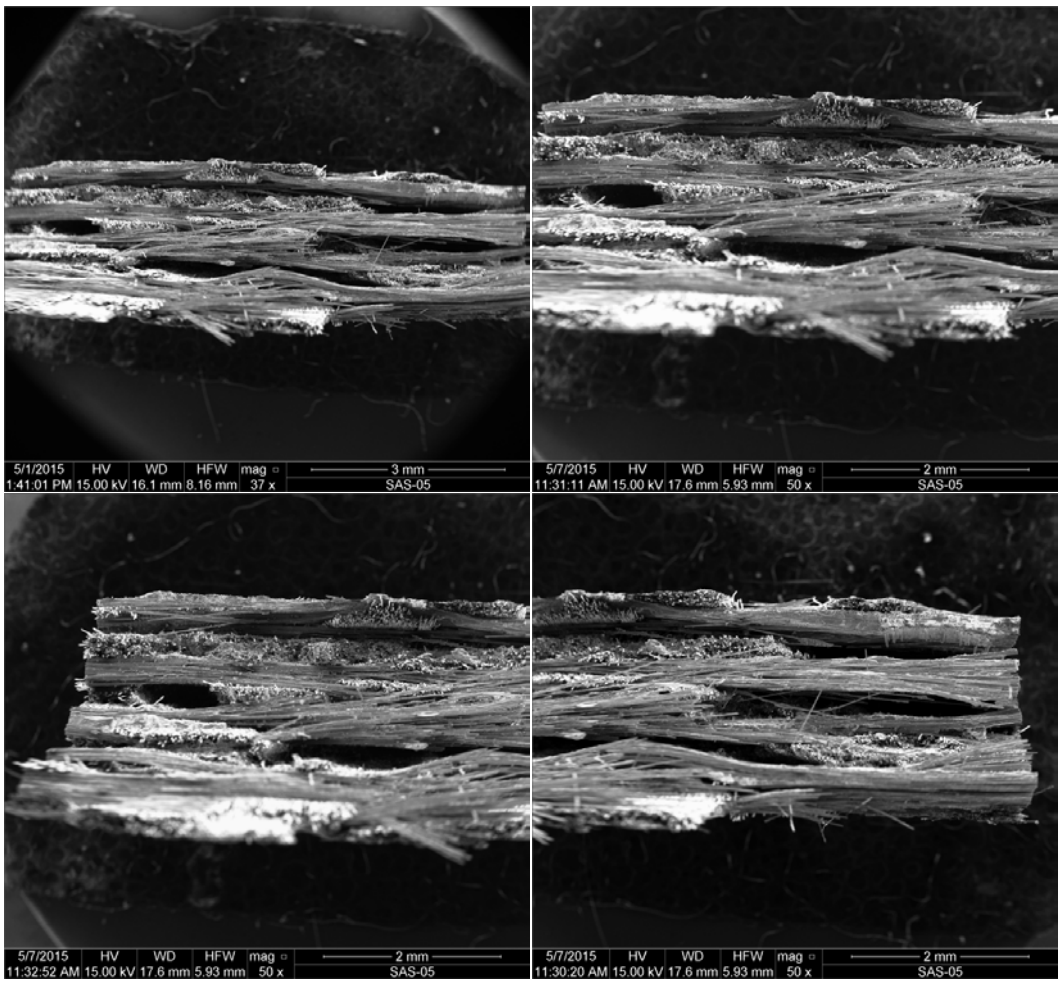

Figure J. 7: SEM micrographs of a fracture surface obtained in tensile test of a Hi-Nicalon™/SiNC specimen subjected to prior heat treatment for 10 h at 1300°C (Plate 11101, Specimen 6)

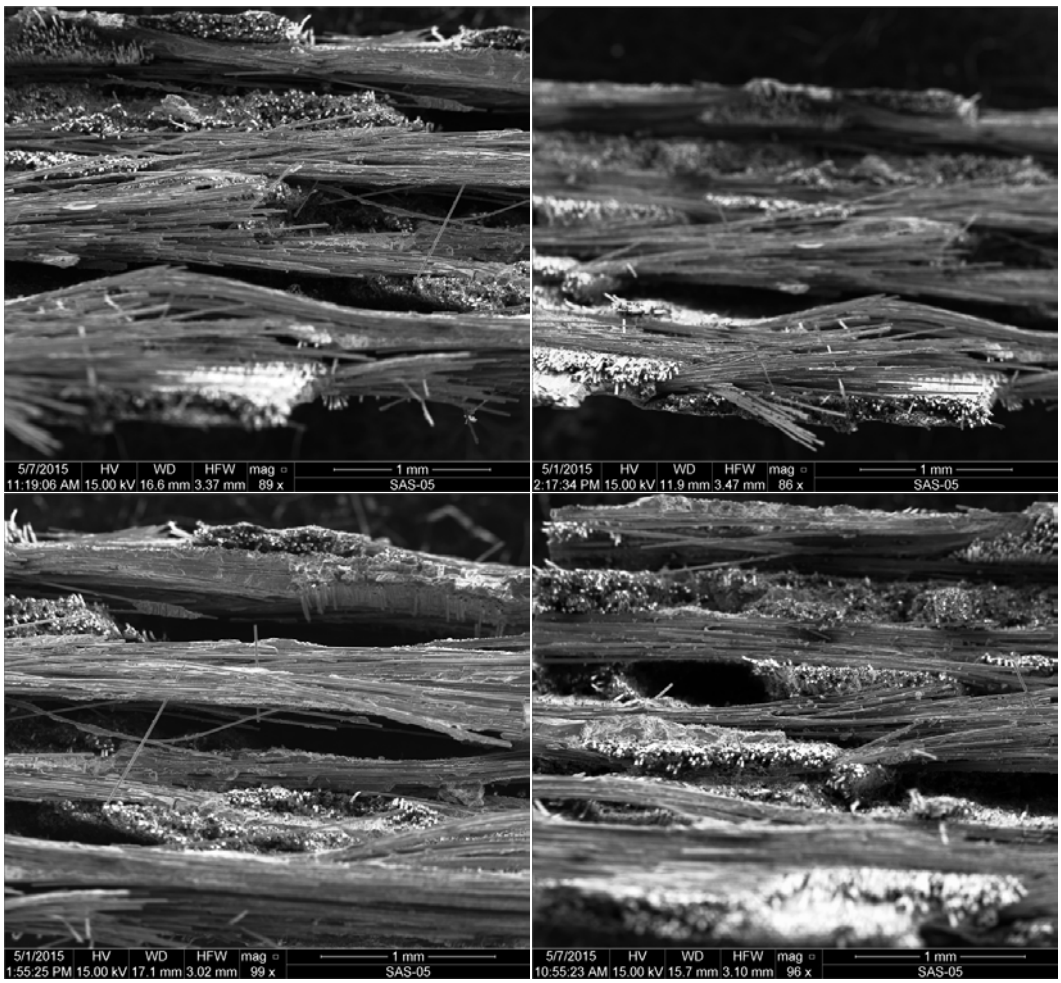

Figure J. 8: SEM micrographs of a fracture surface obtained in tensile test of a Hi-Nicalon™/SiNC specimen subjected to prior heat treatment for 10 h at 1300°C (Plate 11101, Specimen 6)

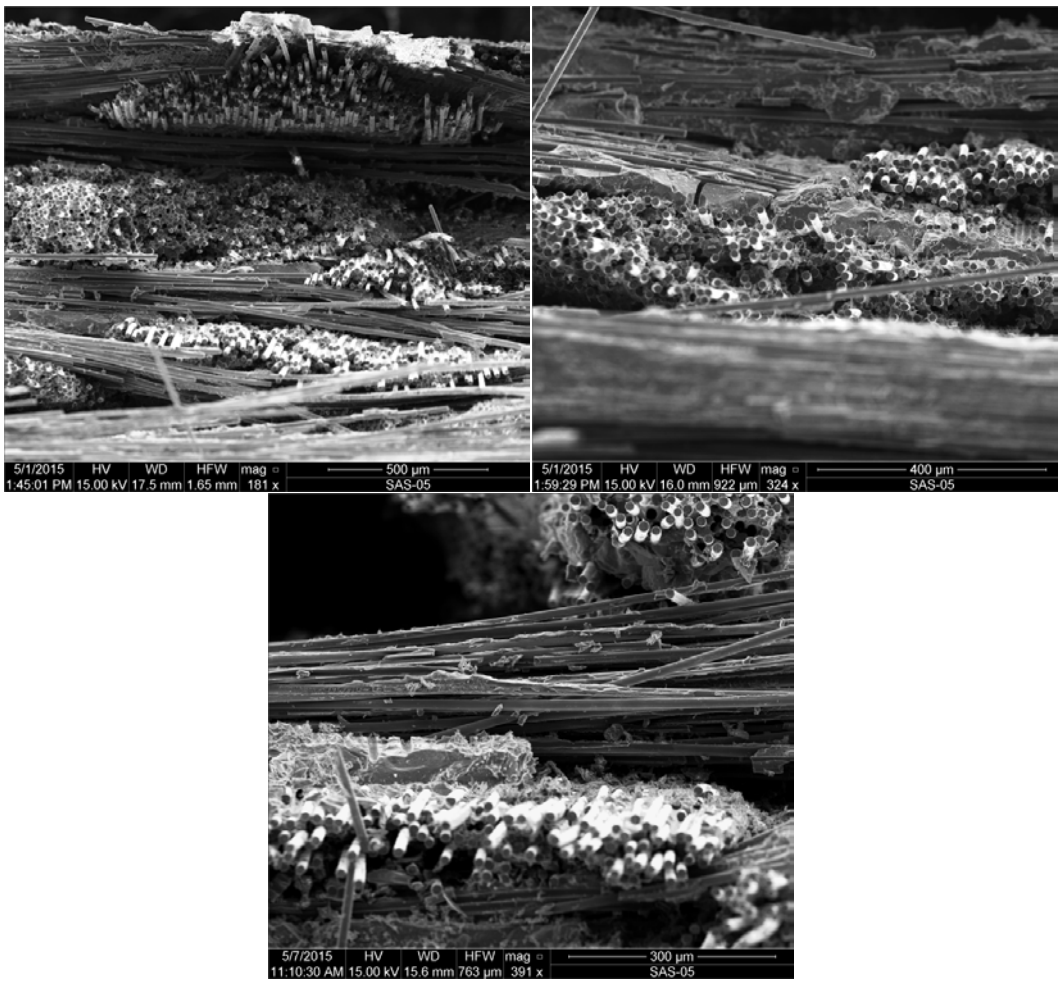

Figure J. 9: SEM micrographs of a fracture surface obtained in tensile test of a Hi-Nicalon™/SiNC specimen subjected to prior heat treatment for 10 h at 1300°C (Plate 11101, Specimen 6)

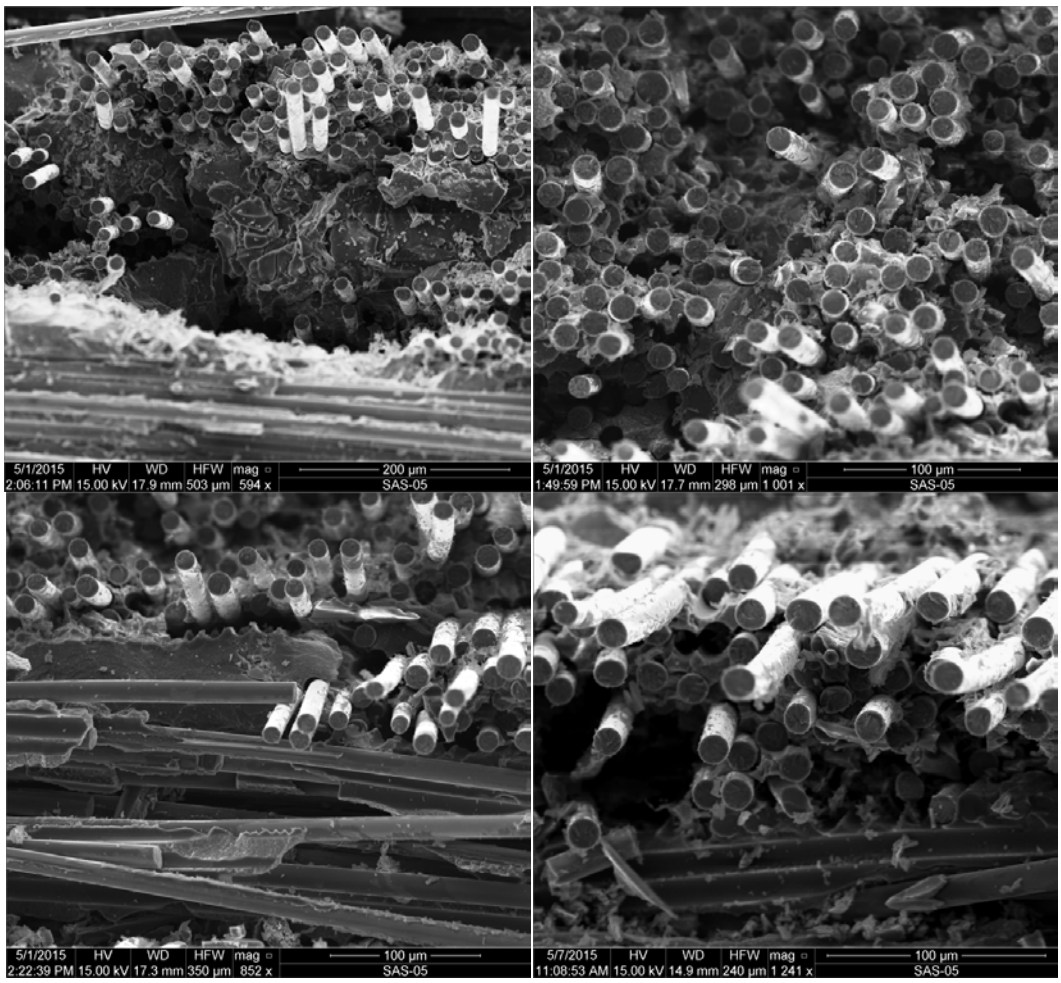

Figure J. 10: SEM micrographs of a fracture surface obtained in tensile test of a Hi-Nicalon™/SiNC specimen subjected to prior heat treatment for 10 h at 1300°C (Plate 11101, Specimen 6)

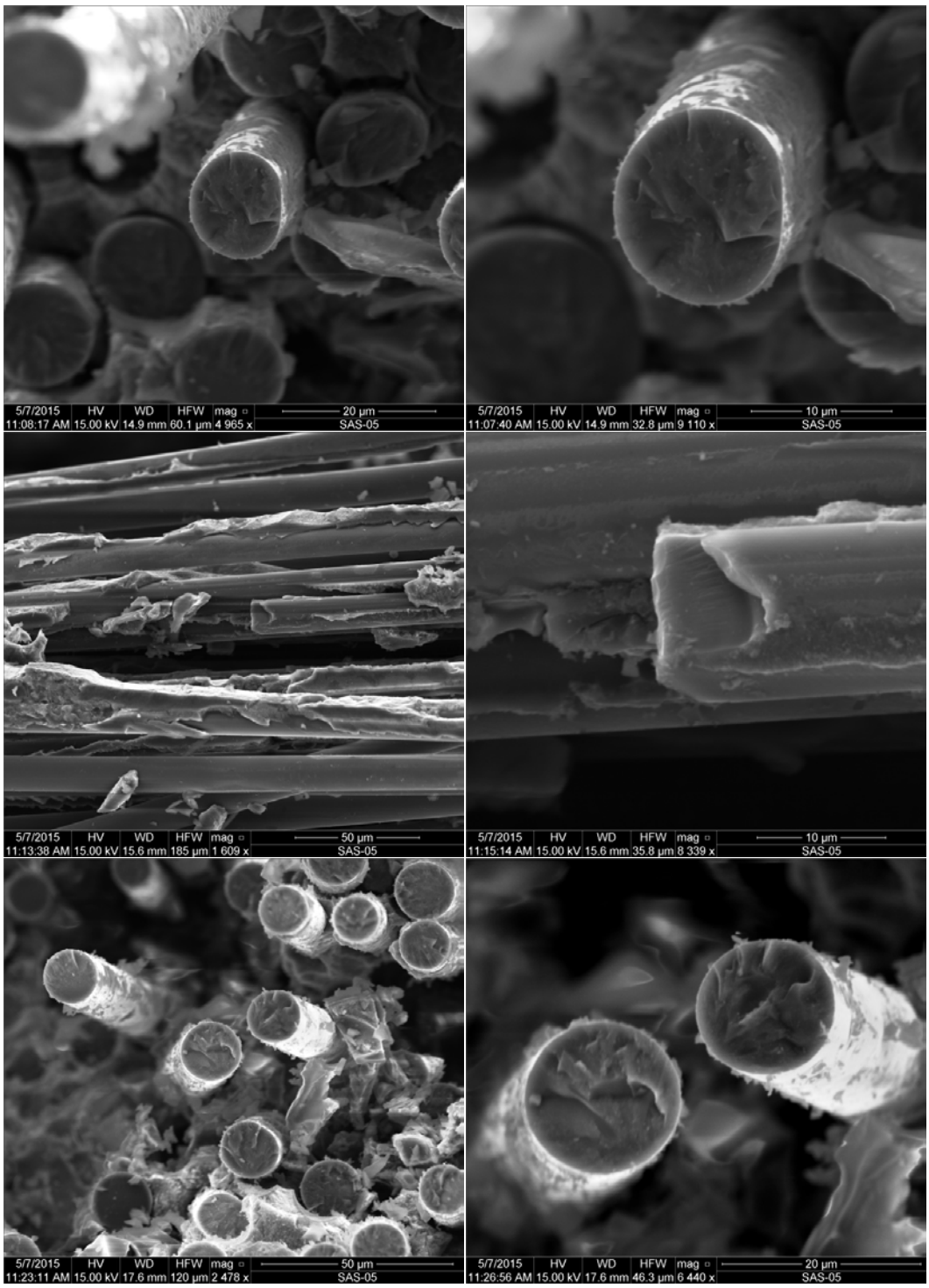

Figure J. 11: SEM micrographs of a fracture surface obtained in tensile test of a Hi-Nicalon™/SiNC specimen subjected to prior heat treatment for 10 h at 1300°C (Plate 11101, Specimen 6)

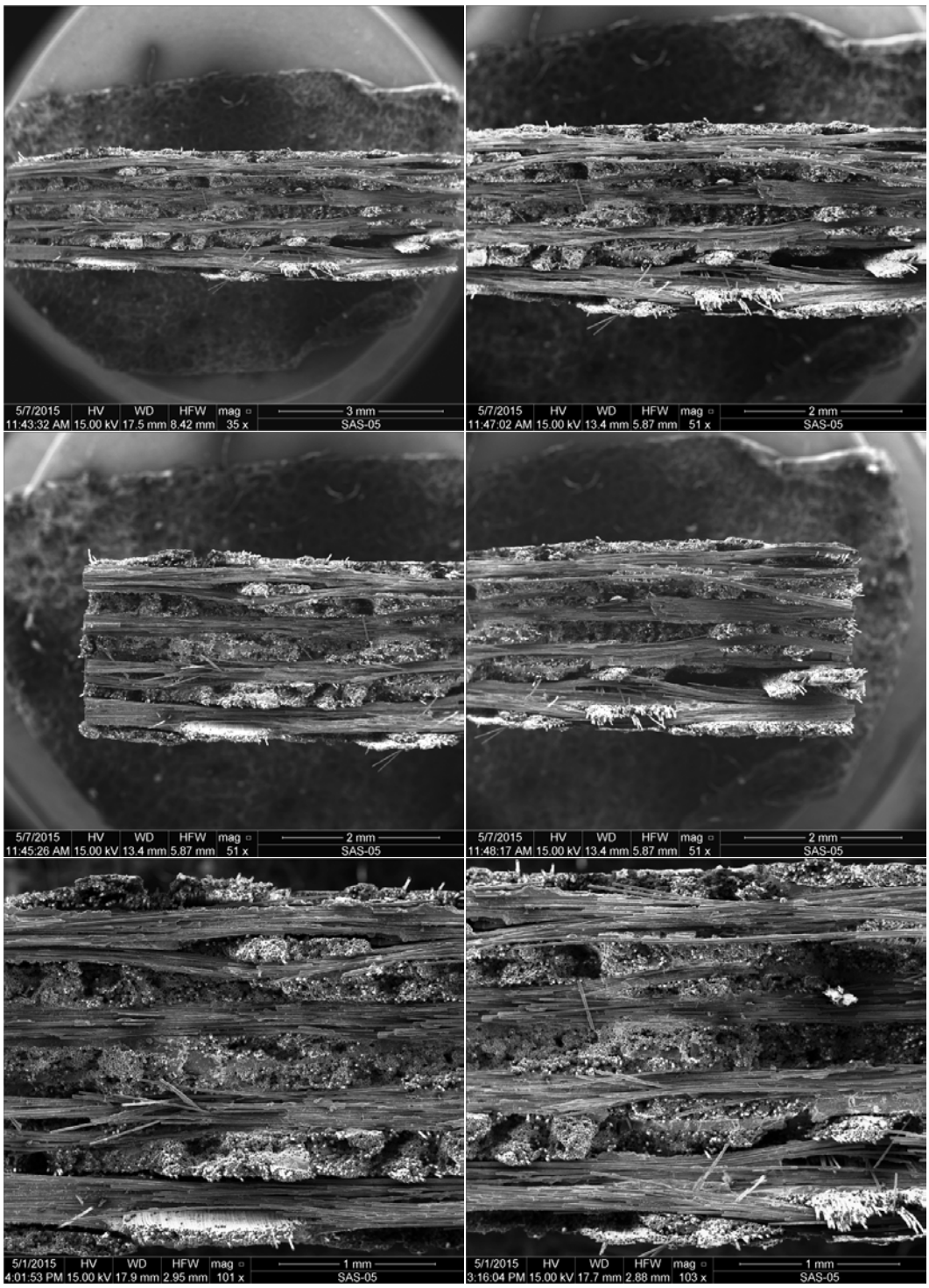

Figure J. 12: SEM micrographs of a fracture surface obtained in tensile test of a Hi-Nicalon™/SiNC specimen subjected to prior heat treatment for 100 h at 1300°C (Plate 11105, Specimen 6)

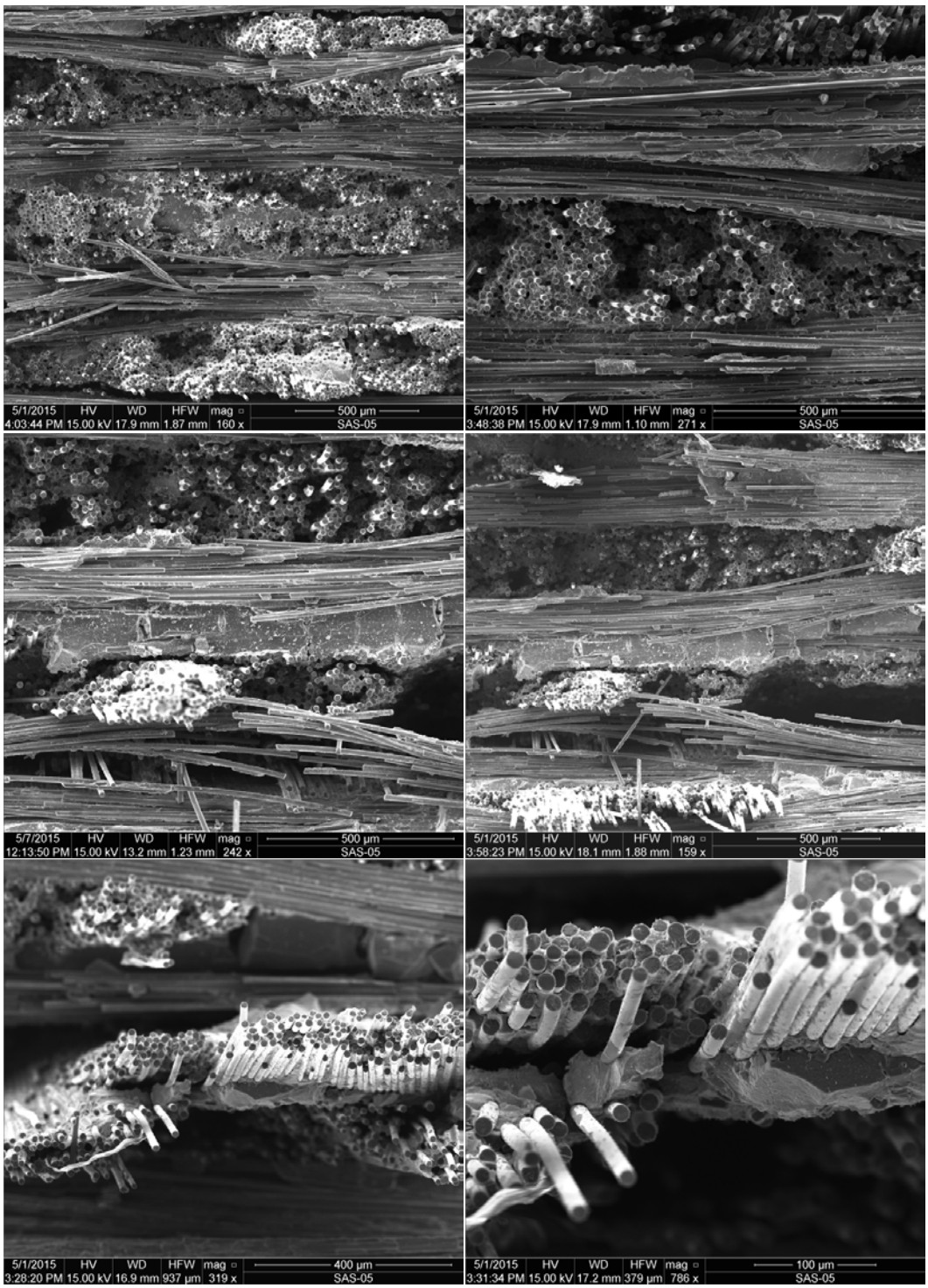

Figure J. 13: SEM micrographs of a fracture surface obtained in tensile test of a Hi-Nicalon™/SiNC specimen subjected to prior heat treatment for 100 h at 1300°C (Plate 11105, Specimen 6)

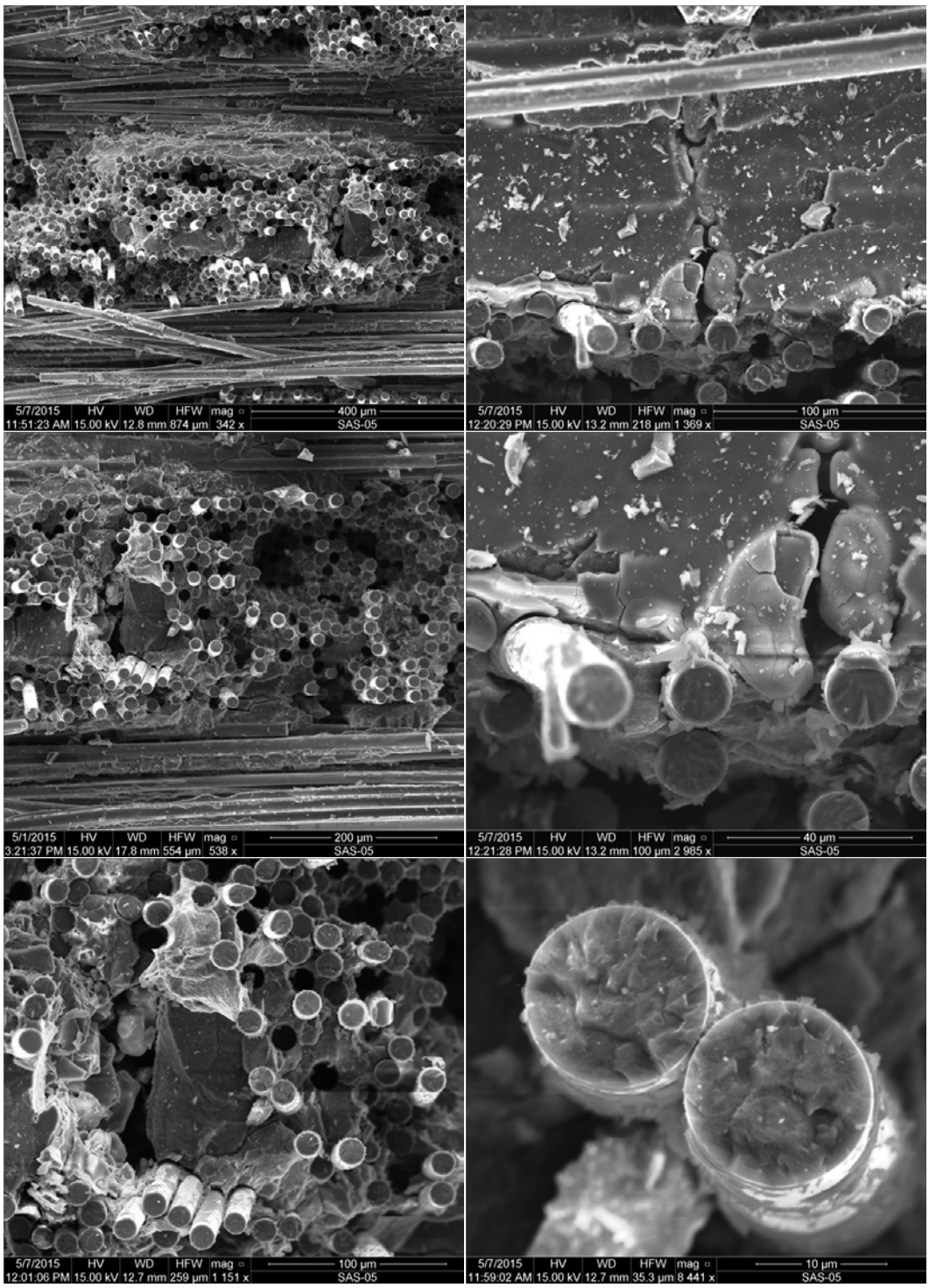

Figure J. 14: SEM micrographs of a fracture surface obtained in tensile test of a Hi-Nicalon™/SiNC specimen subjected to prior heat treatment for 100 h at 1300°C (Plate 11105, Specimen 6)

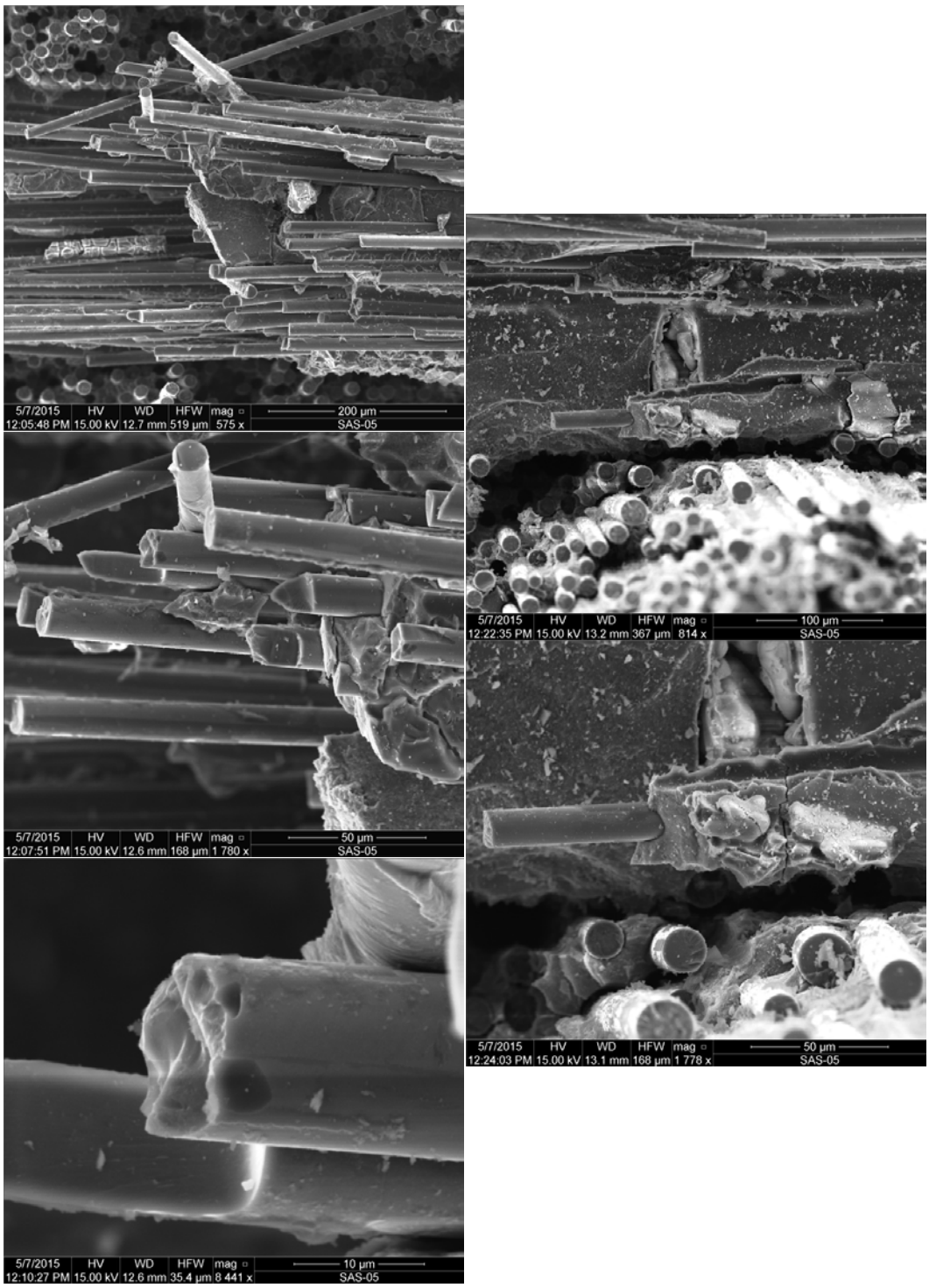

Figure J. 15: SEM micrographs of a fracture surface obtained in tensile test of a Hi-Nicalon™/SiNC specimen subjected to prior heat treatment for 100 h at 1300°C (Plate 11105, Specimen 6)

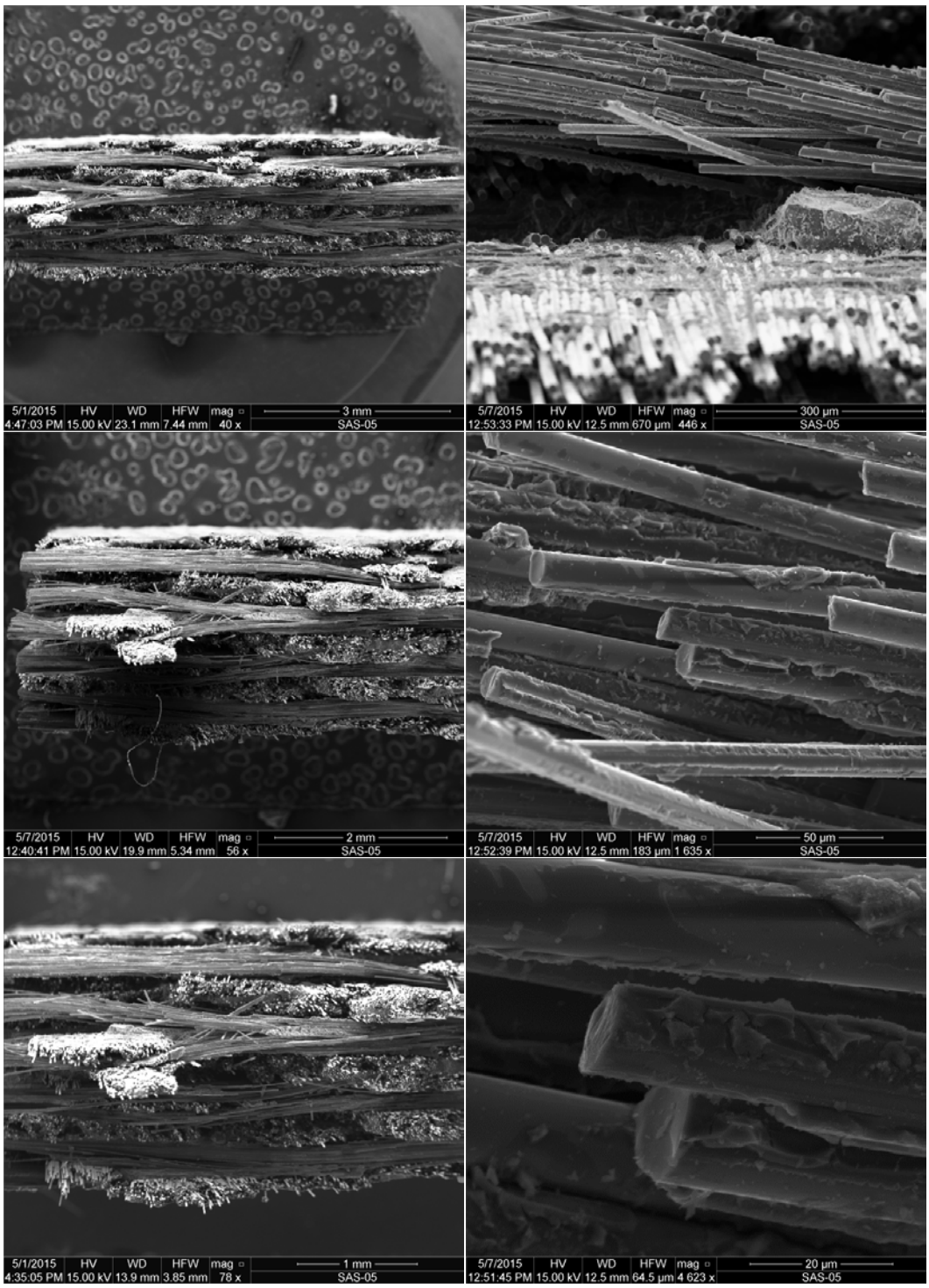

Figure J. 16: SEM micrographs of a fracture surface obtained in tensile test of a Hi-Nicalon™/SiNC specimen subjected to prior heat treatment for 100 h at 1200°C (Plate 11106, Specimen 4)

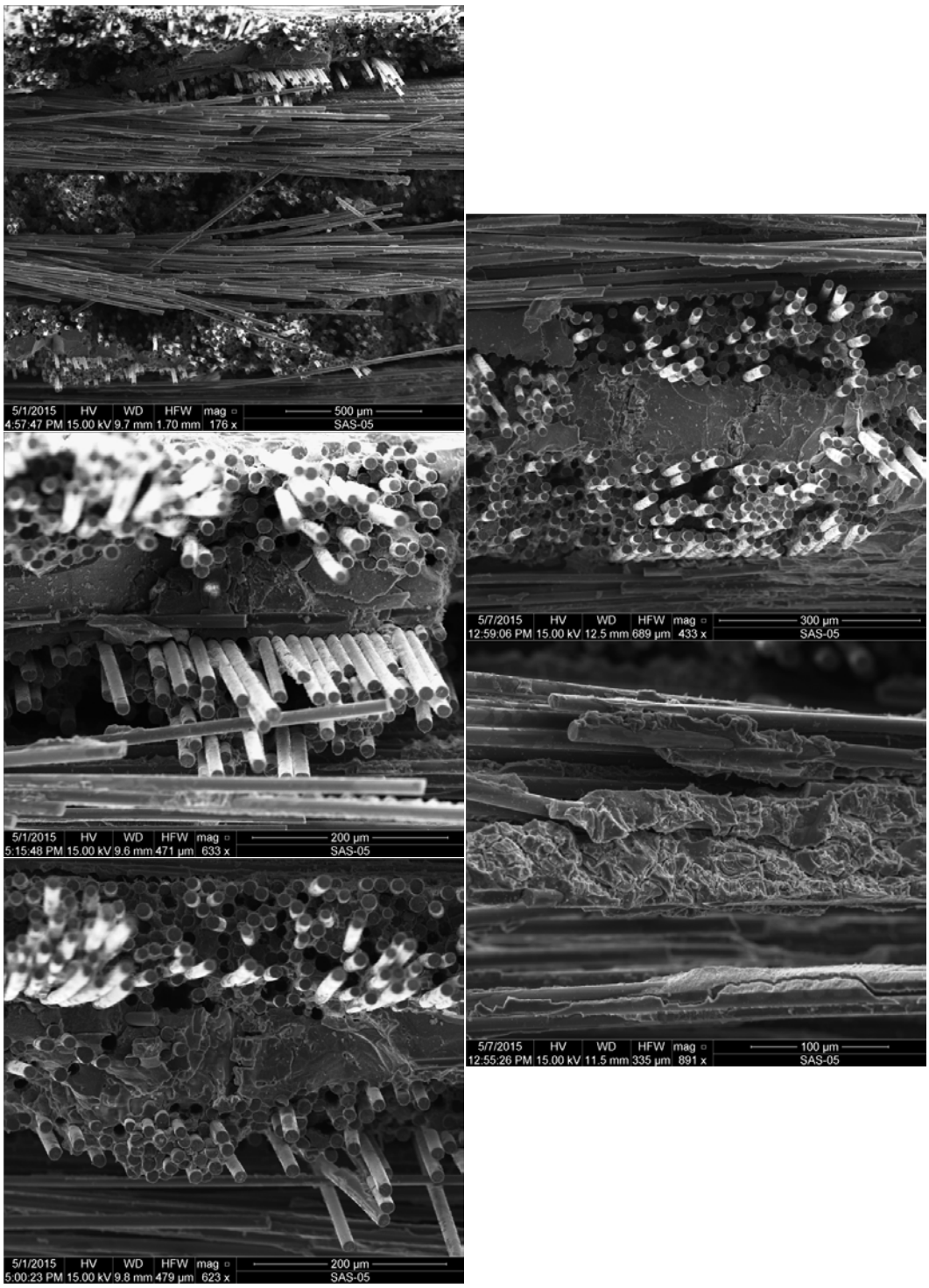

Figure J. 17: SEM micrographs of a fracture surface obtained in tensile test of a Hi-Nicalon™/SiNC specimen subjected to prior heat treatment for 100 h at 1200°C (Plate 11106, Specimen 4)

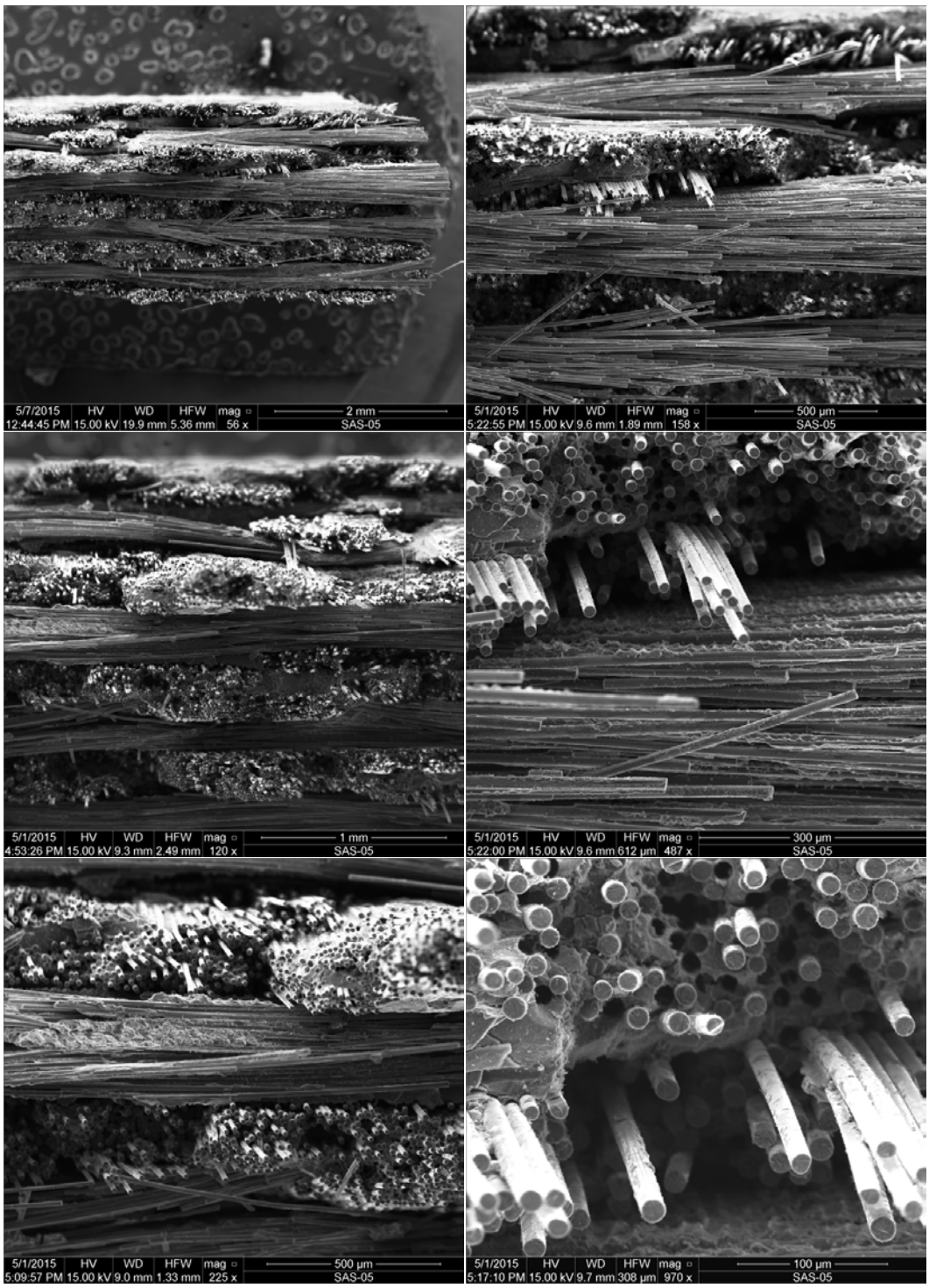

Figure J. 18: SEM micrographs of a fracture surface obtained in tensile test of a Hi-Nicalon™/SiNC specimen subjected to prior heat treatment for 100 h at 1200°C (Plate 11106, Specimen 4)

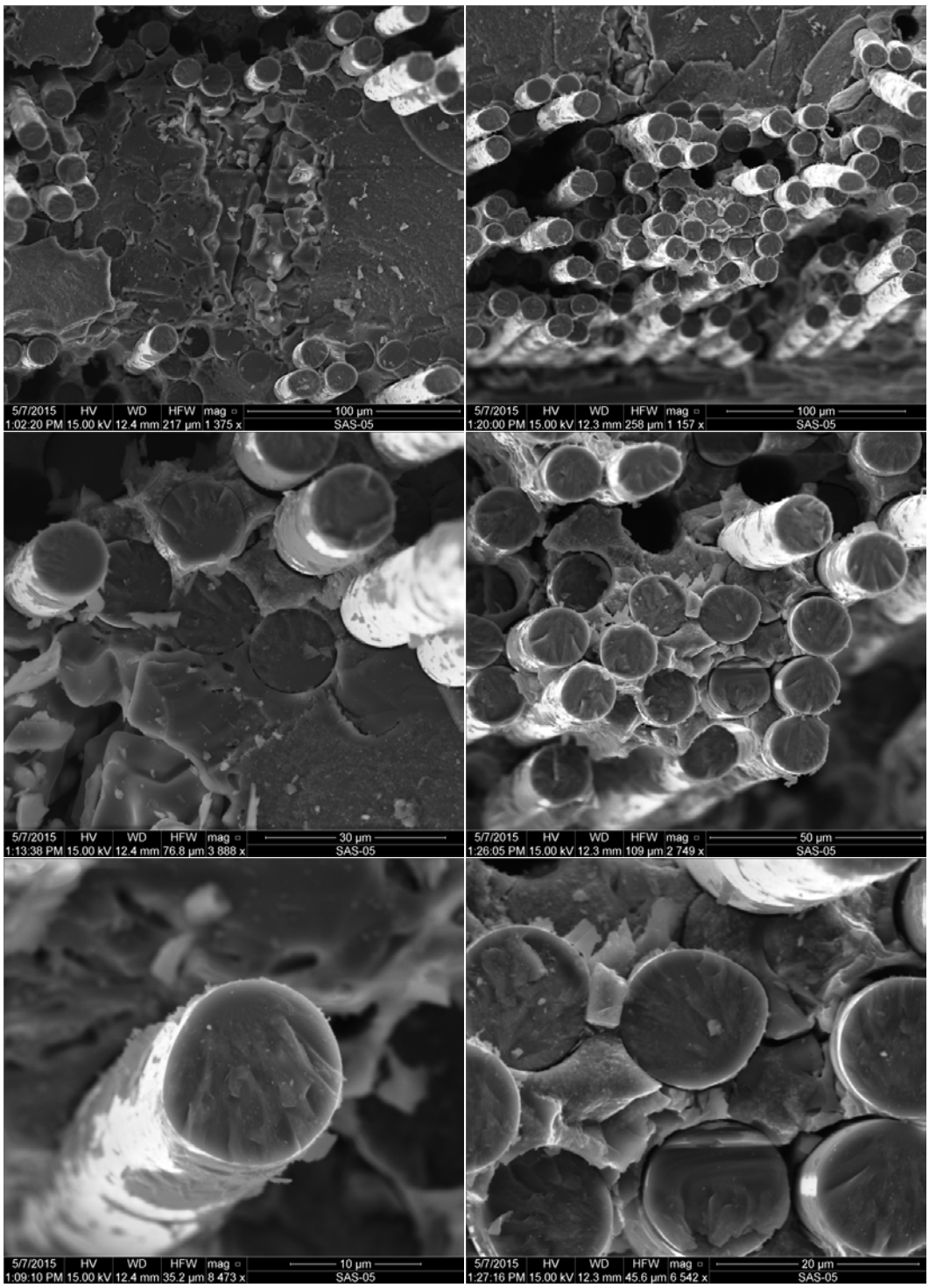

Figure J. 19: SEM micrographs of a fracture surface obtained in tensile test of a Hi-Nicalon™/SiNC specimen subjected to prior heat treatment for 100 h at 1200°C (Plate 11106, Specimen 4)

Appendix K: Additional SEM Micrographs of HexTow® IM7 C/SiC Fracture Surfaces

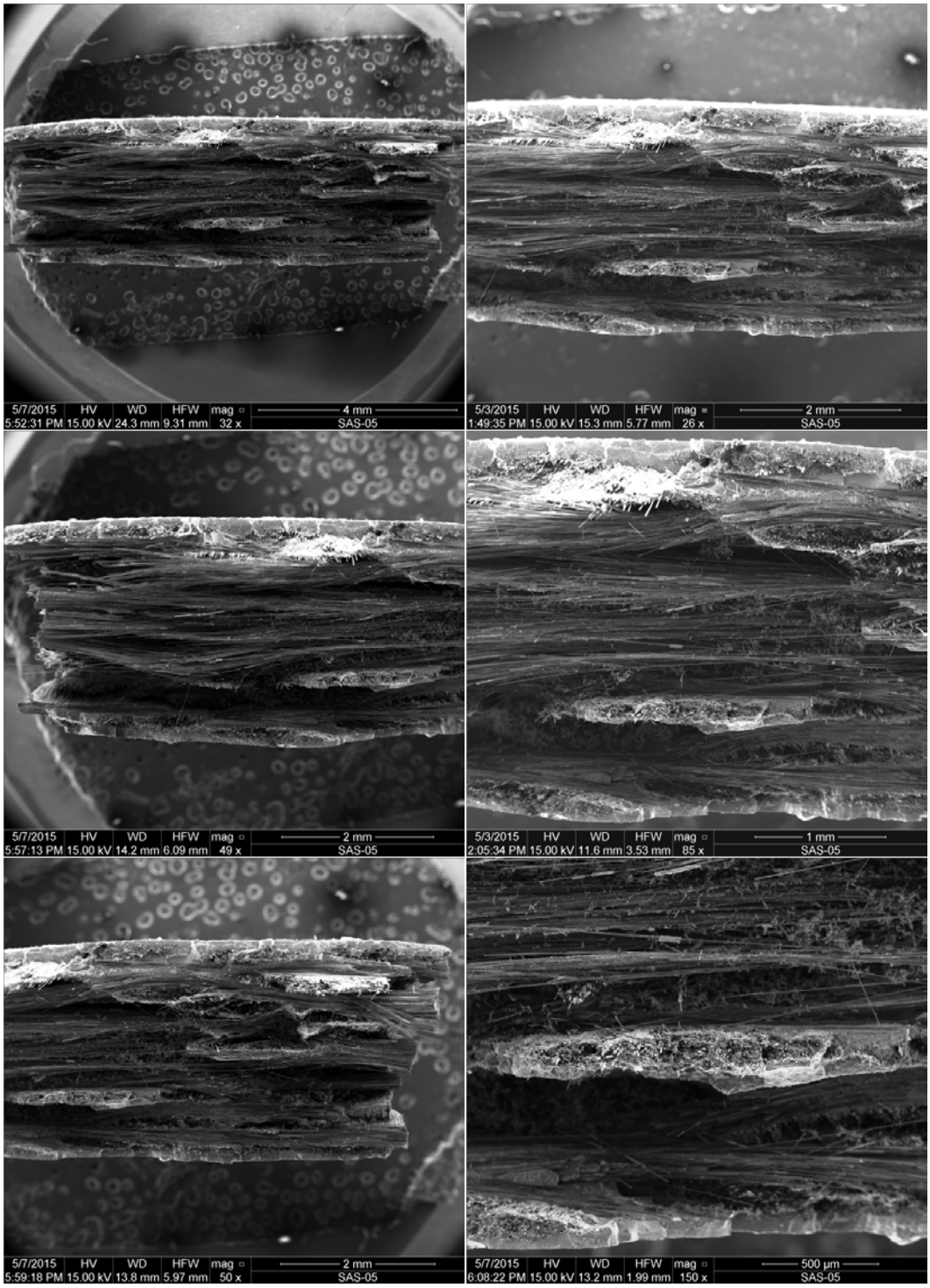

Figure K. 1: SEM micrographs of a fracture surface obtained in tensile test of a virgin C/SiC specimen (Plate 12012, Specimen 6)

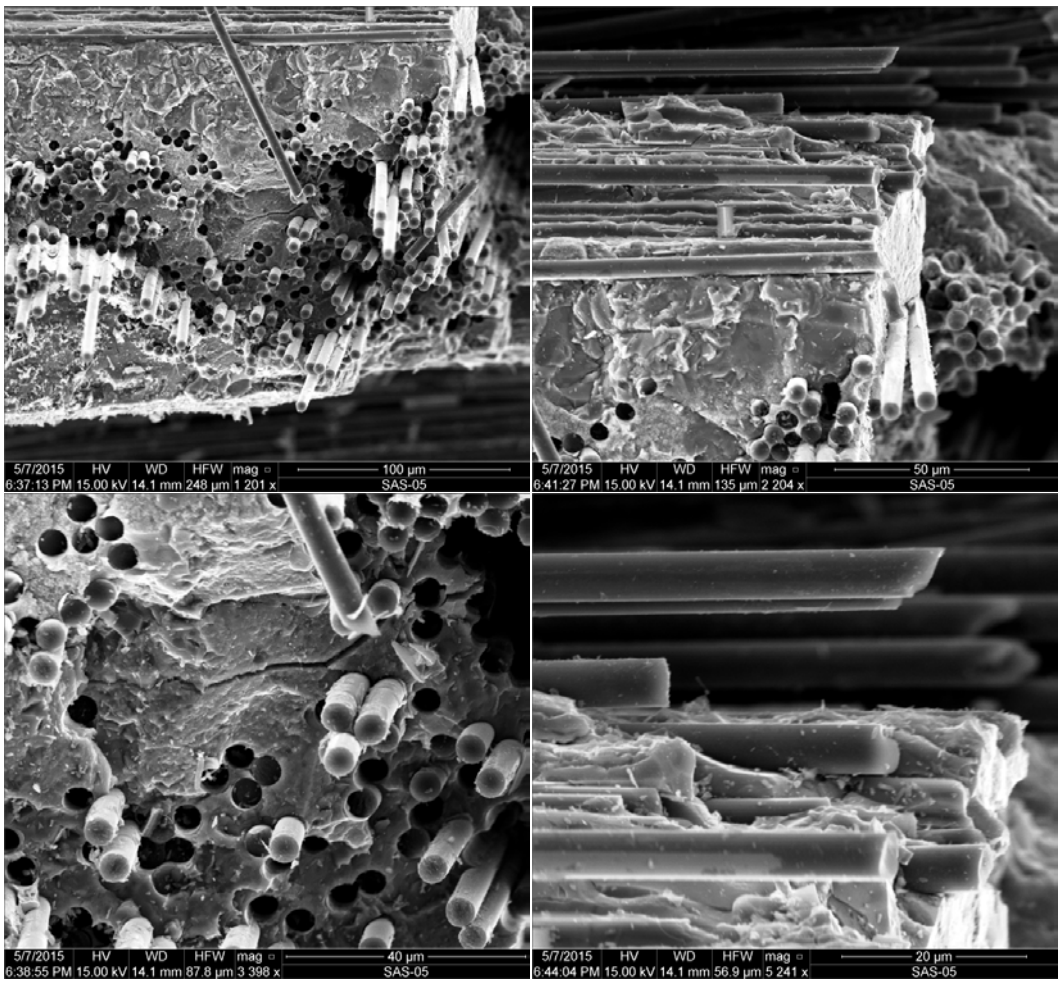

Figure K. 2: SEM micrographs of a fracture surface obtained in tensile test of a virgin C/SiC specimen (Plate 12012, Specimen 6)

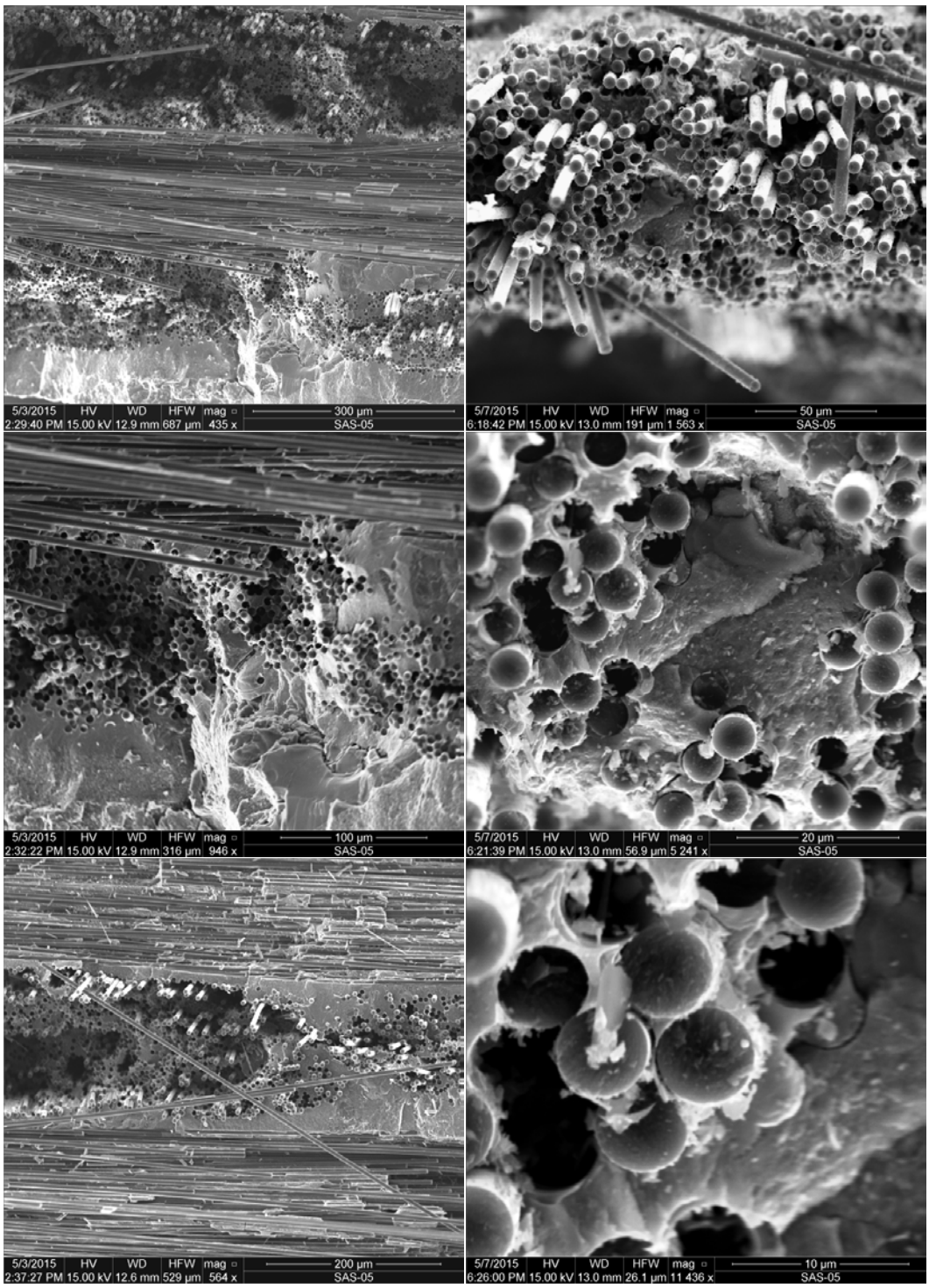

Figure K. 3: SEM micrographs of a fracture surface obtained in tensile test of a virgin C/SiC specimen (Plate 12012, Specimen 6)

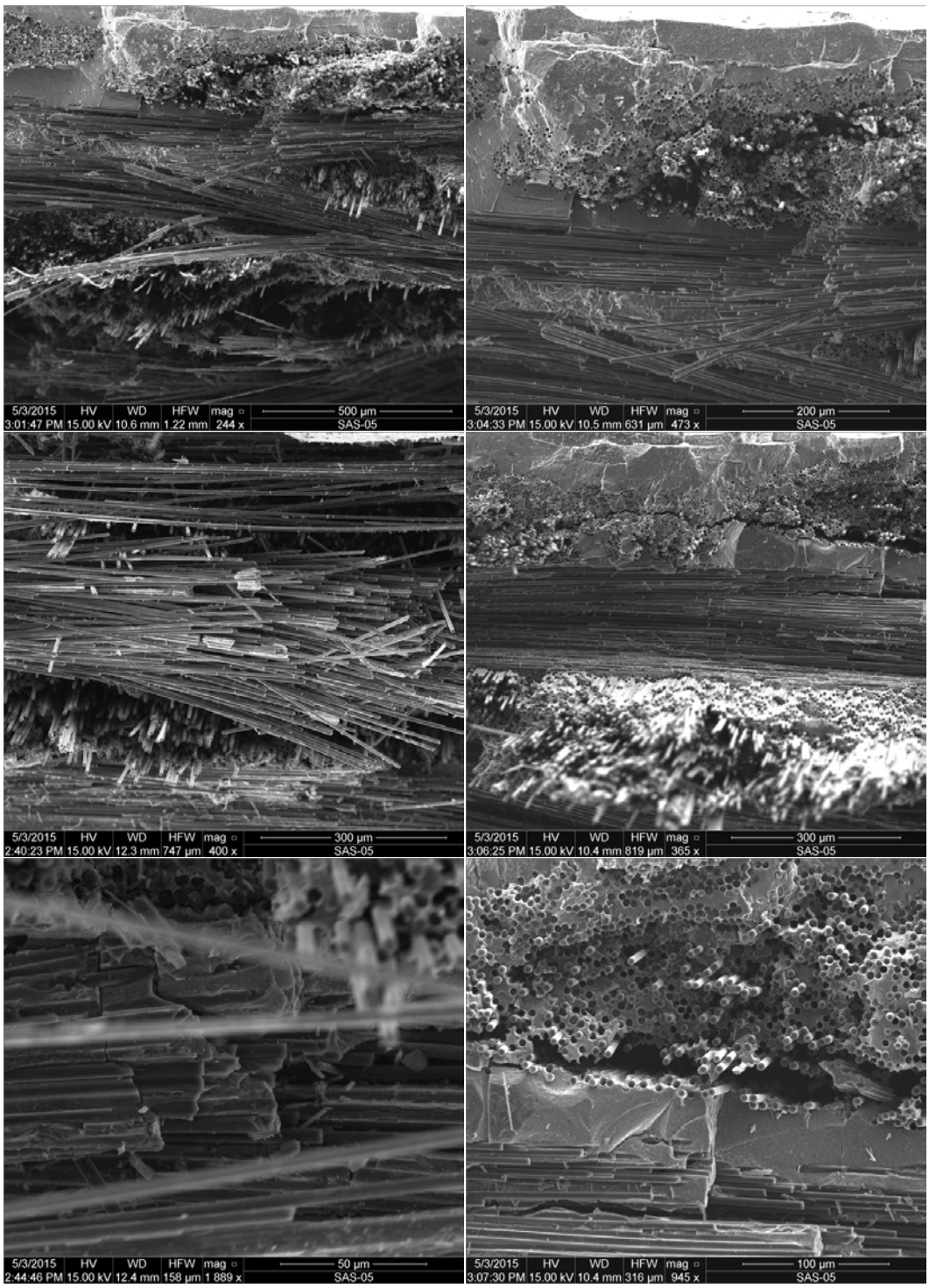

Figure K. 4: SEM micrographs of a fracture surface obtained in tensile test of a virgin C/SiC specimen (Plate 12012, Specimen 6)

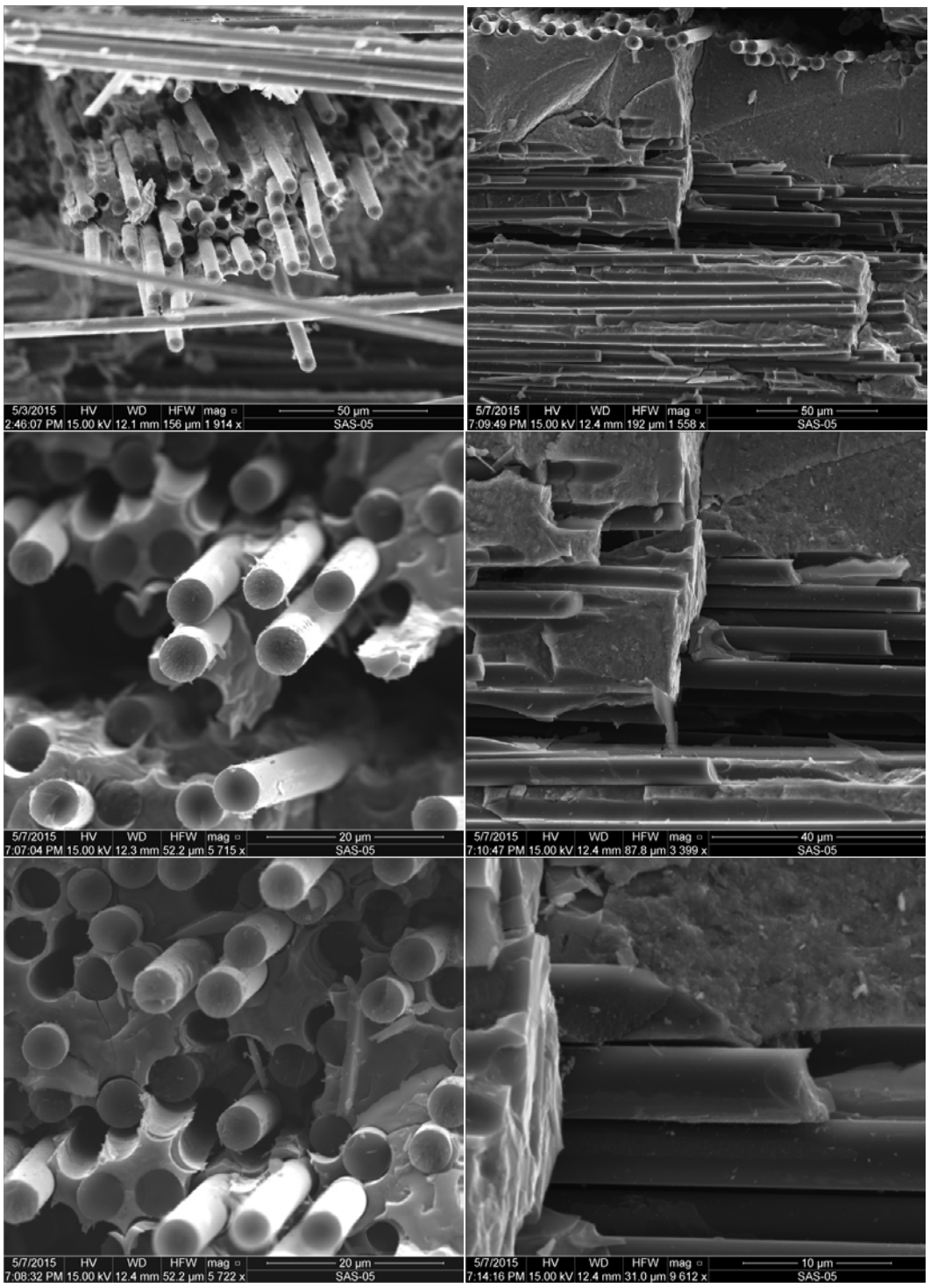

Figure K. 5: SEM micrographs of a fracture surface obtained in tensile test of a virgin C/SiC specimen (Plate 12012, Specimen 6)

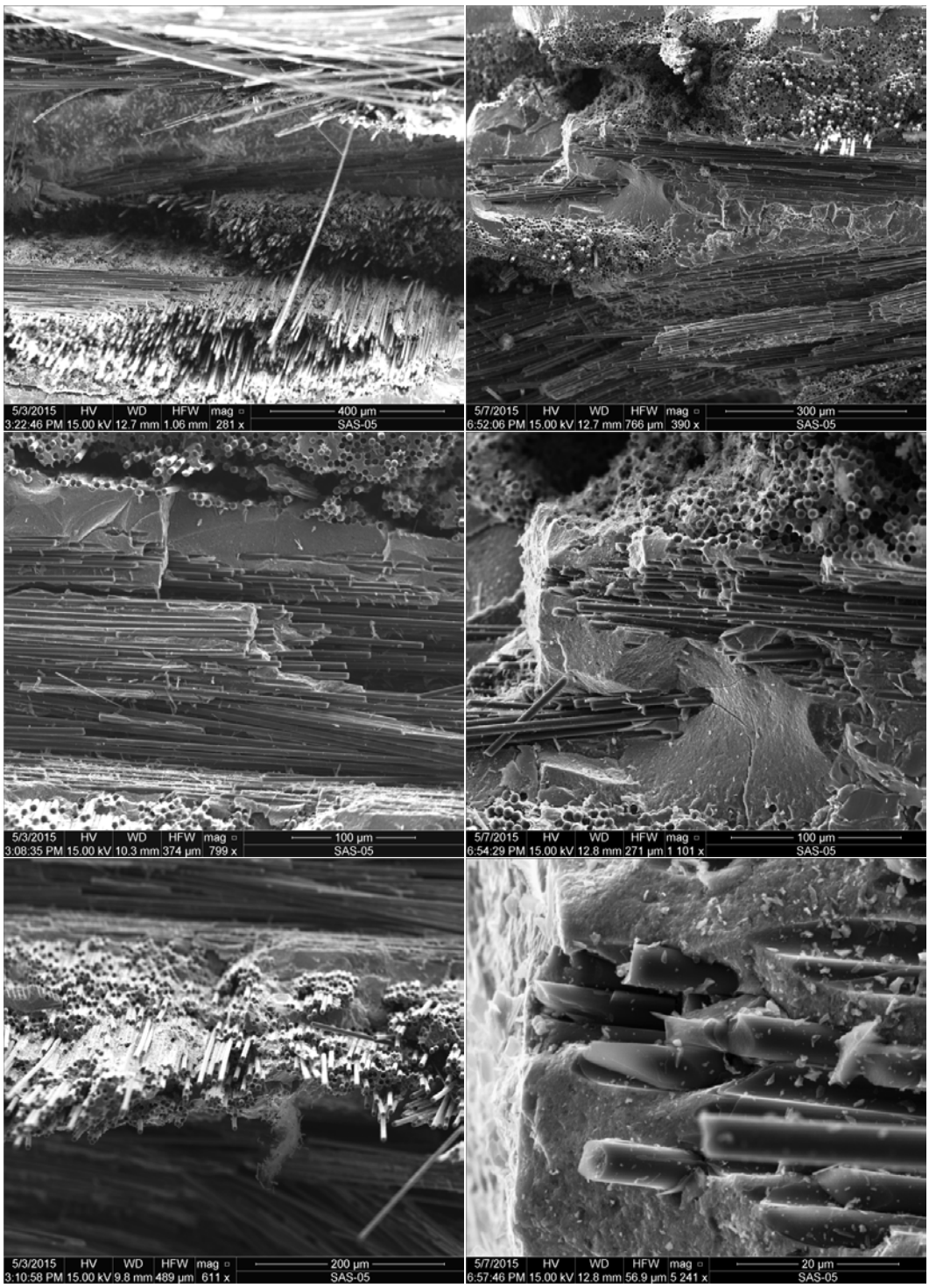

Figure K. 6: SEM micrographs of a fracture surface obtained in tensile test of a virgin C/SiC specimen (Plate 12012, Specimen 6)

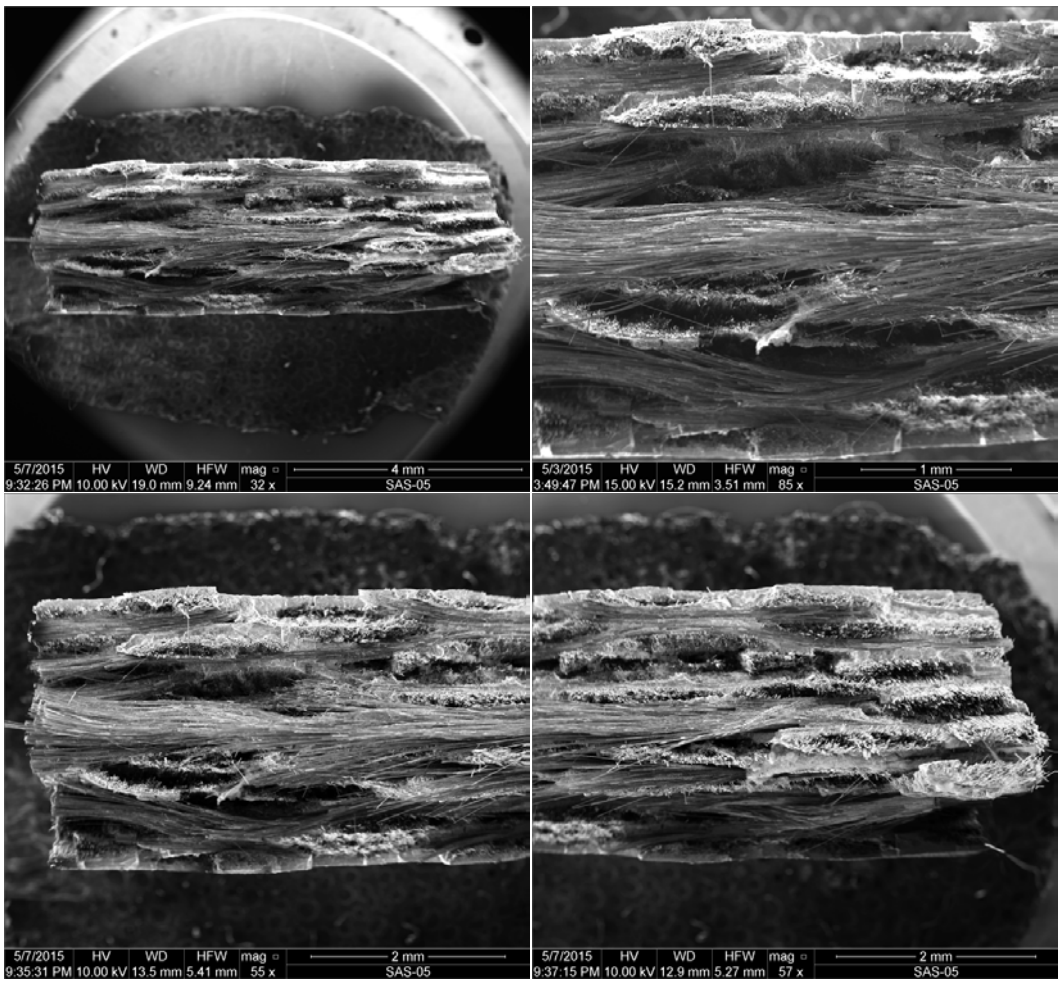

Figure K. 7: SEM micrographs of a fracture surface obtained in tensile test of a C/SiC specimen subjected to prior heat treatment for 40 h at 1300°C (Plate 12018, Specimen 2)

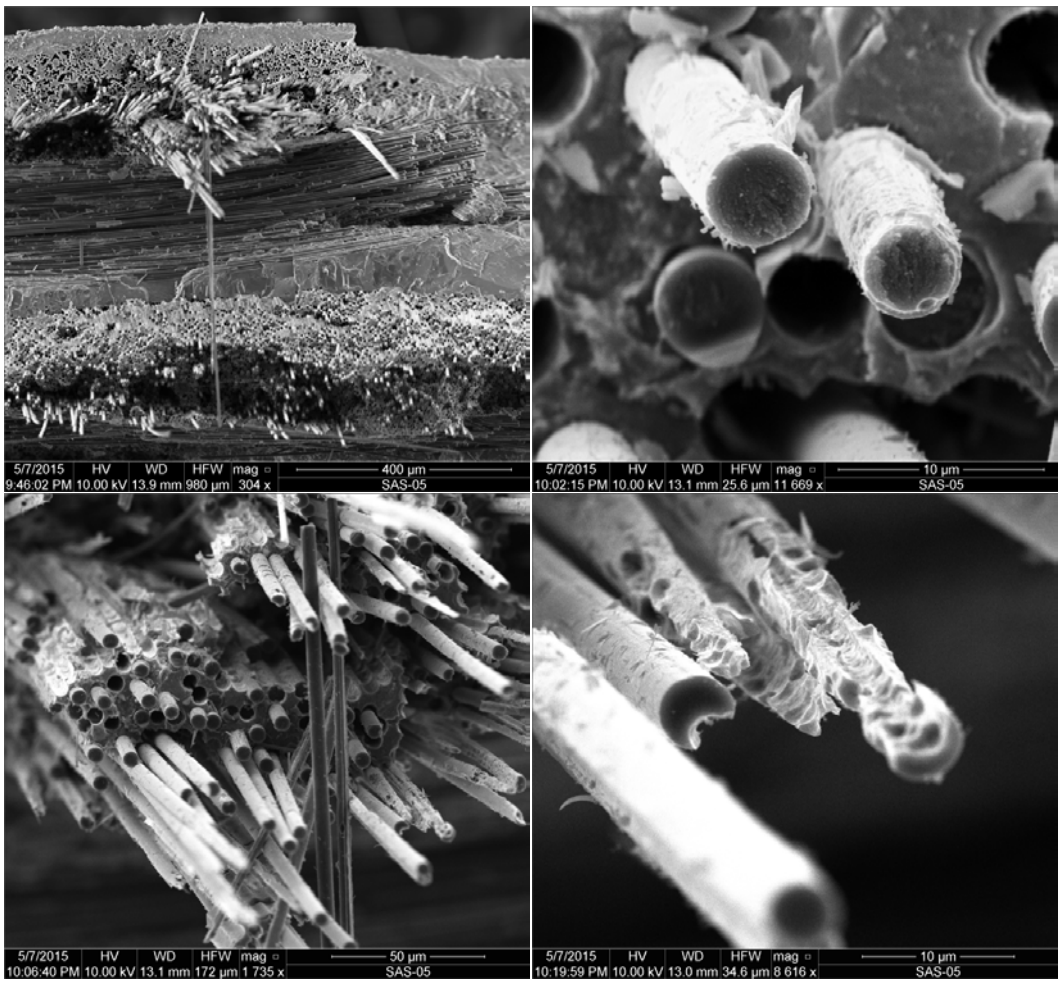

Figure K. 8: SEM micrographs of a fracture surface obtained in tensile test of a C/SiC specimen subjected to prior heat treatment for 40 h at 1300°C (Plate 12018, Specimen 2)

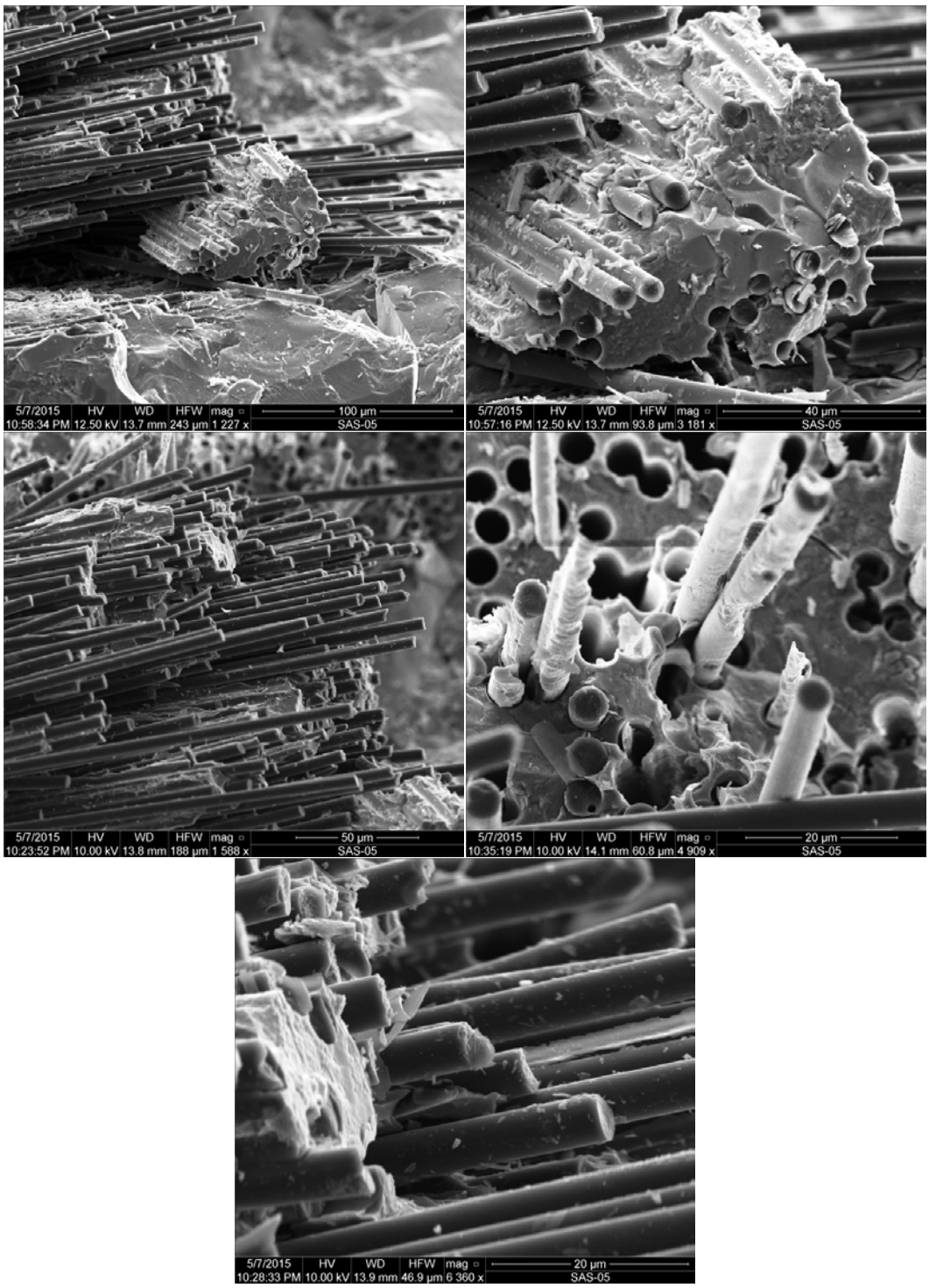

Figure K. 9: SEM micrographs of a fracture surface obtained in tensile test of a C/SiC specimen subjected to prior heat treatment for 40 h at 1300°C (Plate 12018, Specimen 2)

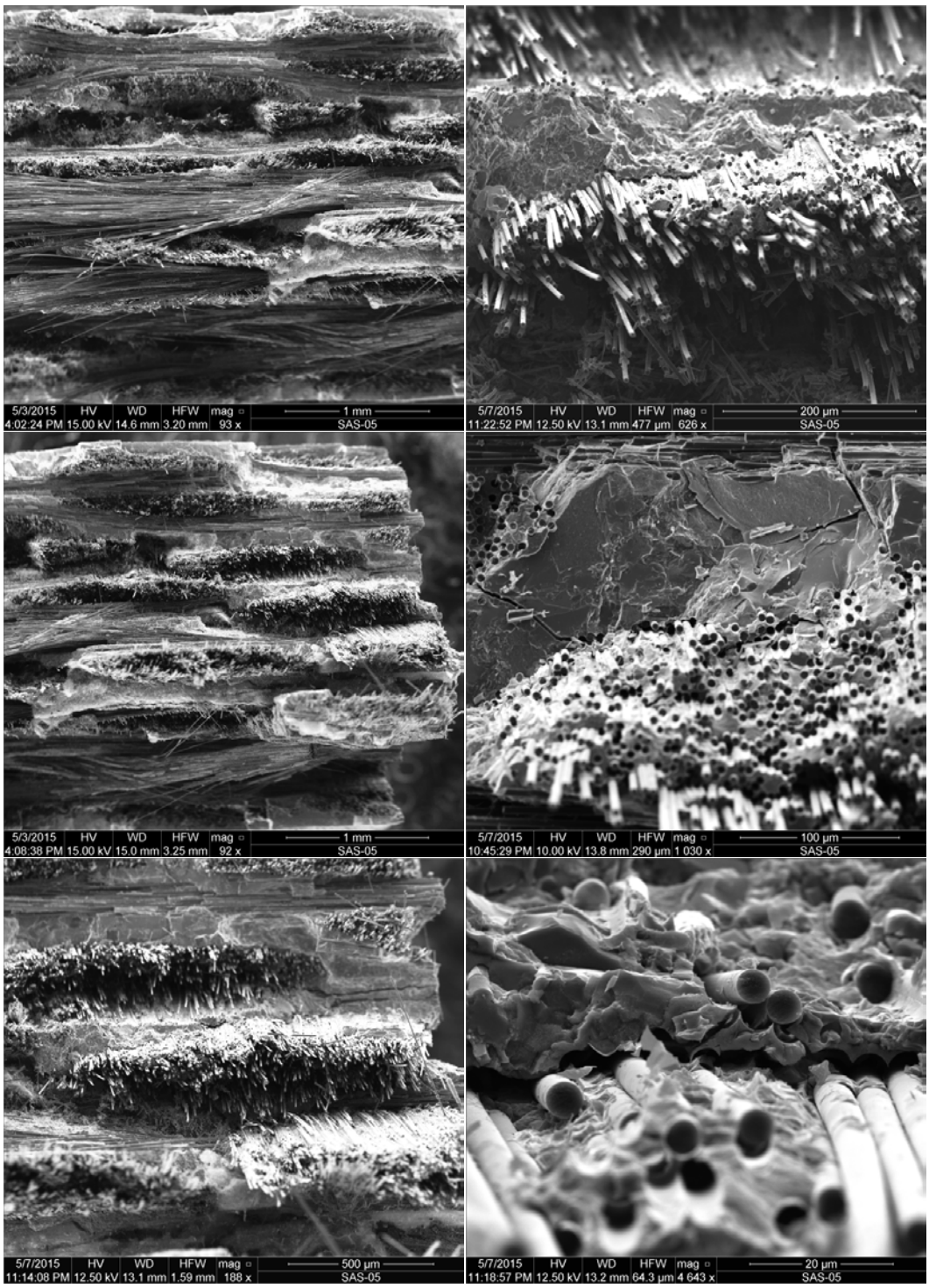

Figure K. 10: SEM micrographs of a fracture surface obtained in tensile test of a C/SiC specimen subjected to prior heat treatment for 40 h at 1300°C (Plate 12018, Specimen 2)

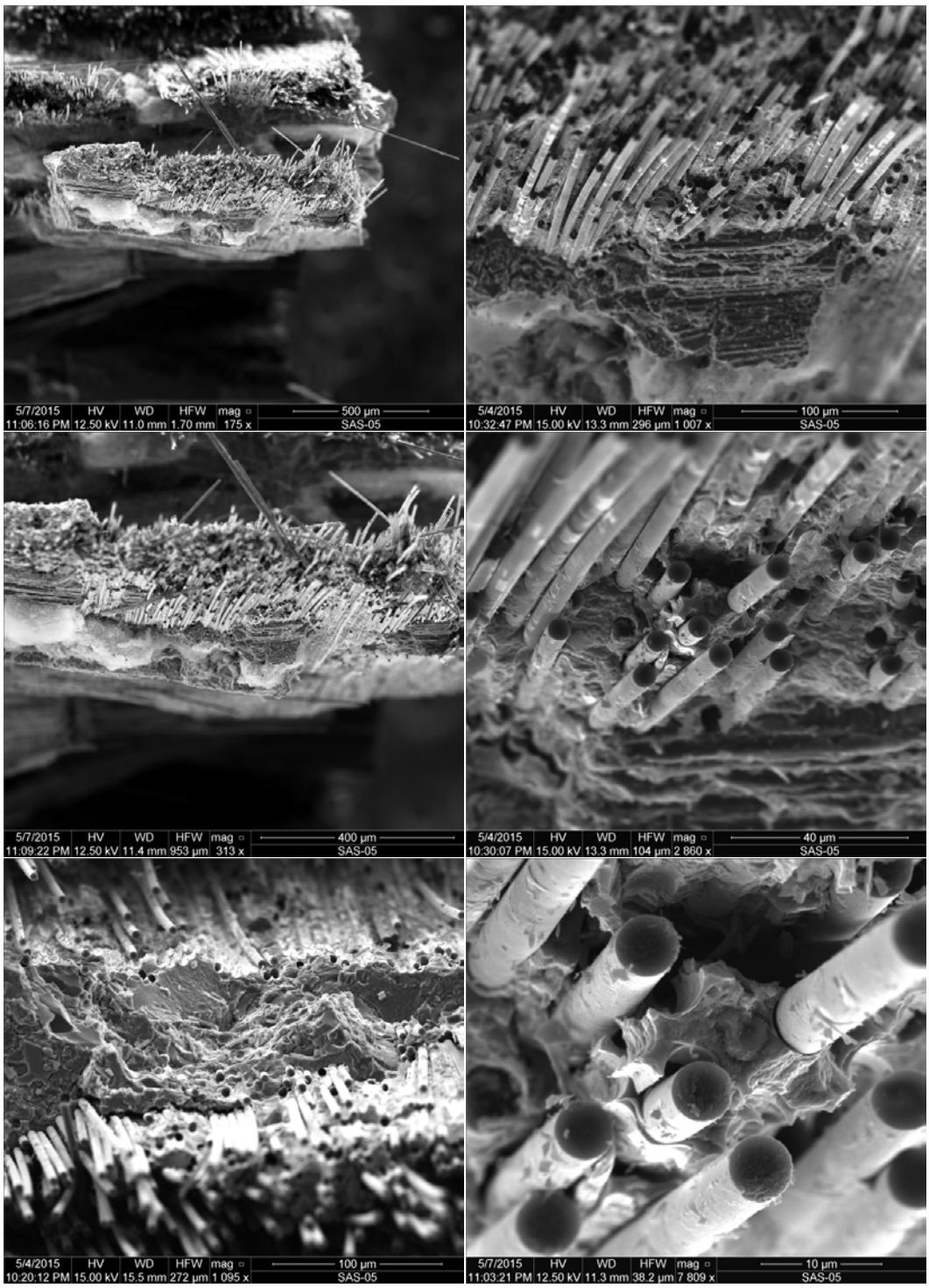

Figure K. 11: SEM micrographs of a fracture surface obtained in tensile test of a C/SiC specimen subjected to prior heat treatment for 40 h at 1300°C (Plate 12018, Specimen 2)

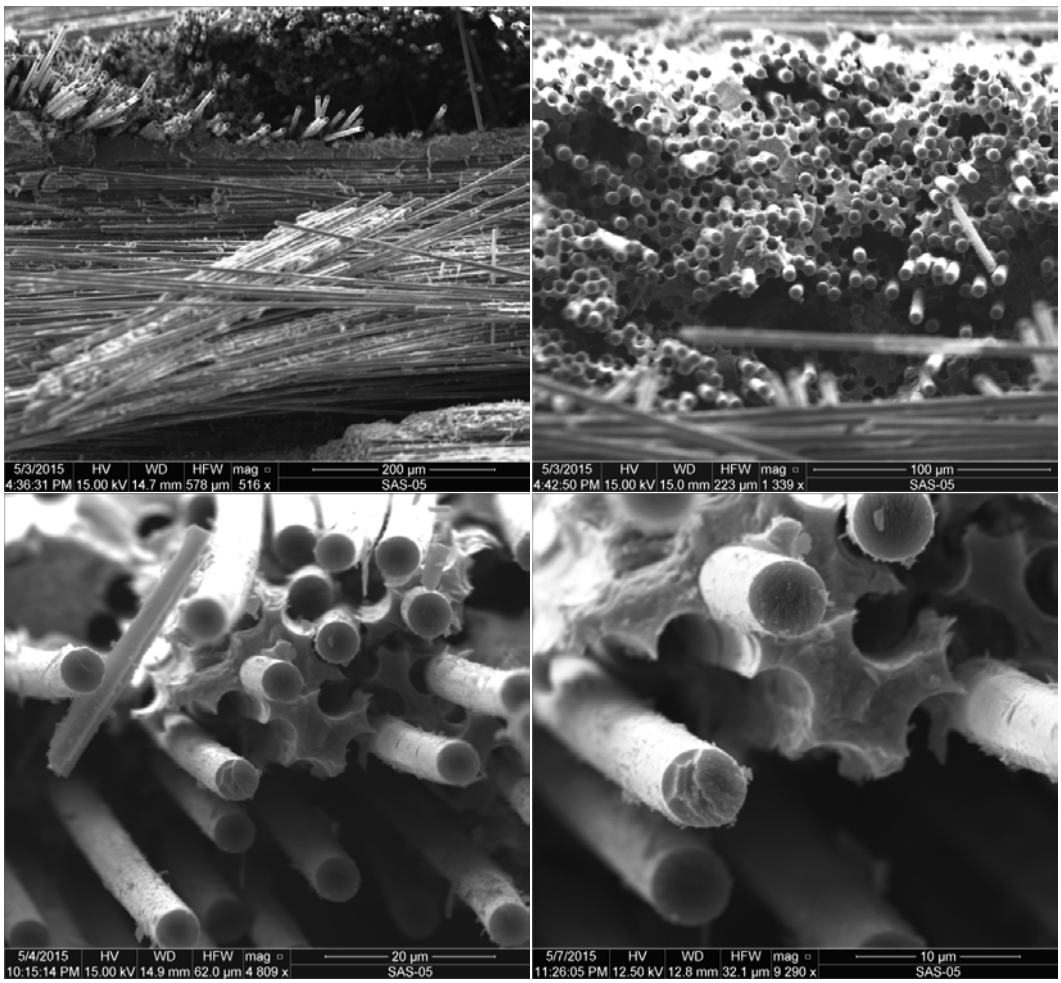

Figure K. 12: SEM micrographs of a fracture surface obtained in tensile test of a C/SiC specimen subjected to prior heat treatment for 40 h at 1300°C (Plate 12018, Specimen 2)

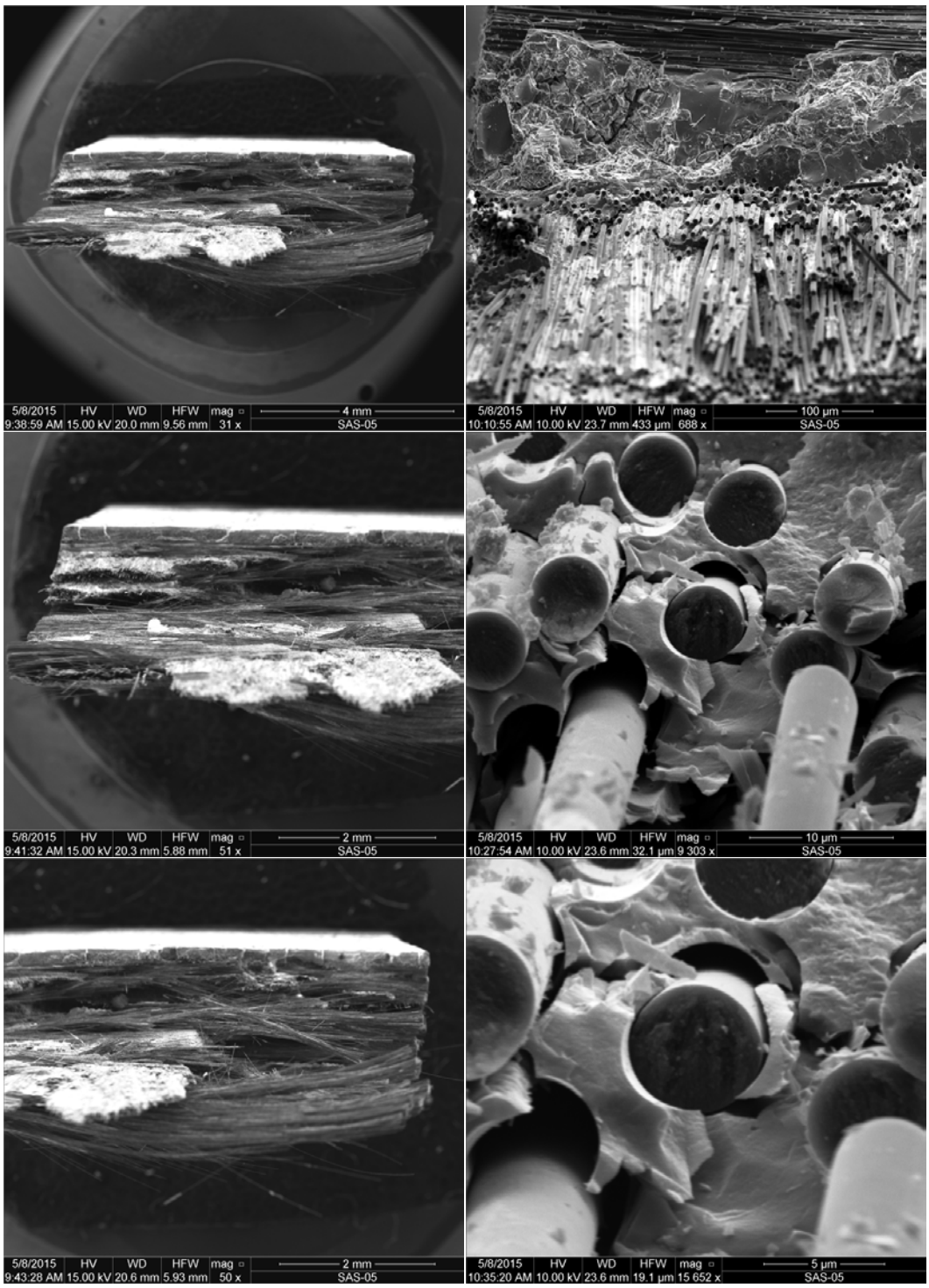

Figure K. 13: SEM micrographs of a fracture surface obtained in tensile test of a C/SiC specimen subjected to prior heat treatment for 100 h at 1300°C (Plate 12015, Specimen 3)

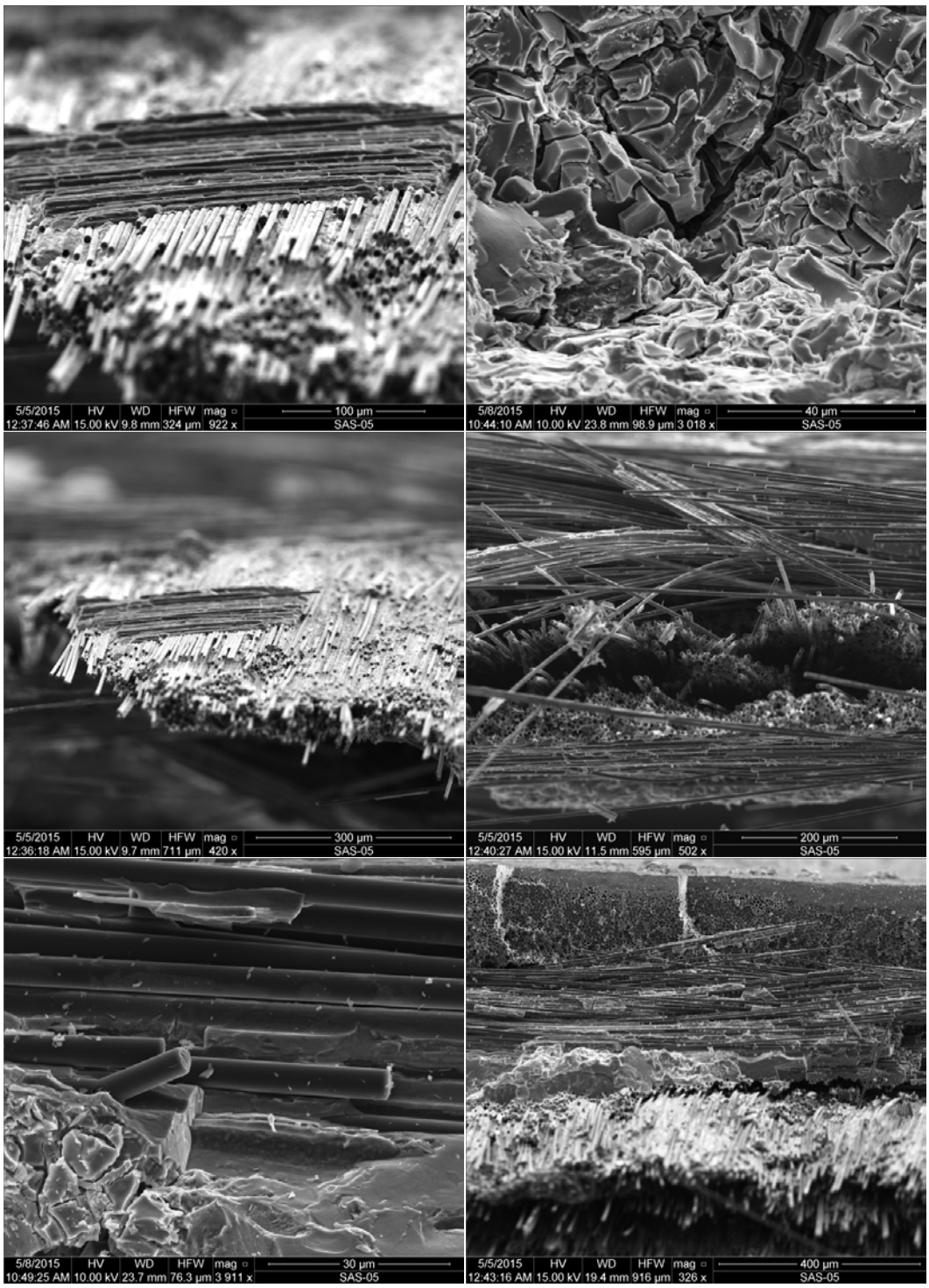

Figure K. 14: SEM micrographs of a fracture surface obtained in tensile test of a C/SiC specimen subjected to prior heat treatment for 100 h at 1300°C (Plate 12015, Specimen 3)

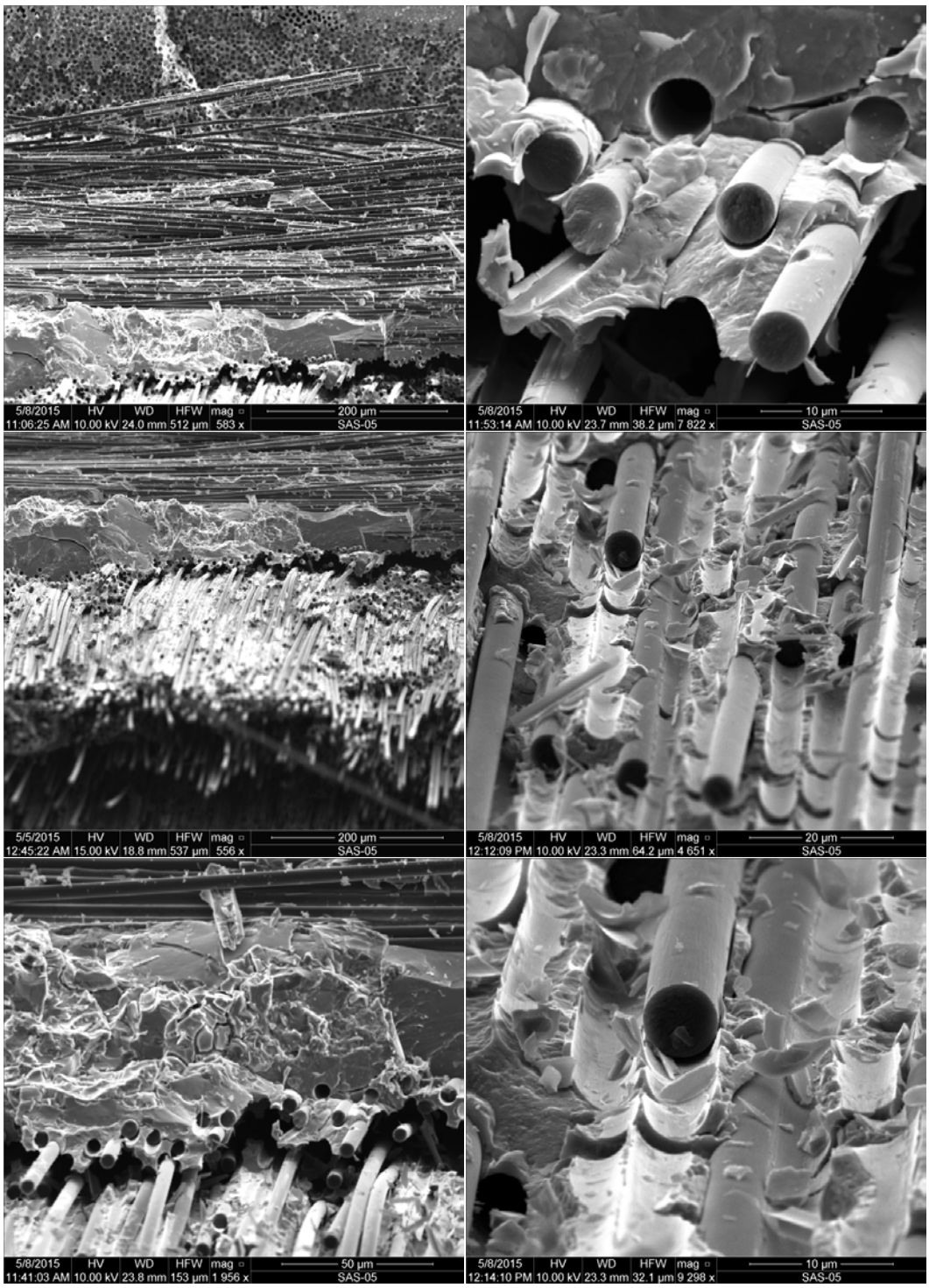

Figure K. 15: SEM micrographs of a fracture surface obtained in tensile test of a C/SiC specimen subjected to prior heat treatment for 100 h at 1300°C (Plate 12015, Specimen 3)

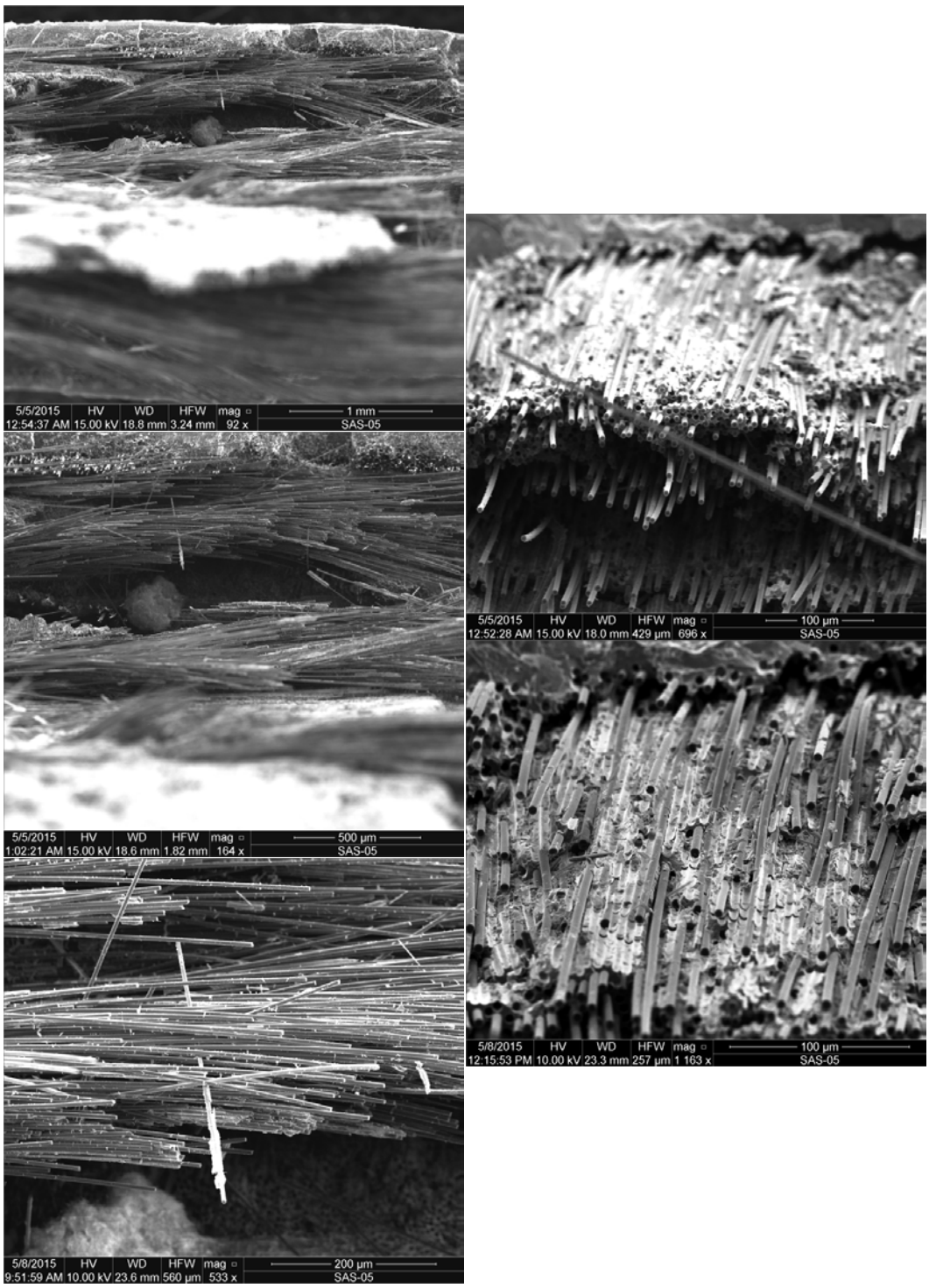

Figure K. 16: SEM micrographs of a fracture surface obtained in tensile test of a C/SiC specimen subjected to prior heat treatment for 100 h at 1300°C (Plate 12015, Specimen 3)

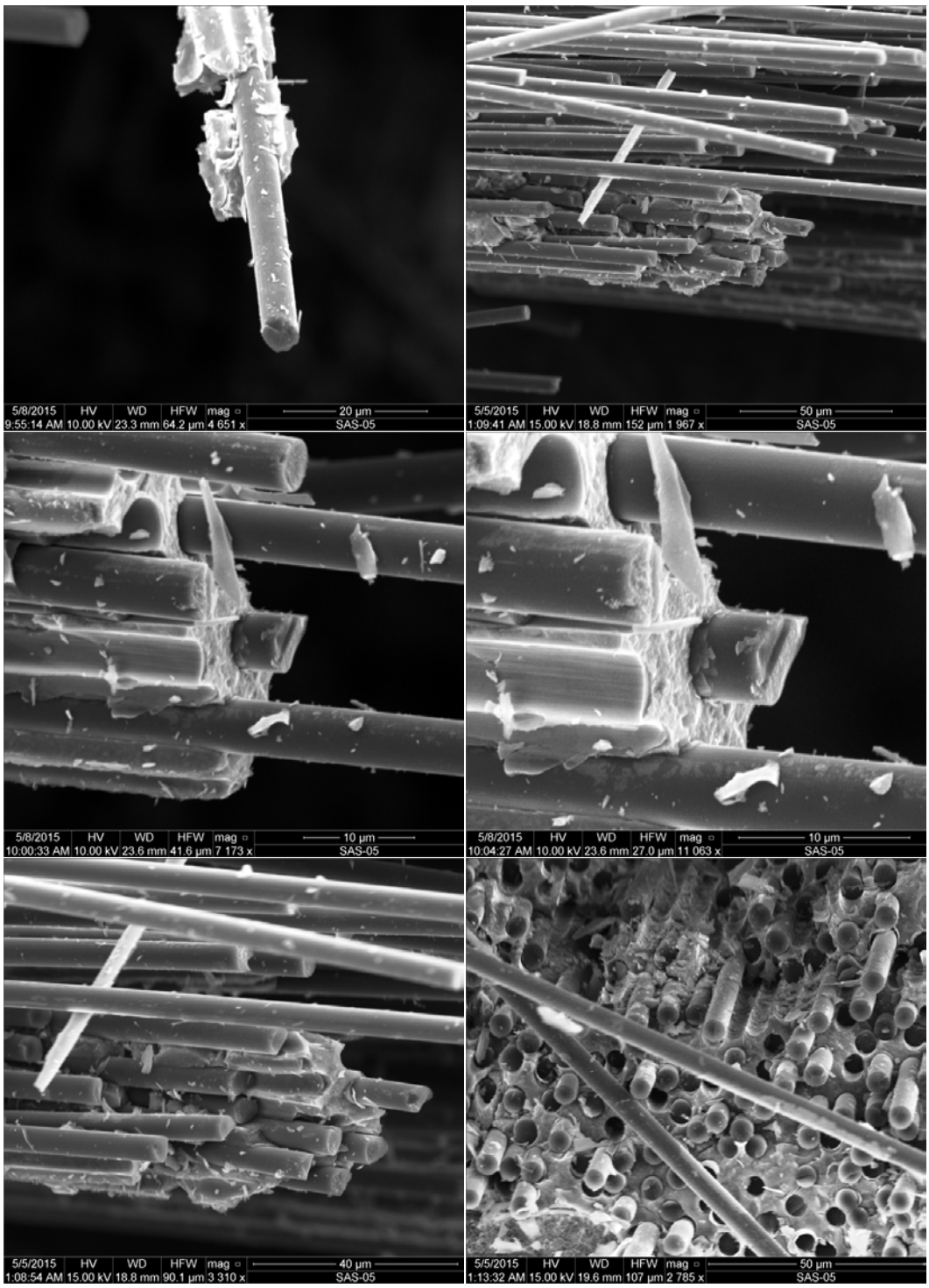

Figure K. 17: SEM micrographs of a fracture surface obtained in tensile test of a C/SiC specimen subjected to prior heat treatment for 100 h at 1300°C (Plate 12015, Specimen 3)

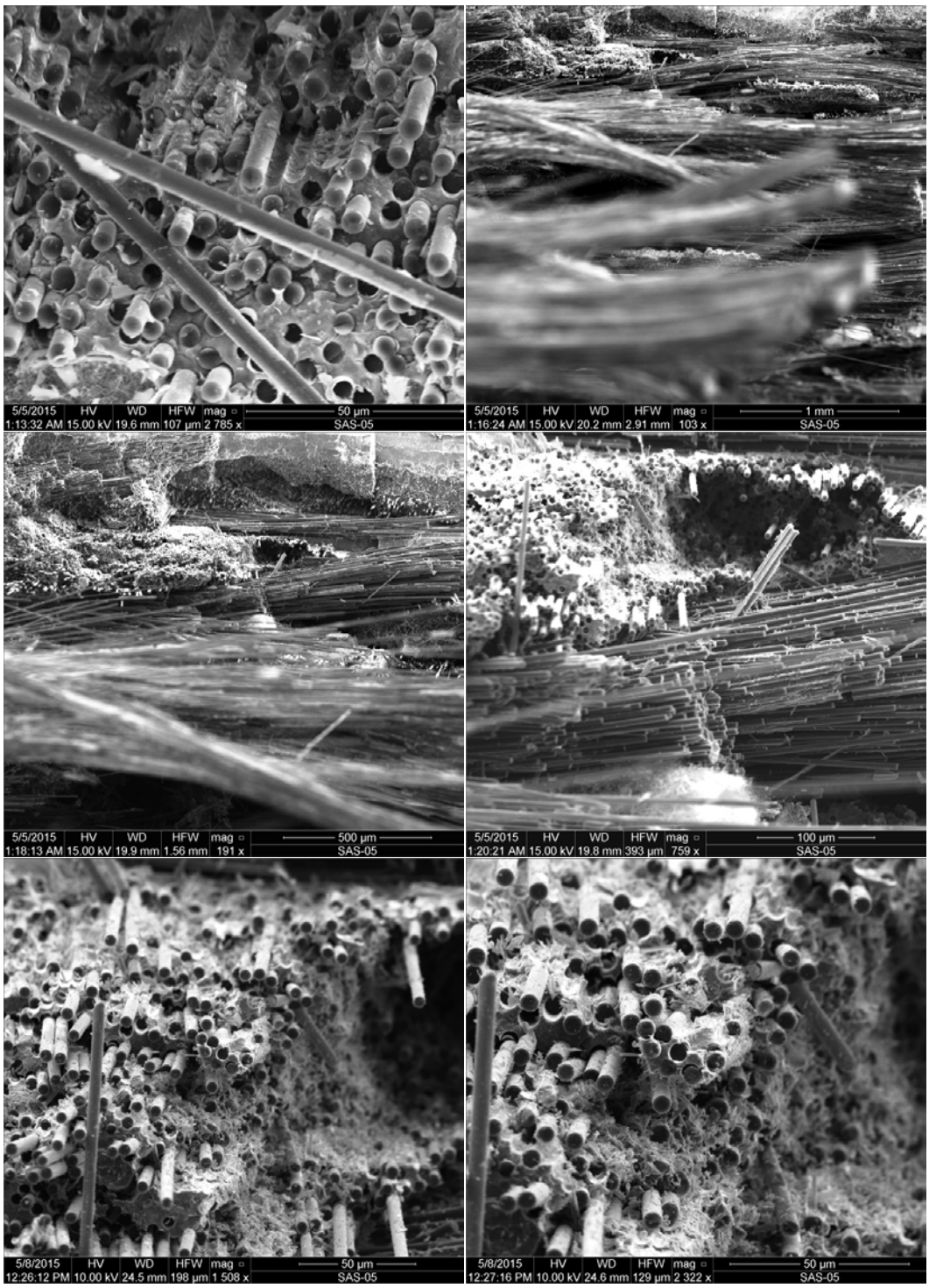

Figure K. 18: SEM micrographs of a fracture surface obtained in tensile test of a C/SiC specimen subjected to prior heat treatment for 100 h at 1300°C (Plate 12015, Specimen 3)

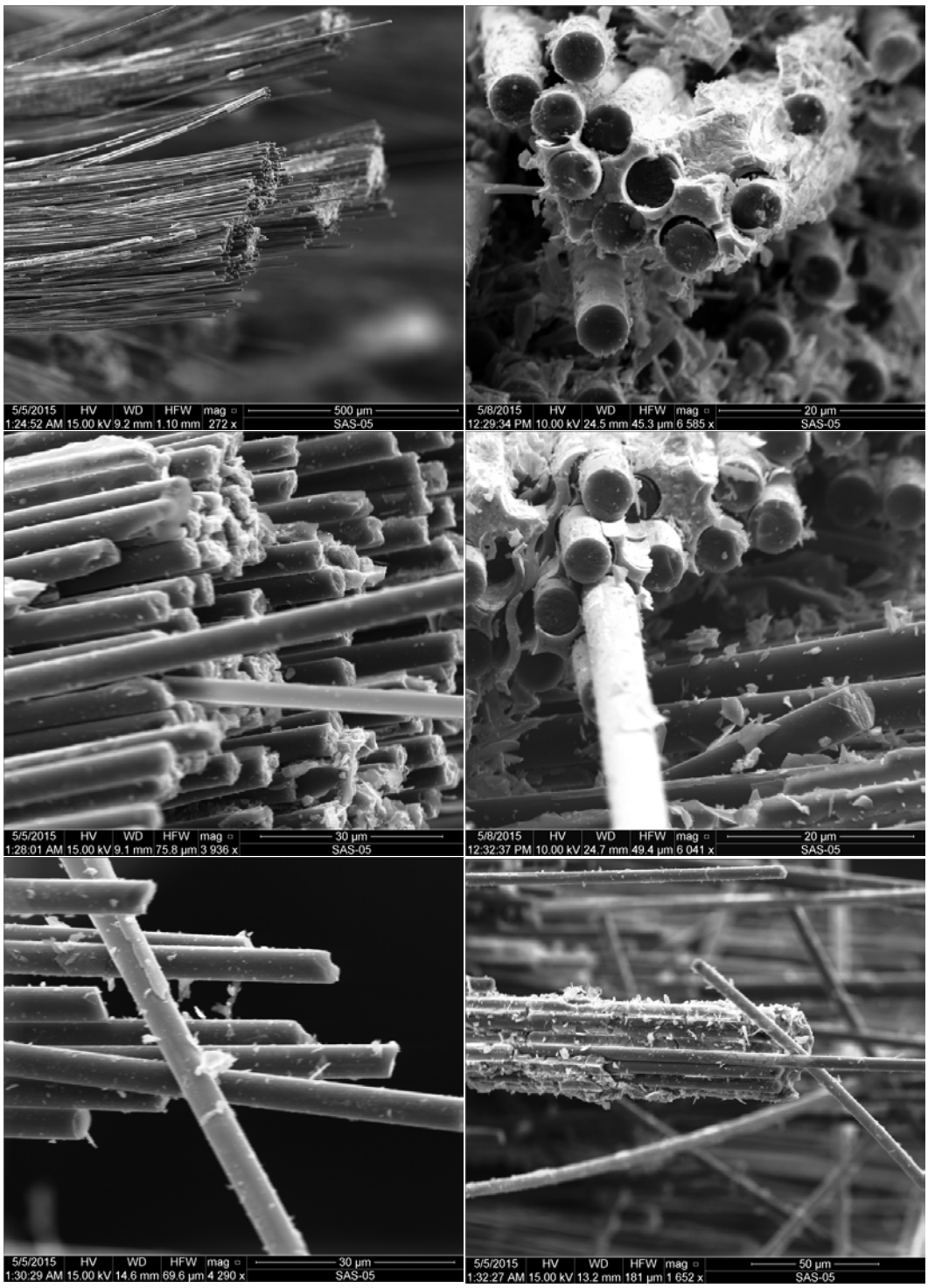

Figure K. 19: SEM micrographs of a fracture surface obtained in tensile test of a C/SiC specimen subjected to prior heat treatment for 100 h at 1300°C (Plate 12015, Specimen 3)

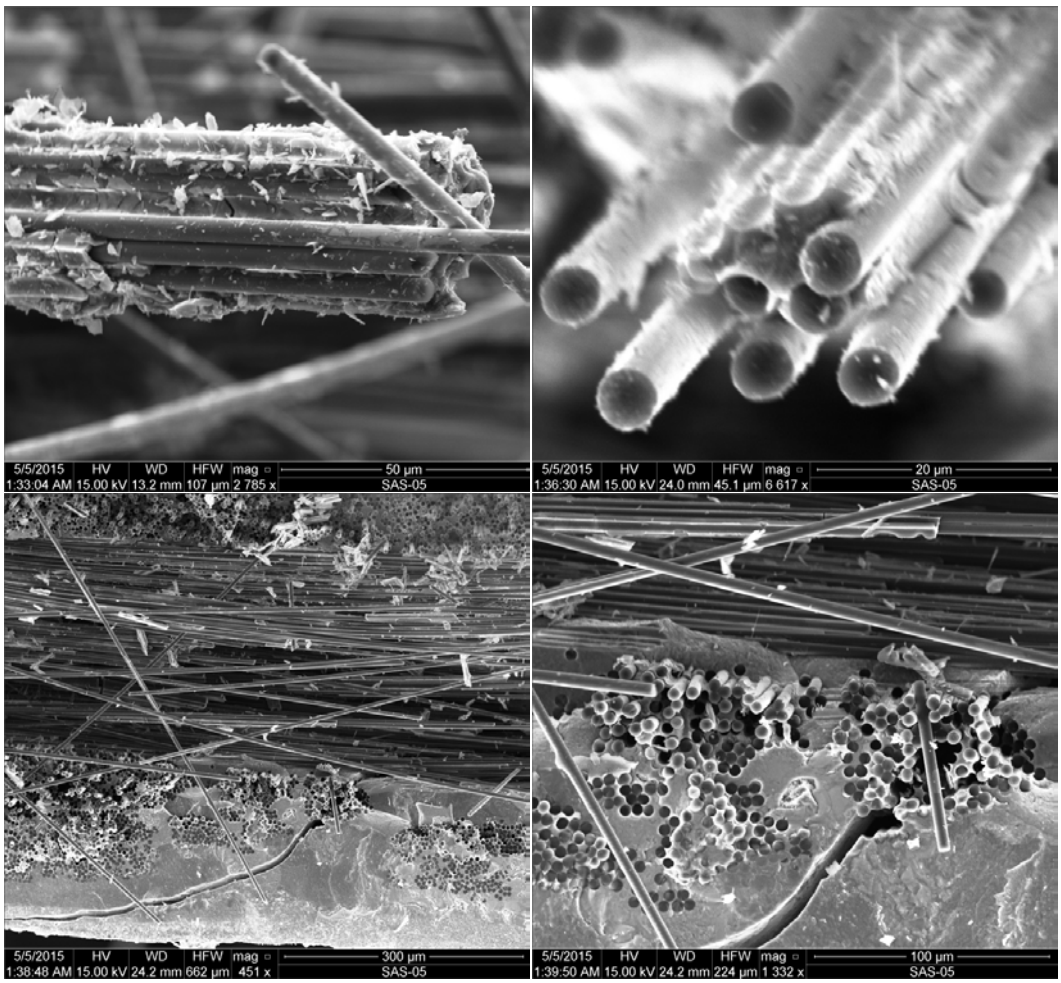

Figure K. 20: SEM micrographs of a fracture surface obtained in tensile test of a C/SiC specimen subjected to prior heat treatment for 100 h at 1300°C (Plate 12015, Specimen 3)

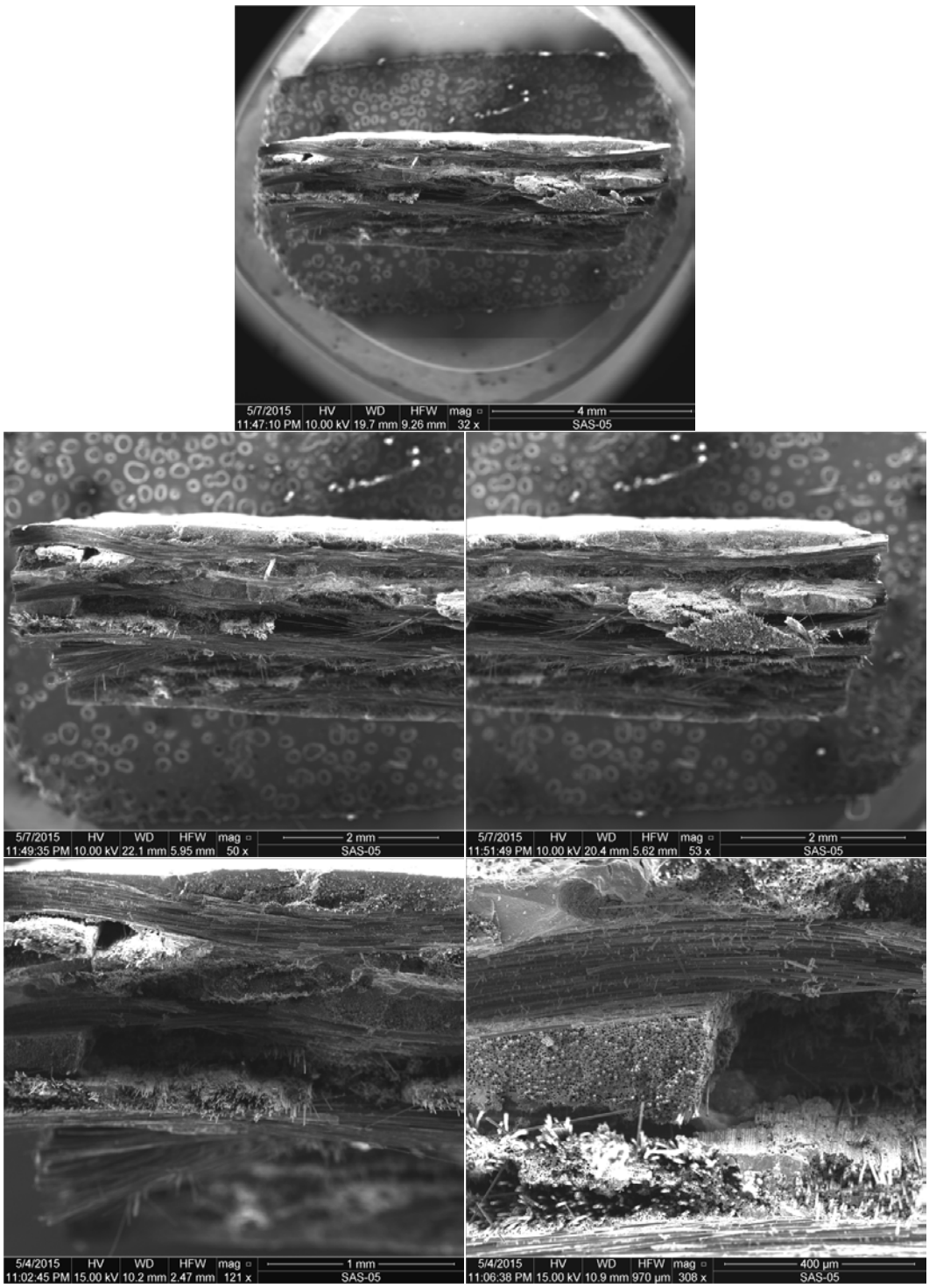

Figure K. 21: SEM micrographs of a fracture surface obtained in tensile test of a C/SiC specimen subjected to prior heat treatment for 100 h at 1200°C (Plate 12016, Specimen 3)

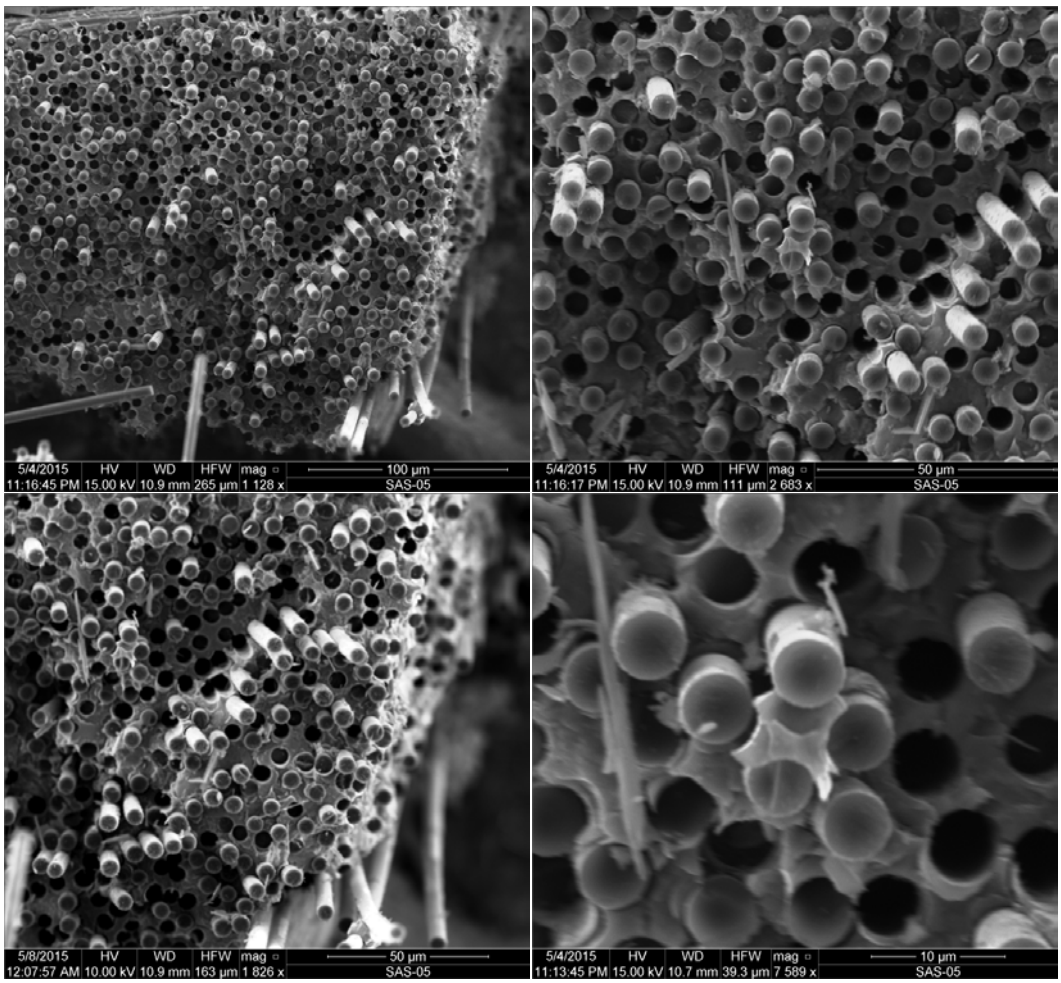

Figure K. 22: SEM micrographs of a fracture surface obtained in tensile test of a C/SiC specimen subjected to prior heat treatment for 100 h at 1200°C (Plate 12016, Specimen 3)

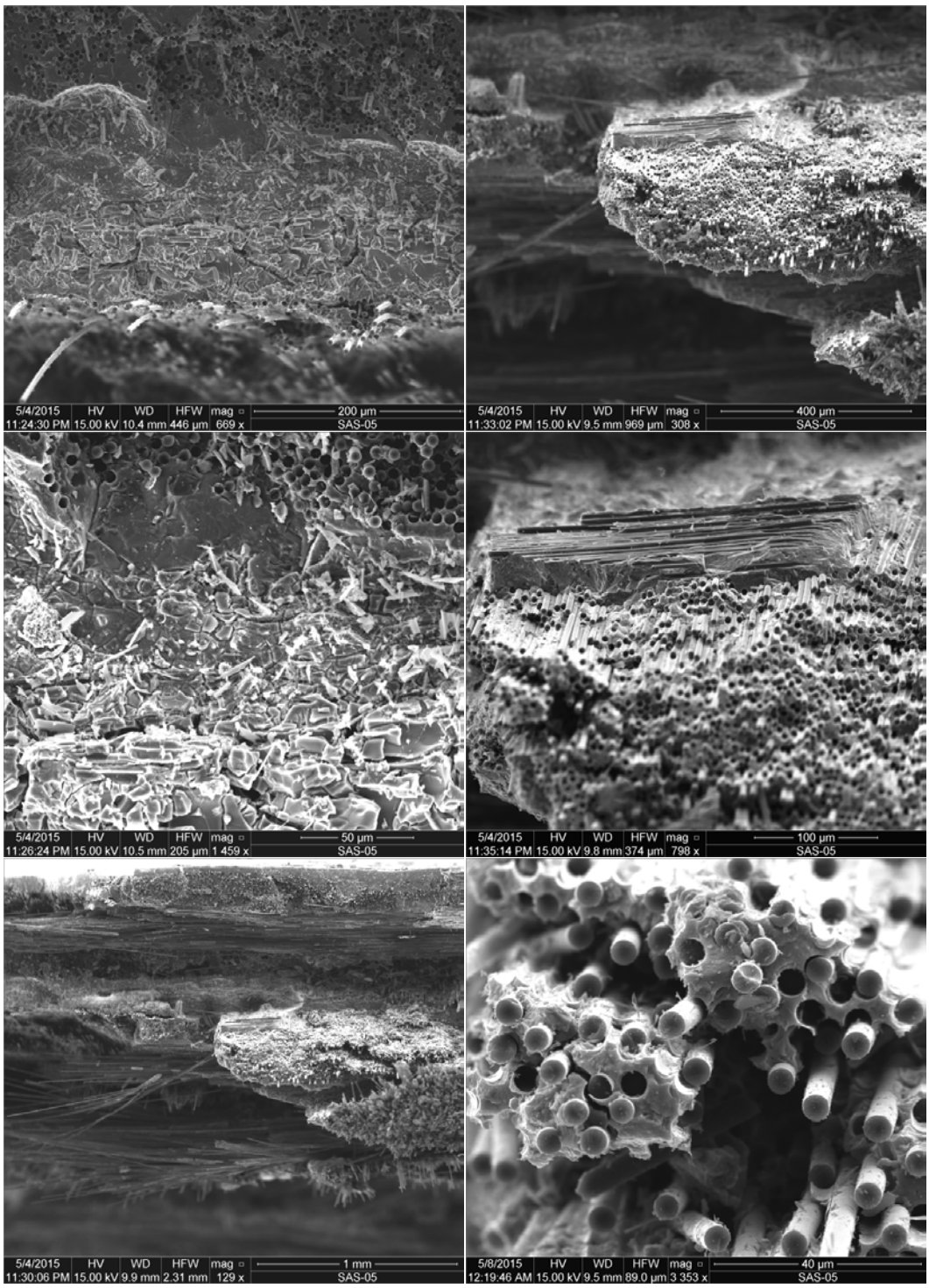

Figure K. 23: SEM micrographs of a fracture surface obtained in tensile test of a C/SiC specimen subjected to prior heat treatment for 100 h at 1200°C (Plate 12016, Specimen 3)

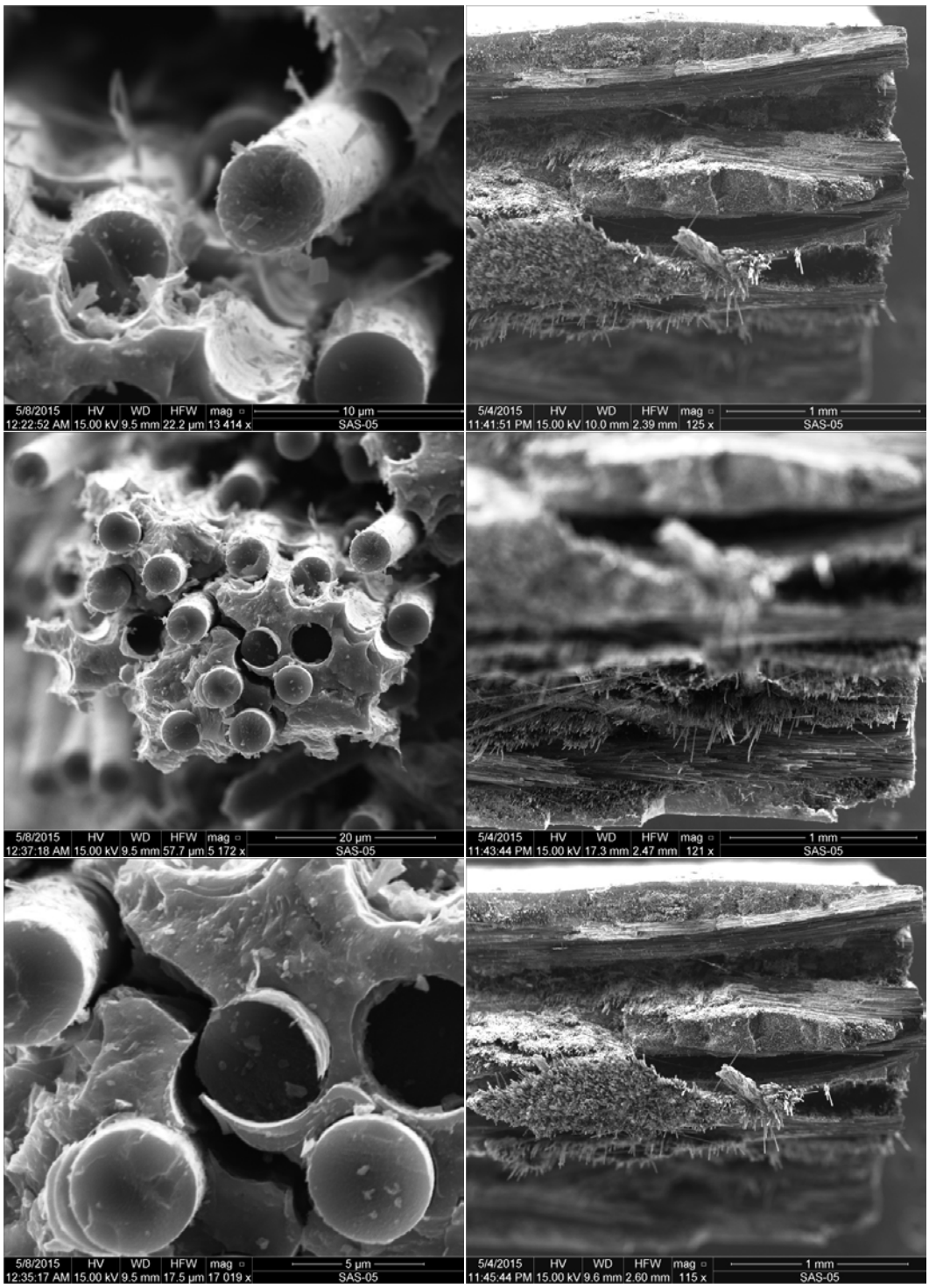

Figure K. 24: SEM micrographs of a fracture surface obtained in tensile test of a C/SiC specimen subjected to prior heat treatment for 100 h at 1200°C (Plate 12016, Specimen 3)

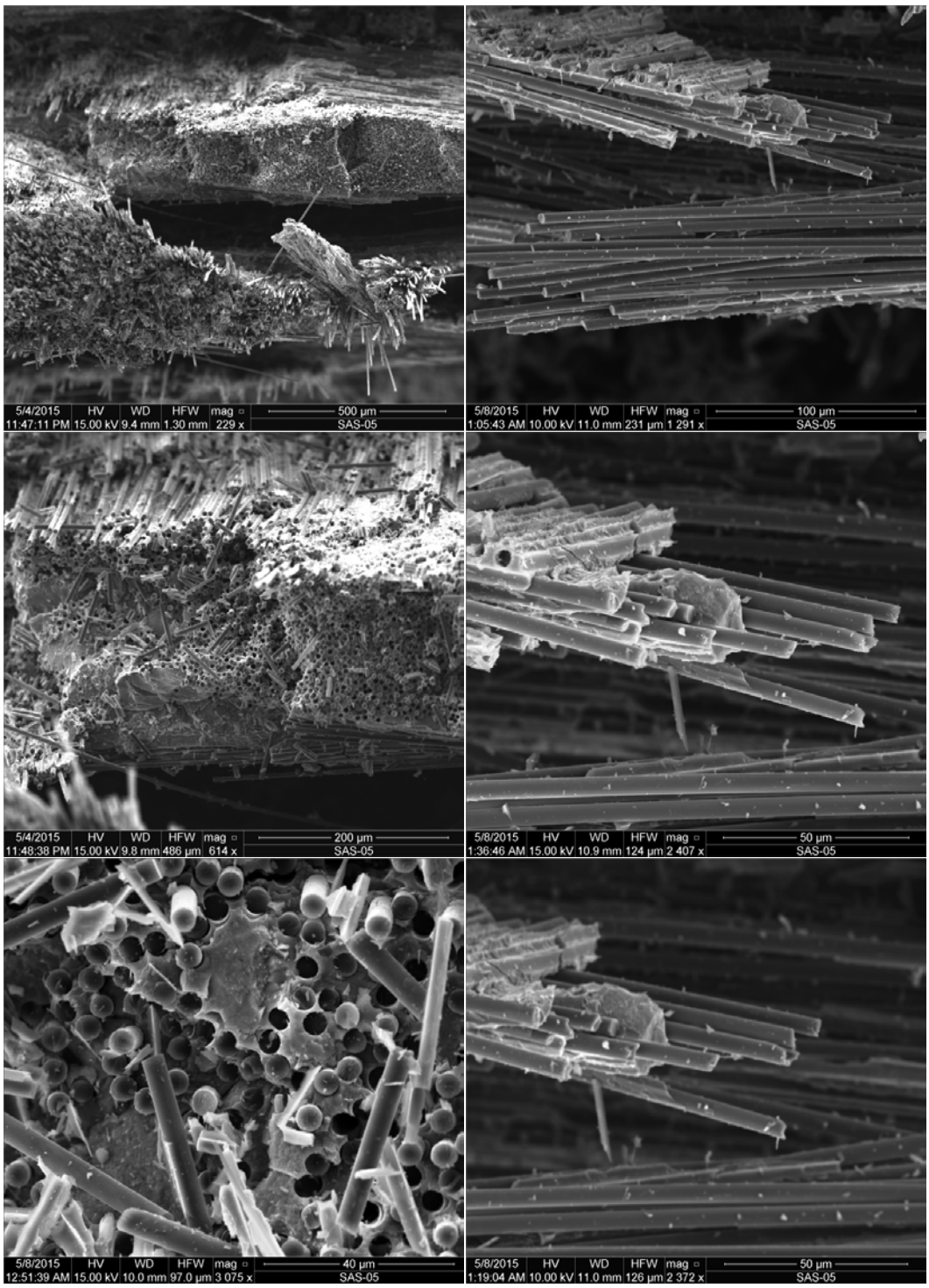

Figure K. 25: SEM micrographs of a fracture surface obtained in tensile test of a C/SiC specimen subjected to prior heat treatment for 100 h at 1200°C (Plate 12016, Specimen 3)

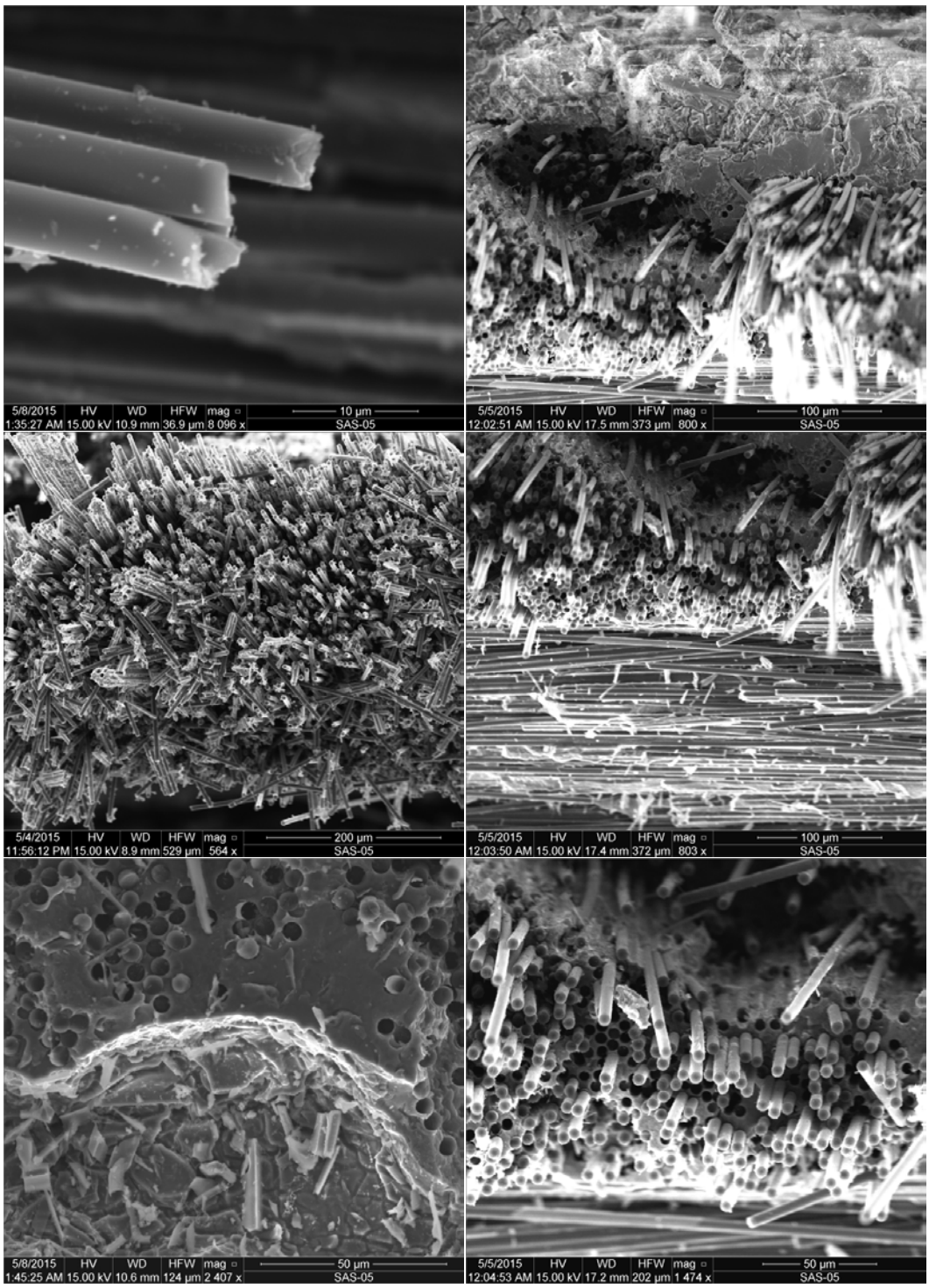

Figure K. 26: SEM micrographs of a fracture surface obtained in tensile test of a C/SiC specimen subjected to prior heat treatment for 100 h at 1200°C (Plate 12016, Specimen 3)

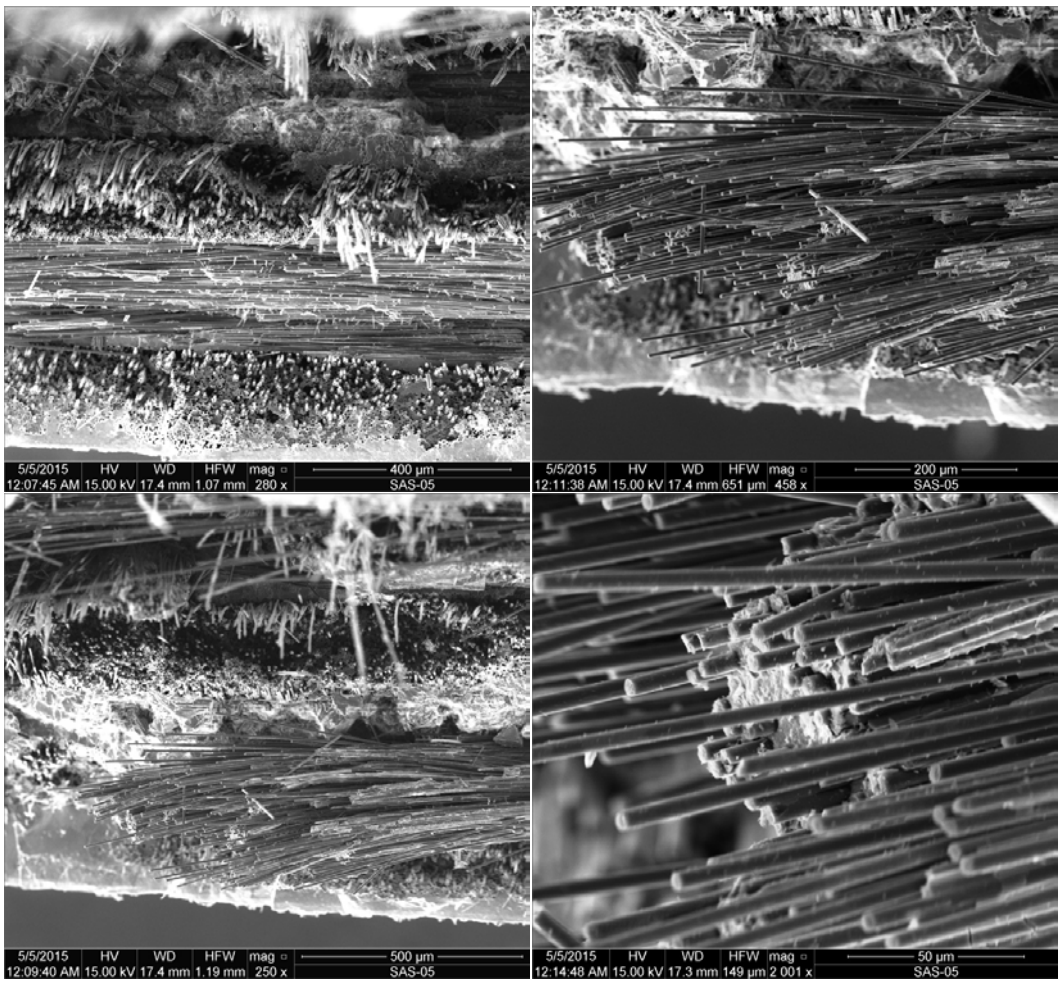

Figure K. 27: SEM micrographs of a fracture surface obtained in tensile test of a C/SiC specimen subjected to prior heat treatment for 100 h at 1200°C (Plate 12016, Specimen 3)

Appendix L: Additional SEM Micrographs of T300 C/HYPR-SiC™ Fracture Surfaces

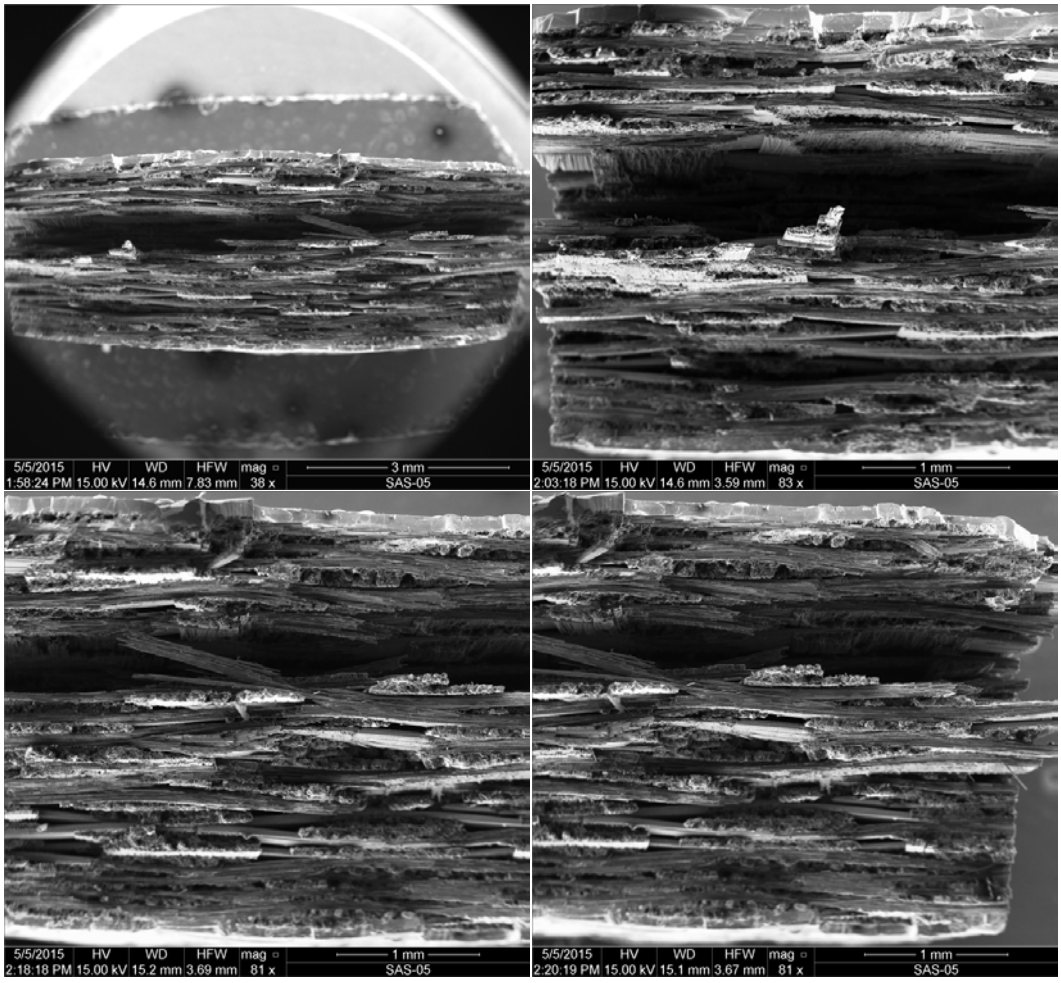

Figure L. 1: SEM micrographs of a fracture surface obtained in tensile test of a virgin C/HYPR-SiC™ specimen (Plate 11126, Specimen 4)

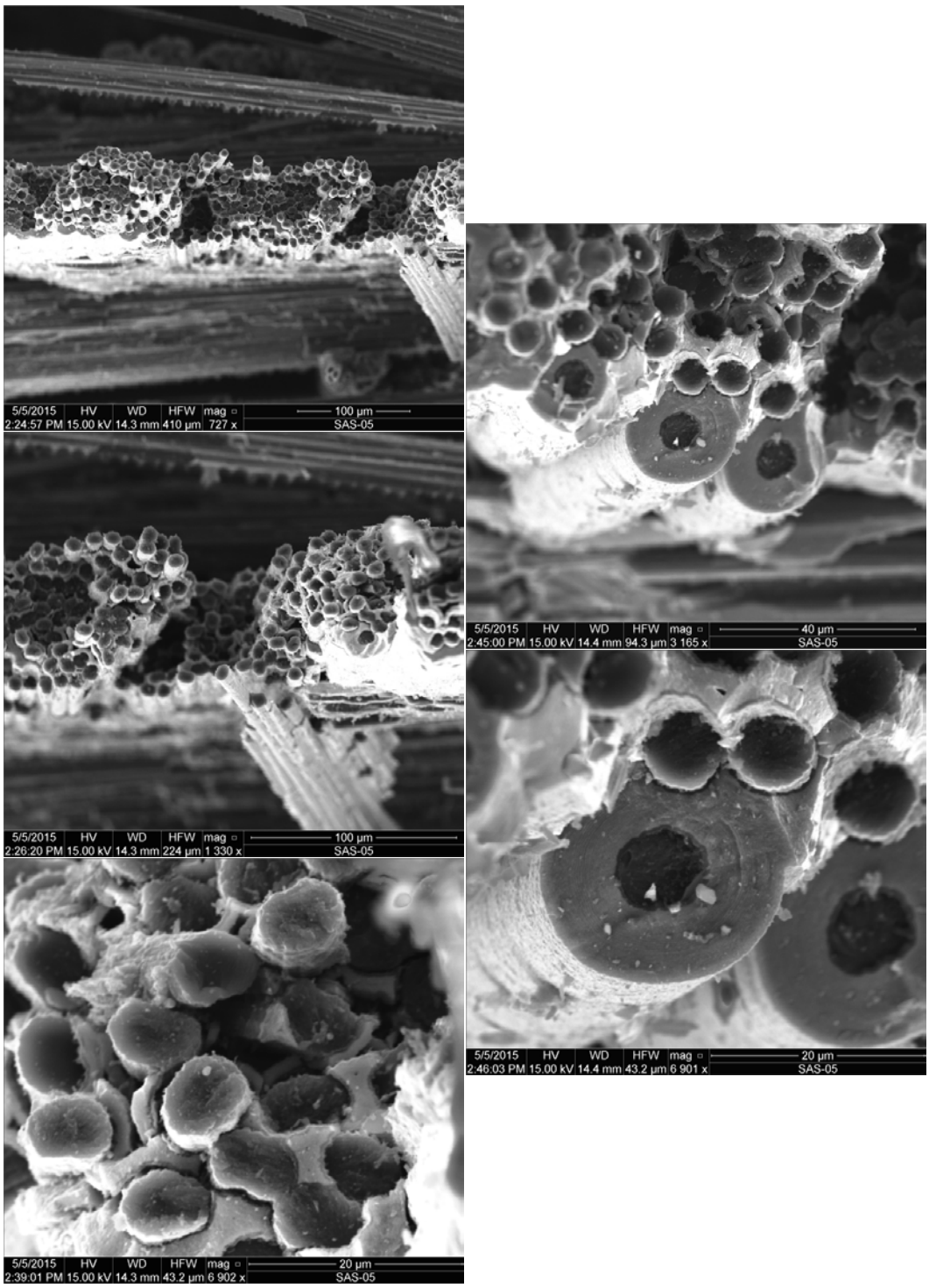

Figure L. 2: SEM micrographs of a fracture surface obtained in tensile test of a virgin C/HYPR-SiC™ specimen (Plate 11126, Specimen 4)

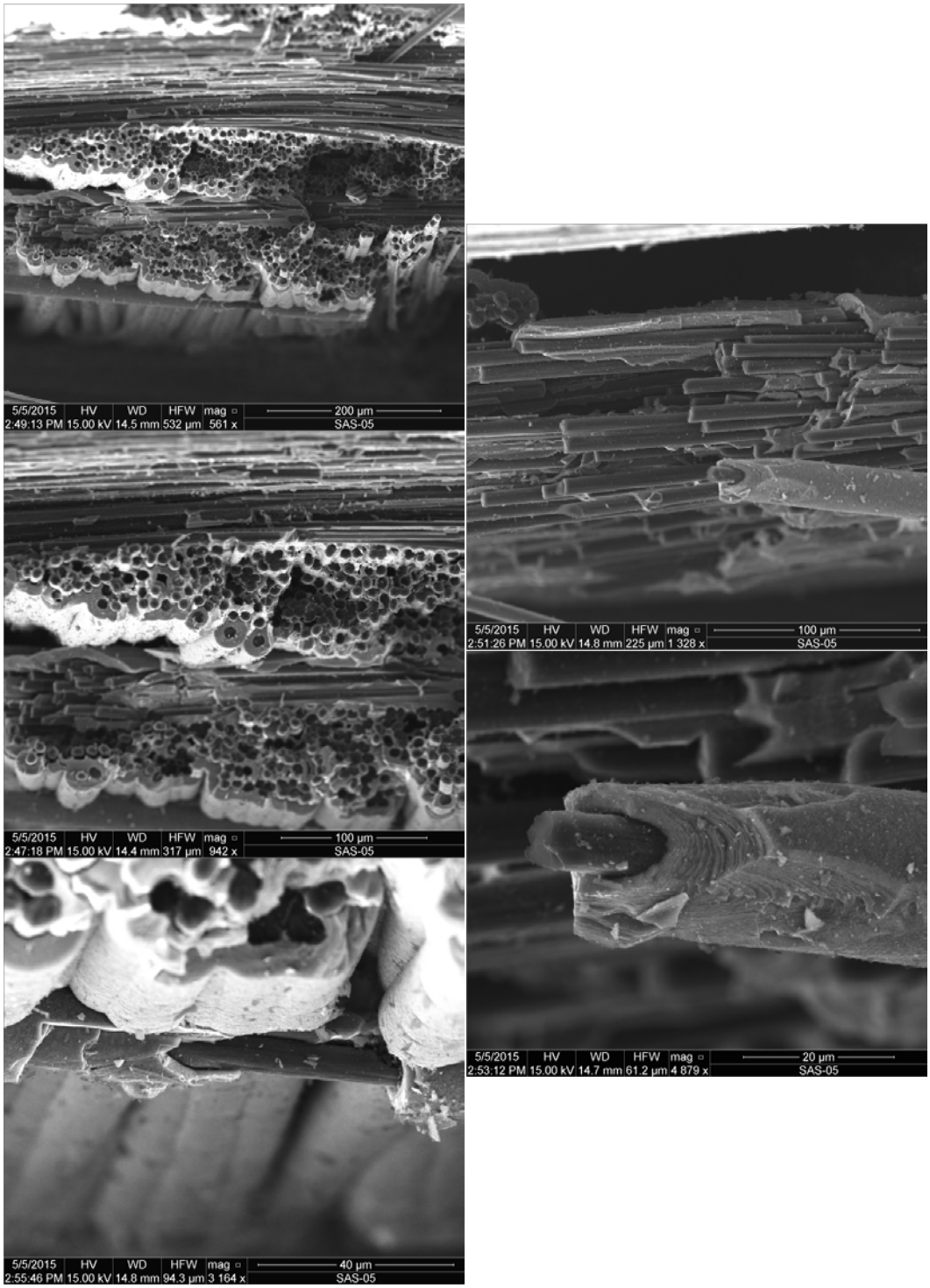

Figure L. 3: SEM micrographs of a fracture surface obtained in tensile test of a virgin C/HYPR-SiC™ specimen (Plate 11126, Specimen 4)

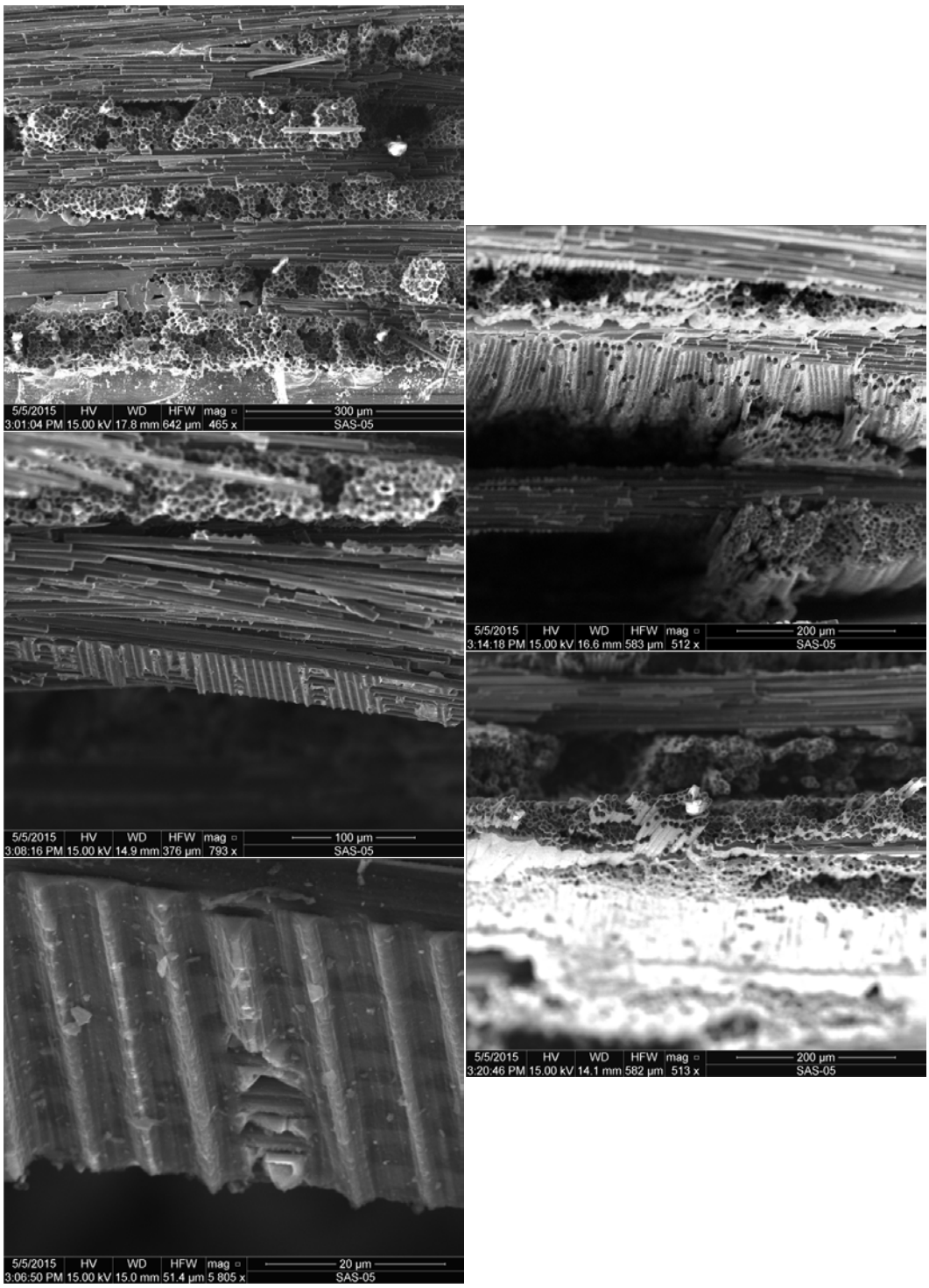

Figure L. 4: SEM micrographs of a fracture surface obtained in tensile test of a virgin C/HYPR-SiC™ specimen (Plate 11126, Specimen 4)

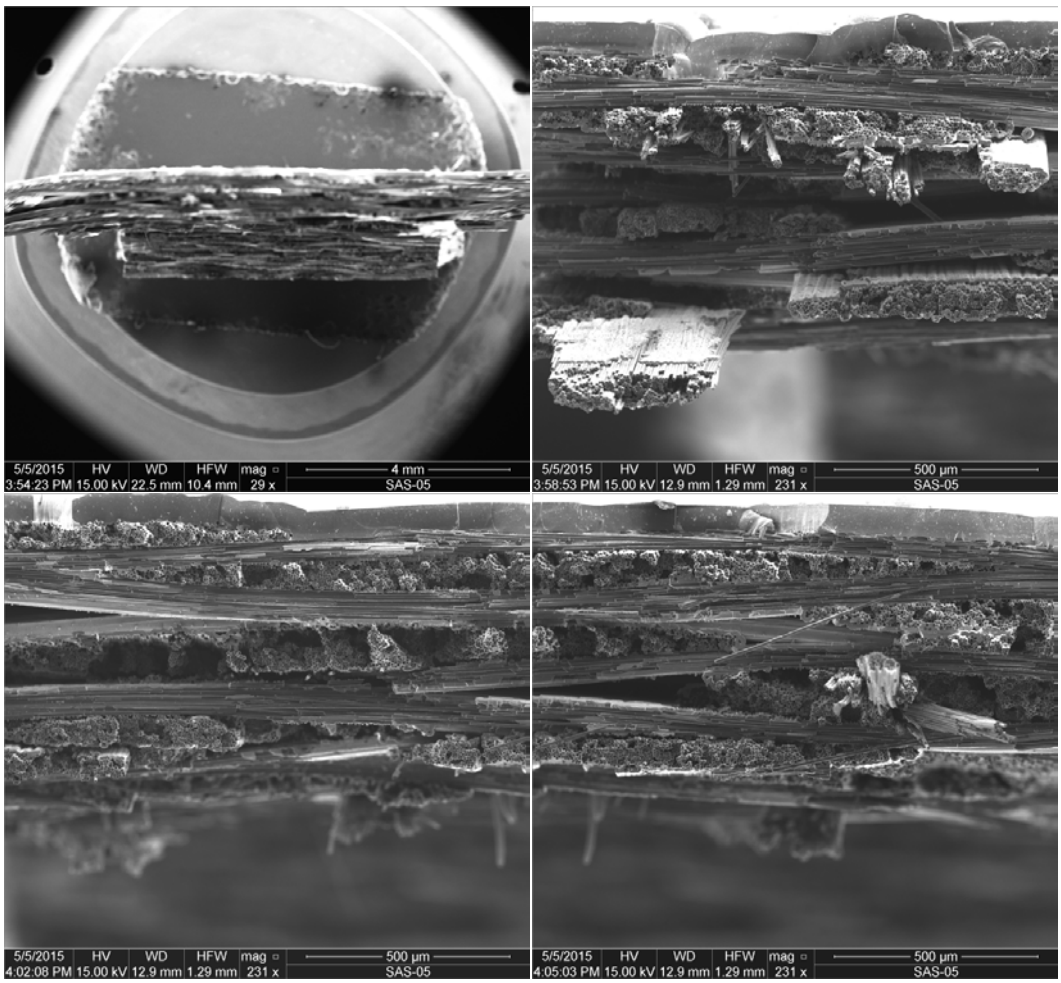

Figure L. 5: SEM micrographs of a fracture surface obtained in tensile test of a C/HYPR-SiC™ specimen subjected to prior heat treatment for 40 h at 1300°C (Plate 11125, Specimen 4)

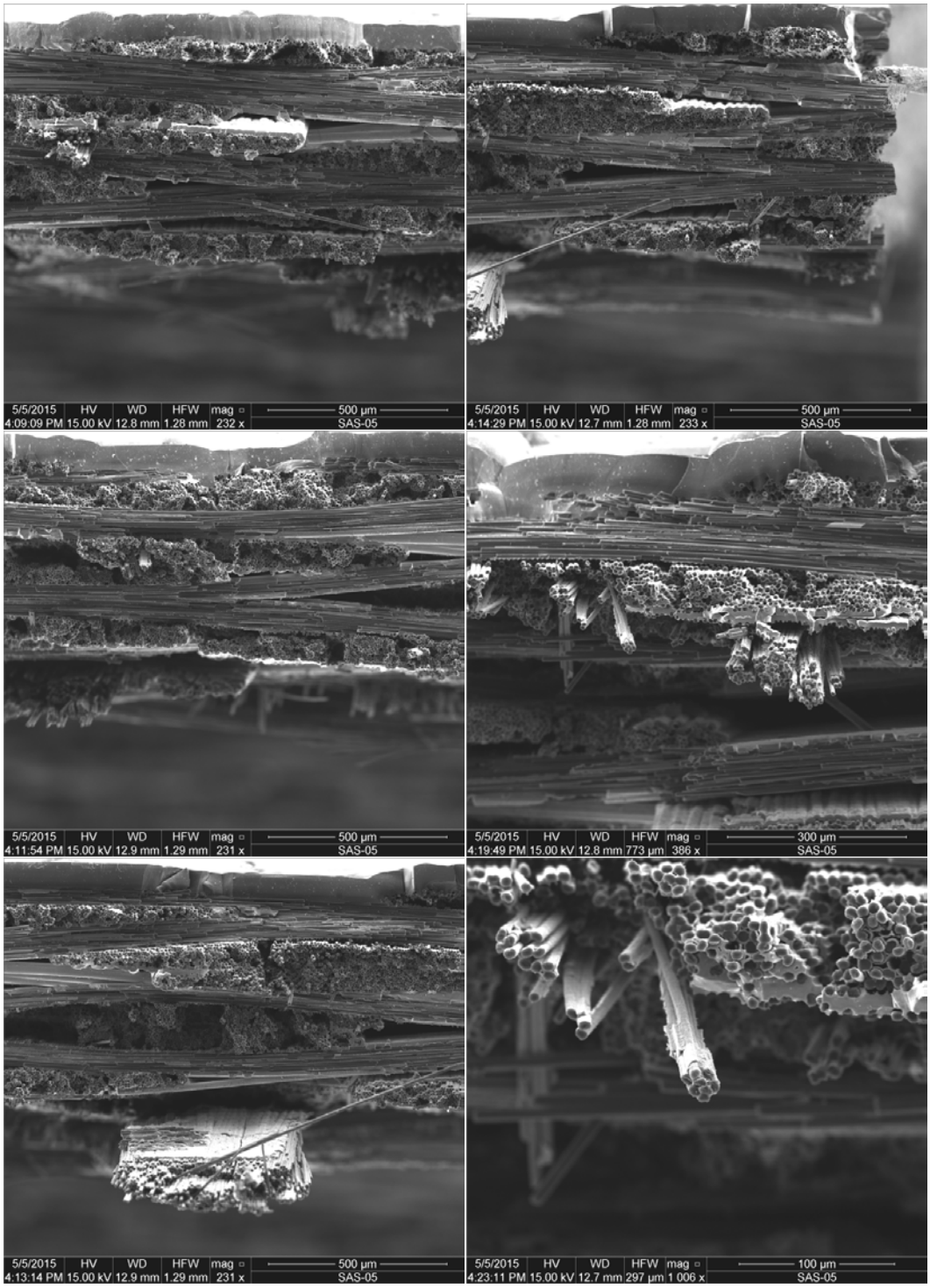

Figure L. 6: SEM micrographs of a fracture surface obtained in tensile test of a C/HYPR-SiC™ specimen subjected to prior heat treatment for 40 h at 1300°C (Plate 11125, Specimen 4)

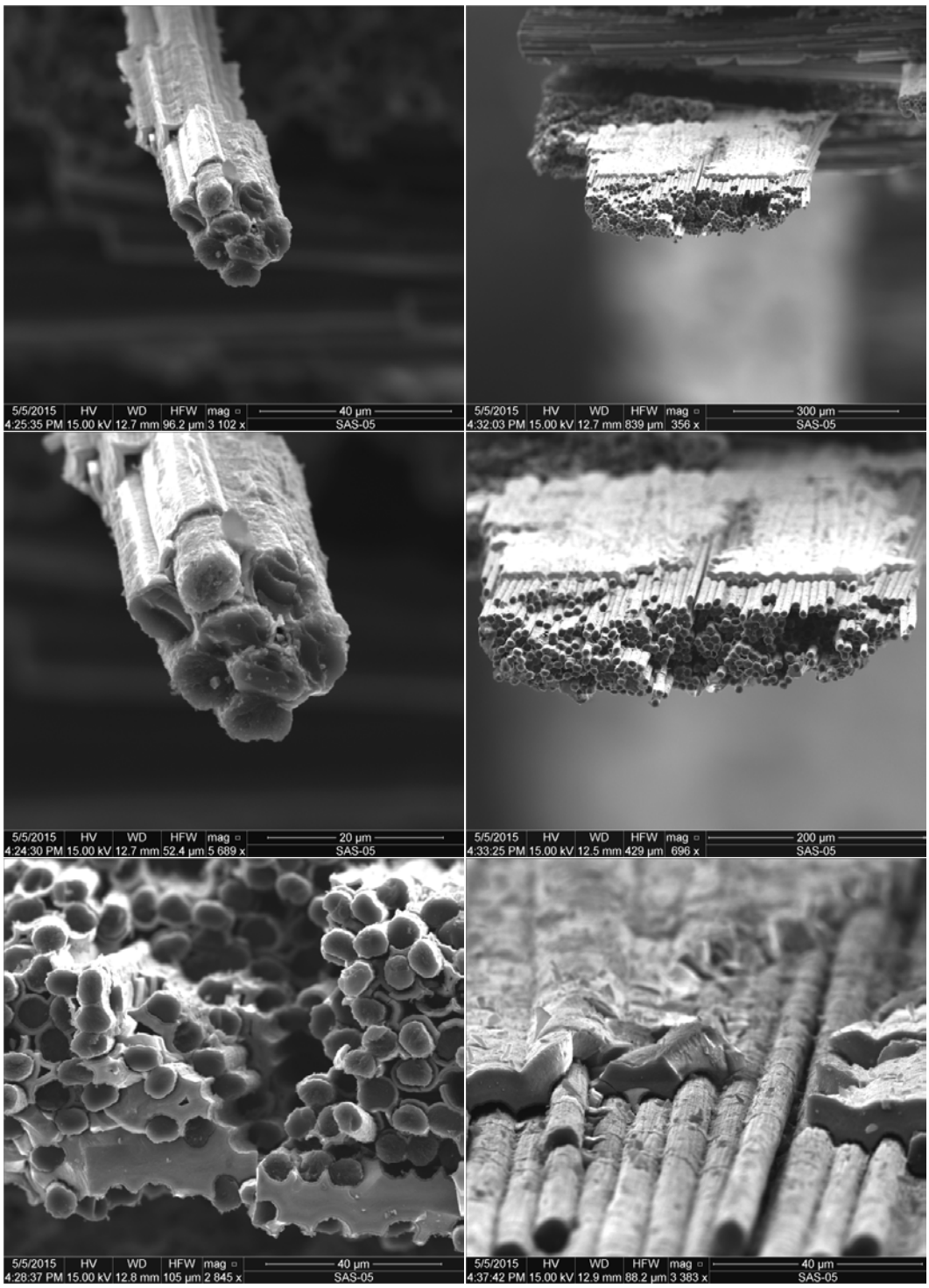

Figure L. 7: SEM micrographs of a fracture surface obtained in tensile test of a C/HYPR-SiC™ specimen subjected to prior heat treatment for 40 h at 1300°C (Plate 11125, Specimen 4)

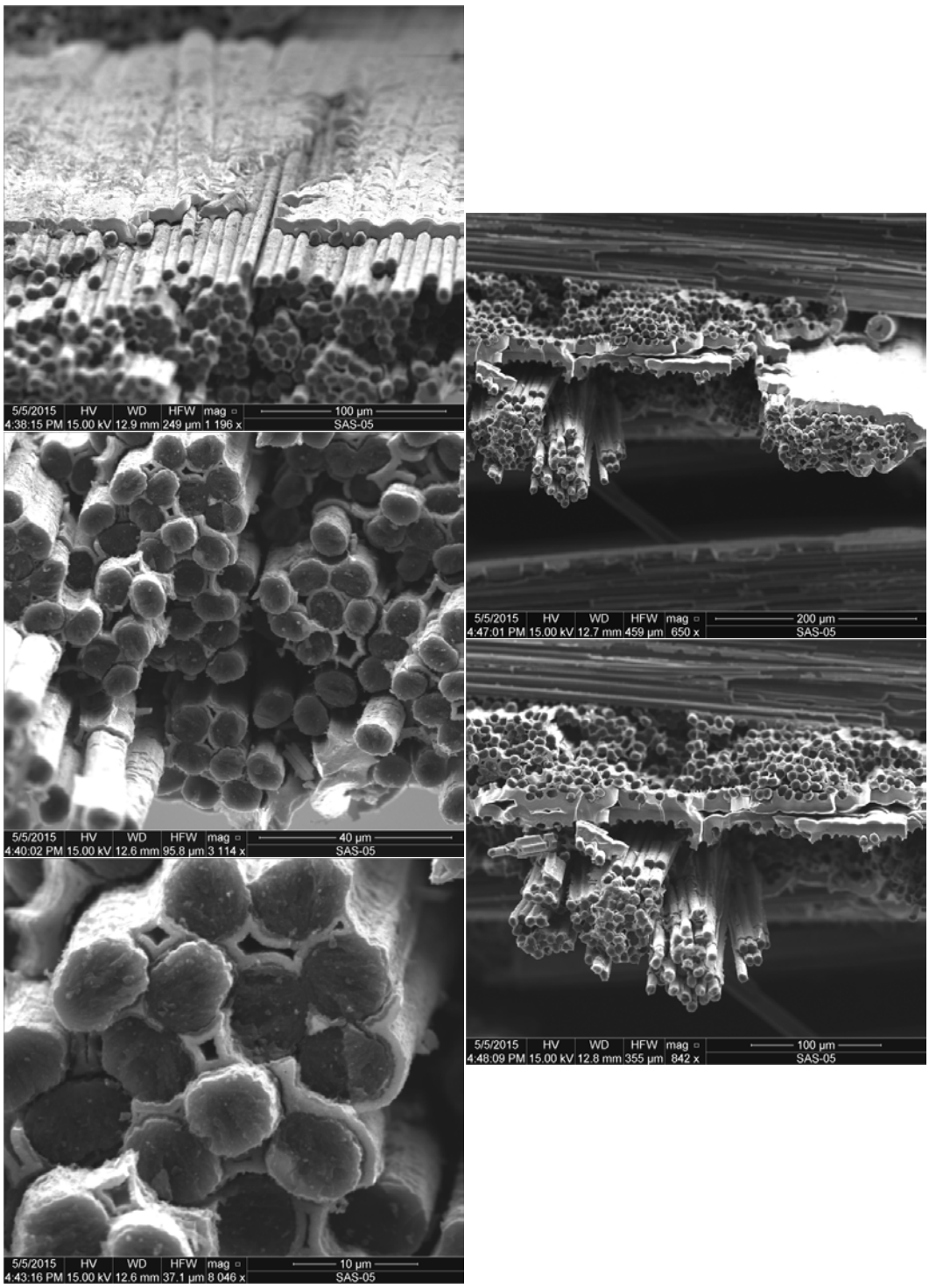

Figure L. 8: SEM micrographs of a fracture surface obtained in tensile test of a C/HYPR-SiC™ specimen subjected to prior heat treatment for 40 h at 1300°C (Plate 11125, Specimen 4)

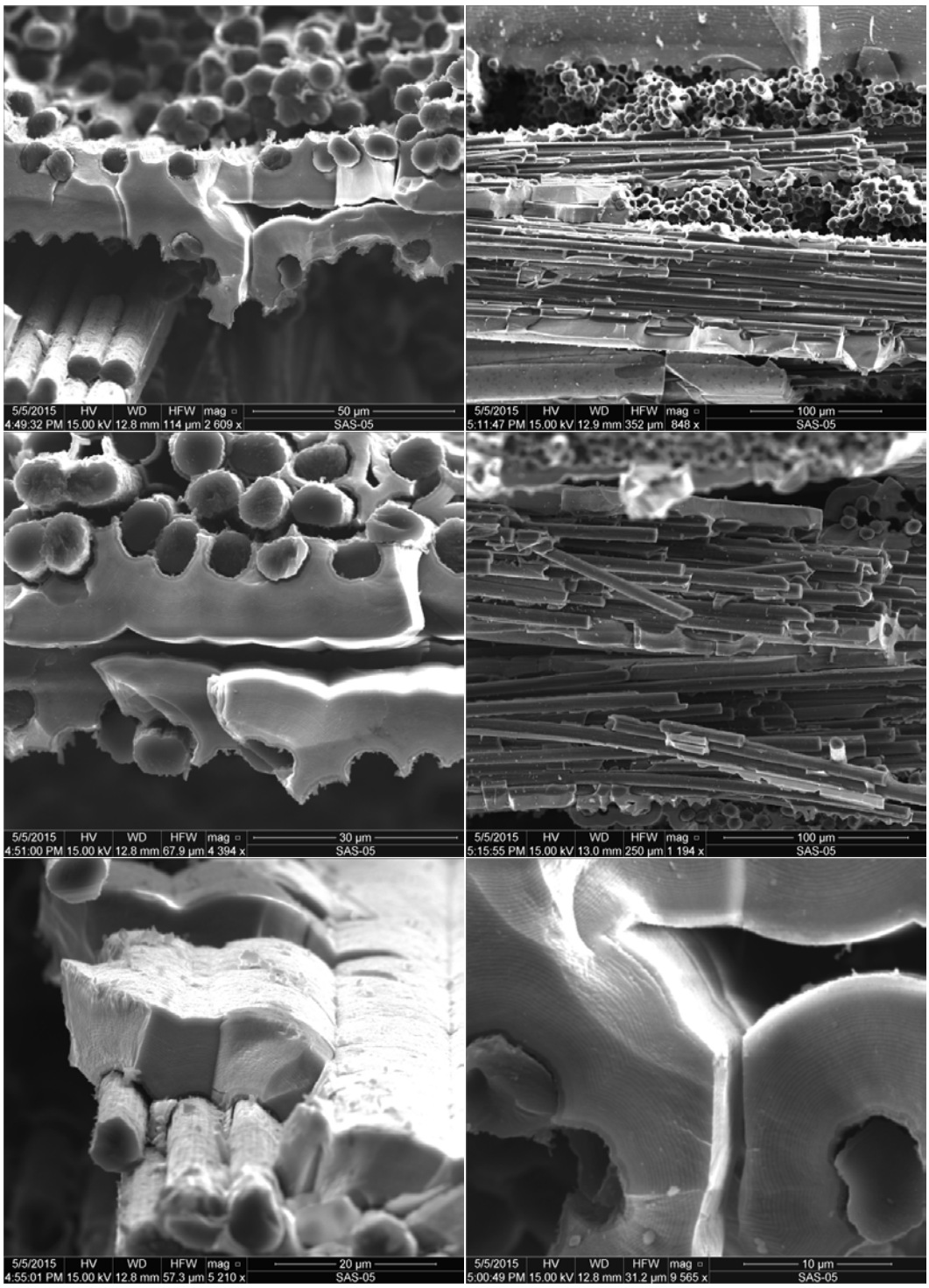

Figure L. 9: SEM micrographs of a fracture surface obtained in tensile test of a C/HYPR-SiC™ specimen subjected to prior heat treatment for 40 h at 1300°C (Plate 11125, Specimen 4)

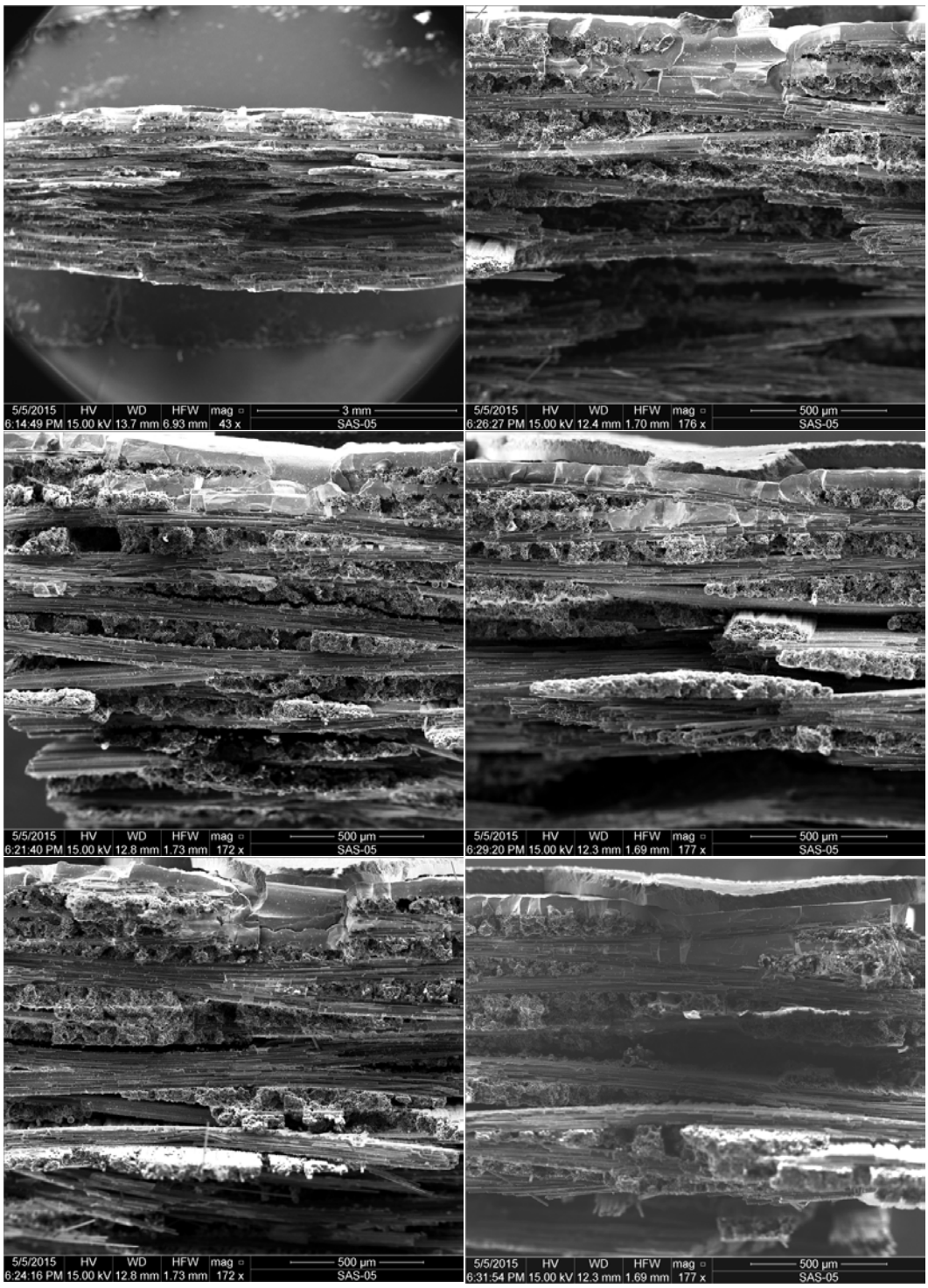

Figure L. 10: SEM micrographs of a fracture surface obtained in tensile test of a C/HYPR-SiC™ specimen subjected to prior heat treatment for 100 h at 1300°C (Plate 11121, Specimen 5)

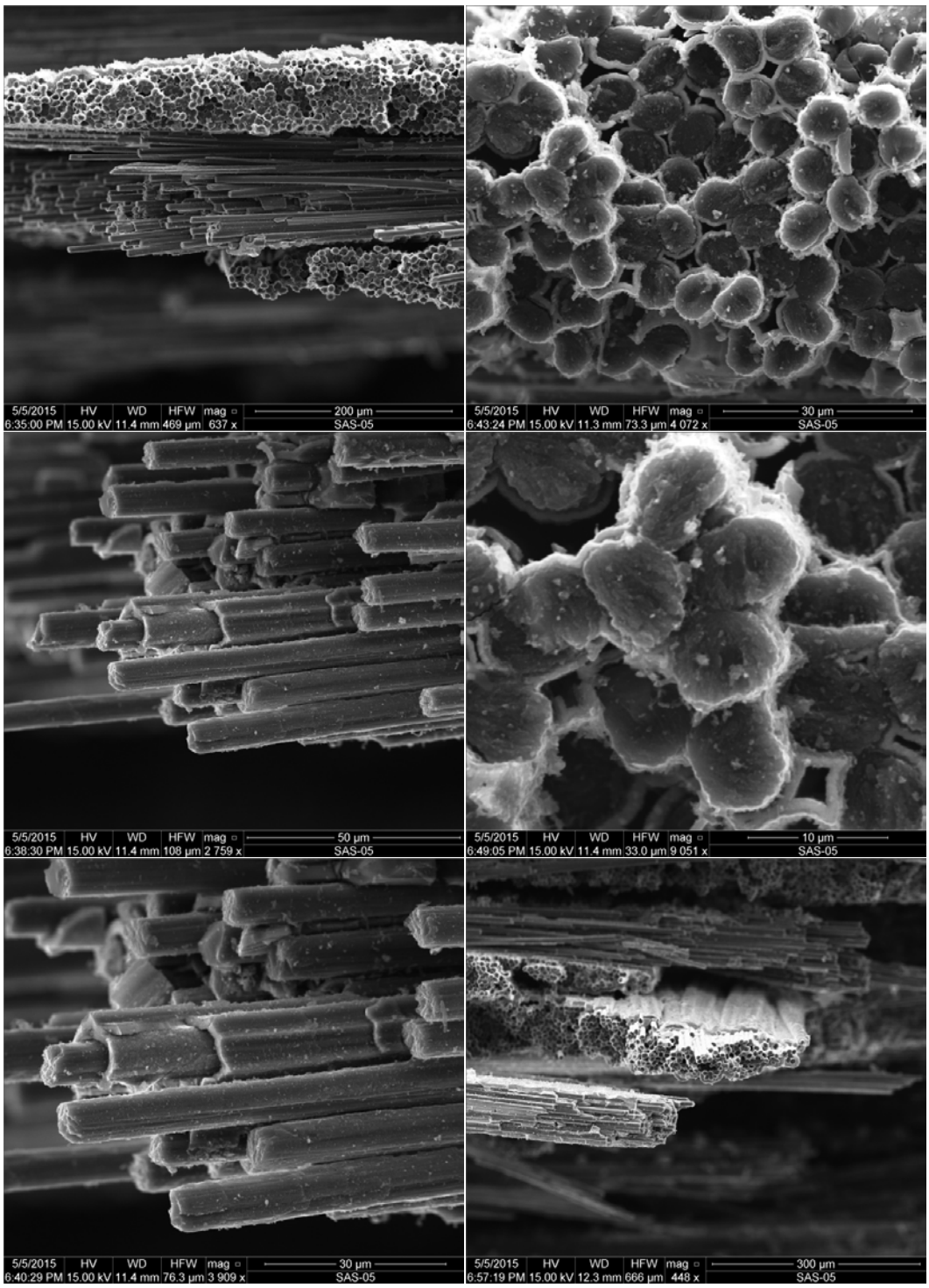

Figure L. 11: SEM micrographs of a fracture surface obtained in tensile test of a C/HYPR-SiC™ specimen subjected to prior heat treatment for 100 h at 1300°C (Plate 11121, Specimen 5)

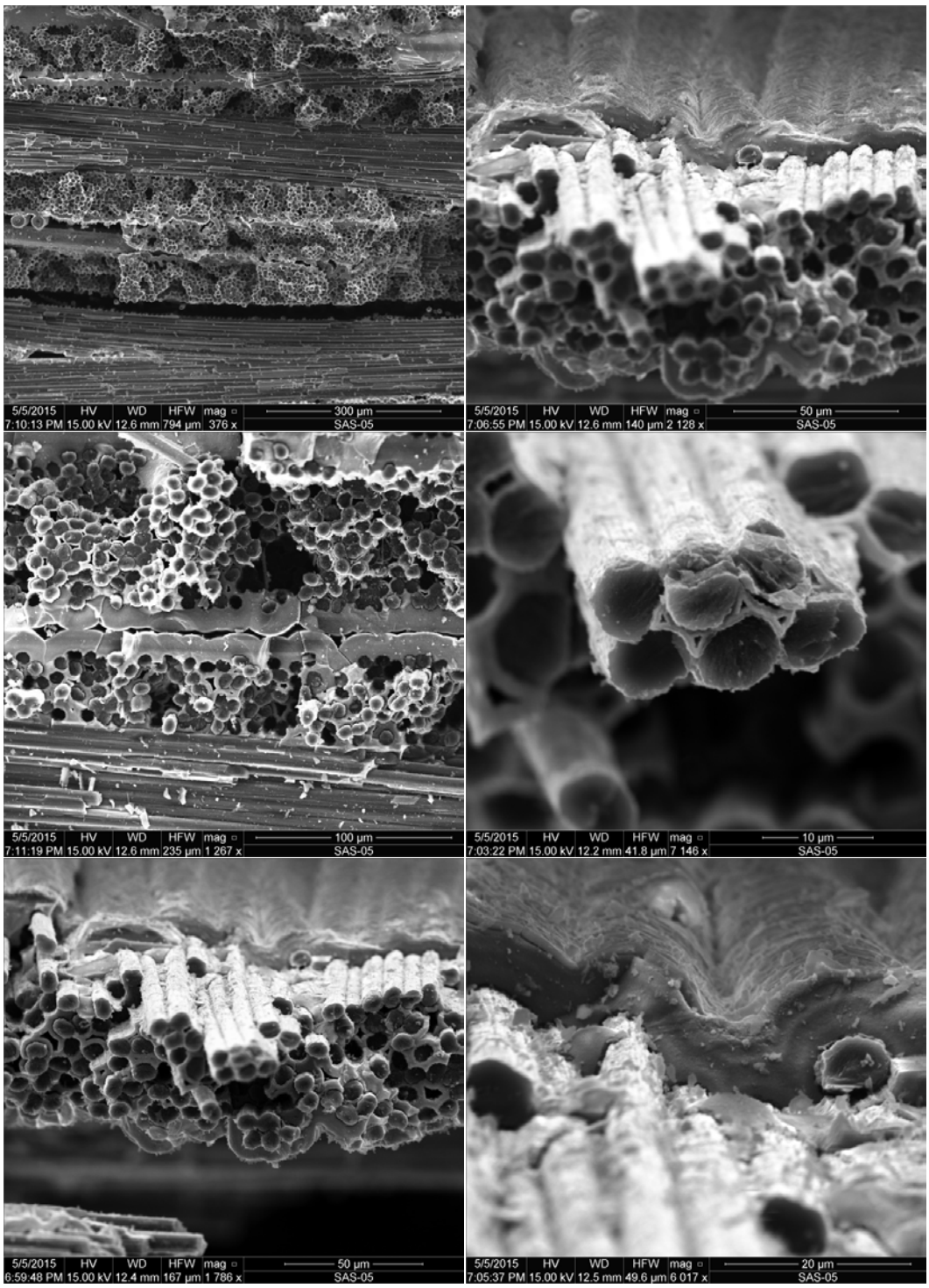

Figure L. 12: SEM micrographs of a fracture surface obtained in tensile test of a C/HYPR-SiC™ specimen subjected to prior heat treatment for 100 h at 1300°C (Plate 11121, Specimen 5)

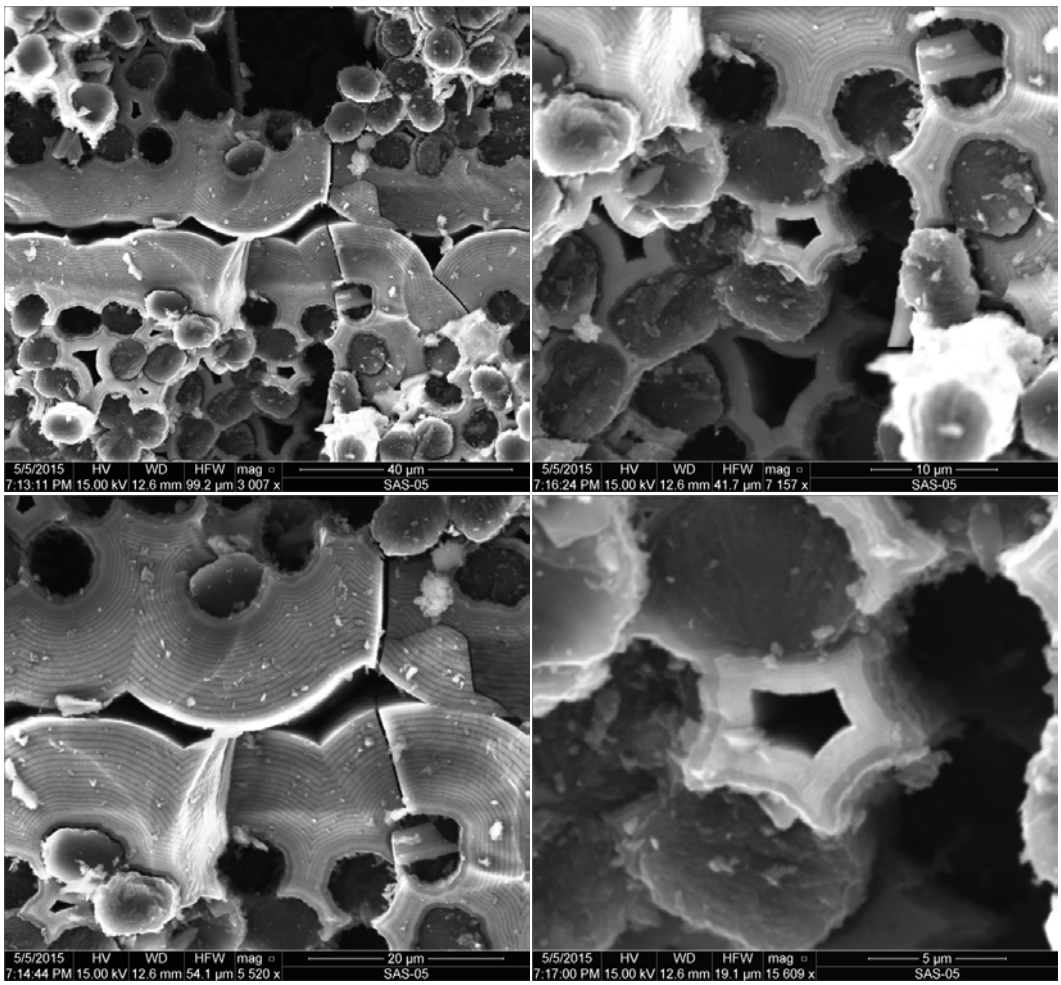

Figure L. 13: SEM micrographs of a fracture surface obtained in tensile test of a C/HYPR-SiC™ specimen subjected to prior heat treatment for 100 h at 1300°C (Plate 11121, Specimen 5)

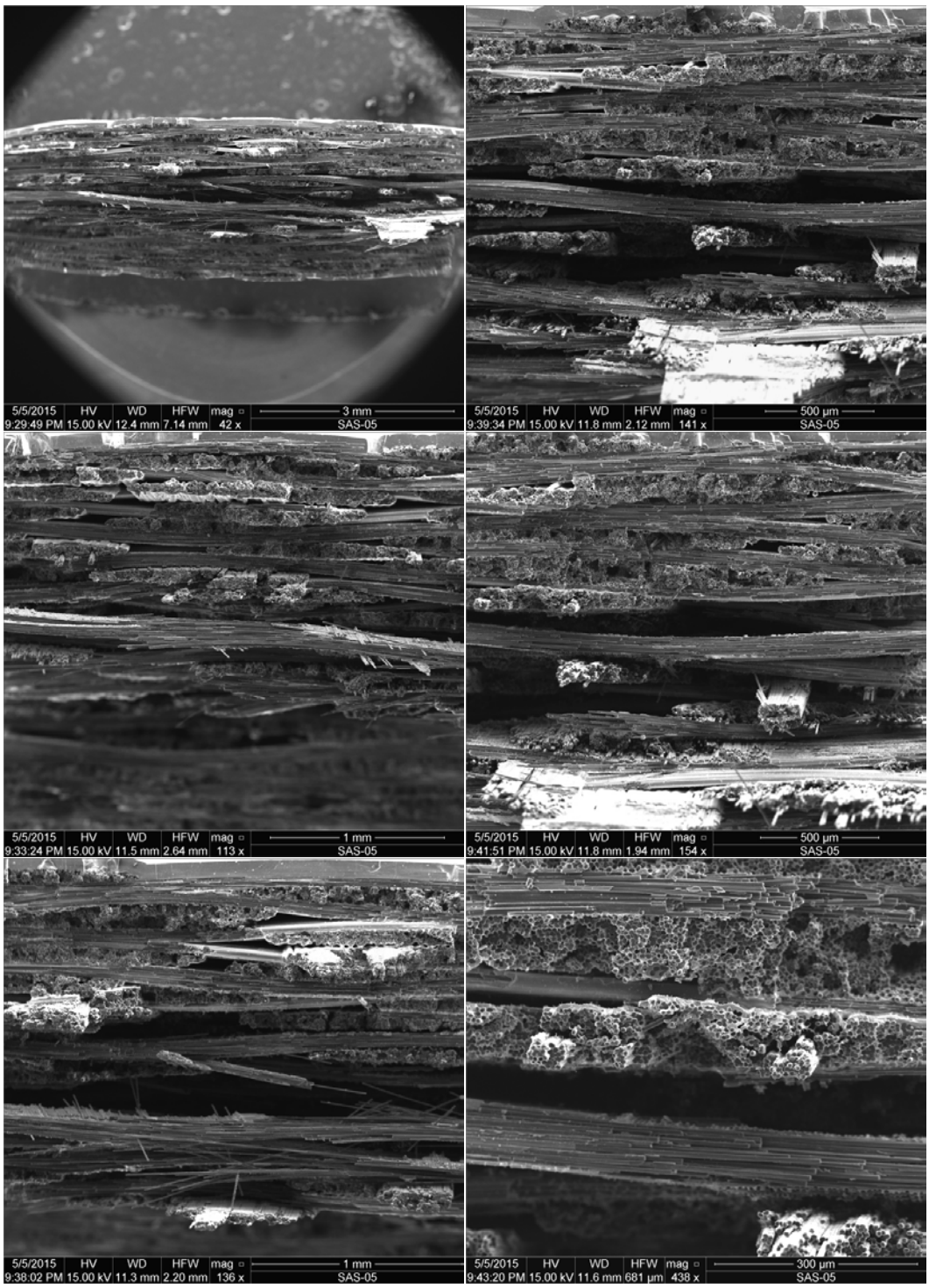

Figure L. 14: SEM micrographs of a fracture surface obtained in tensile test of a C/HYPR-SiC™ specimen subjected to prior heat treatment for 100 h at 1200°C (Plate 11122, Specimen 5)

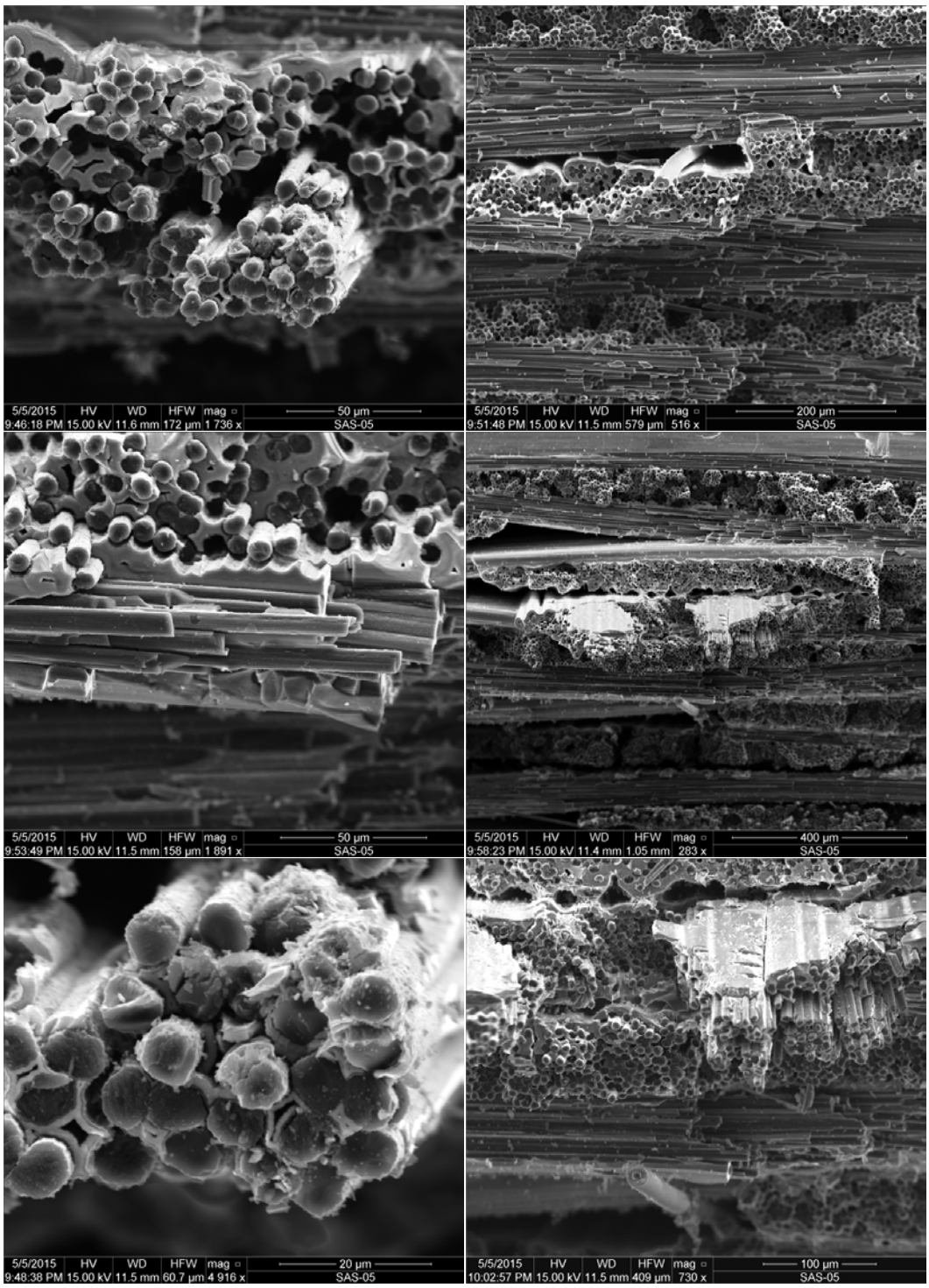

Figure L. 15: SEM micrographs of a fracture surface obtained in tensile test of a C/HYPR-SiC™ specimen subjected to prior heat treatment for 100 h at 1200°C (Plate 11122, Specimen 5)

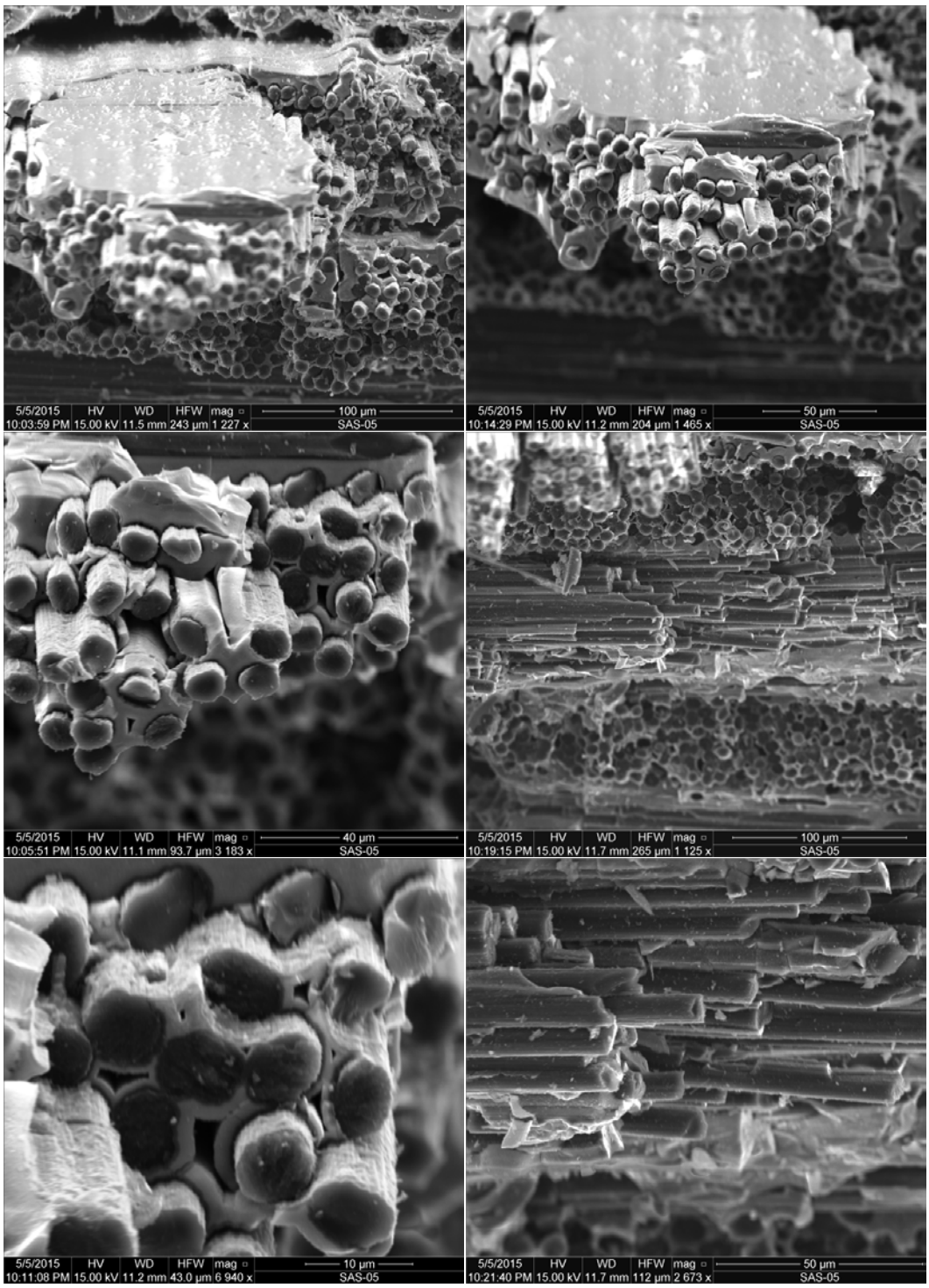

Figure L. 16: SEM micrographs of a fracture surface obtained in tensile test of a C/HYPR-SiC™ specimen subjected to prior heat treatment for 100 h at 1200°C (Plate 11122, Specimen 5)

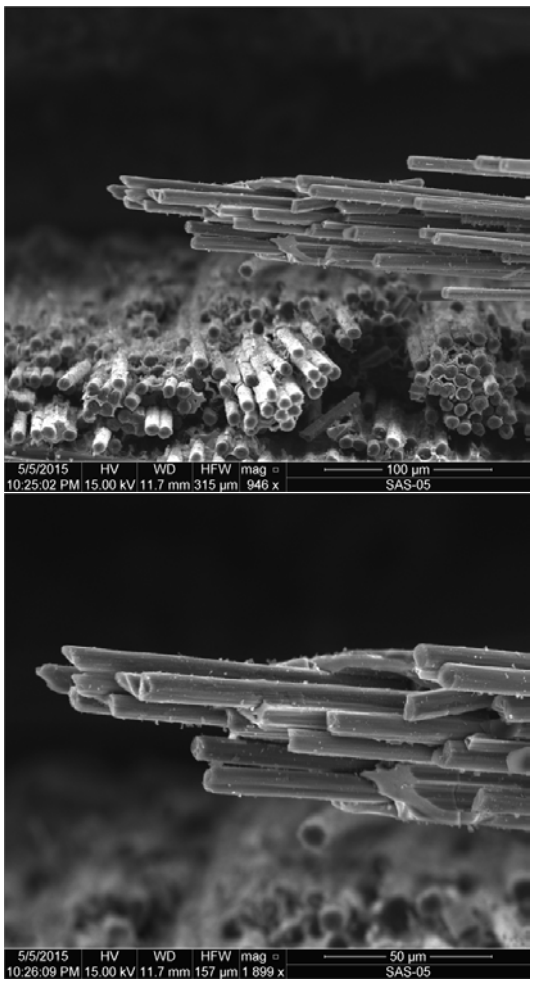

Figure L. 17: SEM micrographs of a fracture surface obtained in tensile test of a C/HYPR-SiC™ specimen subjected to prior heat treatment for 100 h at 1200°C (Plate 11122, Specimen 5)

Appendix M: Additional SEM Micrographs of Hi-Nicalon™/HYPR-SiC™ Fracture Surfaces

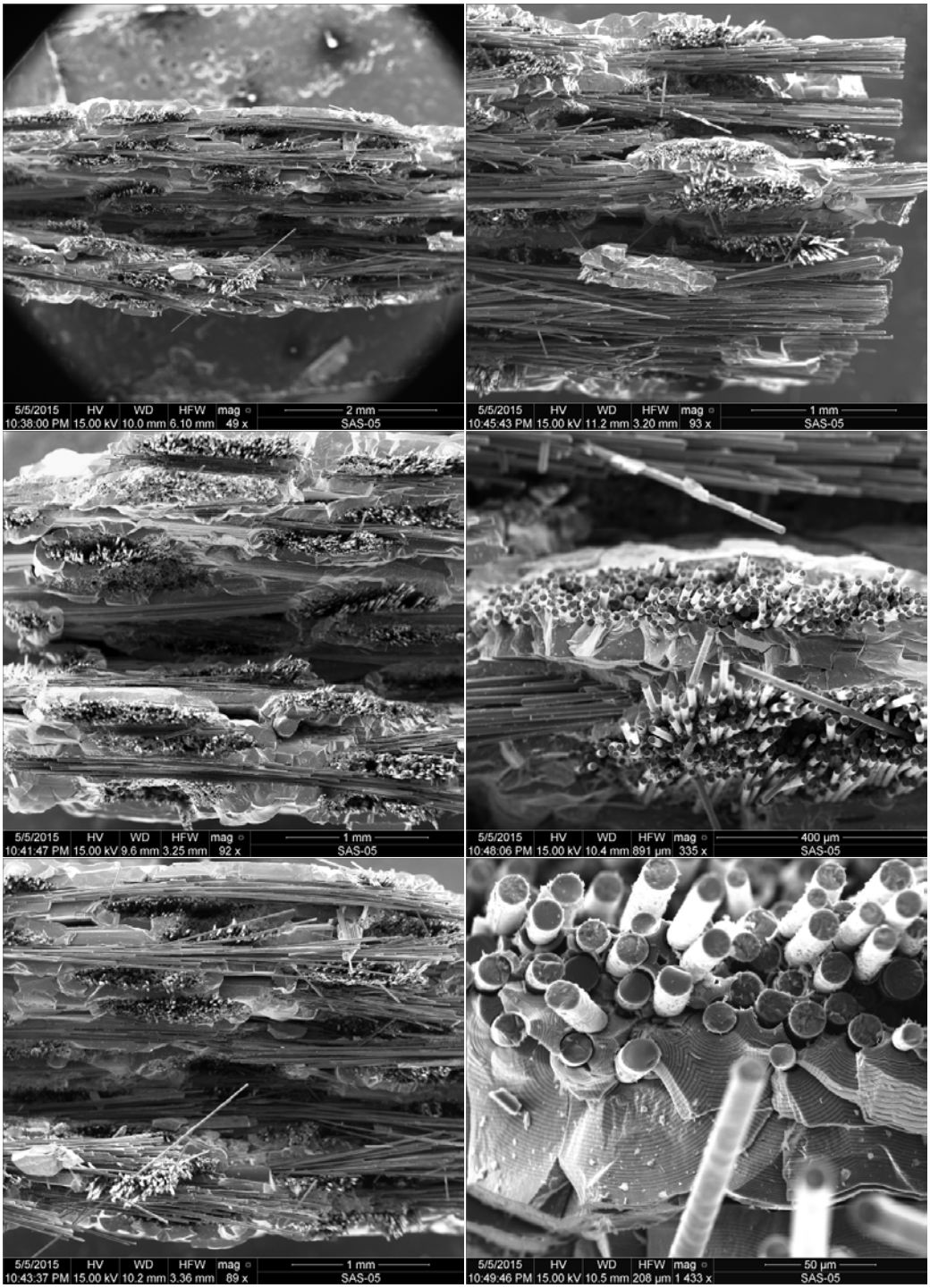

Figure M. 1: SEM micrographs of a fracture surface obtained in tensile test of a virgin Hi-Nicalon™/HYPR-SiC™ specimen (Plate 11138, Specimen 3)

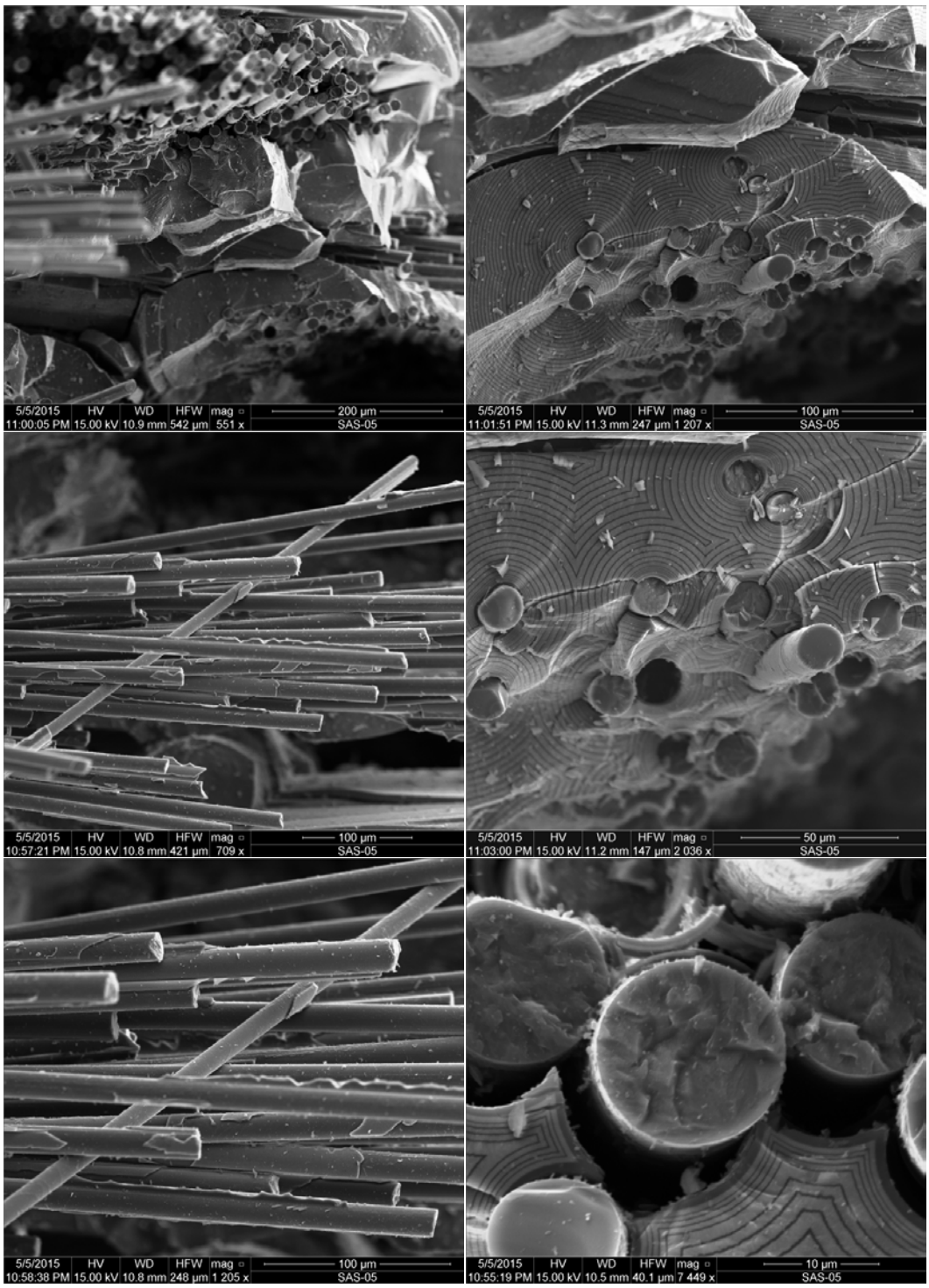

Figure M. 2: SEM micrographs of a fracture surface obtained in tensile test of a virgin Hi-Nicalon™/HYPR-SiC™ specimen (Plate 11138, Specimen 3)

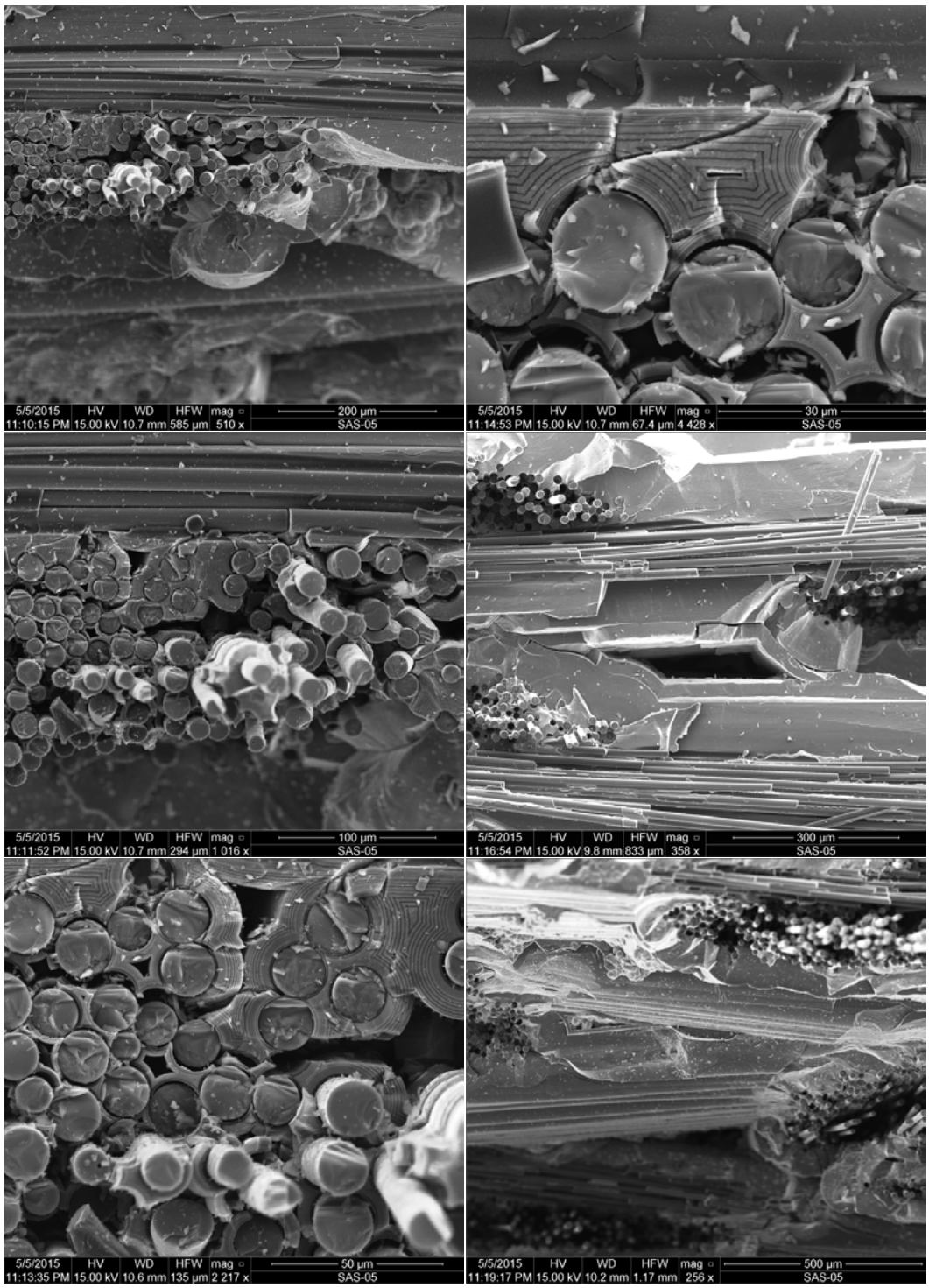

Figure M. 3: SEM micrographs of a fracture surface obtained in tensile test of a virgin Hi-Nicalon™/HYPR-SiC™ specimen (Plate 11138, Specimen 3)

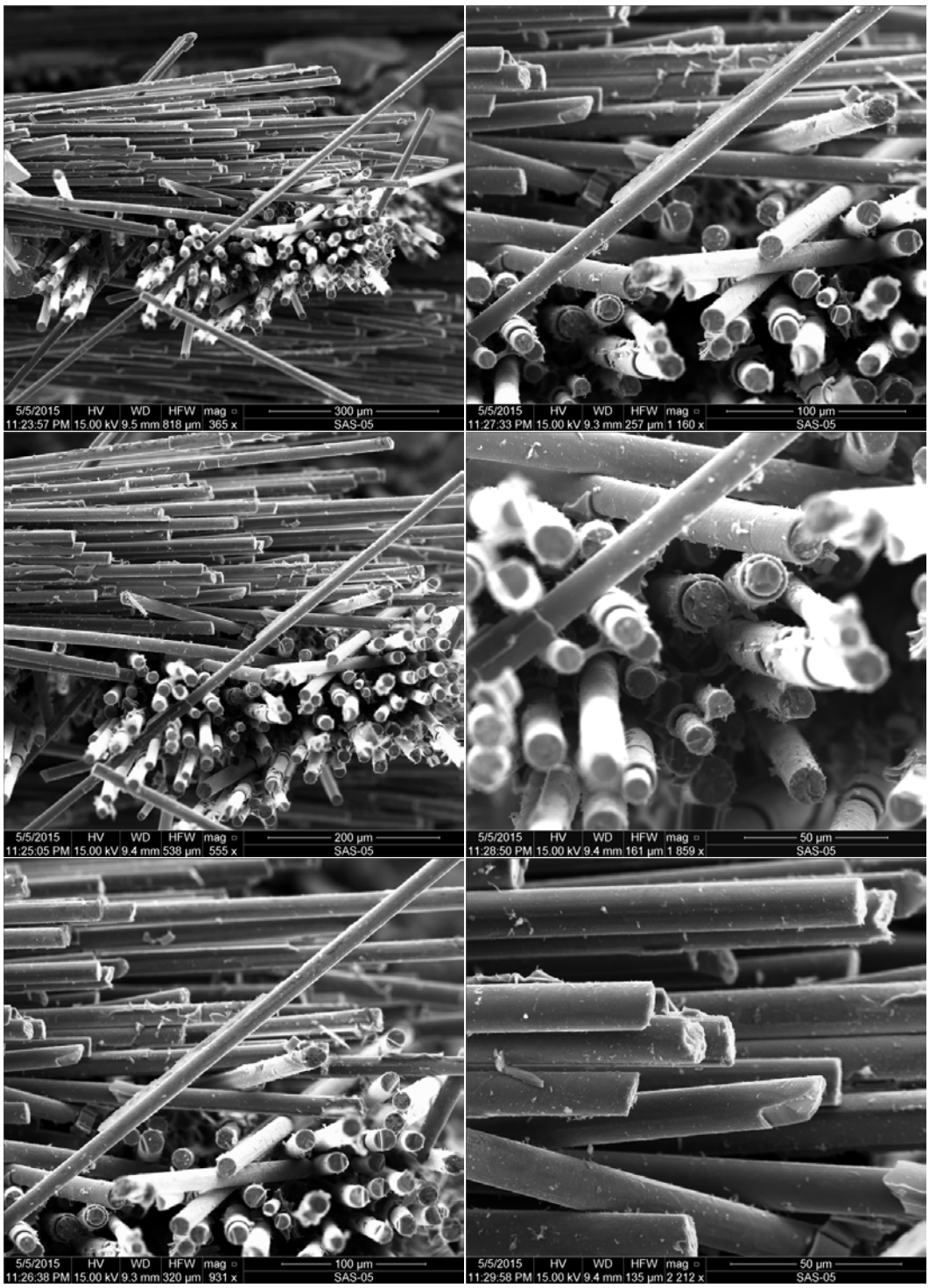

Figure M. 4: SEM micrographs of a fracture surface obtained in tensile test of a virgin Hi-Nicalon™/HYPR-SiC™ specimen (Plate 11138, Specimen 3)

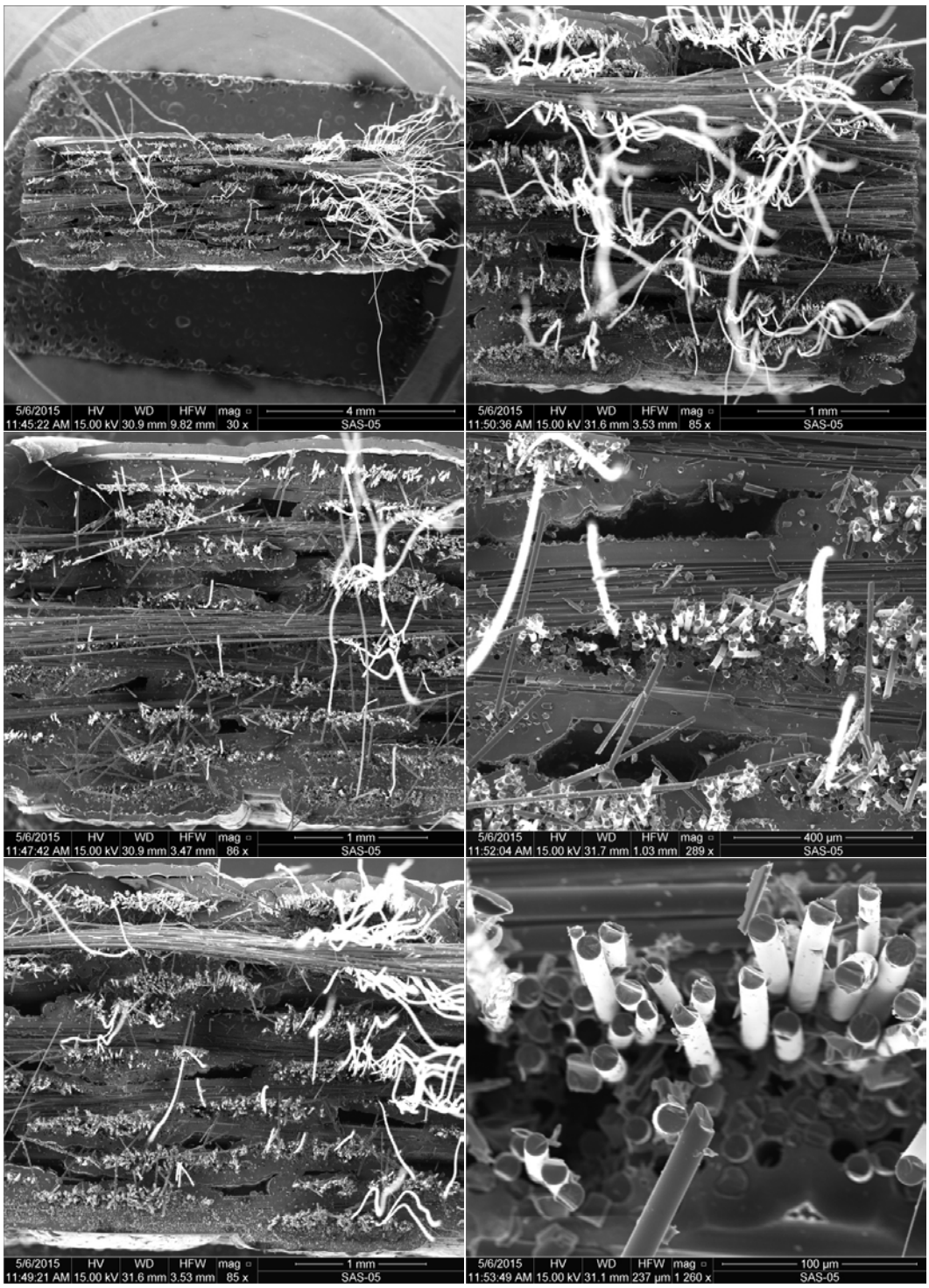

Figure M. 5: SEM micrographs of a fracture surface obtained in tensile test of a Hi-Nicalon™/HYPR-SiC™ specimen subjected to prior heat treatment for 10 h at 1400°C (Plate 11133, Specimen 2)

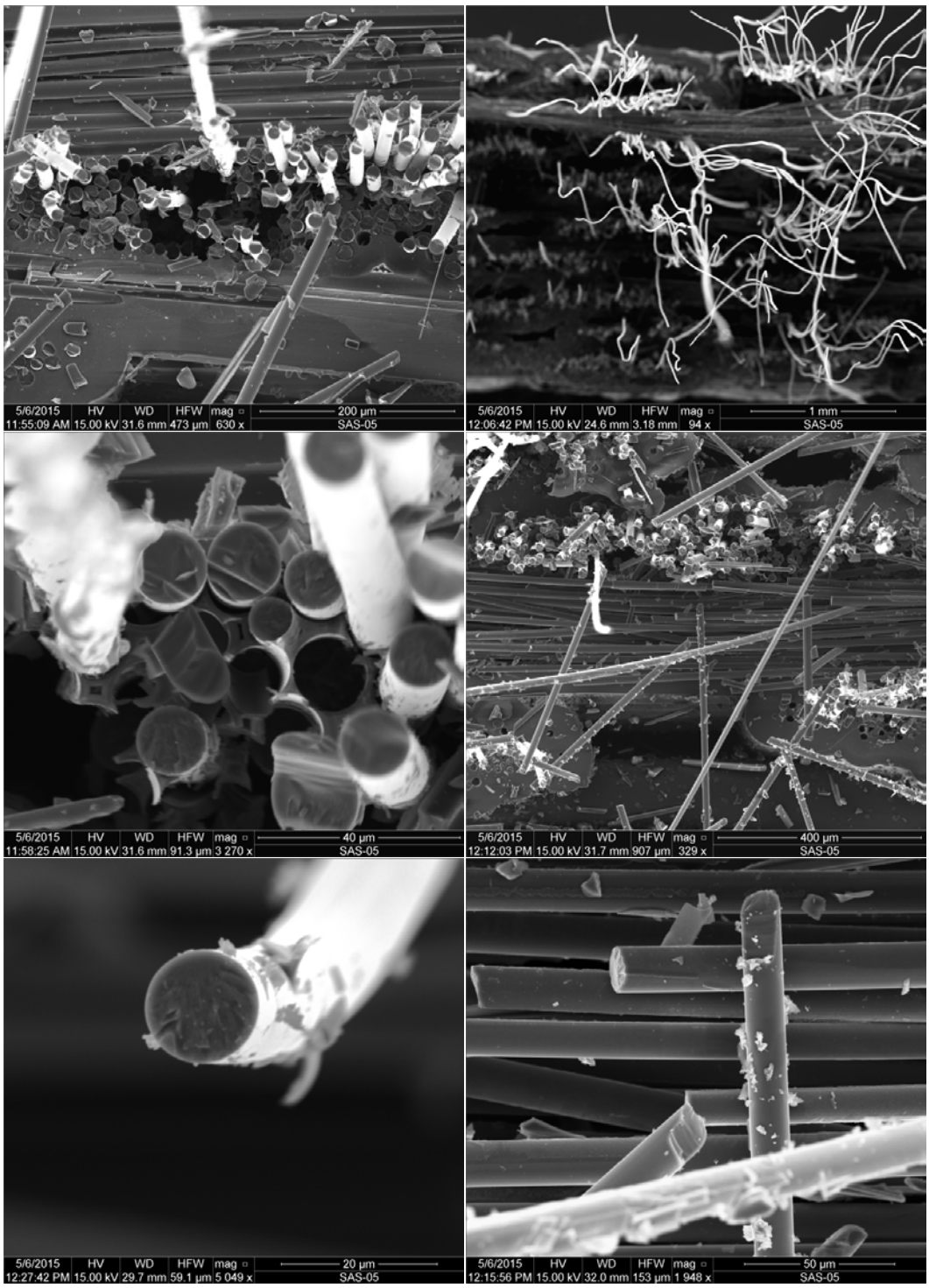

Figure M. 6: SEM micrographs of a fracture surface obtained in tensile test of a Hi-Nicalon™/HYPR-SiC™ specimen subjected to prior heat treatment for 10 h at 1400°C (Plate 11133, Specimen 2)

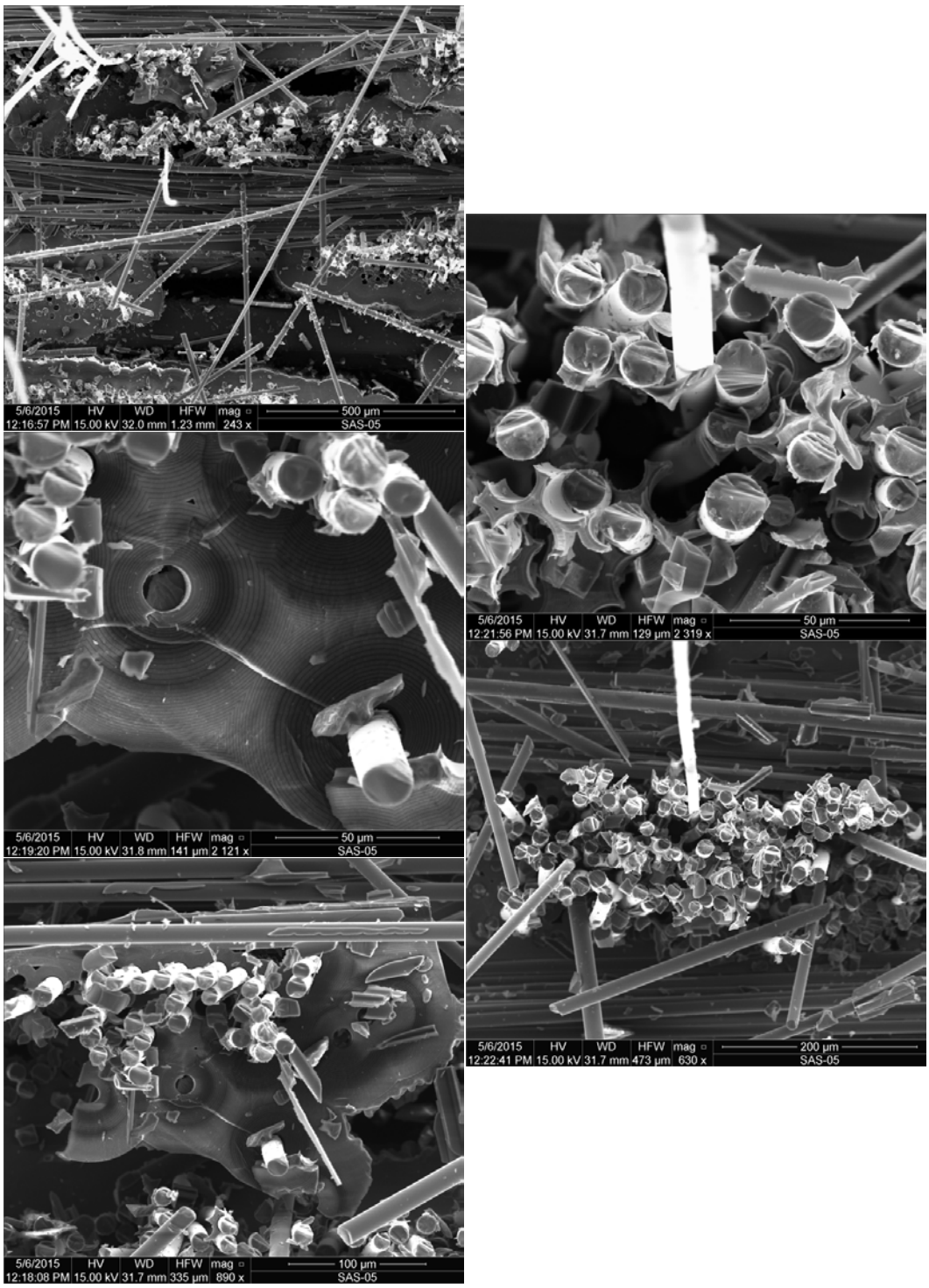

Figure M. 7: SEM micrographs of a fracture surface obtained in tensile test of a Hi-Nicalon™/HYPR-SiC™ specimen subjected to prior heat treatment for 10 h at 1400°C (Plate 11133, Specimen 2)

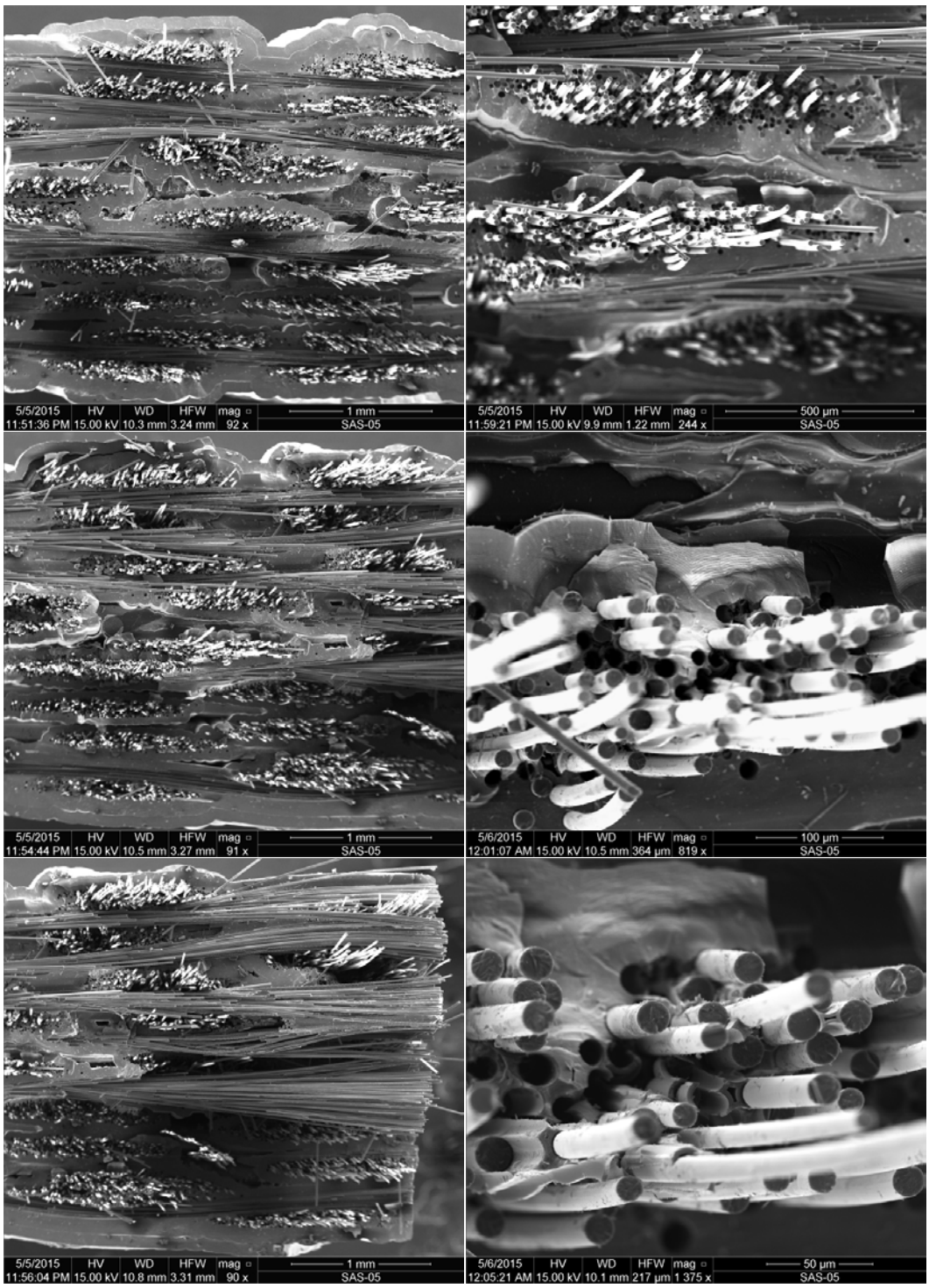

Figure M. 8: SEM micrographs of a fracture surface obtained in tensile test of a Hi-Nicalon™/HYPR-SiC™ specimen subjected to prior heat treatment for 100 h at 1400°C (Plate 11137, Specimen 6)

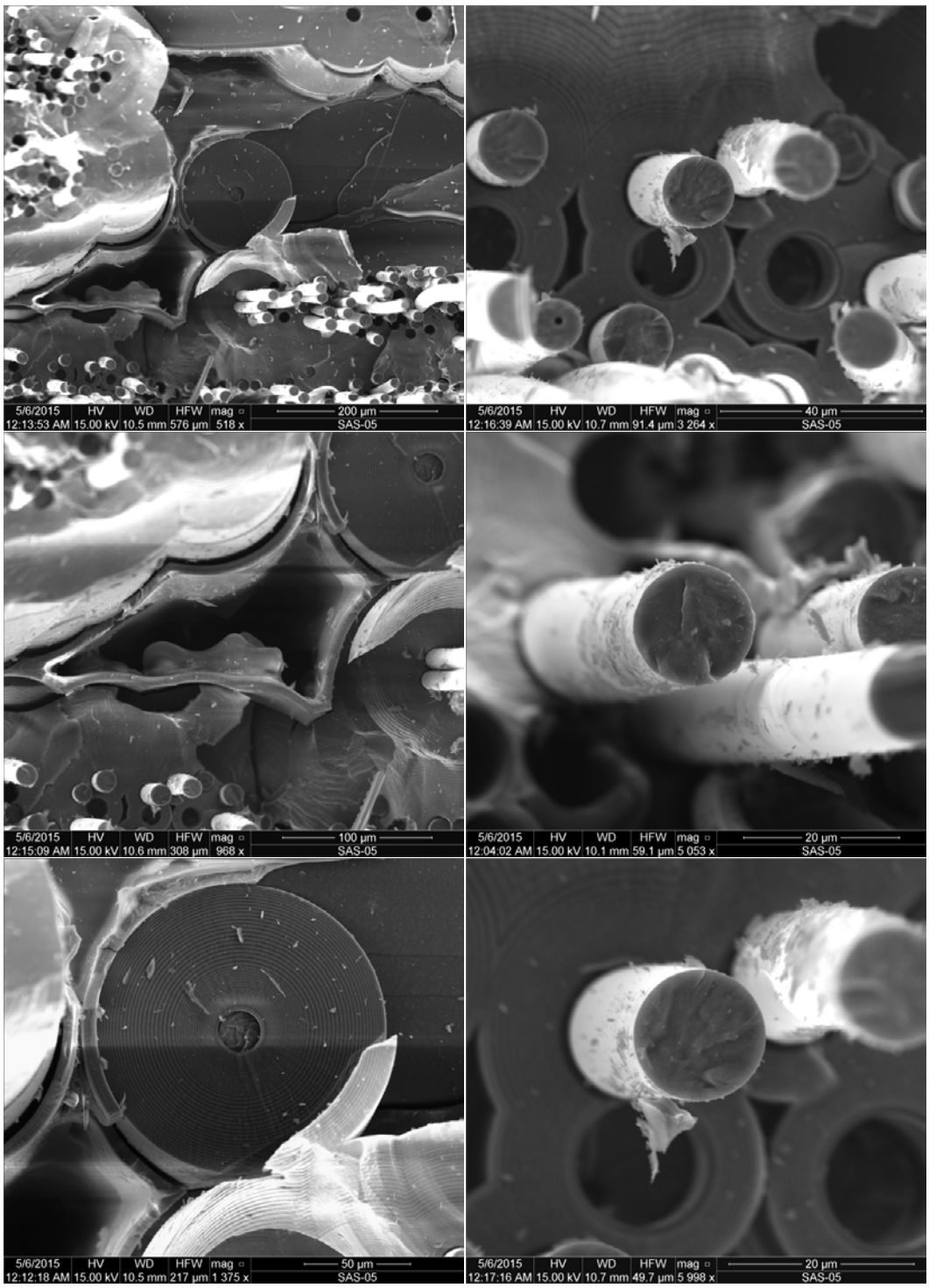

Figure M. 9: SEM micrographs of a fracture surface obtained in tensile test of a Hi-Nicalon™/HYPR-SiC™ specimen subjected to prior heat treatment for 100 h at 1400°C (Plate 11137, Specimen 6)

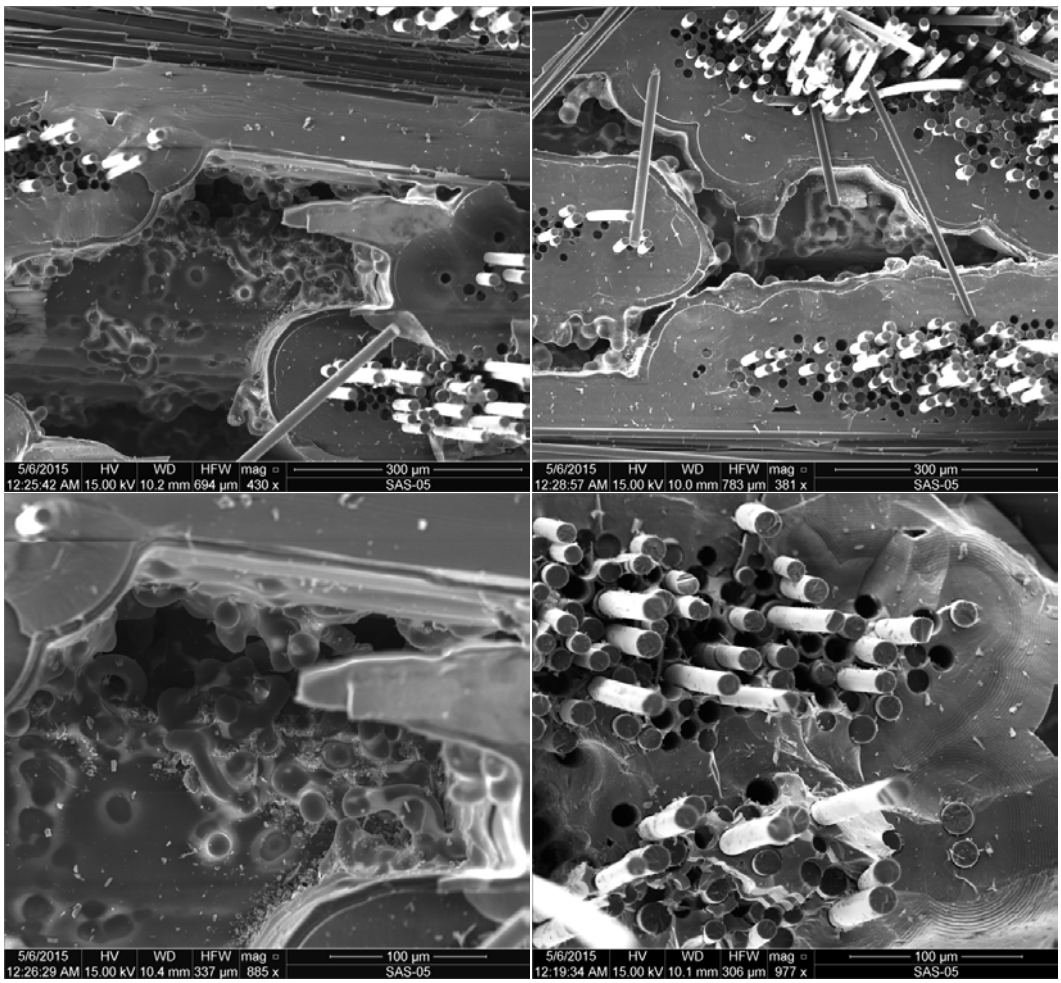

Figure M. 10: SEM micrographs of a fracture surface obtained in tensile test of a Hi-Nicalon™/HYPR-SiC™ specimen subjected to prior heat treatment for 100 h at 1400°C (Plate 11137, Specimen 6)

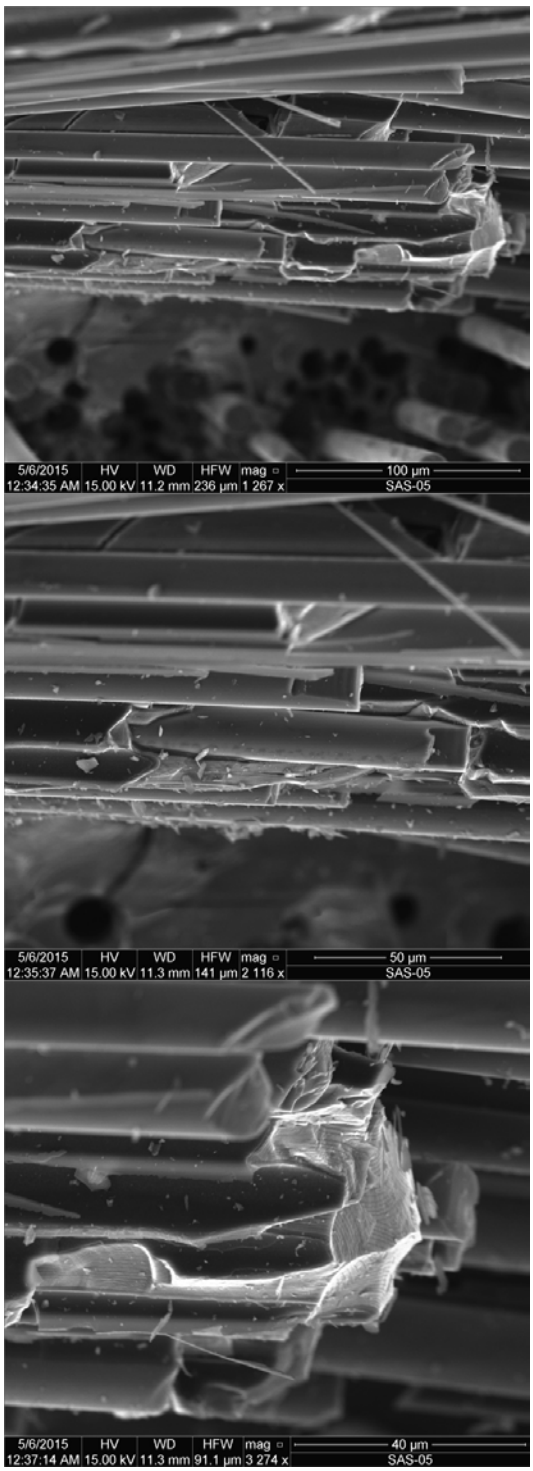

Figure M. 11: SEM micrographs of a fracture surface obtained in tensile test of a Hi-Nicalon™/HYPR-SiC™ specimen subjected to prior heat treatment for 100 h at 1400°C (Plate 11137, Specimen 6)

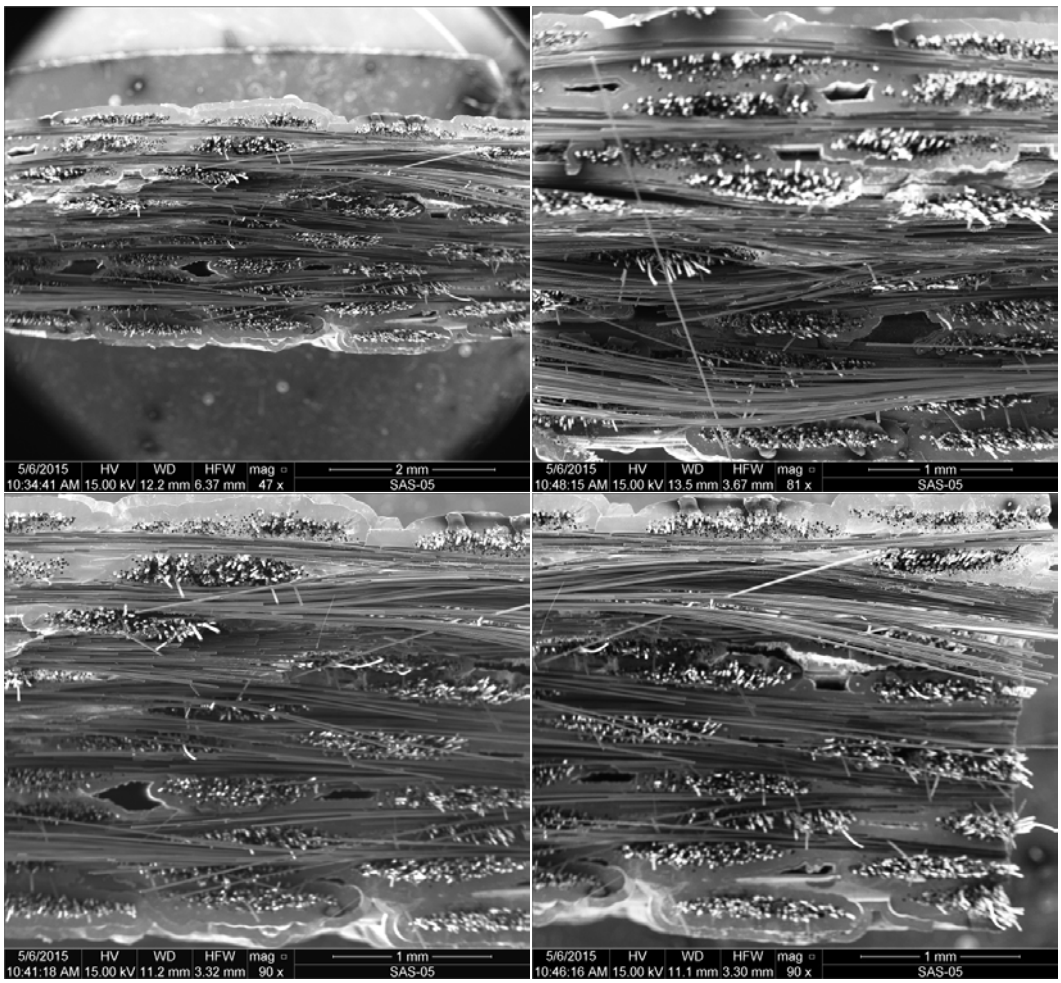

Figure M. 12: SEM micrographs of a fracture surface obtained in tensile test of a Hi-Nicalon™/HYPR-SiC™ specimen subjected to prior heat treatment for 100 h at 1300°C (Plate 11139, Specimen 1)

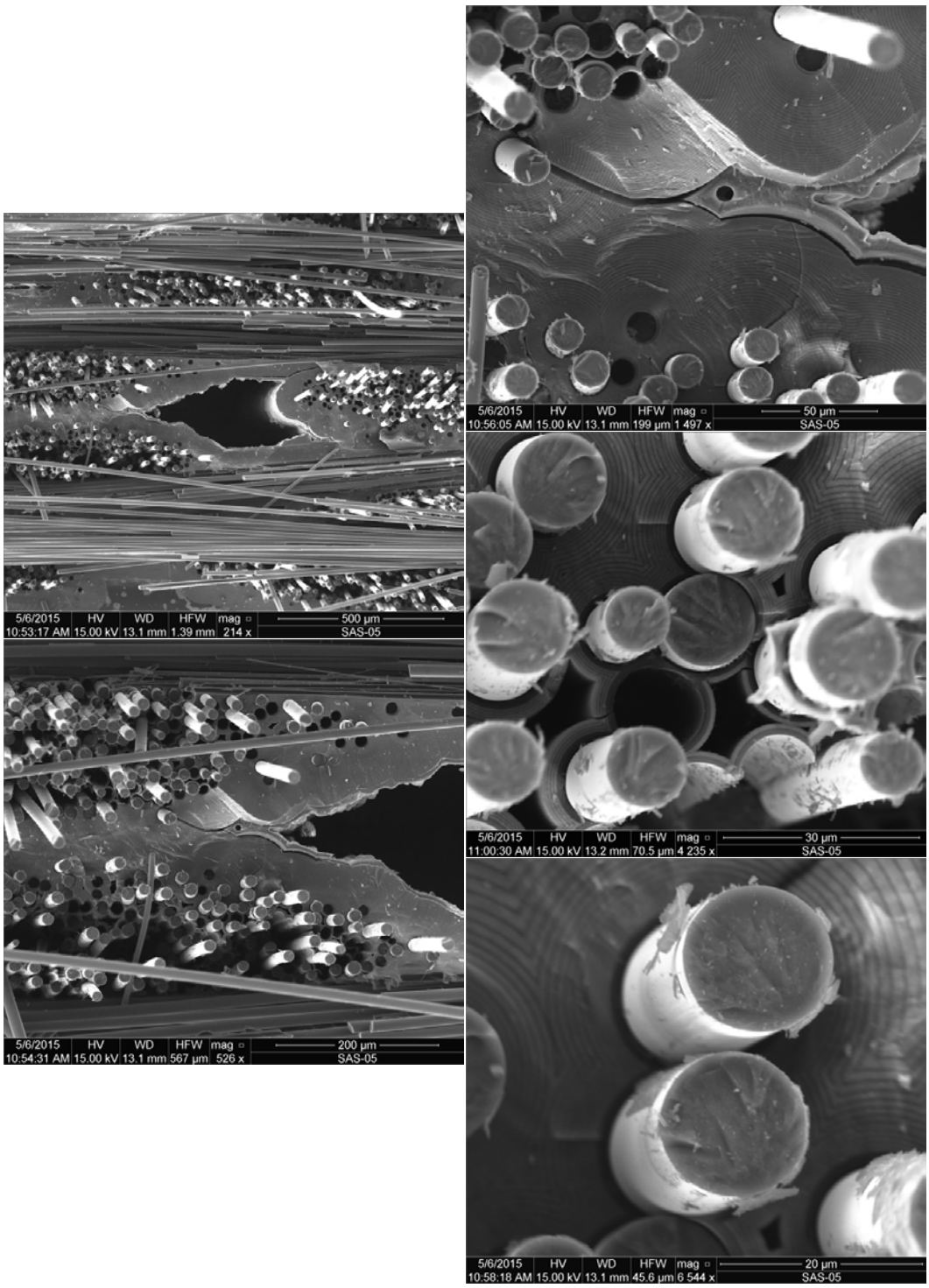

Figure M. 13: SEM micrographs of a fracture surface obtained in tensile test of a Hi-Nicalon™/HYPR-SiC™ specimen subjected to prior heat treatment for 100 h at 1300°C (Plate 11139, Specimen 1)

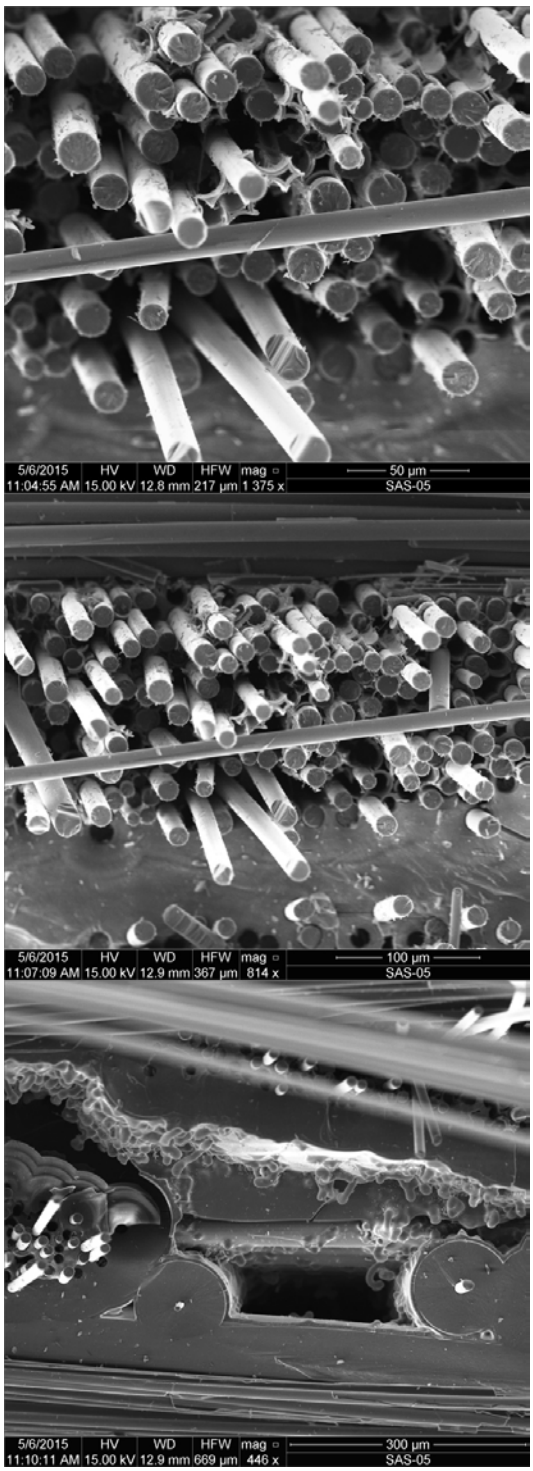

Figure M. 14: SEM micrographs of a fracture surface obtained in tensile test of a Hi-Nicalon™/HYPR-SiC™ specimen subjected to prior heat treatment for 100 h at 1300°C (Plate 11139, Specimen 1)

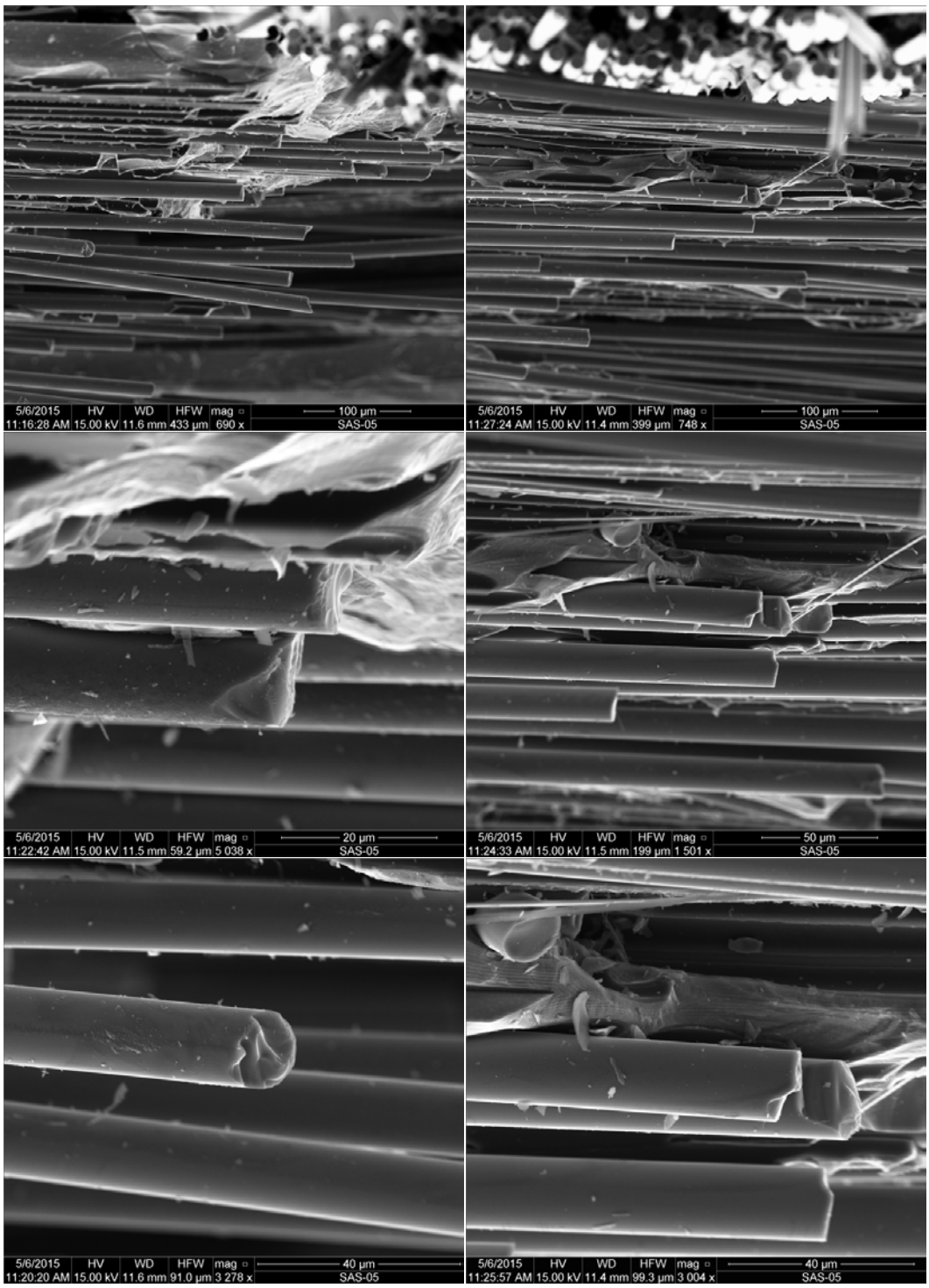

Figure M. 15: SEM micrographs of a fracture surface obtained in tensile test of a Hi-Nicalon™/HYPR-SiC™ specimen subjected to prior heat treatment for 100 h at 1300°C (Plate 11139, Specimen 1)

Bibliography

[1] W. L. Harper, Isaac Newton's Scientific Method: Turning Data Into Evidence about Gravity and Cosmology, New York: Oxford University Press, 2011.

[2] F. Christin, "CMC Materials for Space and Aeronautical Applications," in *Ceramic Matrix Composites*, Weinheim, Wiley-VCH Verlag GmbH & Co, 2008, pp. 327-351.

[3] T.-W. Chou, Microstructural Design of Fiber Composites, Cambridge: Cambridge University Press, 1992.

[4] K. Chawla, Ceramic Matrix Composites, London: Champan & Hall, 1993.

[5] D. F. Adams, L. A. Carlsson and R. B. Pipes, Experimental Characterization of Advanced Composite Materials (Third Edition), Boca Raton: CRC Press LLC, 2003.

[6] M. Ruggles-Wrenn, Interviewee, *MECH 601 Course notes.* [Interview]. 30 June 2014.

[7] W. Kingery, H. Bowen and D. Uhlmann, Introduction to Ceramics, Second Edition, John Wiley & Sons, Inc., 1976.

[8] G. Geiger, "Introduction to Ceramics," American Ceramic Society, 2001.

[9] I. M. Daniel and O. Ishai, Engineering Mechanics of Composite Materials, New York: Oxford University Press, Inc., 2006.

[10] B. Clauss, "Fibers for Ceramic Matrix Composites," in *Ceramic Matrix Composites*, Weinheim, Wiley-VCH Verlag GmbH & Co., 2008, pp. 1-20.

[11] M. Ruggles-Wrenn, J. Delapasse, A. Chamberlain, J. Lane and T. Cook, "Fatigue behavior of a Hi-Nicalon/SiC-B4C composite at 1200C in air and steam," *Materials Science and Engineering - A,* vol. 534, no. 1 February 2012, pp. 119-128, 2012.

[12] M. Ruggles-Wrenn and T. Jones, "Tension-compression fatigue of a SiC/SiC ceramic matrix composite at 1200C in air and in steam," *International Journal of Fatigue,* vol. 47, pp. 154-160, 2013.

[13] M. Ruggles-Wrenn, M. Pope and T. Zens, "Creep behavior in interlaminar shear of a Hi-Nicalon/SiC-B4C composite at 1200C in air and in steam," *Materials Science & Engineering - A,* vol. 610, pp. 279-289, 2014.

[14] J. Ma, Y. Xu, L. Zhang, L. Cheng, J. Nie and N. Dong, "Microstructure characterization and tensile behavior of 2.5D C/SiC composites fabricated by chemical vapor infiltration," *Scripta Materialia,* vol. 54, pp. 1967-1971, 2006.

[15] H. Mei, L. Cheng, L. Zhang and Y. Xu, "Effect of temperature gradients and stress levels on damage of C/SiC composites in oxidizing atmosphere," *Materials Science and Engineering - A,* vol. 430, pp. 314-319, 2006.

[16] H. Mei, L. Cheng and L. Zhang, "Damage mechanisms of C/SiC composites subjected to constant load and thermal cycling in oxidizing atmosphere," *Scripta Materialia,* vol. 54, pp. 163-168, 2006.

[17] F. Lamouroux, S. Bertrand, R. N. R. Pailler and M. Cataldi, "Oxidation-resistant carbon-fiber-reinforced ceramic-matrix composites," *Composites Science and Technology,* vol. 59, pp. 1073-1085, 1999.

[18] C. Zhang, S. Qiao, K. Yan, Y. Liu, Q. Wu, D. Han and M. Li, "Mechanical properties of a carbon fiber reinforced self-healing multilayered matrix composite at elevated temperatures," *Materials Science and Engineering - A,* vol. 528, pp. 3073-3078, 2011.

[19] J. A. DiCarlo and H.-M. Yun, "Non-oxide (Silicon Carbide) Fibers," in *Handbook of Ceramic Composites*, New York, Springer Science+Business Media, 2005, pp. 33-52.

[20] M. B. Ruggles-Wrenn and V. Sharma, "Effects of Steam Environment on Fatigue Behavior of Two SiC/[SiC+Si3N4] Ceramic Composites at 1300C," *Applied Composite Materials,* vol. 2011, no. 18, pp. 385-396, 2011.

[21] COI Ceramics, Inc., "COI Ceramics, Inc.," [Online]. Available: http://www.coiceramics.com/pdfs/1%20Non-oxide%20process.pdf. [Accessed 9 May 2015].

[22] *Personal correspondence with Dr. Kristin Keller and Ms. Jennifer Pierce (AFRL/RXC),* Wright Patterson Air Force Base, 2014.

[23] Hexcel Corporation, *HexTow IM7 Carbon Fiber Product Data,* Stamford: Hexcel Corporation, 2014.

[24] Toray Carbon Fibers America, Inc., *T300 Technical Data Sheet,* Santa Ana: Toray Carbon Fibers America, Inc..

[25] Toray Carbon Fibers America, Inc., "Toray Carbon Fibers America," Design Studio One, 2008. [Online]. Available: http://www.toraycfa.com/index.htm. [Accessed 30 April 2015].

[26] Toray Industries, Inc., "Torayca Carbon Fiber Functional and Composite Properties," 2005. [Online]. Available: http://www.torayca.com/en/techref/index.html. [Accessed 30 April 2015].

[27] Y. M. Tarnopol'skii and T. Kincis, Static Test Methods for Composites, New York: Van Nostrand Reinhold Company Inc., 1985, pp. 45-48.

[28] AFRL/RXC, *AFRL Thermal Stability Test Results Comparison 20131009,* Wright Patterson AFB, 2013.

REPORT DOCUMENTATION PAGE

Form Approved
OMB No. 074-0188

1. REPORT DATE *(DD-MM-YYYY)*	**2. REPORT TYPE**	**3. DATES COVERED** *(From – To)*
18-06-2015	Master's Thesis	September 2013 – June 2015

TITLE AND SUBTITLE
Effect of Prior Exposure at Elevated Temperatures on Tensile Properties and Stress-Strain Behavior of Four Non-Oxide Ceramic Matrix Composites

5a. CONTRACT NUMBER

5b. GRANT NUMBER

5c. PROGRAM ELEMENT NUMBER

6. AUTHOR(S)

Wallentine, Sarah M., Captain, USAF

5d. PROJECT NUMBER

5e. TASK NUMBER

5f. WORK UNIT NUMBER

7. PERFORMING ORGANIZATION NAMES(S) AND ADDRESS(S)
Air Force Institute of Technology
Graduate School of Engineering and Management (AFIT/ENY)
2950 Hobson Way, Building 640
WPAFB OH 45433-8865

8. PERFORMING ORGANIZATION REPORT NUMBER
AFIT-ENY-MS-15-J-048

9. SPONSORING/MONITORING AGENCY NAME(S) AND ADDRESS(ES)
Air Force Research Laboratory
Larry Zawada
2230 10th Street
Wright-Patterson AFB, OH 45433
larry.zawada@us.af.mil

10. SPONSOR/MONITOR'S ACRONYM(S)
AFRL/RXCC

11. SPONSOR/MONITOR'S REPORT NUMBER(S)

12. DISTRIBUTION/AVAILABILITY STATEMENT
DISTRUBTION STATEMENT A.
APPROVED FOR PUBLIC RELEASE; DISTRIBUTION UNLIMITED.

13. SUPPLEMENTARY NOTES
This material is declared a work of the U.S. Government and is not subject to copyright protection in the United States.

14. ABSTRACT

Thermal stability of four non-oxide ceramic matrix composites was studied. The materials studied were commercially available composites: SiC/SiNC; C/SiC; C/SiC-B_4C (C/HYPR-SiC™); and SiC/SiC-B_4C (SiC/HYPR-SiC™). COI Ceramics manufactured the SiC/SiNC and C/SiC composites using polymer infiltration and pyrolysis (PIP). The C/HYPR-SiC™ and SiC/HYPR-SiC™ CMCs were manufactured by Hyper-Therm High-Temperature Composites using chemical vapor infiltration (CVI). All four composites rely on a dense matrix for strength, stiffness, and oxidation protection. Fiber coating provides a fiber-matrix interface that allows fiber-matrix debonding and fiber pullout to occur, imparting fracture toughness to the CMC. The SiC/SiNC, C/SiC, and C/HYPR-SiC™ composites were heat treated in laboratory air for 10 h, 20 h, 40 h, and 100 h at over-temp (1300°C) and for 100 h at operating temperature (1200°C). The SiC/HYPR-SiC™ composite was heat treated in laboratory air for 10 h, 20 h, 40 h, and 100 h at over-temp (1400°C) and for 100 h at operating temperature (1300°C). Room-temperature tensile properties of heat treated and virgin material were measured, and effect of prior heat treatment on tensile properties was evaluated.

Prior heat treatment caused a reduction of tensile strength of at least 10% for all materials. Both PIP-produced CMCs exhibited increased fiber-matrix bonding due to high temperature exposures, contributing to brittle fracture of clumped fiber bundles and thus reduced tensile strength. Both CVI-produced CMCs exhibited considerable matrix voids due to poor infiltration during fabrication. Void prevalence and the associated stress concentrations contributed to premature matrix cracking and composite failure. The CVI CMCs were susceptible to degraded tensile properties and brittle composite fracture due to strengthened fiber-matrix interfaces and fiber degradation caused by prior heat treatment.

15. SUBJECT TERMS
Ceramic Matrix Composites; Composite Materials; Ceramic Fibers; Ceramic Materials; Fiber Reinforced Composites; Non-Oxide; Silicon Carbide; Boron Carbide; Hi-Nicalon™ Fiber; T300 Carbon Fiber; HexTow® IM7 Carbon Fiber; Elevated Temperature; Thermal Stability

16. SECURITY CLASSIFICATION OF:			**17. LIMITATION OF ABSTRACT**	**18. NUMBER OF PAGES**	**19a. NAME OF RESPONSIBLE PERSON**
a. REPORT	**b. ABSTRACT**	**c. THIS PAGE**			Dr. Marina B. Ruggles-Wrenn, AFIT/ENY
U	**U**	**U**	**UU**	271	**19b. TELEPHONE NUMBER** *(Include area code)* 937-255-3636 x4641 marina.ruggles-wrenn@afit.edu

Standard Form 298 (Rev. 8-98)
Prescribed by ANSI Std. Z39-18